FUNCTIONAL CHARACTERISATION OF OPCML CLINICAL MUTATIONS IN OVARIAN CANCER AND CORRELATE TO OPCML CRYSTAL STRUCTURE

Mohammad N Alomary

CID: 00904599

This thesis is submitted in

fulfilment of the requirements for the degree of

PhD in Clinical Medicine Research

Department of Surgery and Cancer

Imperial College London

UK

February 01, 2018

ABSTRACT

Ovarian cancer is a heterogeneous disease, considered the most lethal of all gynaecological malignancies. With an initially high response rate to treatment, ovarian cancer can suddenly relapse, with advanced stages showing loco-regional dissemination. Despite enormous efforts to tackle ovarian cancer, current treatments fail to bring complete remission or significantly extend patient life. OPCML is a promising candidate in ovarian cancer treatment, identified as a tumour suppressor frequently inactivated in ovarian and other cancers. OPCML is a negative regulator of RTKs and regulates different cellular activities.

The aims of this PhD were to identify and functionally characterise clinical OPCML mutations in ovarian cancer guided by the newly resolved crystal structure of OPCML. The project describes how TCGA and COSMIC databases have been used here to identify somatic missense mutations in several tumours. A panel of OPCML mutant constructs was then created and these selected constructs were utilised to transduce three ovarian cancer cell lines (SKOV3, PEA1, and PEO1) for domain I, and SKOV3 cells for domain II and III. Selected transduced mutants were used to characterise the mutants' localisation, interaction with receptor tyrosine kinases, proliferation, cellular transformation, invasion, migration, and their potential role in the adhesion to the extracellular matrix *in vitro*. Furthermore, two *in vivo* models were used to characterise OPCML mutants: the athymic mice model and the chick embryo chorioallantoic membrane assay. The results showed that the OPCML mutants in domain I behave

differently when they interact with receptor tyrosine kinase AXL and FGFR1 compared to wild-type OPCML. These OPCML mutants preserve the ability to inhibit growth in *vitro,* but have a complete loss of function in *vivo*. They also block the OPCML inhibitory activity on anchorage-independent growth, invasion, migration, and adhesion to extracellular matrix components laminin I, fibronectin, and fibrinogen. The OPCML mutants in domain II showed partial loss of function in adhesion to collagen I and IV, and complete loss of tumour suppressor function in cell proliferation *in vitro* and *in vivo*, anchorage-independent growth, invasion, migration, and adhesion to laminin I, fibronectin, and fibrinogen. The OPCML mutants in domain III preserve adhesion to collagen I and IV, but show complete loss of function in the inhibition of tumour growth *in vitro* and *in vivo*, anchorage-independent growth, invasion, migration, and adhesion to laminin I, fibronectin, and fibrinogen.

Therefore, this study identifies a new mechanism of OPCML inactivation by mutations and shows that single amino acid change can abolish OPCML function. These findings suggest that OPCML is an excellent candidate for a new and novel therapeutic strategy in ovarian cancer and other malignancies, as well as other non-cancer diseases.

DECLARATION OF ORIGINALITY

I hereby certify that the work presented in this thesis is my own unless stated otherwise in the body of the text. This thesis has not been submitted for any other degree or equivalent qualification. Information derived from the published and unpublished work of others has been acknowledged in the text and a list of references is given in the bibliography.

Copyright Declaration

The copyright of this thesis rests with the author and is made available under Creative Commons Attribution Non-Commercial No Derivatives licence. Researchers are free to copy, distribute or transmit the thesis on the condition that they attribute it, that they do not use it for commercial purposes and that they do not alter, transform or build upon it. For any reuse or redistribution, researchers must make clear to others the licence terms of this work

TABLE OF CONTENTS

ABSTRACT 2

LIST OF TABLES 15

LIST OF FIGURES 16

LIST OF ABBREVIATION 19

ACKNOWLEDGEMENTS 21

1. Introduction 23

1.1. Cancer 23

1.2. Ovarian cancer 26

1.2.1. Epidemiology 26

1.2.2. Anatomy and biology of ovarian cancer 28

1.2.3. Risk factors 33

1.2.4. Types of ovarian cancer 40

1.2.5. Ovarian cancer staging 44

1.2.6. Grades 47

1.2.7. The origin of ovarian cancer 47

1.2.8. Diagnosis 51

1.2.9. Management of ovarian cancer 52

1.3. RTKs in cancer 53

1.3.1. Introduction 53

1.3.2 Epidermal Growth Factor Receptor (EGFR) Family 55
1.3.3. AXL 58
1.3.4. Insulin-like growth factor I receptor (IGF-IR) 59
1.3.5. H-RYK receptor tyrosine kinase 61
1.3.6. Eph RTK 62
1.4. The IgLON family 64
1.4.1. Introduction 64
1.4.2. IgLON structure and cellular localisation 65
1.4.3. IgLON expression 67
1.4.4. IgLON function 67
1.4.5. IgLON and cancer 69
1.5. OPCML 70
1.5.1. OPCML structure 70
1.5.2. OPCML expression 70
1.5.3. OPCML as a tumour suppressor 71
1.5.4. The role of OPCML in the regulation of RTKs in ovarian cancer 74
1.5.5. Role of OPCML mutations 76
1.6. Hypothesis and Aims 77
2. CHAPTER 2 79
2.1. Chemicals and reagents 80

2.2. Cell culture 80
2.3. Nucleic acid manipulation 83
2.3.1. Agarose Gel Electrophoresis 83
2.3.2. Mutagenic Primers Design 83
2.3.3. Site-Directed Mutagenesis 89
2.3.4. Restriction Endonucleases Digestion 91
2.3.5. Bacterial Transformation and DNA extraction 91
2.3.6. DNA Sequencing 92
2.3.7. The Gateway® cloning system 92
2.4. Lentiviral packaging 96
2.5. Transduction 97
2.6. Whole Cell Lysate Preparation 97
2.7. Protein Concentration Determination 97
2.8. SDS-PAGE and Western Blot 98
2.9. Immunofluorescence Confocal Microscopy 100
2.10. Co-Immunoprecipitation 101
2.11. Proliferation Assay 101
2.12. Lipid raft preparation (Detergent-resistant membranes, DRM) 101
2.13. Duolink (in situ Proximity Ligation Assay) 102
2.14. Wound healing assay 103

2.15. Cell migration and invasion assays 104
2.16. Soft agar colony formation assay 104
2.17. Spheroid formation assay 105
2.18. *In vitro* cell adhesion assay 105
2.19. R428 treatment and IC50 evaluation 106
2.20. Apoptosis Assay 107
2.21. Proteome profiler arrays 107
2.22. In vivo work 108
2.23. Chick Embryo Chorioallantoic membrane (CAM) assay 108
2.24. *In vivo* mouse model 109
2.25. Immunohistochemistry 110
2.26. Data analysis 111
3. CHAPTER 3 112
Introduction 113
3.1. TCGA and COSMIC database 114
3.2. OPCML crystal structure 118
3.3. OPCML mutations mapped onto OPCML's crystal structure 122
3.4. Summary of the findings 124
4. CHAPTER 4 125
Introduction 126

4.1. Identification of OPCML mutations in domain I using public data from TCGA and COSMIC and mapping into the newly discovered OPCML crystal structure. 127

4.2. Creation and characterisation of ovarian cancer cell lines stably expressing OPCML mutants. 133

4.3. The localisation of OPCML mutants in domain I and OPCML wild-type in the cell membrane. 136

4.4. OPCML mutants maintain the lipid raft localisation of OPCML. 138

4.5. The RTK AXL interacts with OPCML wild-type and OPCML mutants. 141

4.6. OPCML mutants disrupt the interaction with AXL upon stimulation with the AXL ligand Gas6 over time. 143

4.7. OPCML mutants do not inhibit GAS6/AXL downstream signalling. 146

4.8. OPCML mutants do not alter cell migration and invasion upon Gas6 stimulation compared to inhibition by wild-type OPCML. 149

4.9. OPCML mutants impair the sensitisation effect of OPCML to AXL inhibitor R428 by altering Caspase 3/7 activation. 153

4.10. OPCML R65L loses the OPCML function in migration by impairing the OPCML-FGFR1 interaction and as consequence, the phosphorylation of downstream AKT……. 157

4.11. OPCML mutants in domain I behave like OPCML wild type in suppressing cell proliferation……..... 161

4.12. OPCML mutants reveal loss of function in anchorage-independent cellular growth……. 163

4.13. OPCML mutants show loss of suppressive function on cellular migration in ovarian cancer *in vitro*..... 170

4.14. OPCML mutants block OPCML function in invasion in ovarian cancer in vitro……. 173

4.15. OPCML mutants in domain I alter OPCML -regulated adherence to extracellular matrix components. 176

4.16. OPCML mutants impair the inhibitory interaction of OPCML with many RTKs…….. 181

4.16.1. OPCML mutants lose of OPCML's activity on the EGFR family downstream signalling. 183

4.16.2. OPCML mutants block the inhibitory function on H-RYK downstream signalling……. 188

4.16.3. OPCML mutants impair OPCML inhibitory effect on IGFIR downstream signalling……. 192

4.17. OPCML mutants do not exhibit anti-tumorigenic properties *in vivo.* 196

4.18. Summary and key findings 201

5. CHAPTER 5 202

Introduction 203

5.1. Identification of OPCML mutations in domain II using the public datasets TCGA and COSMIC and mapping them onto the OPCML crystal structure 204

5.2. Creation and characterisation of mutants in stable ovarian cancer cell lines . 209

5.3. OPCML mutants in domain II block the OPCML function in ovarian cancer cell proliferation in vitro. 212

5.4. OPCML mutants in domain II are loss of function in anchorage-independent cellular growth assays. 214

5.5. OPCML mutants block the function of OPCML in cellular migration and invasion assays 217

5.6. OPCML mutants block the OPCML adherence to extracellular matrix components.… 220

5.7. Summary and key findings 225

6. CHAPTER 6 226

Introduction 227

6.1. Identification of OPCML mutations in domain III using the public datasets TCGA and COSMIC and mapping them onto the OPCML crystal structure 228

6.2. Creation and characterisation of stable ovarian cancer cell lines expressing OPCML domain III mutants. 232

6.3. OPCML mutants in domain III lose their function on proliferation in vitro in ovarian cancer cells. 235

6.4. OPCML mutants in domain III reveal loss of function in the regulation of anchorage-independent cellular growth. 237

6.5. OPCML mutants abolish their function in cellular migration and invasion in ovarian cancer cells *in vitro*. 240

6.6. OPCML mutants block its function toward adherence to extracellular matrix components…. 243

6.7. Summary and key findings 248

7. CHAPTER 7 249

General Discussion 249

7.1. OPCML mutants disrupt OPCML-AXL interaction and thus abolish the inhibitory effect on the downstream signalling and on migration, invasion, and targeted therapy resistance in ovarian cancer cells. 251

7.2. OPCML mutants show different disruption of the interaction with FGFR1. . 253

7.3. OPCML mutant block the inhibitory effect of OPCML on phenotypic properties of ovarian cancer. 254

7.4. The mutants attenuate the OPCML's interaction with the spectrum of receptor tyrosine kinases. 261

7.5. Conclusion 265

7.6. Recommendation for further research 267

7.6.1. Further elucidate the role of OPCML in ovarian cancer metastasis. 267

7.6.2. Explore the role of the discoidin domain receptor family in a cell line expressing OPCML in cell adhesion. 267

7.6.3. Role of OPCML in cartilage regeneration and osteoporosis 268

7.6.4. Role of OPCML dysregulation in other tumours and asthma 268

8. CHAPTER 8 270

References 271

9. CHAPTER 9 316

LIST OF TABLES

TABLE 1.1 RISK AND PROTECTIVE FACTORS FOR THE DEVELOPMENT OF OVARIAN CANCER. 39

TABLE 1.2 FIGO OF OVARIAN, FALLOPIAN TUBE, AND PERITONEAL CANCER STAGING SYSTEM. 45

TABLE 1.3 EXPRESSION OF ERBB RECEPTORS IN HUMAN CARCINOMAS..... 57

TABLE 2.1 CELL LINES, MEDIUM, AND SUPPLEMENTS USED IN THIS STUDY. 82

TABLE 2.2 MUTATED PRIMERS USED IN SITE-DIRECTED MUTAGENESIS TO CONSTRUCT OPCML MUTANTS. 84

TABLE 2.3 OPCML MUTATIONS USED IN THE PROJECT MAPPED IN THE OPCML SEQUENCE. 88

TABLE 2.4 SITE-DIRECTED MUTAGENESIS PCR CYCLING CONDITIONS. 90

TABLE 2.5 LIST OF PRIMARY ANTIBODIES USED IN THE STUDY. 99

TABLE 2.6 LIST OF SECONDARY ANTIBODIES USED IN THE STUDY. 99

TABLE 4.1 PHOSPHOPROTEIN SCREENING ARRAY RESULTS FOR OPCML MUTANTS, OPCML WILD–TYPE AND CONTROL IN OVARIAN CANCER. 182

TABLE 9.3 SUMMARY OF THE NUMBER OF OPCML SNPS FROM GENOME-WIDE ASSOCIATION STUDIES. 323

LIST OF FIGURES

FIGURE 1.1 CANCER INCIDENCE AND MORTALITY IN 2012. 25

FIGURE 1.2 OVARIAN CANCER INCIDENCE AND MORTALITY OBSERVED IN 2012 AND EXPECTED IN 2035. 27

FIGURE 1.3 ANATOMY AND BIOLOGY OF THE FEMALE REPRODUCTIVE SYSTEM. 32

FIGURE 1.4 TYPES OF OVARIAN CANCER. 41

FIGURE 1.5 SCHEMATIC REPRESENTATION OF RECEPTOR TYROSINE KINASE FAMILY. 54

FIGURE 1.6 SCHEMATIC VIEW OF THE IGLON FAMILY PROTEINS. 66

FIGURE 1.7 OPCML HAS FUNCTIONAL FEATURES OF A TUMOUR SUPPRESSOR GENE IN VITRO AND IN VIVO. 73

FIGURE 1.8 OPCML ASSOCIATE AND DOWNREGULATE RECEPTOR TYROSINE KINASES. 75

FIGURE 2.1 MAP OF PENTR4, AND PLENTI VECTORS. 94

FIGURE 2.2 THE GATEWAY® LR CLONASE® II ENZYME MIX. 95

FIGURE 3.1 OPCML IS MUTATED IN DIFFERENT TUMOUR TYPES ACCORDING TO THE TCGA AND COSMIC DATABASE. 117

FIGURE 3.2 CRYSTAL STRUCTURE OF THE OPCML HOMODIMER. 119

FIGURE 3.3 THE PRIMARY AND SECONDARY STRUCTURE OF OPCML. 121

FIGURE 3.4 MUTATIONAL ANALYSIS OF OPCML. 123

FIGURE 4.1 CRYSTAL STRUCTURE OF OPCML WITH DOMAIN I MUTATIONS MAPPED. 132

FIGURE 4.2 OPCML MUTANTS IN DOMAIN I EXPRESSED IN OVARIAN CANCER CELL LINES. 135

FIGURE 4.3 OPCML MUTANTS LOCALISED TO THE CELL MEMBRANE IN OVARIAN CANCER CELL LINES. 137

FIGURE 4.4 OPCML WILD-TYPE AND OPCML MUTANTS RESIDE IN THE LIPID RAFT IN SKOV3 OVARIAN CANCER CELL LINE. 140

FIGURE 4.5 AXL INTERACTS WITH OPCML WILD-TYPE AND MUTANTS. 142

FIGURE 4.6 OPCML MUTANTS DISRUPT THE INTERACTION WITH AXL UPON STIMULATION WITH THE AXL LIGAND GAS6 OVER TIME. 145

FIGURE 4.7 OPCML MUTANTS DO NOT INHIBIT GAS6/AXL DOWNSTREAM SIGNALLING. 148

FIGURE 4.8 OPCML MUTANTS DO NOT ALTER CELL MIGRATION AND INVASION UPON GAS6 STIMULATION COMPARED TO INHIBITION BY WILD-TYPE OPCML. 152

FIGURE 4.9 OPCML MUTANTS IMPAIR THE SENSITISATION EFFECT OF OPCML TO AXL INHIBITOR R428 BY ALTERING CASPASE 3/7 ACTIVATION. 156
FIGURE 4.10 OPCML R65L LOSES THE OPCML FUNCTION IN MIGRATION BY IMPAIRING THE OPCML-FGFR1 INTERACTION AND AS CONSEQUENCE, THE PHOSPHORYLATION OF DOWNSTREAM AKT. 160
FIGURE 4.11 OPCML MUTANTS IN DOMAIN I BEHAVE LIKE OPCML WILD TYPE IN SUPPRESSING CELL PROLIFERATION. 162
FIGURE 4.12.1 OPCML MUTANTS REVEAL LOSS OF FUNCTION IN ANCHORAGE-INDEPENDENT CELLULAR GROWTH IN OVARIAN CANCER CELL LINE SKOV3. 165
FIGURE 4.13 OPCML MUTANTS SHOW LOSS OF SUPPRESSIVE FUNCTION ON CELLULAR MIGRATION IN OVARIAN CANCER IN VITRO. 172
FIGURE 4.14 OPCML MUTANTS BLOCK OPCML FUNCTION IN INVASION IN OVARIAN CANCER IN VITRO. 175
FIGURE 4.15 OPCML MUTANTS IN DOMAIN I ALTER OPCML-REGULATED ADHERENCE TO EXTRACELLULAR MATRIX COMPONENTS. 180
FIGURE 4.16.1 OPCML MUTANTS LOSE OPCML'S ACTIVITY ON THE EGFR FAMILY DOWNSTREAM SIGNALLING. 187
FIGURE 4.17 OPCML MUTANTS DO NOT EXHIBIT ANTI-TUMORIGENIC PROPERTIES IN VIVO. 200
FIGURE 5.1 CRYSTAL STRUCTURE OF OPCML WITH DOMAIN II MUTATIONS MAPPED. 208
FIGURE 5.2 OPCML MUTANTS IN DOMAIN II BEHAVE LIKE OPCML IN EXPRESSION AND LOCALISATION ON THE CELL MEMBRANE IN SKOV3 CELLS. 211
FIGURE 5.3 MUTANTS IN DOMAIN II BLOCK OPCML FUNCTION IN PROLIFERATION OVARIAN CANCER CELLS IN VITRO. 213
FIGURE 5.4 OPCML MUTANTS IN DOMAIN II ARE LOSS OF FUNCTION IN ANCHORAGE-INDEPENDENT CELLULAR GROWTH ASSAYS. 216
FIGURE 5.5 OPCML MUTANTS BLOCK THE FUNCTION OF OPCML IN CELLULAR MIGRATION AND INVASION ASSAYS. 219
FIGURE 5.6 OPCML MUTANTS BLOCK THE OPCML ADHERENCE TO EXTRACELLULAR MATRIX COMPONENTS. 224
FIGURE 6.1 CRYSTAL STRUCTURE OF OPCML WITH DOMAIN III MUTATIONS MAPPED. 231

FIGURE 6.2 OPCML WITH MUTATIONS IN DOMAIN III BEHAVES LIKE WILD-TYPE OPCML IN EXPRESSION AND LOCALISATION ON THE CELL MEMBRANE IN AN OVARIAN CANCER CELL LINE. 234
FIGURE 6.3 OPCML MUTANTS IN DOMAIN III LOSE THEIR FUNCTION ON PROLIFERATION IN VITRO IN OVARIAN CANCER CELLS. 236
FIGURE 6.4 OPCML MUTANTS IN DOMAIN III REVEAL A LOSS OF FUNCTION IN THE REGULATION OF ANCHORAGE-INDEPENDENT CELLULAR GROWTH 239
FIGURE 6.5 OPCML MUTANTS ABOLISH THEIR FUNCTION IN CELLULAR MIGRATION AND INVASION IN OVARIAN CANCER CELLS IN VITRO. 242
FIGURE 6.6 OPCML MUTANTS BLOCK ITS FUNCTION TOWARD ADHERENCE TO EXTRACELLULAR MATRIX COMPONENTS. 247
FIGURE 9.1 SEQUENCING TRACES OF THE OPCML MUTANTS AND OPCML WILD-TYPE PLASMIDS. 321
FIGURE 9.2 RNA-SEQ DATA FROM TCGA SHOWING OPCML WILD-TYPE AND MUTANTS MRNA EXPRESSION IN DIFFERENT CANCERS. 322

LIST OF ABBREVIATION

AKT	Akt murine thymoma viral oncogene homolog
AXL	Greek word *anexelekto*, which means “uncontrolled”
BCA	Bicinchoninic acid
BRCA1	Breast cancer type 1
BRCA2	Breast cancer type 2
BSA	Bovine Serum Albumin
CAM	Chick embryo chorioallantoic membrane
Co-IP	Co-Immunoprecipitation
COSMIC	Catalogue of Somatic Mutations in Cancer
DMSO	Dimethyl sulphoxide
DSM	Detergent Soluble Membrane
DRM	Detergent-Resistant Membrane
EDTA	Ethylenediaminetetraacetic Acid
EGFR	Epidermal Growth Factor Receptor1
EMT	Epithelial-Mesenchymal Transition
EOC	Epithelial Ovarian Cancer
EphA2	Erythropoietin-producing hepatocellular receptor A2
ERK1/2	Extracellular Signal‐Regulated Kinase 1 and 2
FACS	Fluorescence Activated Cell Sorting
FBS	Foetal Bovine Serum
FGFR	Fibroblast Growth Factor Receptor
FIGO	International Federation of Gynaecology and Obstetrics
GAPDH	Glyceraldehyde 3-phosphate Dehydrogenase
GPI	Glycosylphosphatidylinositol
HER2	Human Epidermal growth factor Receptor 2

HER3	Human Epidermal growth factor Receptor 3
HER4	Human Epidermal growth factor Receptor 4
HGSOC	High-Grade Serous Ovarian Cancer
HNT	Neurotrimin
H-RYK	The related to receptor tyrosine kinase
IGFR1	Insulin-like growth factor type 1 receptor
IHC	Immunohistochemistry
Ig	Immunoglobulin
IgLON	Immunoglobulin of LSAMP, OBCAM/OPCML, and Neurotrimin
LOH	Loss-Of-Heterozygosity
LGSOC	Low-Grade Serous Ovarian Cancer
LSAMP	Limbic System-Associated Membrane
MAPK	Mitogen-Activated Protein Kinase
mTOR	Mammalian target of rapamycin
OPCML	Opioid binding Protein/ Cell Adhesion Molecule-Like
OSE	Ovarian Surface Epithelium
PBS	Phosphate Buffered Saline
PCR	Polymerase Chain Reaction
PFA	Para-formaldehyde
PI3K	PhosphoInositide3 Kinase
RTKs	Receptor Tyrosine Kinase
SDS PAGE	Sodium Dodecyl Sulphate – Polyacrylamide gel electrophoresis
STIC	Serous Tubal Intraepithelial Carcinoma
TCGA	Cancer Genome Atlas
WHO	World Health Organisation

ACKNOWLEDGEMENTS

I would first of all express my sincerest and deepest gratitude and thanks Prof. Hani Gabra and Dr Chiara Recchi for giving me the opportunity to do a PhD at Imperial College, their guidance and encouragement throughout the PhD. Without their support, infinite wisdom and constant feedback, this PhD would not have been achievable.

I would also like to thank Elisa Zanini, she gave me countless suggestions on my project. Her vision and passion for research impacted me a lot.

I would like to thank my sponsor King Abdulaziz City for Science and Technology (KACST) and thank extended to the Saudi Ministry of Education for financial support throughout my PhD. I would also like to thank the Saudi Arabian Cultural Bureau for its support.

I would like to thank everyone in the Gabra Lab, both past and present members. I would also like to thank Andrew, Elena, Jane, Evdoxia, Zoe, Aline, Eloise, Haonan, Youngrock, Tommy, Stephan.

Also thank other members in the 4th floor IRDB and others area in Imperial College London Elaina, Manuela, Phil, Joel, Joel Abraham. Thanks to everyone else who has made this possible. It has not always been an easy journey.

I would like also to thank my friends Ali Alkhoushiban, Bader Al-awwad, Saad Al-shahrani, Hadi Al-asmari, Sami Al-yahya, Fahad Al-hoshani for their support and suggestion throughout my PhD journey. I would like to express my deep thank to my family father and Mother Nasser, and Norah for their support and love through my life and my brothers and sisters Ali, Turki, Nawal, Badriah, Asma, Ebtisam and Hind for their loving and supportive. My small

family thank for my wife Nada and my children Abdulaziz and Wateen for their support and thank you so much for your love.

1. Introduction

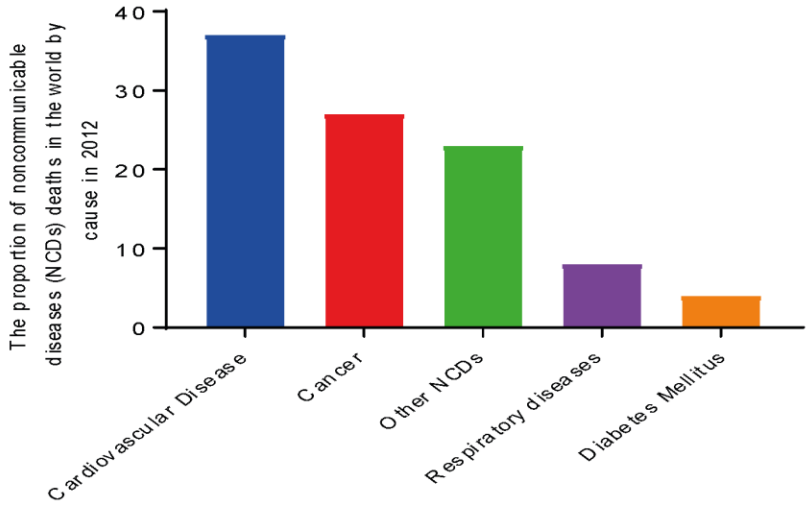
1.1. Cancer

Cancer is considered a major public health problem, although advances have been made over the last century in the prevention, treatment and understanding of the molecular biology of this disease. However, the fundamental mechanisms responsible for the development of cancer remain elusive due to many reasons, including the lack of technology and models, and the complexity of genetic and environmental interactions that may be involved (Ma & Yu, 2006; American Cancer Society, 2015).

Globally, cancer is the second leading cause of death after cardiovascular diseases from the category of non-communicable diseases (these diseases include cardiovascular disease, cancer, mental illness, chronic respiratory disease, and diabetes mellitus; see Figure 1.1 A). In 2012, the International Agency for Research on Cancer estimated cancer incidence at 14.1 million and mortality at 8.2 million worldwide (Figure 1.1 B). By 2030, around the globe, it is predicted that there will be a sharp increase in new cancer cases (21.7 million) and 13 million cancer deaths due to steadily ageing populations (Ferlay et al., 2013; American Cancer Society, 2015).

Financially, cancer is a huge burden on governments, society, patients and their families. Worldwide, in 2008, the economic consequences of cancer cost $895 (£688) billion dollars. This figure excludes the cost of cancer treatment (John & Ross, 2010).

A


The proportion of noncommunicable diseases (NCDs) deaths in the world by cause in 2012
40
30
20
10
0
Cardiovascular Disease
Cancer
Other NCDs
Respiratory diseases
Diabetes Mellitus

B

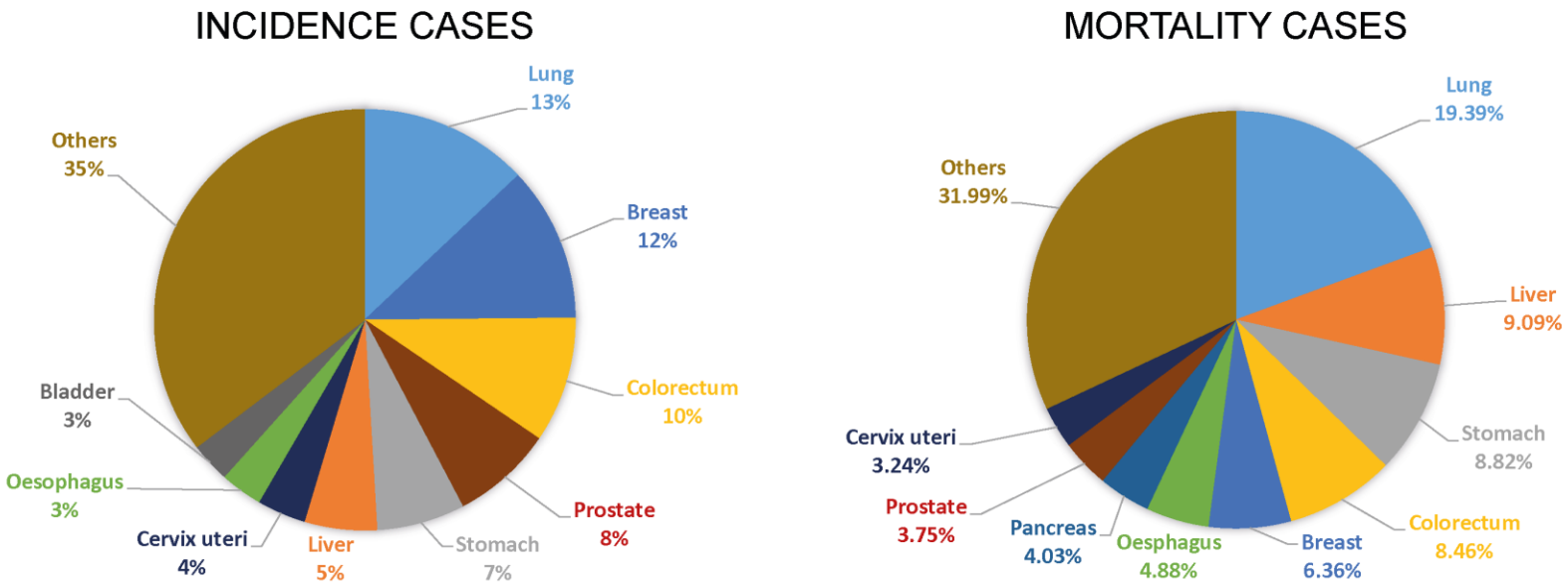

INCIDENCE CASES
Lung 13%
Breast 12%
Colorectum 10%
Prostate 8%
Stomach 7%
Liver 5%
Cervix uteri 4%
Oesophagus 3%
Bladder 3%
Others 35%
MORTALITY CASES
Lung 19.39%
Liver 9.09%
Stomach 8.82%
Colorectum 8.46%
Breast 6.36%
Oesphagus 4.88%
Pancreas 4.03%
Prostate 3.75%
Cervix uteri 3.24%
Others 31.99%

Figure 1.1 Cancer incidence and mortality in 2012.

A. The proportion of non-communicable diseases (NCDs) deaths in the world by cause in 2012 (WHO F. , 2014).

B. Estimated number of incidence and mortality cases in the top 10 cancer types, both sex, in 2012 (Ferlay et al., 2013).

Nationally, in the United Kingdom cancer is the second cause of death after cardiovascular diseases (31%, 29% respectively) (WHO, 2014).

In spite of the advances in the diagnosis, prevention and treatment of cancer, the incidence and the mortality in the United Kingdom are sadly still increasing. The recent projections show that the current cancer incidence is expected to rise in 2035 by 32.6% for males and 26.7% for females, while the mortality is expected to grow by 26% for males and 19.7% for females (Maddams et al., 2012; Smittenaar et al., 2016).

1.2. Ovarian cancer

The outlook for ovarian cancer, the most deadly of the gynaecological malignancies, has not changed in the last century despite an increase in cancer awareness (including increased public education and sentience), initial detection, genetic testing and substantial improvements in advanced therapies.

1.2.1. Epidemiology

Globally, in 2015, an estimated 251,000 women were diagnosed with ovarian cancer and 161,000 died from the disease (Ferlay et al., 2013; Fitzmaurice, 2015; Smittenaar et al., 2016). In the United Kingdom, ovarian cancer is the fifth leading cause of cancer death in women and represented roughly 5% of all female deaths in 2014 (Smittenaar et al., 2016). The ovarian cancer incidence in the United Kingdom in 2012 was 6,692 cases, and the mortality was of 4,040 cases (Ferlay et al., 2013; Smittenaar et al., 2016). The projection of ovarian cancer in 2035 shows a sharp increase in the

incidence with 8,485 women diagnosed with ovarian cancer, around a 27% increase compared to the 2012 cases. The projected mortality figures for 2035 show a 36% increase with approximately 5,493 women who will have died due to ovarian cancer, as shown in Figure 1.2 (Ferlay et al., 2013; Smittenaar et al., 2016). The five-year relative survival rate in Europe, based on figures from the Eurocare-4 database (Berino et al., 2009), is 36.5%; more recent figures for the United Kingdom show it at 42.9% (Office for National Statistics, 2011).

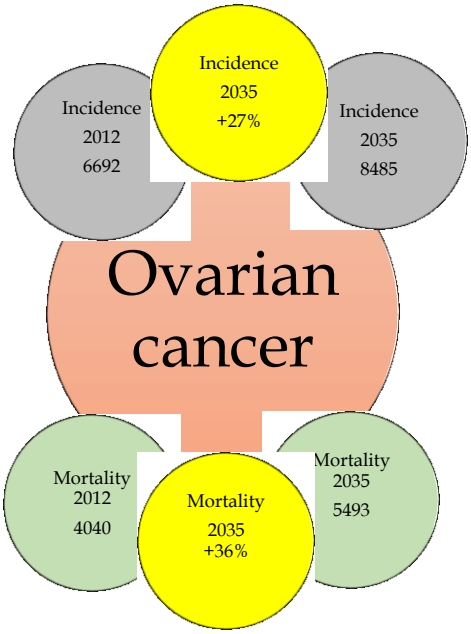


Figure 1.2 Ovarian cancer incidence and mortality observed in 2012 and expected in 2035.

The figure shows the proportion of total ovarian cancer incidence and mortality cases in 2012 (observed) and 2035 (projected), adapted and modified from (Ferlay et al., 2013).

1.2.2. **Anatomy and biology of ovarian cancer**

The female reproductive organs are composed of two parts: internal and external organs. The internal organs comprise the vagina, cervix, uterus, fallopian tube and ovary (Figure 1.3 A), while the external organs are composed of the perineum and the vulva (Ramírez-González et al., 2016).

The fallopian tube connects the ovary to the uterus and plays an important role in the transport of sperm and oocytes, sperm storage and in early embryogenesis (Lyons et al., 2006) .The fallopian tube wall consists of three different types of layers, the outer serosal layer, the intermediate muscular layer (myosalpinx), and the internal mucosa layer (endosalpinx) (Ezzati et al., 2014).

The internal mucosal layer of the fallopian tube is covered with a single epithelium layer composed of three different cell types: non-ciliated secretory cells, ciliated cells, and peg cells (Lyons et al., 2006). The non –ciliated secretory cells play an essential role in the capacitation of spermatozoa by secreting a fluid that contains nutrients that are nourishing and protective for oocytes (Ezzati et al., 2014). The ciliated cells are found in substantial amounts compared to the other cell types in the fallopian tube and they play an important role in the transport of oocytes and sperms. The third type of cells (non-ciliated Peg cells) are known as resting secretory cells (or intercalated cells) and are thought to represent a quiescent maturational stage of secretory cells(non-functional) (Blaustein and Kurman, 2002).

The ovary consists of two parts: a surface outer layer and an internal part. The surface layer is composed of a simple cuboidal epithelium, called germinal epithelium (it is worth noting that this kind of specialised cells can withstand more trauma and play a

significant role in diffusion and secretion). The inside of the ovary is divided into a further two components: the outer part is known as the cortex (which encompasses the ovarian follicles), and the inner part is known as the medulla (which includes the neurovascular structure) (Clement, 1987; Auersperg et al., 2001).

Each woman holds two ovaries; these ovaries are each about three cm in length and play two important roles:

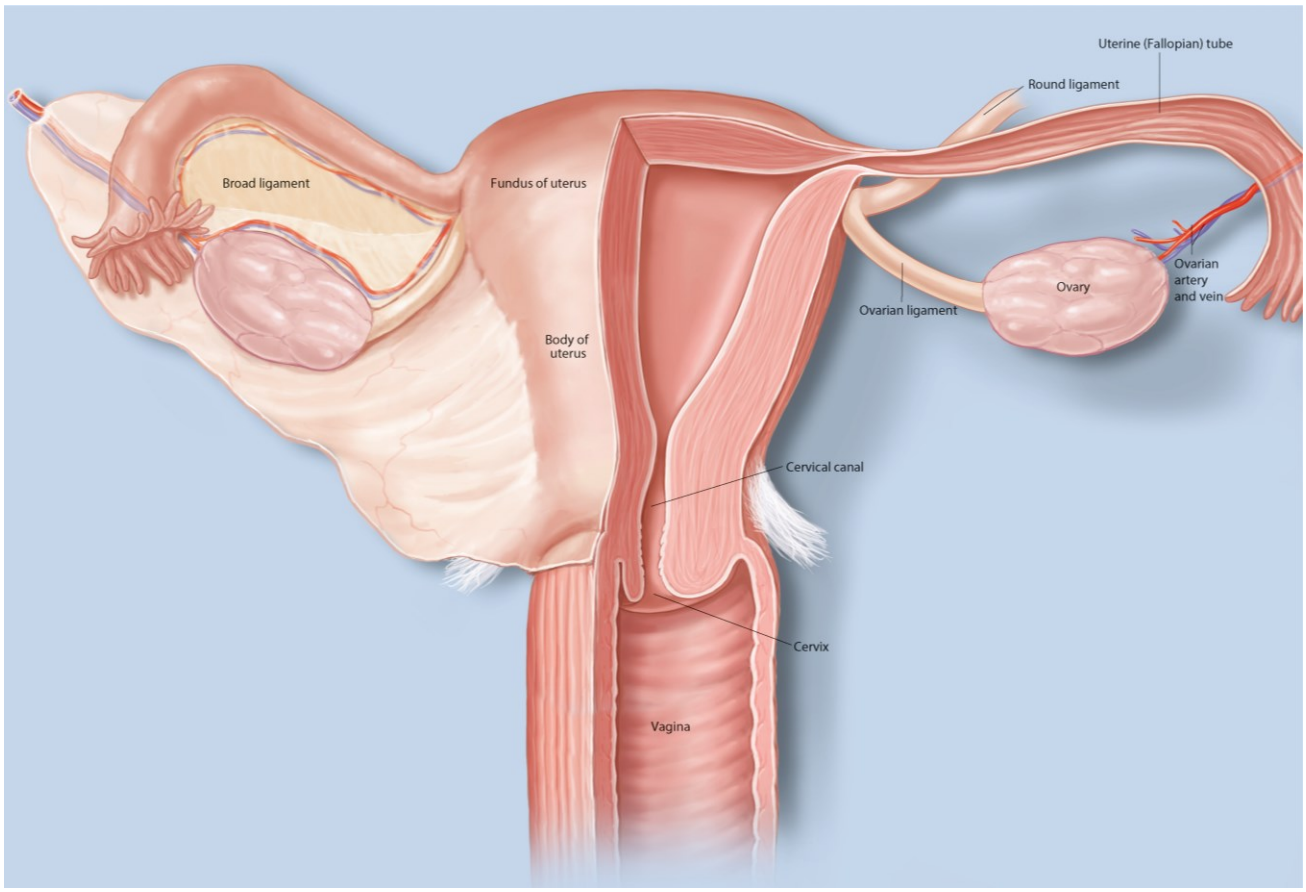
1) The oogenesis.
2) They produce oestrogen and progesterone hormones (Knudtson & Mclaughlin, 2013; Drake et al., 2015).

Anatomically, each ovary is held in place by three types of ligaments: the mesovarium, which is part of the broad ligament (the thin layer of peritoneum associated also to the fallopian tube and the uterus); the ovarian ligament, which connects the side of the uterus to the ovary; and the suspensory ligament, which connects the ovary to the abdominal wall and holds the ovarian artery, vein, nerve plexus and lymphatic vessels (Knudtson & Mclaughlin, 2013; Drake et al., 2015).

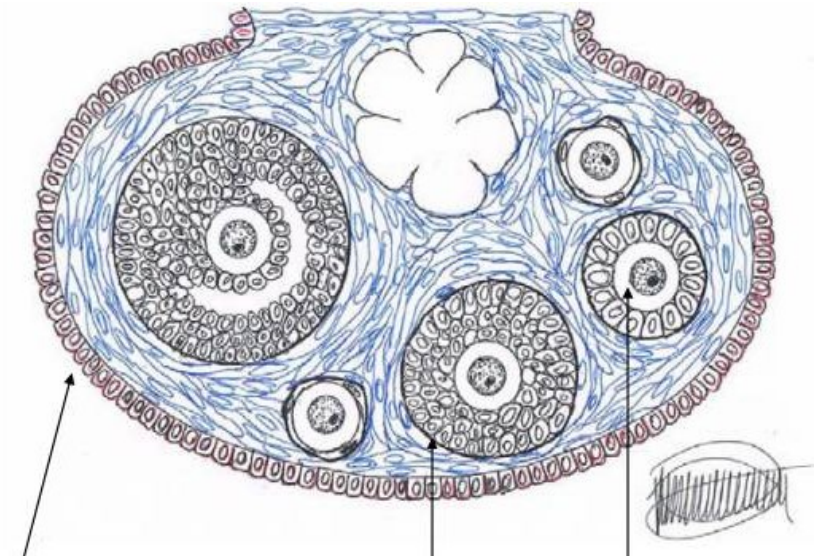
The ovary primarily contains three different cell types – namely, the surface epithelium cells covering each ovary (90%), the sex cord-stromal cells (7%) that mainly form the inner ovarian structure, and the germ cells within the follicles (3%) (Figure 1.3 B). Ovarian cancer is believed to be able to originate from all three cell types (Chen et al., 2003; Romero & Bast, 2012). Epithelial ovarian cancer accounts for approximately 90% of ovarian cancers, and it is considered rare among young women and more common in postmenopausal women (Berek & Bast, 2003; Romero & Bast, 2012).

Sex cord stromal tumours are more common in young women but can occur at any age. They generally represent 7% of all ovarian cancer cases and have a good prognosis (Soslow, 2008; Romero & Bast, 2012). Germ cell tumours, such as sex cord cells, more frequently occur in young women and ascend from the germ cells that form the oocyte. This type of a tumour represents approximately 3% of ovarian cancer cases and has a good prognosis (Soslow, 2008; Romero & Bast, 2012).

A



B



Surface epithelium (90%) Sex cord -stroma (7%) Germ cell (3%)

Figure 1.3 Anatomy and biology of the female reproductive system.

A) Anatomy of a female reproductive system illustrating the internal organs: vagina, cervix, uterus, fallopian tube, ovary, and the ligament connected to the ovary (Anatomical chart company, 2008) .

B) Different ovarian cell types can give rise to different ovarian cancers (Romero & Bast, 2012) .

1.2.3. **Risk factors**

The leading causes of ovarian cancer are still elusive, although several risk factors may contribute to causing ovarian cancer. They include environmental factors, genetic susceptibility, and medical factors.

Some factors seem to promote ovarian cancer such as age, family history of cancer, mutations in p53 and RB, BRCA mutations, fertility drugs, hormonal replacement therapy, smoking, obesity, talcum powder and asbestos.

On the other hand, some factors would be protective from ovarian cancer such as multiparty, breastfeeding, oral contraceptives, tubal ligation and hysterectomy, and salpingo-oophorectomy.

The factors that increase or protect against the risk of ovarian cancer are illustrated in table 1.1.

1.2.3.1. Age

Ovarian cancer risk shows a strong correlation with older age. Ovarian cancer develops in all age groups, although its occurrence is rare in women younger than 40 years. It develops more frequently after menopause and in women older than 63 years old (Edmondson & Monaghan, 2001; McLemore et al., 2010; American Cancer Society, 2015; UK Cancer Research, 2017).

1.2.3.2. Genetic risk factors

Genetic risks include a family history of cancer (such as ovarian and breast cancers, human hereditary non-polyposis colorectal carcinoma) and other syndromes (including the PTEN hamartoma tumour syndrome) (Boyd & Rubin, 1997; Sansal & Sellers, 2004).

About 3% of ovarian cancer cases occur in women with a genetic family history of ovarian, breast or colorectal cancers (Granström, Sundquist, & Hemminki, 2008). The risk increases by 2.7 to 3.5 times in women whose direct relatives had ovarian cancer (Granström, Sundquist, & Hemminki, 2008; Hemminki, Sundquist, & Brandt, 2011; Jervis et al., 2014; Webb & Jordan, 2017). Almost 90% of the family history cases are attributed to mutations in BRCA1 and BRAC2 genes, while the last 10% is attributed to hereditary human non-polyposis colorectal carcinoma (lynch syndrome) and other syndromes (Doufekas & Olaitan, 2014).

Other genetic factors are mutations in p53 and RB. The tumour suppressor protein 53 (p53) is encoded by the *TP53* gene and is also broadly mutated in high-grade serous ovarian carcinomas (Ahmed et al., 2010) and in approximately 50% of human cancers

(Soussi et al., 2006). The Retinoblastoma 1 (RB) gene encodes for RB, a tumour suppressor protein, and is found mutated in approximately 50% of epithelial ovarian cancers (Hashiguchi et al., 2001; Corney et al., 2008).

1.2.3.3. Reproductive factors

1.2.3.3.1. Pregnancy (Multiparty)

Pregnancy (multiparty) is thought to reduce the risk of ovarian cancer following the assumption that incessant ovulation and an increase in the release of pituitary gonadotropin are increasing risk factors for ovarian cancer (Rostgaard et al., 2003; Pike et al., 2004).

Incessant ovulation, in fact, sees the constant damaging and repair of the epithelial surface. During pregnancy, ovulation stops and the trauma to the surface of the ovary is decreased. The release of pituitary gonadotropin stimulates the release of the follicle-stimulating hormone (FSH), which, in turn, stimulates the maturation of the ovarian follicle and the production of oestrogen and the luteinizing hormone (LH), causing ovulation and hence increasing the risk of ovarian cancer (Pike et al., 2004). During pregnancy, the pituitary gonadotropin is inhibited, decreasing the risk of ovarian cancer.

1.2.3.3.2. Breastfeeding

Studies have shown that breastfeeding reduces the risk of ovarian cancer irrespective of the number of births (Jordan et al., 2012; Luan et al., 2013). As ovulation and the production of gonadotropin are suppressed during breastfeeding, as a consequence the risk of ovarian cancer is also reduced (Risch, 1998).

1.2.3.4. Fertility drugs

Some studies on using fertility drugs such as clomiphene citrate (Clomid, which was approved in 1967 to treat primary infertility) for more than one year show an increase in the risk of ovarian cancer, with a higher prevalence of the low malignant potential type of ovarian cancer (borderline epithelial ovarian cancer). As the gonadotropin theory explained above suggests, exposure of the ovaries to excessive exogenous gonadotropins is believed to be carcinogenic (Diergaarde & Kurta, 2014).

1.2.3.5. Menstrual cycle

Several studies failed to show a significant correlation between early menarche or late menopause and ovarian cancer. One study showed an insignificant reduction in ovarian cancer risk in women who started their menarche at 12 years old, compared to women who were younger than 12 years. As a consequence, early menarche is unlikely to be a major factor in ovarian cancer pathogenesis (Whittemore et al., 1992; Hankinson et al., 1995; Doufekas & Olaitan, 2014).

1.2.3.6. Exogenous hormones

1.2.3.6.1. The oral contraceptive pill

Oral contraceptives are the most widely used drugs worldwide and are associated with an almost 30% reduction in ovarian cancer (Beral et al., 2008; Doufekas & Olaitan, 2014). The effect of oral contraceptive pills persists up to 10 years after 5 years of use, and an even greater reduction of ovarian cancer risk is associated with a longer use of the oral contraceptive pill (Beral et al., 2008; Doufekas & Olaitan, 2014).

1.2.3.6.2. Hormonal replacement therapy

Recent studies show that using hormonal replacement therapy for menopause is associated with an increase in the risk of ovarian cancer by nearly 13% if used for more than 5 to 10 years (Zhou et al., 2008; Beral et al., 2015).

1.2.3.7. Smoking Tobacco

Smoking contributes to increasing the risk of several cancers, including ovarian cancer.

Several studies have confirmed the relationship between tobacco use and the mucinous type of ovarian cancer, but some studies failed to confirm the relationship with the non-mucinous type of ovarian cancer (Modugno et al., 2002). Nevertheless, the risk to develop mucinous ovarian cancer returns to normal after ceasing smoking for 20–30 years (Jordan et al., 2006; McLemore et al., 2010). Smoking risk can be an exhibit by founding smoking metabolites residue in ovarian follicular cells (Modugno et al., 2002; McLemore et al., 2010).

1.2.3.8. Medical history

1.2.3.8.1. Hysterectomy and Laparoscopic sterilization

It has been suggested that hysterectomy reduces the risk of ovarian cancer and it is also used as a preventive measure for high-risk patients (McLemore et al., 2010). The potential for ovarian cancer is reduced by roughly 26–30% after tubal ligation and hysterectomy. Furthermore, hysterectomy reduces ovarian cancer risk by 50% in high-risk women (Green et al., 1997; Rice et al., 2012).

1.2.3.9. Diet and Obesity

Obesity alters sex hormone metabolism, inflammatory regulation, insulin and growth factor signalling, thus creating several metabolic and endocrine abnormalities that are associated to the risk of developing cancer (Calle & Kaaks, 2004; Renehan et al., 2015).

1.2.3.10. Talcum powder and asbestos

Talcum powder was shown in several studies to increase the risk of ovarian cancer (Harlow, Cramer, Bell, & Welch, 1992; Tzonou et al., 1993), which can also be increased by two-fold in women exposed to asbestos (McLemore et al., 2010).

Table 1.1 Risk and protective factors for the development of ovarian cancer.

The table shows the factors that increase or decrease the risk of ovarian cancer and whether the evidence is strong or weak (Whiteman et al., 2015; UK Cancer Research, 2017; Webb & Jordan, 2017).

OVARIAN CANCER	RISK FACTOR	PROTECTIVE FACTOR
SUFFICIENT OR SUBSTANTIAL EVIDENCE	• Asbestos • Hormone replacement therapy (HRT) (oestrogen-only) • Smoking (MUC) • Adult-attained height • Obesity (none-HGSC) • The family history of ovarian cancer • Endometriosis (END & CCC) • BRCA mutations	• Pregnancy • Breastfeeding • Oral contraceptive use • Hysterectomy and tubal ligation Salpingo-oophorectomy
LIMITED OR PLAUSIBLE EVIDENCE	• Talcum powder (perineal use) • X-radiation, gamma radiation • Younger age at menarche • Diabetes Mellitus • Older age at menopause	• Older age at last birth • Aspirin • Vitamin D

CCC: clear cell cancers; **END:** Endometriosis cancers; **NHGSC**: Non-high-grade serous cancers; **MUC:** mucinous cancers

1.2.4. **Types of ovarian cancer**

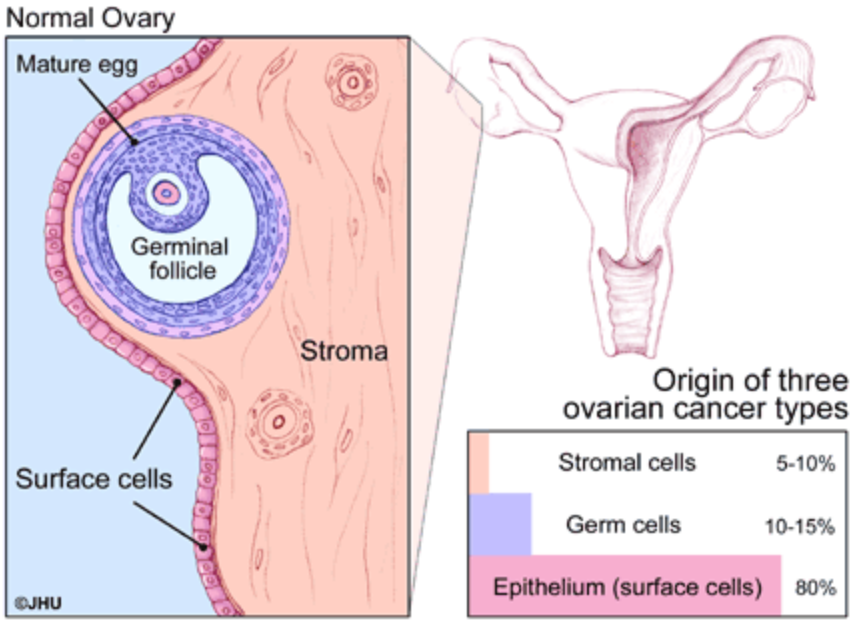
Ovarian cancer can result from any cells in the ovary, which, as mentioned before, is composed of three types of cells: epithelial, germ and sex cord-stromal cells (Figure 1.4 A).

Epithelial cells are the most common type and account for 90% of ovarian cancer (Shih & Kurman, 2004), which is further sub-classified based on histologic features into serous, mucinous, clear cell, endometrioid, squamous, transitional cell, and undifferentiated carcinomas (Kurman, 2013).

Based on clinical, pathological and molecular features, epithelial ovarian cancers can be classified into two main types. Type I epithelial tumours are composed of low-grade serous, mucinous, endometrioid, clear cell, squamous, and transitional cell carcinomas. Type I are characterised by slow-growing tumours that are mostly confined to the ovary. It accounts for 10% of ovarian cancer cases and has a good prognosis (Shih & Kurman, 2004) (Figure 1.4 B).

Type II tumours include high-grade serous carcinomas, carcinosarcomas (malignantly mixed mesodermal) and undifferentiated carcinomas. Type II is distinguished by fast-growing tumours; it is unusual for it to be confined to the ovary and it metastasises to other tissues. It constitutes the majority of ovarian cancer cases and it is the cause of most deaths (Jonathan et al., 2003; Tavassoli & Devilee, 2003; McCluggage, 2008; Kurman & Shih, 2011) (Figure 1.4 B).

A



B

	Type I	Type II
Tumour Type	- Serous - Mucinous - Endometrioid - Clear cell	- Serous carcinomas - Malignant mixed mesodermal tumours (carcinosarcoma) - Undifferentiated carcinomas
Mutations	*- KRAS* *-BRAF* *-PTEN* *-β-catenin (CTNNB1)*	*- TP53* *-BRCA mutations*
Chromosomal Instability	Steady increase	High
Confined to ovary	Yes	No

Figure 1.4 Types of ovarian cancer.

A. The figure illustrates the ovary cell types, and ovarian cancer types and their percentages of occurrence (SAMCI, 2017).

B. The table shows the Summary of Clinicopathological features of ovarian cancer Type I and Type II (Shih & Kurman, 2004).

1.2.4.1. Serous epithelial ovarian cancer

Serous is the most widespread type of epithelial ovarian cancer and accounts for almost 75% of epithelial ovarian cancers. Such tumours are formed from cells that are similar to the cells in the fallopian tube. Serous cancer is the most aggressive type of ovarian cancer and is associated with a poor five-year survival rate, mainly due to cases of high-grade serous carcinoma (Vang et al., 2009; Seidman et al., 2012). 97% of high-grade serous carcinoma is associated with mutations in TP53 (Ahmed et al., 2010), while low-grade serous carcinoma is associated with mutations in KRAS, BRAF, and ERBB2 (Singer et al., 2003; Anglesio et al., 2008).

1.2.4.2. Mucinous epithelial ovarian cancer

The mucinous type of ovarian cancer represents 10% of epithelial ovarian cancer cases, and tumours are formed from cells that resemble those of the endocervical epithelium or intestinal epithelium. Generally, this type of ovarian cancer has a good prognosis in the early stages while, in the later stages, it presents poor prognosis and platinum resistance (Harrison et al., 2008).

1.2.4.3. Endometrioid epithelial ovarian cancer

The endometrioid type of epithelial ovarian cancer is malignant and accounts for 10–20% of epithelial ovarian cancer cases. Additionally, the cells forming endometrioid carcinomas resemble the endometrium (Rosen et al., 2009). Moreover, endometrioid tumours are more frequently associated with PTEN mutations (almost 43% of the cases) (Obata et al., 1998).

1.2.4.4. Clear cell epithelial ovarian cancer

The clear cell type of epithelial ovarian cancer accounts for approximately 5% of all ovarian cancer cases. Moreover, advanced stages are associated with poor prognosis and platinum resistance, even though the tumour occurrence is relatively rare. Ovarian clear cell carcinomas occur more frequently in women with endometriosis (Rosen et al., 2009).

1.2.4.5. Transitional cell epithelial ovarian cancer

The transitional cell type of epithelial ovarian cancer is known as the Brenner tumour, and it develops from cells that look like those lining the urinary bladder. It is considered a rare tumour. Generally, patients with a transitional cell type of epithelial ovarian cancer have good prognosis depending on the stage of diagnosis and they respond well to chemotherapy (Jelovac & Armstrong, 2011).

1.2.5. **Ovarian cancer staging**

Staging of ovarian tumours reveals where a tumour is located and to what extent it has metastasised. Paradigm criteria facilitate the comparison of patients in different centres worldwide to allocate them into the right categories for precise treatments (Prat, 2015).

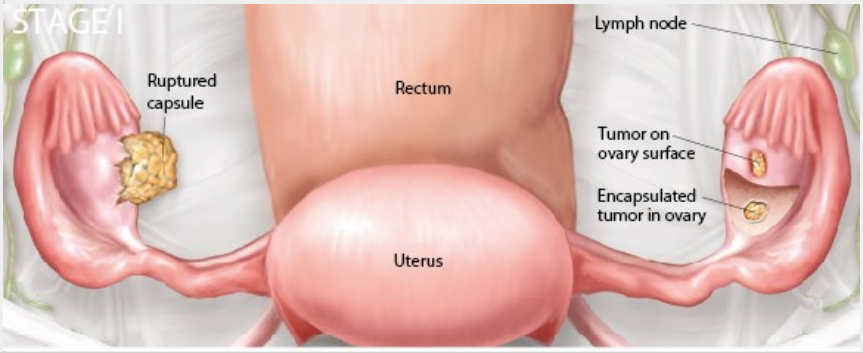
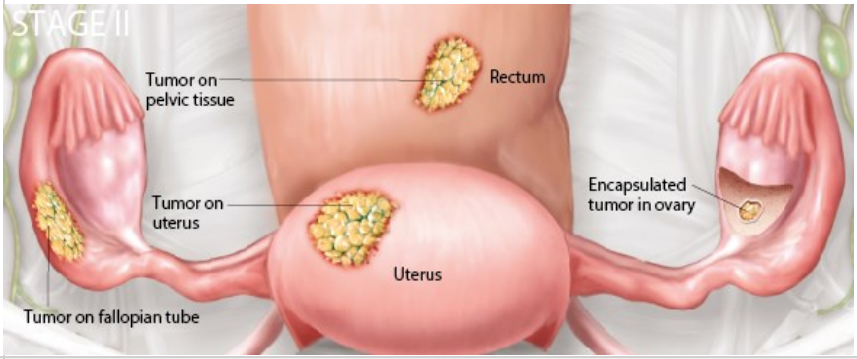
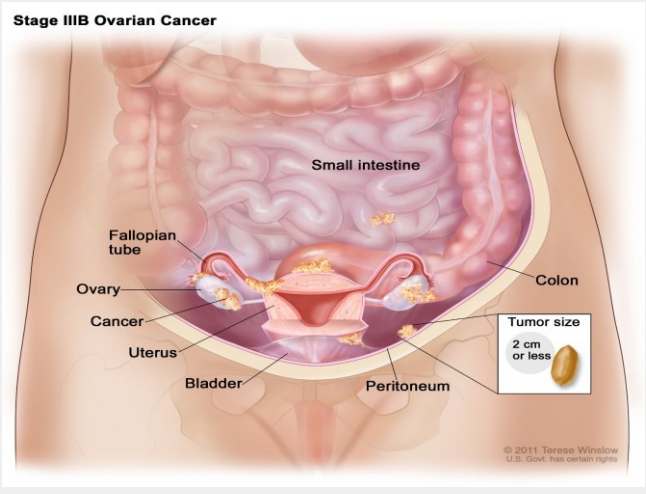
Ovarian cancers are classified according to the American Joint Committee on Cancer (AJCC) tumor-node-metastasis (TNM) staging system or the International Federation of Gynaecology and Obstetrics (FIGO) system. These systems are necessary for patient diagnosis, prognosis and treatment. The AJCC TNM system describes the extent of a primary tumour, combined with its metastasis to adjacent tissue or the lymph nodes. The FIGO system is based on surgical pathology judgement (Prat, 2014). The FIGO system is the most widely used worldwide for ovarian cancer staging.

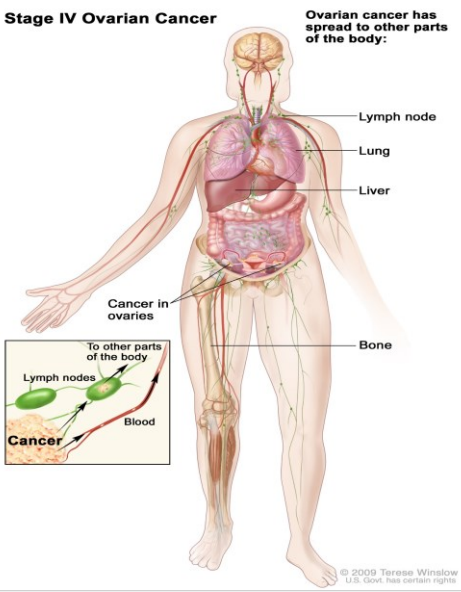
Ovarian cancer is described as a heterogeneous disease from the histopathological and morphological point of view. Ovarian cancer is staged into four stages based on the primary site and the surgical histopathological behaviour of the tumours, and the general definition of each stage is explained in Table 1.2.

The five-year survival rates based on ovarian cancer stages are as follows: stage I (93%), stage II (70%), stage III (37%), and stage IV (25%) (Holschneider & Berek, 2000). Stage I represents only 15% of cases of women with ovarian cancer. Most women are diagnosed with an advanced disease, and their five-year survival rate is currently less than 30% (Raja et al., 2012).

Table 1.2 FIGO of ovarian, fallopian tube, and peritoneal cancer staging system.

The table illustrate the staging system, definition of each stage and site of the tumour (Prat, 2014; Anatomical Chart Company, 2008; NCI, 2009).

Stage	Definition	Site of the tumour
STAGE I	Tumour confined to ovary or fallopian tube	
STAGE II	Tumour involves one ovary or both or fallopian tubes with pelvic extension or primary peritoneal cancer	
STAGE III	Tumour include one ovary or both or fallopian tubes, or primary peritoneal cancer, with histopathological, confirmed spread to the peritoneum and metastasis to the retroperitoneum lymph nodes	

STAGE IV	Distant metastasis to the other organs such as liver, lung, and brain	
Tumour size	Tumour scale representation	

1.2.6. **Grades**

The grading system defines the morphological and histological differences between tumour cells and their particular healthy tissue. Subsequently, the tumours are classified on the basis of the extent to which the cells are less differentiated.

There are four grades of ovarian cancer: grade 0 or borderline; grade I or a well-differentiated tumour (<5% solid tumour); grade II or a moderately differentiated tumour (>5% to <50% solid tumour); and grade III or a poorly differentiated tumour (>50% solid tumour) (Silverberg, 2000; Benedet et al., 2000).

1.2.7. **The origin of ovarian cancer**

Ovarian cancer is composed of multiple and heterogeneous diseases, and identifying its cellular origin in the ovary is still considered a priority.

The source of ovarian cancer has been the subject of intense debate within the scientific community. Three anatomical sites have been proposed as the main sites of origin: the surface ovarian epithelium, the mesothelium of the peritoneum, and the fallopian tubes (Kurman & Shih, 2011; Li et al., 2011).

Currently, four theories have tried to explain the origin of ovarian cancer. The first theory, the incessant ovulation theory, proposes that the mechanism that causes ovarian cancer is the exposure of susceptible ovarian surface epithelium to mutations due to damage and repair during each cycle of ovulation (Fathalla, 1971). The best evidence that supports this theory is the regular ovulation during a woman's lifecycle, which exposes the ovarian surface epithelium to the risk of repeated damage and repair. It is

also supported by the decreased risk associated with pregnancy, lactation, or the use of oral contraceptives, which all reduce the number of ovulation cycles.

The second theory, the gonadotropin theory, explains the possibility of mutations due to the promotion of cell growth during ovulation as a consequence of stimulation by gonadotropin hormones (Risch, 1998; Kulkarni & McGarry, 1989). Gonadotropin hormones are controlled and produced by the pituitary gland, which also produces Follicle-stimulating hormone (FSH). Their primary role is to stimulate follicle maturation and trigger oestrogen production from the follicle. Luteinizing hormone (LH) rises in response to the increase in oestrogen, and the shifts from FSH to LH induces the mature follicle to rupture and release the ovum. The remainder of the follicle forms the corpus luteum, which produces progesterone (which plays a primary role in sustaining pregnancy) (Fauser & Heusden, 1997; Richards & Pangas, 2010). The best evidence that supports this theory is that infertility and polycystic ovary syndrome (PCOS) increase the risk of ovarian cancer.

A third theory, the hormonal theory, postulates that excessive stimulation by androgen promotes ovarian cancer (Risch, 1998; Lukanova & Kaaks, 2005).

A fourth theory, the inflammation theory, proposes that excessive damage to the ovarian surface epithelium provokes inflammation, subsequently inducing a predisposition to mutations (Fleming et al., 2006; Yang et al., 2004). The inflammatory responses associated with cytokines and reactive oxygen species (ROS) are also linked to ovulation cycles.

As previously mentioned, the four theories above postulate different origins for ovarian cancer with three different sites. Each of these locations has its own evidence to support these theories.

The first hypothesis is that the ovarian surface epithelium is the source of ovarian cancer, which is supported by all the previous theories. However, the weakness of this argument is that it does not reveal the distinct genetic alterations observed among ovarian cancer subtypes (Karst & Drapkin, 2010).

The second hypothesis assumes that a Müllerian-derived organ (a secondary Müllerian system) is the origin of ovarian cancer, which is explained as frequent invagination in the cortical stroma forming cortical inclusion cysts (CICs) (circular structures that line the ovarian surface epithelium) and hence exposing it to hormones that are thought to induce cell differentiation (Lauchlan, 1972; Lauchlan, 1994).

The third hypothesis suggests that the fallopian tube is the origin of ovarian cancer. This has been supported by several anatomical, phenotypic and biological findings, including the fact that salpingo-oophorectomy reduces ovarian cancer risk and that serous tubal intraepithelial carcinomas (STICs) show the same mutations (germline *BRCA1* and *BRCA2*) as high-grade serous carcinoma, which are different from non-serous epithelial ovarian cancer (Tone et al., 2012).

Serous tubal intraepithelial carcinomas (STICs) are identified following fallopian tube epithelial examination in *BRCA* mutation women undergoing risk-reducing salpingo-oophorectomies (RRSO). These STICs lesions have distinct characteristic features such as an abnormal p53 expression, high-proliferative index, pleomorphic nuclei (different shape and size nuclei), loss of polarity, lack of ciliated cells, and

epithelial tufting (epithelial dysplasia) (Piek et al., 2001; Piek et al., 2003; Lee et al., 2007; Folkins et al., 2008; George and Shaw, 2014; and Lheureux et al., 2015; George, et al., 2016).

It is also supported by the fact that if only the oophorectomy is carried out, the risk of developing peritoneal high-grade serous carcinoma is increased (Piek et al., 2004). Also, several studies support the notion that fallopian tube fimbriae are the origin of sporadic high-grade serous carcinoma (HGSC) in patients without hereditary BRCA1 and BRCA2 associated breast-ovarian cancer history (Gilks et al., 2015; Morrison et al., 2015). Phenotypically evidence support the fallopian tube origin of ovarian cancer as gene expression patterns (Marquez et al., 2005), proteomic profiles (Levanon et al., 2010) and heterogeneous populations of cells (Roh et al., 2009; Banet & Kurman, 2015) in HGSC and fallopian tube epithelium share many similarities. For example, HGSC and STIC share similar P53 signature and DNA damage (Lee et al., 2007) and p53 mutations (Leonhardt et al., 2011). Also, the human HGSC gene expression and morphology resemble that of a tumour generated from transformed human fallopian tube epithelial cells (Yamamoto et al., 2016). Furthermore, the genetically modified tubal secretory mice model with *p53, Pten* and *BRCA1* or *BRCA2* mutations result in STIC and HGSC (Perets et al., 2013).

Ultimately, as the debate regarding the origin of ovarian cancer continues, it is crucial to recognise and understand its source and the mechanism of tumour progression in order to establish a more efficient approach for early detection, prevention and treatment.

1.2.8. **Diagnosis**

Women with ovarian cancer often complain of the following symptoms: permanent abdominal bloating or swelling, persistent abdominal or pelvic pain, dyspepsia, early satiety, urinary urgency, changes in bowel habits, and unusual fatigue and weight loss (Goff et al., 2007).

Currently, accurate screening of low-risk patients to detect ovarian cancer in its early stages has not been achieved yet, and the tests mostly used to follow the patient's clinical symptoms are the levels of the tumour marker cancer antigen 125 (CA-125) and transvaginal ultrasound (TVUS) (Badgwell & Bast, 2007). It is worth noting that CA-125 is used primarily to monitor ovarian cancer during treatment, and it is not approved as a population screening test. Advanced imaging is also unlikely to be used for screening patients due to costs. High-risk patients are recommended to undertake risk-reducing salpingo-oophorectomy, which includes the removal of the fallopian tube and ovaries (Berek et al., 2010; Daly et al., 2017).

The diagnosis of patients consists of a combination of the patients' history, physical examination, tumour marker CA-125, CT scan, TVUS, three-dimensional power Doppler (3DPD) ultrasound (Vrachnis et al., 2012; Daly et al., 2017).

1.2.9. **Management of ovarian cancer**

Regardless of the substantial effort made over the last years, ovarian cancer endures as the most lethal gynaecological malignancy due to late diagnosis and frequent relapse. Improving the prevention, diagnosis and treatment is an urgent need.

The gold standard treatment of ovarian cancer is cytoreductive surgery and chemotherapy containing platinum and paclitaxel. The operation includes total abdominal hysterectomy, bilateral salpingo-oophorectomy, omentectomy, and evaluation and assessment of the entire abdominal cavity by removal of any remaining deposits and biopsy examination (Raja et al., 2012; Narod, 2016).

1.3. RTKs in cancer

1.3.1. Introduction

Receptor tyrosine kinases (RTKs) play a substantial role in normal human physiology, and the deregulated expression of RTKs can lead to a wide variety of cellular aberrations such as uncontrolled cell proliferation and survival, motility, invasion, migration and chemotherapy resistance (Hanahan & Weinberg, 2000; Blume-Jensen & Hunter, 2001).

The RTK superfamily is composed of 58 members belonging to 20 different receptor families (Lemmon & Schlessinger, 2010). RTKs are transmembrane proteins containing three domains: an extracellular ligand binding domain, a transmembrane domain and an intracellular cytoplasmic tyrosine kinase domain (Figure 1.5) (Lemmon & Schlessinger, 2010). Typically, RTK activation involves two steps. Upon ligand binding, the receptor is activated, then it homo- or heterodimerises through the extracellular domain and it is autophosphorylated (either in cis within the receptor or in trans between receptors). The activated intracellular kinase domain leads to the regulation of a range of cellular functions (Rehn et al., 1998; Lemmon & Schlessinger, 2010; Hubbard & Till, 2000).

Nearly two-thirds of the RTK families have been reported to be deregulated, contributing to the development of several human cancers either by receptor overexpression, chromosomal translocation, gene amplification or mutations. As a consequence, RTKs are thought to be potential therapeutic targets for cancer therapy (Blume-Jensen & Hunter, 2001; Lemmon & Schlessinger, 2010).

Some RTK families will be described more in details below.

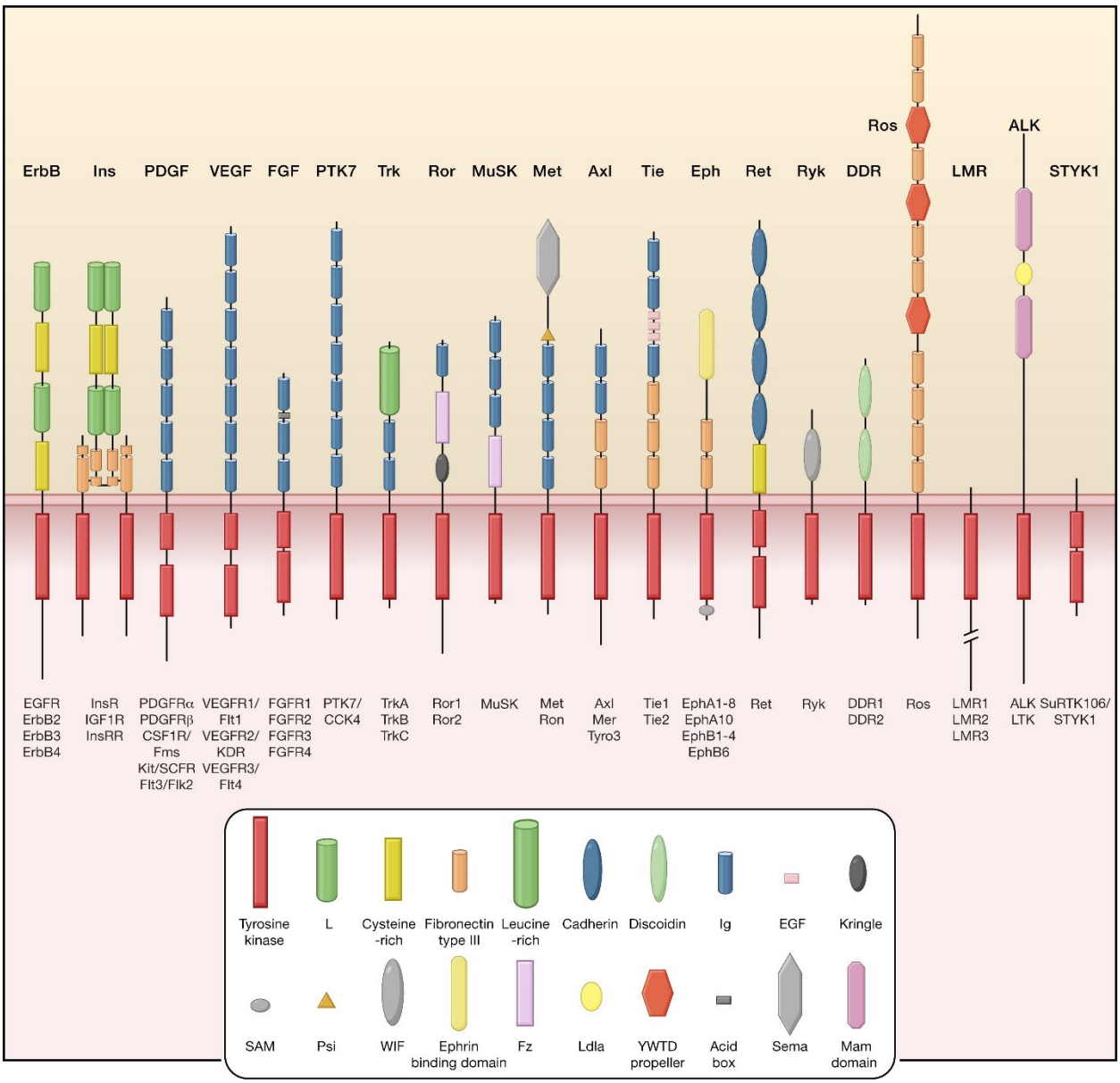


Figure 1.5 Schematic representation of receptor tyrosine kinase family.

All members of receptor tyrosine kinases share a similar molecular architecture including an extracellular domain, a single transmembrane domain, and an intracellular domain having tyrosine kinase activity.

Structure analysis is marked according to the key. The intracellular domains are shown as red squares. Adapted from (Lemmon & Schlessinger, 2010).

1.3.2 Epidermal Growth Factor Receptor (EGFR) Family

The EGFR family consists of four members: EGFR (Her1, erbB1, v-erb-b), the paradigm of the group (Ullrich & Schlessinger, 1990); HER2 (neu, erbB2) (Holbro & Hynes, 2004); HER3 (erbB3) (Citria et al., 2003); and HER4 (erbB4) (Carpenter, 2003). EGFR and HER2 were identified to be overexpressed in breast cancer, epithelial ovarian cancer and several other malignancies (Normanno et al, 2003**;** English et al., 2013; Yan et al., 2015)**.**

As mentioned previously, the EGFR family members – such as other RTKs – share high sequence and similar structures, and are composed of the extracellular ligand binding domain, the hydrophobic transmembrane domain and a cytoplasmic tyrosine kinase domain. Moreover, they are able to form homo- and heterodimers within the family with up to 28 different combinations with each other (Lemmon & Schlessinger, 2010).

EGFR is known to have seven ligands: epidermal growth factor (EGF), transforming growth factor-α (TGF-α), amphiregulin, betacellulin, epigen, epiregulin, and heparin-binding EGF-like (HB-EGF) (Yarden, 2001). There is no known ligand for HER2, and it is considered the preferred partner for all other EGFR family members because it is always in an open conformation, not needing activation. When bound to EGFR, it leads to a reduced ligand dissociation rate and increased receptor recycling (Roskoski, 2014). HER3 binds to two ligands: neuregulin (NRG) 1/heregulin (HRG) isoforms, and NRG-2α and β. HER4 binds to seven ligands: NRG-1/HRG isoforms, NRG-2α and β, NRG-3, NRG-4, tomoregulin, HB-EGF, BTC, and EP (Graus-Porta et al., 1997; Falls, 2003; Normanno et al., 2003). HER3 has an impaired tyrosine kinase domain, but it

forms one of the most potent dimers by binding to HER2 and strongly activating PI3K-AKT and ERK-MAPK pathways, leading to enhanced proliferation and the evasion of apoptosis (Guy et al., 1994; Yarden & Pines, 2012).

In normal physiology, EGFR and HER2 show moderate levels of expression in the epithelium of the ovary and undetectable levels in the ovarian stroma, whereas HER3 is absent in both tissues. HER4 has a low-level expression in the epithelium, while it is undetected in the ovarian stromal tissues (Wilken et al., 2012).

EGFR overexpression is associated with many solid malignancies, including ovarian, brain, colorectal, pancreas, oesophageal, gastric, bladder, kidney, prostate, breast, and head and neck tumours, as well as non-small cell lung carcinoma. Furthermore, EGFR is involved in chemotherapy resistance and is associated with poor prognosis (Wilken et al., 2012). The HER2 expression is also deregulated in many cancers, including ovarian, breast, head and neck, prostate, gastric, oesophageal, and endometrial cancers, and it is associated with aggressive and poor prognosis (Moasser, 2007).

In ovarian epithelial carcinoma, EGFR is overexpressed in 30–98% of the cases (Gui & Shen, 2012), HER2 in 40% (Slamon et al., 1989), HER3 in 48% (Stern, 2000) and HER4 in 71% (Stern, 2000). Table 1.3 shows the expression of the EGFR family members in ovarian cancer and other different human types of cancer (Normanno et al., 2003). It is worth noting that the discrepancies in the expression of the EGFR family members between different studies are due to variations in the antibodies and reagents used, techniques and methodology employed, the sample size, the histopathology, and patients' age and race (Wilken et al., 2012).

Table 1.3 Expression of ERBB receptors in human carcinomas.

Expression of ERBB receptors in different types of cancer, ((NA) not assessed). Modified and adapted from (Normanno et al, 2003)

Type of cancer	EGFR (%)	ERBB-2 (%)	ERBB -3 (%)	ERBB -4 (%)
Ovary	30-70	8-32	85	93
Lung	40-80	18-60	25-85	NA
Breast	14-91	9-39	22-90	82
Stomach	33-74	8-40	35-100	NA
Colon	25-77	11-20	65-89	NA
Esophagus	43-89	7-64	64	NA
Liver	47-68	0-29	84	61
Pancreas	30-50	19-45	57-63	81
Prostate	40-80	40-80	22-96	NA
Kidney	50-90	0-40	0	NA
Bladder	35-86	9-50	30-56	30
Head and Neck	36-100	17-53	81	28-69

1.3.3. AXL

AXL belongs to the TAM family of RTKs, which consists of three members: TYRO-3 (Sky, Etk-2), AXL (UFO, Ark) and MER (c-EyK, Tyro-12) (Linger et al., 2008). Structurally, the TAM family members include an extracellular domain (two immunoglobulin-like domains and two Fibronectin-III domains), a transmembrane domain, and a cytoplasmic kinase domain (which varies between family members). TAM family members are broadly expressed in normal tissues, and AXL is expressed in the ovary (Sun et al., 2004), hippocampus and cerebellum ((Bellosta et al., 1995), monocytes-macrophages, platelets, endothelial cells, the heart, skeletal muscles, liver, kidney, and testis (Neubauer et al., 1994; Graham et al., 1995; Angelillo-Scherrer et al., 2001).

Gas6 (growth arrest-specific 6) is a vitamin K-dependent protein that was identified as a ligand for the TAM family of RTKs, with higher affinity for AXL (Varnum et al., 1995).

The typical mechanism of activation of AXL includes ligand binding to its extracellular domain, then dimerisation and consequent autophosphorylation of the cytoplasmic domain (Schlessinger, 2000). Atypical activation of the AXL receptor (ligand-independent) can occur through four different mechanisms: homotypic dimerisation, heterotypic dimerisation, crosstalk with other RTKs, and transcellular activation (Linger et al., 2008).

AXL plays a major role in signalling pathways promoting cell growth and survival (Stenhoff et al., 2004). AXL is associated with several malignancies, such as epithelial ovarian cancer (Rea et al., 2015; Sun et al., 2004), chronic myelogenous leukaemia (CML) (Dufies et al., 2011), B-cell chronic lymphocytic leukaemia (Ghosh et al., 2011),

metastatic breast cancer (Meric et al., 2002), glioblastoma (Onken et al., 2016), hepatocellular carcinoma (Tsou et al., 1998), melanoma (Quong et al., 1994), prostate carcinoma (Sainaghi et al., 2005), metastatic colon carcinoma (Craven et al., 1995), gastric cancer (Wu et al., 2002), and thyroid carcinoma (Ito et al., 2009). In particular, AXL expression has been observed at high levels in metastases and advanced-stage human ovarian tumours (Rankin et al., 2010).

1.3.4. Insulin-like growth factor I receptor (IGF-IR)

IGF-IR is a transmembrane tyrosine kinase receptor that belongs to a larger family composed of three other members: an insulin receptor (IR), an insulin-like growth factor II receptor (IGF-IIR) and a hybrid receptor of insulin-like growth factor (IGF) and insulin (Samani et al., 2007).

IGF function is regulated by six insulin-like growth factor-binding proteins (IGFBPs), IGFBP-1 through IGFBP-6. These control ligand bioavailability and the interaction between IGF receptors and ligands (Clemmons, 1998). Generally, IGF-IR is activated and stimulated through binding to its cognate ligand IGF-I; two types of ligands are known to the IGF receptor family, namely IGF-I and IGF-II (Samani et al., 2007; Gennigens et al., 2006).

Structurally, the IGF-IR RTK shows a 70% homology to the insulin receptor and is constituted of two alpha (α) subunits in the extracellular domain (which are critical for ligand binding) and two beta (β) subunits linked by disulfide bonds that form the transmembrane and intracellular cytoplasmic domains (and are vital for kinase activity) (Wu & Yu, 2014). Like other RTKs, these receptors are stimulated by ligand binding to

the alpha subunits, which induces conformational changes and a series of events, including the activation of the kinase domain in the beta units. Hence, they activate downstream signalling, most commonly the phosphorylation of insulin receptor substrate-1 (IRS-1) and the activation of the phosphatidylinositol 3-kinase (PI3K) and the mitogen-activated protein kinase (MAPK) pathways. Consequently, they are essential for cell proliferation, survival and transformation (Baserga et al., 2003; Adams et al., 2000).

IGF-IR is widely expressed in the fetal and postnatal tissues and has important roles in regulating cell cycle, breathing, the anabolic effect (in children) and ageing (Baserga et al., 2003; Dupont et al., 2003). However, aberrant IGR-IR signalling is linked to tumour transformation, disease progression, antiapoptotic effects and chemotherapy resistance (Grothey et al., 1999). Overexpression of IGF-IR is associated with oncogenic formation and is detected in various tumours, including ovarian (Yee et al., 1991), breast (Pollak et al., 1987), prostate (Gennigens et al., 2006), colorectal (Pollak et al., 1987), small and non-small cell lung cancer (Rotsch et al., 1992), melanoma (Furlanetto et al., 1993) and several other types of tumours (Khandwala et al., 2000).

1.3.5. H-RYK receptor tyrosine kinase

The RYK receptor (the receptor related to tyrosine kinase) is an atypical member of the RTK family. RYK is named H-RYK in humans, Derailed (derailed-2, doughnut) in Drosophila melanogaster and Lin-18 in Caenorhabditis elegans (C. elegans) (Hovens et al., 1992). It was first identified in 1992 as a result of screening for novel RTKs (Paul et al., 1992; Hovens et al., 1992; Stacker et al., 1993; Inoue et al., 2004).

The structure of the RYK family is composed of an extracellular domain, including a cysteine-rich domain (CRD) that resembles the Wnt inhibitory factor-1 (WIF-1). It is able to bind Wnt ligands and tetrabasic cleavage sites (KRRK), and its intracellular domain lacks tyrosine kinase activity, even though it is able to activate MAP kinase pathways, presumably through its association with the Src kinase family (Katso et al., 2000).

RYK is ubiquitously expressed in all adult and foetal tissues (Halford & Stacker, 2001) and acts as a Wnt co-receptor; as a consequence, it activates the canonical β-catenin-dependent pathway. Moreover, it plays an indispensable role in the central nervous system by affecting typical axon guidance and neuronal differentiation during development and regeneration during injury. Therefore, it could play a vital role in Wnt-mediated signalling (Fradkin et al., 2010; Clark et al., 2014). It is also known that RYK plays a significant role in mammalian planar cell polarity (PCP) (the β-catenin-independent Wnt signalling pathway) (Macheda et al., 2012) and a possible role in the congenital syndrome remains elusive (Keeble & Cooper, 2006). RYK exerts a tumorigenic role through aberrant expression in multiple tumours, including ovarian cancer (Katso et al., 2000; Wang et al., 1996), glioblastoma (Adamo et al., 2017) and

osteosarcoma (Gobin et al., 2014). It is also detected in the stromal tissue of most tumours (Katso et al., 1999) and paediatric brain tumours (Weiner et al., 1996).

1.3.6. Eph RTK

Eph receptors represent a quarter of RTK members, and they include two significant subgroups: EphA receptors (composed of nine EphA receptors) and Eph B receptors (consisting of five Eph B receptors). EphA receptors bind to the GPI-linked ephrin-A ligand (five ligands), whereas the Eph B receptors bind to transmembrane ephrin-B ligands (three ligands) (Pasquale, 2005). Exceptionally, Eph A4 also binds any members of ephrin-B, Eph B2 binds to ephrin-A5, and Eph B4 specially binds to ephrin-B2 only (Pasquale, 2005; Himanen et al., 2004).

The family of Eph receptors is activated in response to a binding complex between their receptor and ligands (Eph–ephrin) by generating a signal like other RTKs, but it also has an exceptional capacity to initiate an intercellular signal known as bi-directional signalling through two ways. The first way is forward signalling, where the receptor-bearing cell (receptor-expressing cell) is activated upon ligand-bound receptor, and the receptor initiates the signal following cell-cell contact. The second method is reverse signalling, where the opposing ephrin-bearing cell (ligand-expressing cell) initiates signalling through the ligand following cell-cell contact.

Furthermore, this family is also able to signal through cross-talk with other family receptors and has feedback regulation (Davy et al., 1999; Cheng et al., 2002; Palmer et al., 2002; Himanen & Nikolov, 2003; Carvalho et al., 2006).

Eph receptors regulate cell-cell communication and are involved in numerous biological functions. They play a significant role in embryogenic and neural development (Yamaguchi & Pasquale, 2004), immune function (Luo et al., 2004), insulin regulation (Kulkarni & Kahn, 2007; Konstantinova et al., 2007), and bone homeostasis (Zhao et al., 2006). When deregulated, they play a crucial role in cancer and angiogenesis (Cheng et al., 2002). The Eph2 receptor is upregulated in a myriad of malignancies, including in ovary (Thaker et al., 2004), breast (Zelinski et al., 2001), brain (Wykosky et al., 2005), urinary bladder (Abraham et al., 2006), prostate (Walker-Daniels et al., 1999), pancreas (Duxbury et al., 2004), lung (Kinch et al., 2003), oesophagus (Miyazaki et al., 2003), and stomach malignancies (Yuan et al., 2009).

1.4. The IgLON family

1.4.1. Introduction

IgLON stands for the Immunoglobulin LSAMP, OPCML and neurotrimin. The IgLON family is one of several groups of immunoglobulin cell adhesion molecules (IgCAMs), a type of immunoglobulin superfamily (IgSF) of cell adhesion molecules (IgSF, integrins and cadherins) (Struyk et al., 1995; Funatsu et al., 1999; Miyata et al., 2003). The IgLON family is composed of five members: OPCML/OBCAM, located on chromosome 11q25 (Schofield et al., 1989; Sellar et al., 2003; Reed et al., 2007); LSAMP, located at chromosome 3q13.2–q21 (Levitt, 1984; Brümmendorf et al., 1997); neurotrimin (HNT, CEPU-1) located at chromosome 11q25 (Struyk et al., 1995); the neuronal growth regulator 1 (NEGR1, kilon, neurotractin), located at chromosome 1p31.1 (Funatsu et al., 1999; Marg et al., 1999); and IgLON5, located at chromosome 19q13.41 (Grimwood, et al., 2004; Sabater, et al., 2014).

The IgLON members are associated with aberrant expression in epithelial ovarian cancer and two of its members are linked to cancer: the opioid binding protein/cell adhesion molecule-like (OPCML/OBCAM) and the limbic system-associated membrane protein (LSAMP) have been associated with epithelial ovarian cancer and clear cell renal cell carcinoma, respectively, as tumour suppressor proteins (Sellar et al., 2003; Chen et al., 2003). Hence, the IgLON family may be considered a promising new therapeutic or diagnostic biomarker (Ntougkos et al., 2005).

1.4.2. IgLON structure and cellular localisation

All members of the IgLON family share a general structure, which contains three C2-type immunoglobulin domains, and are attached to the cell membrane by a glycosyl-phosphatidylinositol (GPI) anchor. They all have a high level of glycosylation that varies among the family members (Itoh et al., 2008; Reed et al., 2004). Figure 1.6 shows the structure of the IgLON family members and their high glycosylation pattern.

GPI anchor proteins are localised in detergent-resistant membranes, which are enriched with cholesterol and sphingolipids. As a consequence, these proteins are able to modulate protein organisation in response to intracellular or extracellular stimuli (Simons & Toomre, 2000; Mishra & Joshi, 2007).

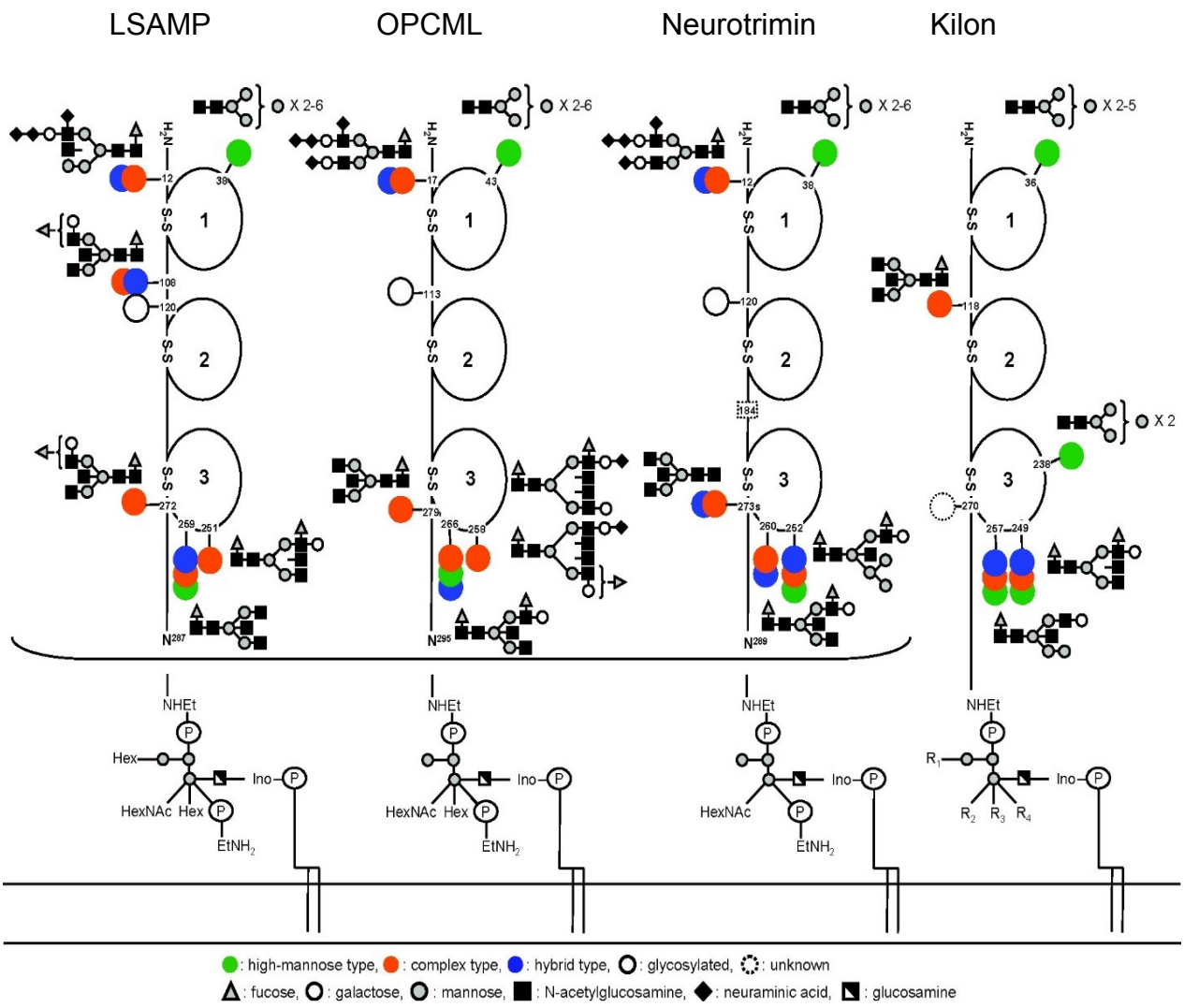


Figure 1.6 Schematic view of the IgLON family proteins.

Summary of glycosylation of IgLON family proteins including opioid-binding protein cell adhesion molecule (OPCML), limbic system-associated membrane protein (LSAMP), Neurotrimin, and Kilon, which are all part of the immunoglobulin (Ig) superfamily cell adhesion molecules. These molecules are composed of three immunoglobulin domains and a glycosylphosphatidylinositol (GPI) anchor and contain six or seven potential N-glycosylation sites. Adapted and modified from (Itoh et al., 2008).

1.4.3. IgLON expression

High expression of IgLONs was first observed in the brain as the result of studies on rat and chick brains. IgLONs are expressed in a variety of tissues, such as nerve system tissues, with OPCML being primarily expressed in the grey matter and the inner plexiform layer of the retina (Hachisuka et al., 1999), neurotrimin in the sensorimotor cortex and the cerebellum and outer plexiform layer (Struyk et al., 1995; Lodge et al., 2000), LSAMP in the cortical and subcortical neurons of the limbic system (Levitt, 1984), and NEGR1 in the cerebrum and brain stem (Funatsu et al., 1999). A recent study shows that IgLONs are expressed both in neurons and oligodendrocytes, except for neurotrimin (Sharma et al., 2015), which has been found to be expressed specifically in neurons (Hashimoto et al., 2009). The spatial and temporal expression of the IgLON family also varies during neuronal development (Miyata et al., 2000; Miyata et al., 2003).

1.4.4. IgLON function

IgLONs can heterodimerise both in cis and in trans between cells at the cell membrane level to form dimeric IgLONs (DIgLONs) (Reed et al., 2004). IgLONs, as mentioned previously, have been studied in the brain during neuronal development. They have also been shown to play a significant role in the regulation of synaptic structure, synapse formation and function, axon migration, cell recognition, and aggregation (Struyk et al., 1995; Varma & Mayor, 1998; Mann et al., 1998; Gil et al., 2002). Furthermore, they have been shown to play a role in cell adhesion and signal transduction (Zhukareva et al., 1997; McNamee et al., 2002). Their function as tumour suppressor genes has also been reported in a number of malignancies (Sellar et al.,

2003; Ntougkos et al., 2005; Reed et al., 2007; Cui et al., 2008; Barøy et al., 2014; Kim et al., 2014).

The *NEGR1* gene has been associated with white matter integrity disruption, which is linked to the preclinical stage of Alzheimer's disease (Dennis et al., 2014), depression (Hyde et al., 2016) and obesity (Melén et al., 2010; Poveda et al., 2014).

The *LSAMP* gene is associated with the regulation of emotional and social behaviour in mouse models, such as locomotion, anxiety, learning, fear reaction and a lack of acclimatisation (Innos et al., 2013; Philips et al., 2015). It has also been associated with psychiatric disorders, such as major depressive disorders and schizophrenia in humans (Behan et al., 2009; Innos et al., 2013; Koido et al., 2014).

The *neurotrimin* gene is associated with intelligence (Pan et al., 2011) and linked to axon fasciculation (axon guidance) (Chen et al., 2001; Yu et al., 2012), while *Iglon5*, a recently discovered member of the IgLON family, is associated with encephalopathy with protuberant sleep dysfunction, chronic neurodegeneration (Alzheimer's disease, Parkinson's disease) and autoimmunity of the cell surface (Sabater et al., 2014; Leypoldt et al., 2015).The function of OPCML will be discussed below.

1.4.5. IgLON and cancer

Remarkably, most studies identify aberrant methylation and a loss of heterozygosity as mechanisms that silence the OPCML member of the IgLON family in cancer. So far, most studies have focused on gene expression profiling of tumours, while functional analyses remain elusive (Sellar et al., 2003). OPCML was the first of the family to be linked to several types of tumours: epithelial ovarian cancer (Sellar et al., 2003), brain tumours (Reed et al., 2007), non-small cell lung carcinoma (Tsou et al., 2007), bladder cancer (Duarte-Pereira et al., 2011), Cholangiocarcinoma (Sriraksa et al., 2011), primary nasopharyngeal (Cui et al., 2008), oesophageal (Cui et al., 2008), gastric (Wang et al., 2006), hepatocellular (Cui et al., 2008), colorectal (Chunhong et al., 2015), breast and cervical cancers (Cui et al., 2008), as well as lymphomas (Cui et al., 2008).

Epithelial ovarian cancer is characterised by loss of expression of three members of the IgLON family – namely OPCML, LSAMP and NEGR1 – while neurotrimin shows increased expression (Ntougkos et al., 2005). LSAMP has also been suggested as acting as a tumour suppressor gene in sporadic and hereditary clear cell renal cell carcinoma (Chen et al., 2003), osteosarcoma (Barøy et al., 2014; Kresse et al., 2009) and aggressive prostate cancer (Petrovicsa et al., 2015).

1.5. OPCML

1.5.1. OPCML structure

Like other IgLON family members, the structure of the OPCML protein is composed of three C2-type immunoglobulin domains bound to the cell membrane via a GPI anchor attached to the C-terminal portion of the protein (Lodge et al., 2000). The gene comprises seven exons, spans nearly 600 kb, and the protein sequence size is around 345 amino acid (Sellar et al., 2003; Cui et al., 2008). In humans, two major splice variants, variant α1 and variant α2, can be found that give rise to the same protein (Reed et al., 2007).

OPCML interacts with other IgLON members to heterodimerise both in cis within the same cell and in trans between cells at the cell membrane level to form DIgLONs (Reed et al., 2004).

1.5.2. OPCML expression

As mentioned earlier, due to alternative splicing, the OPCML gene gives rise to two different variants whose expressions vary in different tissues. While the OPCML variant α1 expression is absent in placenta and peripheral blood mononuclear cells (PBMC), it is expressed widely in the brain, kidney, spleen, stomach, trachea, testis, cervix, ovary and prostate, and is weakly expressed in the lungs, breast and bone marrow (Cui et al., 2008). OPCML variant α2, on the other hand, is hardly detected in the kidney, spleen, pancreas, breast, testis, lungs, colon, liver and bone marrow, while it is expressed in all foetal tissues except the placenta, suggesting a role in embryonic development (Cui et al., 2008).

Two alternative variants of OPCML, variant 1 and variant 2, were previously identified in human, which only differ in their exon number 5 but encode very similar mature proteins (345 and 338 amino acids respectively) with the same function (Reed et al., 2007; Cui et al., 2008).

1.5.3. OPCML as a tumour suppressor

Originally, OPCML was isolated as a potential opioid receptor and cell-cell adhesion and recognition molecule (Cho et al., 1986; Schofield et al., 1989; Miyata et al., 2003; Lodge et al., 2000). More recently, it has been recognised as a tumour suppressor protein that is often inactivated by loss of heterozygosity and promoter hypermethylation in ovarian and lung adenocarcinoma (Sellar et al., 2003; Tsou et al., 2007) and other several tumours (Cui et al., 2008). Its expression is lost in 83% of primary ovarian tumours, 88% of ovarian cancer cell lines, and 71% of non-ovarian cancer cell lines; as a consequence, epigenetic methylation and loss of heterozygosity have been attributed to OPCML inactivation (Gabra et al., 1996; Sellar et al., 2003).

OPCML is a tumour growth suppressor and promotes cell aggregation (Sellar et al., 2003). Our group previously found that, in *in vitro* growth assays, OPCML expression in SKOV-3 cells reduced cell growth compared to both SKOV-3 parent cells and cells transfected with OPCML antisense sequences (Figure 1.7 A). Also, *in vitro* aggregation assays showed that cells expressing OPCML have higher ability to aggregate compared to control cells (Figure 1.7 B).

OPCML was transfected into SKOV3 cells after cloning the OPCML PCR product into the pcDNA3.1 Zeo plasmid in both the sense and antisense orientations and

verifying the inserted sequences. Then, OPCML sense- and antisense-transfected clonal cell lines were established (Sellar et al., 2003).

Furthermore, re-expression of OPCML in an *in vivo* xenograft model strongly suppressed tumour growth formation (Sellar et al., 2003). In fact, the study in a nude mice model showed that OPCML expression in SKOV-3 cells suppressed tumour growth compared with parent and control cells transfected with OPCML antisense sequence in both a subcutaneous model (Figure 1.7 C) and an intraperitoneal model (Figure 1.7 D, E) (Sellar et al., 2003). Furthermore, evidence in our lab showed – through using SKOV3 and OV90 cells expressing OPCML –that OPCML sensitises cells to both lapatinib and erlotinib in HER2-expressing ovarian cancer cell lines and could be potential beneficial target therapy for positive HER2 expressing breast cancer patients. (Zanini et al., 2017).

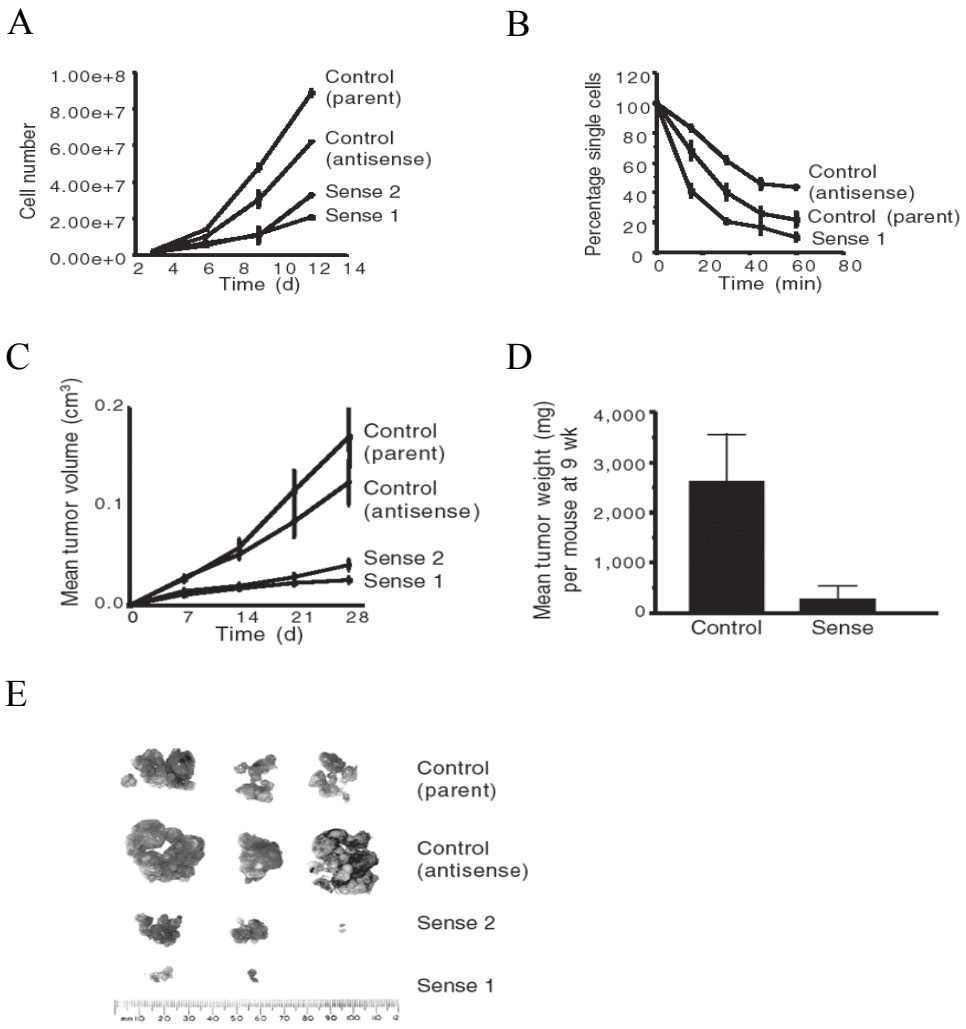


Figure 1.7 OPCML has functional features of a tumour suppressor gene in vitro and in vivo.

The figure illustrates the characterisation of two independent SKOV3 clones transfected with a sense OPCML sequence compared to clonal control SKOV3 lines (parental and antisense-transfected) in several functional assays.

A. *In vitro* growth assay of clonal SKOV3 cell lines. The values shown are the mean ± SD of triplicate assays.
B. *In vitro* aggregation assay. The graph shows standard error of the mean (SEM) for three experiments.
C. *In vivo* subcutaneous tumour growth assay.
D. *In vivo* intraperitoneal tumour growth assay. Mean tumour weight per mouse.
E. Photograph of tumours from *D.*

Figures adapted and modified from (Sellar et al., 2003).

1.5.4. The role of OPCML in the regulation of RTKs in ovarian cancer

As mentioned previously, aberrant RTK expression is observed in ovarian cancer and several other malignancies. Our group found that the inactivation of OPCML correlates with the upregulation of a spectrum of RTKs (McKie et al., 2012). Indeed, OPCML binds to (Figure 1.8 A) and downregulates a subset of RTKs by inducing their distribution in lipid rafts, followed by ubiquitination and proteasomal degradation, thus causing the attenuation of their downstream signalling (McKie et al., 2012). Among the receptors downregulated by OPCML, there are HER2, HER4, Eph A2, FGFR1 (McKie et al., 2012) (Figure 1.8 B), and AXL (unpublished data). As a consequence of their interaction with OPCML and their subsequent downregulation, their downstream signalling through the MAPK and AKT pathways becomes also attenuated.

It is important to note that OPCML modulates cellular effects by downregulating multiple RTKs in several cancerous (SKOV3, PEO1) and non-cancerous (ovarian surface epithelium C2) cell lines (McKie et al., 2012) (Figure 1.8 B). In the latter, the abolition of OPCML expression promotes the RTKs' expression, which upregulates the downstream signalling (Figure 1.8 B). Therefore, this study defines OPCML as a therapeutic candidate agent in treating ovarian cancer.

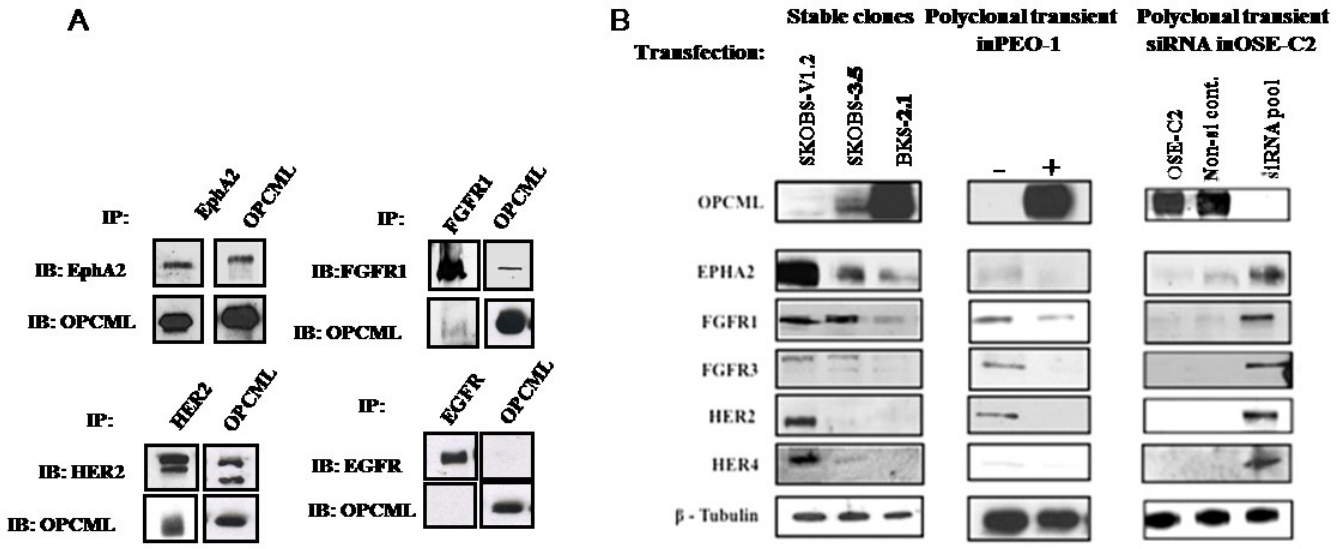


Figure 1.8 OPCML associate and downregulate receptor tyrosine kinases.

A. Co-Immunoprecipitation assay. It demonstrates that OPCML associates with a diverse array of receptor tyrosine kinase such as EPHA2, FGFR1, and HER2, likewise associated with OPCML in a reciprocal way. Moreover, OPCML does not bind to EGFR.

B. Western blots. They illustrate that OPCML negatively regulates EPHA2, FGFR1, FGFR3, HER2, and HER4 in stably transfected SKOV-3 cells. Left panel containing pcDNA3.1 vector (SKOBS V1.2), pcDNA3.1-OPCML with low OPCML expression (SKOBS-3.5), and pcDNA3.1-OPCML with high OPCML expression (BKS2.1). The middle panel shows polyclonal transiently PEO1 cells (B) transfected with vector only (–) or OPCML (+). The right panel shows normal ovarian surface epithelial cells (OSE-C2, physiologically expressing OPCML) which were either untreated (OSE-C2), or transiently transfected with non-silencing duplex (Non-si), or OPCML-directed siRNA duplexes. The bottom panel shows β-tubulin as a loading control. Figure adapted and modified from McKie et al., 2012.

1.5.5. Role of OPCML mutations

As we mentioned above, the inactivation of the OPCML tumour suppressor is a frequent event in many tumours and it usual occurs upon loss of heterozygosity and epigenetic methylation (Sellar et al., 2003). However, one alternative mechanism leading to the inactivation of OPCML could be by mutations. Mutations may for example affect OPCML's function by modifying its RTK binding sites, by creating potential alterations in protein stability, by inducing protein aggregation or by impairing post-translational modifications. Therefore, protein malfunction may occur, which would affect OPCML's tumour suppressor function.

Sellar et al., 2003 had previously identified a single somatic missense mutation in a primary ovarian tumour (P95R) and the partial characterisation of this mutant showed that it behaved like OPCML in suppressing tumour growth but it had lost the ability to promote cell aggregation compared to wild-type OPCML (Sellar et al., 2003).

Here, analysing the TCGA and COSMIC datasets we identified many mutations in the OPCML gene that occur in different types of malignant transformations. However, the prevalence and clinical significance of these OPCML mutations in ovarian and other cancers remain elusive.

Therefore, studying OPCML mutations would provide a guide for a broad understanding of OPCML's role in normal and cancer tissues. Also, it will provide further insight into the function of each domain, which will help us refine the regions of OPCML that could be used as either biomarkers or personalised targeted therapies.

1.6. Hypothesis and Aims

Our goal in this study is to investigate the roles and mechanisms of OPCML mutations in ovarian cancer, guided by the hypothesis that somatic mutation of OPCML causes the loss of its function as a tumour suppressor partially or wholly. As such, to test our hypothesis, we seek to answer the following questions:

1. Do OPCML mutations affect the localisation of the protein in the cell?

2. Do OPCML mutations influence the function of OPCML? If yes, what is their role?

3. Do OPCML mutants still sensitise cells to AXL inhibitor R428 treatment?

To answer these questions, the aims of this doctoral project are to:

A. Create stable cell lines in ovarian cancer cells (SKOV3, PEA1, and PEO1) expressing OPCML-WT or OPCML mutants in domain I, and SKOV3 cell line for domain II, and domain III.

B. Characterise protein expression and localisation of the OPCML mutants by Western blot analysis and immunofluorescence microscopy.

C. Identify whether OPCML mutations affect the interaction with RTKs, initially focusing on AXL, using co-Immunoprecipitation and Duolink® assays.

D. Determine the *in vitro* effects of OPCML mutations on critical downstream signalling pathways.

E. Validate *in vitro* the role of OPCML mutations on adhesion, invasion and migration.

F. Investigate whether OPCML mutations affect sensitisation or resistance to an AXL inhibitor.

G. Determine the *in vivo* effects of OPCML mutations in mouse and CAM xenograft models.

The outcomes of this study may, therefore, enhance our understanding of OPCML and its role in ovarian cancer. As a consequence, our results may promote novel therapeutic opportunities for the treatment and the management of ovarian cancer and other tumour types.

2. CHAPTER 2

Materials and Methods

2.1. Chemicals and reagents

Chemicals were obtained from Sigma Aldrich (Merck, USA) unless otherwise indicated. Some basic reagents and solutions were prepared by the Institute of Reproductive and Developmental Biology (IRDB) technical staff.

2.2. Cell culture

All ovarian cancer cell lines (SKOV3, PEA1, and PEO1) were maintained in RPMI-1640 medium (Sigma-Aldrich, USA) supplemented with 10 % Foetal calf serum (FCS, First link, UK), 0.2 mM L-Glutamine (Gibco, USA), 50 U/ml penicillin, and 50 µg/ml streptomycin (Gibco, USA).

HEK293T (Human embryonic kidney) were maintained in Dulbecco's Modified Eagle Medium (DMEM) supplemented with Foetal calf serum, 0.2 mM L-Glutamine, and Penicillin (50 U/ml) with streptomycin (50 µg/ml).

All cell lines were cultured at 37°C in a 5 % CO_2 humidified incubator. Transduced cells were maintained in full medium supplemented with Puromycin dihydrochloride (Gibco, USA) (10 µg/ml for SKOV3; 5 µg/ml for PEO1; and 2.5 µg/ml for PEA1) (Table 2.1). When cells reached 80-85% confluence, they were passaged by washing twice with Phosphate buffered saline (PBS, Sigma Aldrich, USA) and by detaching using 1X Trypsin in Ethylenediaminetetraacetic acid (EDTA, Gibco, USA). The three immortalised cell lines used in this study (two of which are of mesenchymal type) are i) SKOV3, derived from ascitic high grade serous adenocarcinoma cells, ii) PEA1, platinum-sensitive cells derived from ascitic serous adenocarcinoma cells, and iii) epithelial type PEO1, which is a platinum sensitive ascitic serous adenocarcinoma cell line. The

advantage of using these cell lines is that these are heterogeneous cells and mimic the actual ovarian cancer tumour compared to clone expansion of one single clone, which could lose the characteristics of the real tumour.

These cell lines lack OPCML expression and we confirmed our results by analysing the OPCML expression using Western Blot and immunofluorescence microscopy.

Table 2.1 Cell lines, medium, and supplements used in this study.

OVARIAN CANCER CELL LINE	MEDIUM	SUPPLEMENTS
Tumour cell line transduced with either pLenti-OPCML mutants, pLenti-OPCMLWT, or pLenti-Empty vector stable cell lines in SKOV3	RPMI-1640	10 % Foetal bovine serum (First link) 50 U/ml Penicillin 50 µg/ml Streptomycin 10 µg/ml Puromycin dihydrochloride (Gibco, USA)
Tumour cell line transduced with either pLenti-OPCML mutants, pLenti-OPCMLWT, or pLenti-Empty vector stable cell lines in PEA1	RPMI-1640	10 % Foetal bovine serum (First link) 50 U/ml Penicillin 50 µg/ml Streptomycin 2.5 µg/ml Puromycin dihydrochloride (Gibco, USA)
Tumour cell line transduced with either pLenti-OPCML mutants, pLenti-OPCMLWT, or pLenti-Empty vector stable cell lines in PEO1	RPMI-1640	10 % Foetal bovine serum (First link) 50 U/ml Penicillin 50 µg/ml Streptomycin 5 µg/ml Puromycin dihydrochloride (Gibco, USA)
Tumour cell line transduced with GFP and either pLenti-OPCML mutants, pLenti-OPCMLWT, or pLenti-Empty vector stable cell lines in SKOV3	RPMI-1640	10 % Foetal bovine serum (First link) 50 U/ml Penicillin 50 µg/ml Streptomycin 10 µg/ml Puromycin dihydrochloride (Gibco, USA)
HEK293T cell line	DMEM	10 % Foetal bovine serum (First link) 0.2 mM L-Glutamine 50 U/ml Penicillin 50 µg/ml Streptomycin

2.3. Nucleic acid manipulation

2.3.1. Agarose Gel Electrophoresis

DNA samples were prepared for analysis by gel electrophoresis by mixing them with an appropriate volume of 5X DNA loading buffer (Bioline). Gels were made with 1% (w/v) agarose in 1X TAE buffer (Tris-base: 242 g, Acetate (100 % acetic acid): 57.1 ml, EDTA: 100 ml 0.5 M sodium EDTA, for a final volume of 1000 ml) containing 0.01% Ethidium bromide (10 mg/ml).

Electrophoresis was carried out at 90-100V for 1 hour in a 1X TAE buffer, and DNA was visualised under UV light with Uvitec Cambridge - Gel Documentation Systems - Fire Reader V4.

2.3.2. Mutagenic Primers Design

Primers were designed using the Quick-change Agilent primer design program available online at www.agilent.com/genomic/qcpd.

The primers for site-directed mutagenesis were designed to have a complementary sequence ranging from 12 to 20 bases on either side of the desired mutation site. Details of the primer sequences used can be found in table 2.2, OPCML Mutations used in the project mapped in the OPCML sequence table 2.3.

Table 2.2 Mutated primers used in site-directed mutagenesis to construct OPCML mutants.

Mutation	Sequence	Primer
R65L	GAT GAC CGG GTA ACC CTG GTG GCC TGG CTA AAC Arginine CGG to Leucine CTG	Forward
R65L	GTT TAG CCA GGC CAC CAG GGT TAC CCG GTC ATC Arginine CGG to Leucine CTG	Reverse
N70H	CGG GTG GCC TGG CTA CAC CGC AGC ACC ATC CTC Asparagine AAC to Histidine CAC	Forward
N70H	GAG GAT GGT GCT GCG GTG TAG CCA GGC CAC CCG Asparagine AAC to Histidine CAC	Reverse
R71C	GTG GCC TGG CTA AAC TGC AGC ACC ATC CTC TAC Arginine CGC to Cysteine UGC	Forward
R71C	GTA GAG GAT GGT GCT GCA GTT TAG CCA GGC CAC Arginine CGC to Cysteine UGC	Reverse

P95R	ATC ATC CTG GTC AAT ACA CGA ACC CAG TAC AGC ATC ATG Proline CCA to arginine CGA	Forward
P95R	CAT GAT GCT GTA CTG GGT TCG TGT ATT GAC CAG GAT GAT Proline CCA to Arginine CGA	Reverse
P95L	ATC ATC CTG GTC AAT ACA CTA ACC CAG TAC AGC ATC ATG Proline CCA to Leucine CTA	Forward
P95L	CAT GAT GCT GTA CTG GGT TAG TGT ATT GAC CAG GAT GAT Proline CCA to Leucine CTA	Reverse
P95S	ATC ATC CTG GTC AAT ACA TCA ACC CAG TAC AGC ATC Proline CCA to Serine TCA	Forward
P95S	TAG TAG GAC CAG TTA TGT AGT TGG GTC ATG TCG TAG Proline CCA to Serine TCA	Reverse
E201Q	CAG TCC GGG GAG TAC CAA TGC AGC GCG TTG AAC Glutamic acid GAA to Glutamine CAA	Forward

E201Q	GTC AGG CCC CTC ATG GTT ACG TCG CGC AAC TTG Glutamic acid GAA to Glutamine CAA	Reverse
S203R	GGG GAG TAC GAA TGC CGC GCG TTG AAC GAT GTC Serine AGC to Arginine CGC	Forward
S203R	CCC CTC ATG CTT ACG GCG CGC AAC TTG CTA CAG Serine AGC to Arginine CGC	Reverse
R214Q	GCT GCG CCC GAT GTG CAG AAA GTA AAA ATC ACT Arginine CGG to Glutamine CAG	Forward
R214Q	CGA CGC GGG CTA CAC GTC TTT CAT TTT TAG TGA Arginine CGG to Glutamine CAG	Reverse
K230R	CCC TAT ATC TCA AAA GCC AGG AAC ACT GGT GTT TCA GTC Lysine AAG to Arginine AGG	Forward
K230R	GGG ATA TAG AGT TTT CGG TCC TTG TGA CCA CAA AGT CAG Lysine AAG to Arginine AGG	Reverse

K239N	GTT TCA GTC GGT CAG AAC GGC ATC CTG AGC TGT Lysine AAG to Asparagine AAC	Forward
K239N	CAA AGT CAG CCA GTC TTG CCG TAG GAC TCG ACA Lysine AAG to Asparagine AAC	Reverse
M278I	GAA AAC AAA GGC CGC ATC TCC ACT CTG ACT TTC Methionine ATG to Isoleucine ATC	Forward
M278I	CTT TTG TTT CCG GCG TAG AGG TGA GAC TGA AAG Methionine ATG to Isoleucine ATC	Reverse

Table 2.3 OPCML Mutations used in the project mapped in the OPCML sequence.

Mutations in domain I are denoted in violet, domain II in green, domain III in dark red.

ATG GGG GTC TGT GGG TAC CTG TTC CTG CCC TGG AAG TGC CTC GTG GTC GTG TCT CTC
AGG CTG CTG TTC CTT GTA CCC ACA GGA GTG CCC GTG CGC AGC GGA GAT GCC ACC TTC CCC AAA
GCT ATG GAC AAC GTG ACG GTC CGG CAG GGG GAG AGC GCC ACC CTC AGG TGT ACC ATA GAT GAC
CGG GTA ACC CGG GTG GCC TGG CTA AAC CGC AGC ACC ATC CTC TAC GCT GGG AAT GAC AAG
TGG TCC ATA GAC CCT CGT GTG ATC ATC CTG GTC AAT ACA CCA ACC CAG TAC AGC ATC ATG ATC
CAA AAT GTG GAT GTG TAT GAC GAA GGT CCG TAC ACC TGC TCT GTG CAG ACA GAC AAT CAT CCC
AAA ACG TCC CGG GTT CAC CTA ATA GTG CAA GTT CCT CCT CAG ATC ATG AAT ATC TCC TCA GAC
ATC ACT GTG AAT GAG GGA AGC AGT GTG ACC CTG CTG TGT CTT GCT ATT GGC AGA CCA GAG CCA
ACT GTG ACA TGG AGA CAC CTG TCA GTC AAG GAA GGC CAG GGC TTT GTA AGT GAG GAT GAG TAC
CTG GAG ATC TCT GAC ATC AAG CGA GAC CAG TCC GGG GAG TAC GAA TGC AGC GCG TTG AAC
GAT GTC GCT GCG CCC GAT GTG CGG AAA GTA AAA ATC ACT GTA AAC TAT CCT CCC TAT ATC TCA
AAA GCC AAG AAC ACT GGT GTT TCA GTC GGT CAG AAG GGC ATC CTG AGC TGT GAA GCC TCT
GCA GTC CCC ATG GCT GAA TTC CAG TGG TTC AAG GAA GAA ACC AGG TTA GCC ACT GGT CTG GAT
GGA ATG AGG ATT GAA AAC AAA GGC CGC ATG TCC ACT CTG ACT TTC TTC AAT GTT TCA GAA AAG
GAT TAT GGG AAC TAT ACT TGT GTG GCC ACG AAC AAG CTT GGG AAC ACC AAT GCC AGC ATC ACA
TTG TAT GGG CCT GGA GCA GTC ATT GAT GGT GTA AAC TCG GCC TCC AGA GCA CTG GCT TGT CTC
TGG CTA TCA GGG ACC CTC TTA GCC CAC TTC TTC ATC AAG TTT TGA

Domain I mutations R65L, N70H, R71C, P95R, P95L, and P95S

Domain II mutations E201Q, S203R, and R214Q

Domain III mutations K230R, K239N, and M278I

2.3.3. **Site-Directed Mutagenesis**

Mutagenesis reactions were performed following a Quick-Change® Site-Directed Mutagenesis protocol (Agilent) using Pfu DNA Polymerase (Thermo-scientific). The plasmid DNA template, used to generate the desired mutants, was pENTR4 containing the OPCML wild-type cDNA. The mutagenesis reaction was prepared to make a final volume of 20 µl that contained the following components: up to 20 µl of autoclaved distilled water; 2 µl of 10x buffer+MgSO4; 0.5 µl of 25 mM dNTPs; 1 µl of each mutagenic primer (100 ng/µl); 20 ng/µl plasmid DNA template; 1 µl of Pfu DNA Polymerase; (Thermo-scientific, UK) and 3 % of DMSO (Table 2.4).

The reaction mixture was run in the MJ Research PTC-200 PCR Thermal Cycler - GMI using PCR cycling conditions as follows:

Table 2.4 Site-directed mutagenesis PCR cycling conditions.

Segment	Cycle	Temperature	Time
1	1	95ºC	30 seconds
2	12-18(15)	95ºC	30 seconds
3		55ºC	1 minute
4		68ºC	6 minutes (1 minute/Kb of plasmid length)
5		4ºC	∞

After the reaction was completed, it was incubated with 1 µl of *DpnI* restriction enzyme (New England Biolabs®, UK) at 37ºC for one hour. The digested mutagenesis product was then transformed into competent bacterial cells.

2.3.4. **Restriction Endonucleases Digestion**

10 ul of the analytical digestion reaction was composed of the following: 2 µl of plasmid DNA, 1 µl 10X Fast digest green buffer (Thermo Scientific™ Fast Digest™ Restriction Enzymes, Fisher Scientific, UK), 0.5 µl of each restriction enzyme (BamHI, XhoI) and up to 10 µl of autoclaved distilled water. The digestion reaction was incubated at 37°C for 15-30 minutes. Agarose gel electrophoresis was used to analyse the digestion products.

2.3.5. **Bacterial Transformation and DNA extraction**

A vial of chemically modified competent XL-1 *Escherichia Coli* (Agilent, UK) was thawed briefly by placing it on ice. 25 µl of competent bacteria were transferred into 1.5 ml Eppendorf tubes and were mixed with 2.5 µl of the DNA/PCR mixture and incubated on ice for at least 15 minutes. After the incubation, the bacteria were heat-shocked by placing them in a water bath at 42°C for 45 seconds. They were then immediately placed back on the ice and incubated for 3 minutes. Following that, 300 µl of 2x-YT medium was added to the bacteria and incubated in the shaker at 37°C for 1 hour. Bacteria were plated onto agar plates containing the suitable antibiotics and incubated at 37°C for 16-20 hours. The following day, single colonies were picked and inoculated into a liquid culture of 2x-YT medium containing the appropriate antibiotic (Ampicillin or Kanamycin) and left to grow for 16-20 hours at 37°C. The following day, the plasmid DNA was extracted using the Gene JET plasmid miniprep kit (Thermo-scientific, UK) or the Qiagen maxi-prep Kit (Qiagen), following the manufacturer's instructions. DNA concentration was determined by Nanodrop-1000 (Thermo-scientific).

2.3.6. **DNA Sequencing**

In order to confirm that the mutations of interest were present, samples were analysed by automated DNA sequencing, which was provided by Beckman Coulter Genomics (GENEWIZ, UK).

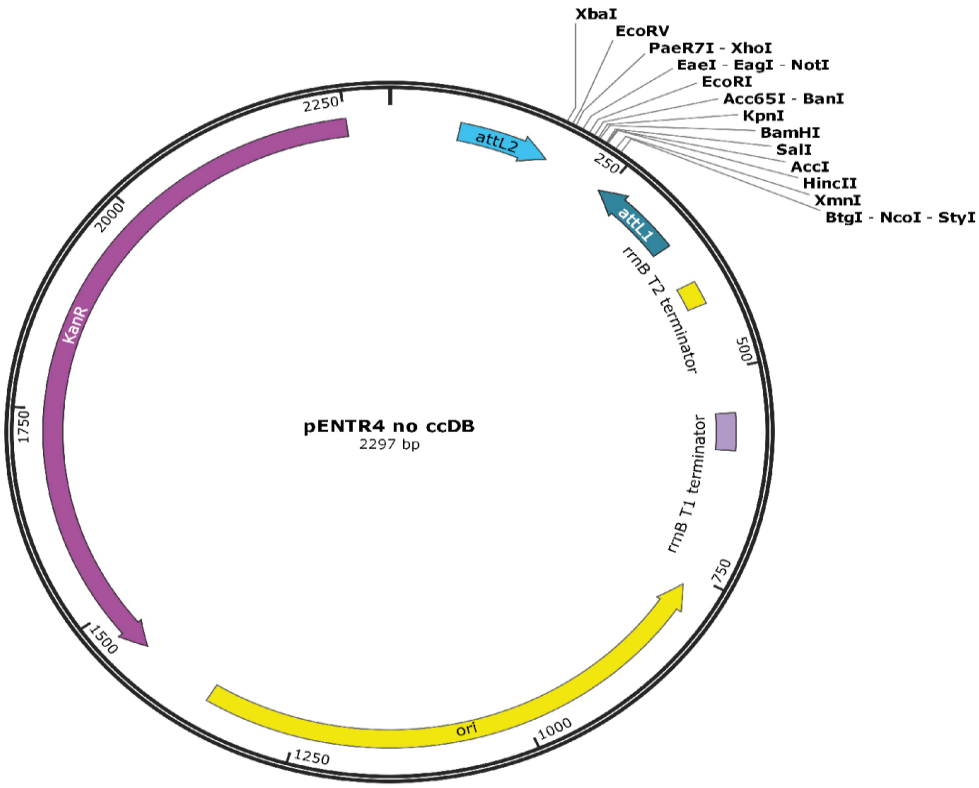
2.3.7. **The Gateway® cloning system**

Sequenced pENTR4-OPCML wild -type/-OPCML mutants were used to shuttle the sequence of interest to the Destination vector, pLenti CMV Puro DEST. This reaction was performed by an enzyme mixture, the Gateway® LR Clonase® II Enzyme Mix (Thermo Fisher Scientific, USA), which contains the necessary components to form the expression plasmid by shuttling the gene of interest from the Entry clone and integrate it into the Destination vector.

Reactions were carried out mixing 50 ng of entry vector and 150 ng of destination vector with 1X LR Clonase reaction buffer in a total volume of 10 µl. Reactions were incubated at 25°C for 1 hour, after which 4 µg of proteinase K solution was added, and samples were incubated for further 10 minutes at 37°C. When the reaction terminated, 1µl of the reaction was used for bacterial transformation using HB101 competent cells.

In figure 2.1 the map of the two vectors used is shown, and figure 2.2 reveals the schematic representation of the gateway cloning system process.

A


Created with SnapGene®
XbaI
EcoRV
PaeR7I - XhoI
EaeI - EagI - NotI
EcoRI
Acc65I - BanI
KpnI
BamHI
SalI
AccI
HincII
XmnI
BtgI - NcoI - StyI
attL2
attL1
rrnB T2 terminator
rrnB T1 terminator
KanR
ori
pENTR4 no ccDB
2297 bp
250
500
750
1000
1250
1500
1750
2000
2250

B

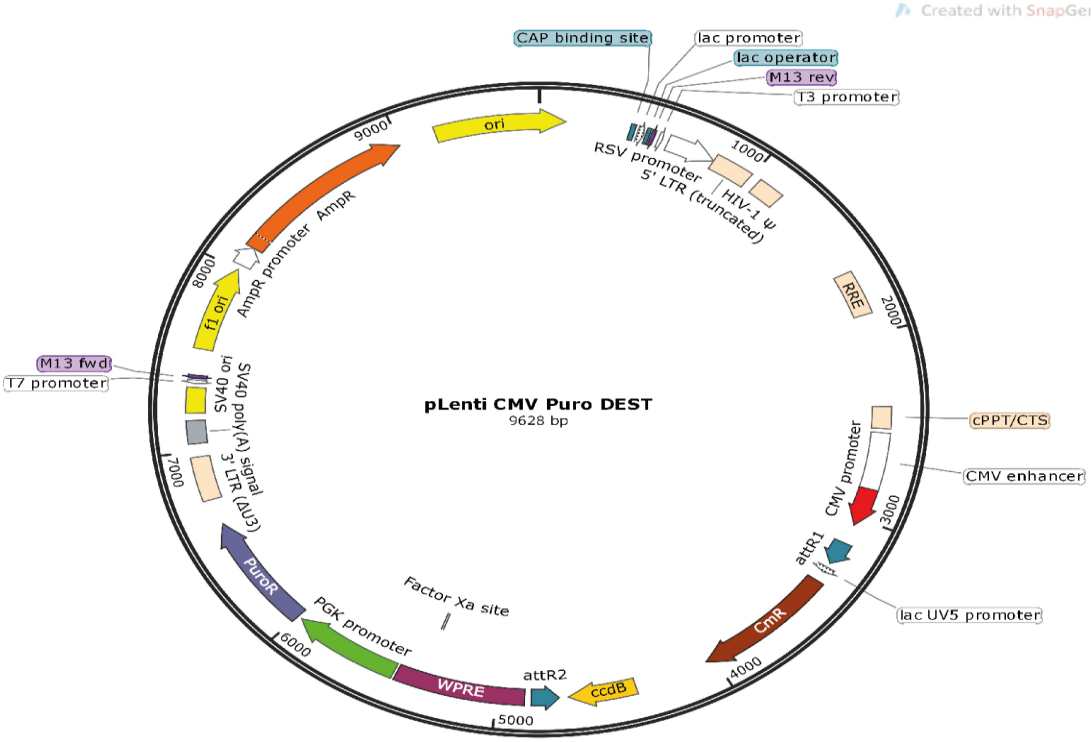

Created with SnapGene®
CAP binding site
lac promoter
lac operator
M13 rev
T3 promoter
ori
RSV promoter
5' LTR (truncated)
HIV-1 ψ
RRE
cPPT/CTS
CMV enhancer
CMV promoter
attR1
lac UV5 promoter
CmR
attR2
ccdB
WPRE
PGK promoter
Factor Xa site
PuroR
3' LTR (ΔU3)
SV40 poly(A) signal
SV40 ori
f1 ori
AmpR promoter
AmpR
M13 fwd
T7 promoter
pLenti CMV Puro DEST
9628 bp
1000
2000
3000
4000
5000
6000
7000
8000
9000

Figure 2.1 Map of pENTR4, and pLenti vectors.

The figure shows the map of the vectors used and their components: T3 promoter (Promoter for bacteriophage T3 RNA polymerase), M13 rev (Common sequencing primer, one of multiple similar variants), lac promoter (Promoter for the E. coli lac operon), RSV promoter (Rous sarcoma virus enhancer/promoter), Ori (High-copy-number ColE1/pMB1/pBR322/pUC origin of replication), 5' LTR (Truncated 5' long terminal repeat (LTR) from), HIV-1 Ψ (Packaging signal of human immunodeficiency virus type 1), RRE(The Rev response element (RRE) of HIV-1 allows for Rev-dependent mRNA export from the nucleus to the cytoplasm), cPPT/CTS (Central polypurine tract and central termination sequence of HIV-1), CMV enhancer (Human cytomegalovirus immediate early enhancer), CMV promoter (Human cytomegalovirus (CMV) immediate early promoter), lac UV5 promoter (E. coli lac promoter with an "up" mutation), CmR (Chloramphenicol acetyltransferase), ccdB (CcdB, a bacterial toxin that poisons DNA gyrase), WPRE (Woodchuck hepatitis virus posttranscriptional regulatory element), PGK promoter (Mouse phosphoglycerate kinase 1 promoter), PuroR (Puromycin N-acetyltransferase), 3' LTR (ΔU3) (Self-inactivating 3' long terminal repeat (LTR) from HIV-1), SV40 poly(A) (Signal SV40 polyadenylation signal), SV40 ori (SV40 origin of replication), T7 promoter (Promoter for bacteriophage T7 RNA polymerase), M13 fwd (Common sequencing primer, one of multiple similar variants), f1 ori (f1 bacteriophage origin of replication; arrow indicates direction of (+) strand synthesis), AmpR (β-lactamase), ori (high-copy-number ColE1/pMB1/pBR322/pUC origin of replication), Factor Xa site (Factor Xa recognition and cleavage site), rrnB T2 terminator (Transcription terminator T2 from the E. coli rrnB gene), rrnB T1 terminator (Transcription terminator T1 from the E. coli rrnB gene), and KanR (Aminoglycoside phosphotransferase). Adapted and modified using vector sequence from Addgene. Map created using SnapGene software (Campeau et al., 2009).

A) pENTRA4, B) pLenti CMV PURO DEST.

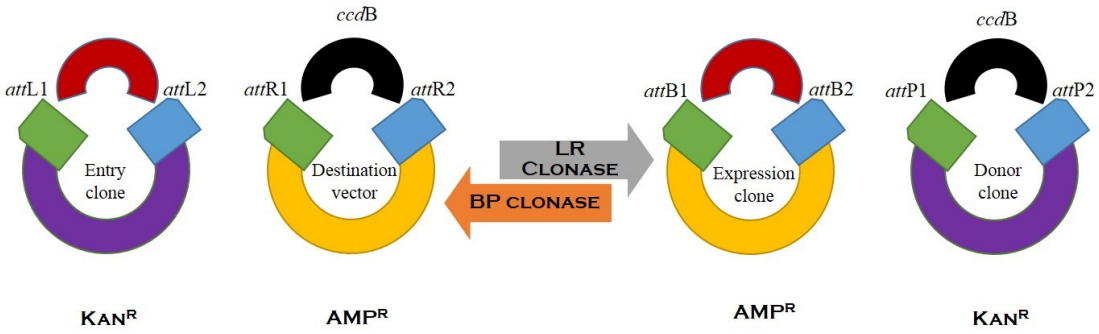


Figure 2.2 The Gateway® LR Clonase® II Enzyme Mix.

The panel shows the reaction between the two vectors with different antibiotic resistance. Adapted and modified from (Thermo Fisher Scientific, 2017).

2.4. Lentiviral packaging

Human Embryonic Kidney HEK293T cells were used to produce the virus necessary for the creation of stable cancer cell lines expressing OPCML-WT, OPCML mutants and the empty vector (pLenti CMV Puro DEST).

The cells were seeded into 60 X 15 mm tissue culture dishes at $3x10^6$, 24 hours before transfection, which was performed following the Lipofectamine 2000™ Reagent protocol (Invitrogen). A mix of 4 µg of DNA, 3.5 µg of packaging plasmid (p8.9) and 0.5 µg of envelope plasmid (pMDG) was incubated in 500 µl of Opti-MEM medium for 5 minutes at room temperature. At the same time, 20 µl of Lipofectamine2000™ was diluted in 500 µl of Opti-MEM medium and also incubated for 5 minutes. After the incubation, the DNA and Opti-MEM mixture was mixed with the diluted Lipofectamine™2000- Opti-MEM and incubated at room temperature for a further 20 minutes. The transfection complex was then added to the cells drop-wise and incubated for six hours, after which the medium was changed to full growth medium with antibiotic (Penicillin /Streptomycin).

After 48 hours the medium containing the virus was collected, centrifuged at 1,500 rpm for 4 minutes and filtered using 0.20 µm filter to remove cells and cell debris. Aliquots were made into 1.5 ml Eppendorf tubes and frozen at -80°C.

2.5. Transduction

Ovarian cancer cell lines (SKOV3, PEA1, and PEO1) were seeded into 24-well plates (Corning, USA) at a suitable density, transduced with different amounts of virus (50-450 µl) (pLenti-OPCML mutants, pLenti-OPCML WT, and pLenti-Empty vector) and incubated for 24h before changing the medium and adding the selective antibiotic (Puromycin). Cells were then expanded and protein expression tested by Western blot.

2.6. Whole Cell Lysate Preparation

Cultured mammalian cells in 6 well plate (Corning, USA) were lysed in 100 µl of RIPA buffer (25 mM Tris-hydrochloride pH 7.6, 150 mM NaCl, 1 % NP-40, 1 % sodium deoxycholate, 0.1 % SDS) supplemented with phosphatase and protease inhibitors. Cells were lysed on ice for 15 minutes, collected into Eppendorf tubes and subjected to centrifugation at 13,000 rpm for 20 minutes at 4°C. After centrifugation, supernatants were transferred to new Eppendorf tubes and used for protein concentration determination.

2.7. Protein Concentration Determination

The concentration of proteins in the lysate was determined by using the BCA protein assay kit (Pierce) following the manufacturer's instructions. The assay is based on bicinchoninic acid (BCA) for colourimetric detection and quantification of total proteins.

2.8. SDS-PAGE and Western Blot

The protein samples (20-50 µg) were loaded on 8-12 % Sodium Dodecyl Sulphate-Polyacrylamide Gels and separated by gel electrophoresis. Following the separation, the protein samples were transferred onto a nitrocellulose membrane (Merck, Millipore) in an ice-cold transfer buffer (20 % methanol, 10 g/100 ml Tris-base (TB), and 70 % dH2O) at a constant voltage of 250 Amp for 120 minutes. The nitrocellulose transfer membrane was then blocked in either 5% dried skimmed milk or 5% bovine serum albumin (BSA, Fisher Scientific, USA) in 1x Tris-based buffered saline (TBS-T: 100 mM Tris-HCl, pH 7.5, 150 mM NaCl, 0.1 % v/v Tween 20, TBST) or PBS-T for one hour at room temperature, with gentle rocking. The membrane was incubated with the desired primary antibody overnight at 4 ^{o}C and then washed three times for 10 minutes each in 1 x TBS-T or PBS-T (Table 2.5). The membrane was then incubated with the appropriate secondary antibodies (DAKO) diluted in 5% non-fat dry skimmed milk or BSA in TBS-Tor PBS-T for 1h at room temperature with gentle rocking and washed again (Table 2.6). Proteins were detected using Immobilon Western Chemiluminescent HRP Substrate system (Millipore) and developed on GE Healthcare Amersham™ Hyperfilm™ ECL film using a Kodak SRX2000 (Rochester, NY, USA) developer machine.

Table 2.5 List of Primary antibodies used in the study.

PRIMARY ANTIBODY	COMPANY	APPLICATION
Anti-OPCML	R&D systems	IP/WB/IHC
Anti-HER2	Cell signaling	IP/WB
Anti-EGFR	Cell signaling	WB
Anti-EphA2	Cell signaling	WB
Anti-Axl	Cell signaling	IP/WB
Anti H-RYK	R&D systems	IP/WB
Anti-p-AKT	Cell signaling	WB
Anti-AKT	Cell signaling	WB
Anti-p-Tyrosine	R&D systems	IP/WB
Anti-ERK	Abcam	WB
Anti-pERK	Abcam	WB
Anti-IGFIR	Abcam	WB
Anti-p-IGFIR	R&D systems	WB
Anti-GAPDH	Cell signaling	IP/WB
Anti-caveolin-1	Cell signaling	WB
Anti-p-Her2	Cell signaling	WB
Anti-p-EGFR	Cell signaling	WB
Anti-p-Axl	Cell signaling	WB

Table 2.6 List of Secondary antibodies used in the study.

SECONDARY ANTIBODY	COMPANY	APPLICATION
Polyclonal Rabbit Anti-Goat	DAKO	IP/WB/IHC
Polyclonal Goat Anti-Mouse	DAKO	IP/WB/IHC
Polyclonal Goat Anti-Rabbit	DAKO	IP/WB/IHC

2.9. Immunofluorescence Confocal Microscopy

Coverslips with adherent monolayer cells were rinsed twice in PBS. Cells were fixed with ice-cold methanol for 5 minutes at -20°C and then washed three times with PBS. The cells were then blocked with 3 % Bovine serum albumin (BSA) in PBS for 30 minutes at room temperature and then incubated with the appropriate primary antibody diluted in 1% BSA at room temperature for 1 hour in a wet chamber. Once the incubation was complete, they were washed three times with PBS and incubated with a suitable secondary antibody at room temperature for 30 minutes. After that, they were washed three times with PBS, and the coverslips were mounted with a drop of Prolong gold 4', 6-diamidino-2- phenylindole (DAPI, Invitrogen, UK) and left to dry in the dark at room temperature overnight before being examined under a fluorescence microscope. Images were captured with an SP5 confocal microscope (Leica).

As an alternative method of fixation, 4 % PFA (Paraformaldehyde, Santa Cruz, USA) was used for 20 minutes, followed by quenching with 50 mM NH_4CL in PBS for 5 minutes and washed with Perm/Wash for 5 minutes (PBS, 2 % Foetal calve serum (FCS), and 0.05 % Saponin). Coverslips were next incubated with the desired primary antibody for 1 hour in wet chambers and, after three washes, with the appropriate secondary antibody for 30 minutes in wet chambers. Finally, coverslips were mounted on slides with mounting medium (ProLong™ Diamond Antifade Mountant with DAPI, Thermo Fisher Scientific, USA). Lastly, the slides were left to dry at room temperature before the observation by confocal microscope.

2.10. Co-Immunoprecipitation

Immunoprecipitation experiments were performed using a Pierce@ crosslink Immunoprecipitation kit protocol (Thermo-scientific) following the manufacturer's instructions. Briefly, 10µg of the antibody of interest were cross-linked to the resin; any unbound antibody was washed away by the elution buffer before using the resin for the actual IP. The eluted antigen was analysed with SDS-PAGE gel.

2.11. Proliferation Assay

To study cell proliferation, we used MTS-1 proliferation assay (Promega, USA) following the manufacturer protocol. We first did a pilot study by seeding different amount of cells in 96 well plates. Baseline readings were taken on the same day of the seeding as soon as the cells settled down, and at each time-point (6h, 24h, 48h, 72h, 96h) 10 µl of the MTS-1 solution was added to each 100 µl of cells, incubated for 1 hour at 37°C and absorbance was measured at 490 nm. Based on this experiment, we decided to use 2,000 cells per well in all subsequent experiments.

2.12. Lipid raft preparation (Detergent-resistant membranes, DRM)

Cells were grown in 2-3 x 100 mm or x 150 mm dishes and, when the cell confluency reached 80-90%, cells were washed once with PBS. Cells were then detached with either 1x Ethylenediaminetetraacetic acid (EDTA) without Trypsin or cell dissociation solution (Sigma, UK) and centrifuged at 3,000 rpm for 5 minutes. Cells were resuspended in cold PBS, centrifuged at 3,000 rpm for 5 minutes and then re-

suspended in 1 ml 20 mM Tris-HCl (pH 7.0) with complete protease (Roche, USA) and phosphatase inhibitors (Millipore Calbiochem, USA).

Samples were then incubated at 4°C on a rotator for 30 minutes. Samples were then centrifuged at 45,000 rpm for 1 hour at 4°C, and the pellet was resuspended in 1 ml of cold PBS (Total membrane fraction (TMF)) and re-centrifuged at 45,000 rpm for 30 minutes at 4°C. The pellet from this centrifugation step was resuspended in 150-200 µl (depending on the pellet size) in 1% Triton X-100/PBS, and the sample was then incubated at 4°C on a rotator for 30 minutes. After this, it was centrifuged at 45,000 rpm for 1 hour at 4°C. The supernatant was retained for analysis as the detergent soluble membrane (DSM) sample, and the pellet (detergent-resistant membranes, DRM) solubilised in 1% Sodium dodecyl sulphate (SDS) same volume as detergent soluble membrane.

2.13. Duolink (in situ Proximity Ligation Assay)

The Duolink kit (Olink, Sweden, distributed by Sigma Aldrich) was used for proximity ligation assays (PLA). Cells were seeded at 0.5x10^{4} cells per well on coverslips in 24-well plates and stimulated with Gas6 for the time indicated or left untreated. The cells were fixed and incubated with blocking buffer (3% BSA) for 30 minutes at room temperature and then incubated with the primary antibodies for 1 hour at room temperature. For the rest of the protocol, the manufacturer's protocol was followed. Briefly, the cells were washed with PBS three times and incubated with "plus" and "minus" PLA probes for one hour at 37°C in a humid chamber. Washes in Buffer A followed this, then the ligation reaction was carried out at 37°C for 30 minutes in a

humid chamber followed by further washes in Buffer A. The cells were then incubated with the amplification mix for 100 minutes at 37°C in an incubator. After washing twice with 1X Buffer B for 10 minutes followed by a 1-minute wash with 0.01X buffer B, the cells were mounted using the mounting media supplied with the kit.

The slides were then examined and observed using inverted Leica SP5 confocal microscope (Leica, Germany).

2.14. Wound healing assay

Cells were seeded in u-plate 24-well (Ibidi) using culture inserts (Ibidi) so that they would be completely confluent; they were let adhere and, if needed, serum-starved for 6 hours before the experiment. Membrane dye (Cell Mask™ Deep Red Plasma membrane Stain 1 µl per 3 ml of medium) was then added and removed after 45 minutes. Cells were then washed with PBS after the insert was removed and the well was filled with medium without serum supplemented with a specific ligand (rhGas6 400 ng/ml, rhFGF1 10 ng/ml) before placing the plate under the microscope.

The gap closure was monitored over a 15-hour period using inverted Leica SP5 confocal microscope (Leica, Germany) and the results were analysed using ImageJ.

2.15. Cell migration and invasion assays

Collective cell migration and invasion assays were performed using 8 μm pore PET Membrane chambers for 24-well plates (Corning, UK). The chambers for invasion were coated with Matrigel. SKOV3 and PEA1 cells expressing OPCMLWT, OPCML mutants and the empty vector were grown in full medium and then re-suspended in serum-free media when added to the chamber. 2.5 $X10^4$ cells/chamber were seeded in triplicate. Cells were allowed to migrate/invade for 24 hours in an incubator at 37°C 5 % CO_2, after which the cells that had not migrated/invaded were removed with a cotton tip from inside the chamber and the inserts washed in Phosphate-Buffered Saline (PBS). Cells that had migrated/invaded were fixed with ice-cold methanol and stained with 0.1% crystal violet in 25% methanol solution. At least six images were taken for each insert at 10× magnification using a Nikon Eclipse TE2000-U microscope and Q-Capture Pro software. Analysis and quantitation were performed using ImageJ.

2.16. Soft agar colony formation assay

Anchorage-independent growth was assessed by plating three densities of cells: 2, 4 and $8x10^3$ cells in 2 ml 0.6 % Difco Noble agar (Difco, USA) supplemented with 2X RPMI medium 10.4 gm/ 1L (Gibco, USA) and 1 gm / 1 L sodium bicarbonate (Fisher Scientific, USA) over a base of 1 % Nobel agar in 6-well plates (Corning, USA). Cells were allowed to grow for 2-4 weeks, during which time the media was replaced every week, and colonies were then stained by adding 0.015 % neutral red in PBS (Sigma Aldrich, USA) in PBS (Sigma Aldrich, USA) to the media and incubated overnight.

Images were captured by using TE2000-V inverted microscopes with a digital camera (Nikon, UK).

Average colony size and number was determined by measuring the area (in pixels) of each colony, with ImageJ software, from four random fields per condition. The data were obtained from three independent cultures, and each experiment was repeated in triplicate.

2.17. Spheroid formation assay

A spheroid formation assay was used to study 3D invasion *in vitro*. Briefly, 0.5×10^4 cells per 100 µl were seeded in full medium in 96-well ultra-low attachment plates and incubated at 37°C, 5 % CO_2 for five days to form spheroids. These were then serum starved for 24 hours and subsequently embedded in Matrigel (Matrigel 1: 1 serum-free medium contain cell) and incubated for further 24 hours with the desired treatment. Images were captured by using a TE2000-V inverted microscopes with a digital camera (Nikon, UK).

2.18. *In vitro* cell adhesion assay

The effect of OPCML mutants on cell adhesion to fibronectin, collagen I, collagen IV, laminin I and fibrinogen was evaluated using the CytoSelect cell adhesion assay (Cell Biolabs, USA). The assay was performed according to manufacturer's protocol. Concisely, SKOV3 cancer cell lines expressing OPCML-WT, OPCML mutants and the empty vector were suspended in serum-free media at a concentration of 1×10^6 cell/ml. A total of 150 µl (1.5×10^5 cells) was seeded into each well of a plate pre-coated with

different ECM proteins. The plate was incubated at 37 °C for 90 minutes, after which the wells were gently washed five times with PBS, followed by staining with cell stain solution (0.09% crystal violet) for 10 minutes at room temperature. Wells were then washed five times with deionised water, and the plate was left to dry before dissolving cells in 200 µl of cell extraction solution (10% acetic acid) on an orbital shaker for 10 minutes. 150 µl of each extract sample was finally transferred into a 96-well plate and the optical density (OD) was measured at 560 nm in a computer-interfaced 96- well tunable microtiter plate reader (OPTImax Molecular Devices).

2.19. R428 treatment and IC50 evaluation

Cells were seeded in 96 well plate at 5,000 cells / well and then left overnight in the incubator at 37°C, 5% CO_2. On the following day, cells were treated with different concentrations of the drug (Axl inhibitor, R428, Selleckchem). Each treatment was done in triplicate on the same plate. Cells with medium only were used as a control, and medium only without cells as plate background. The plate was then incubated for 48 h before evaluating cell viability using the CellTiter MTS cell proliferation assay (Promega, USA) as explained above. The experiment was repeated at least three times with a minimum of three replicates and IC50 values were calculated with the GraphPad Prism software (USA).

2.20. Apoptosis Assay

Cells were seeded in two 96 well plates at 5,000 cells / well and left overnight in the incubator at 37°C, 5% CO_2. One plate was used to assess the levels of apoptosis using the Caspase-Glo® 3/7 Assay (Promega, UK), which measures cleaved Caspase-3 and Caspase-7 activities, whereas the second plate was used to determine viable cells by MTS proliferation assay (Promega, USA). The assay was performed according to manufacturer's guidelines. Briefly, following drug treatment, an equal volume of Caspase-Glo® 3/7 reagent was added to each well and the plates were incubated for 1 hour at room temperature. Following Caspase-Glo® 3/7 reagent addition to the cells, cells release active caspase-3/7 that cleaves the tetra-peptide DEVD substrate releasing amino luciferin, which is oxidised by the luciferase, producing a luminescent signal that is proportional to the Caspase 3/7 activity. Luminescence was then measured using a LUMIstar OPTIMA microplate reader (BMG Labtech, UK).

2.21. Proteome profiler arrays

Tumour cell lines transduced with pLenti-OPCML mutants, pLenti-OPCML WT, or pLenti-empty vector were analysed to determine the relative phosphorylation levels of RTKs by using Proteome Profiler™ human phospho-RTK antibody arrays (R&D Systems). Cells were seeded in one 150 mm tissue culture dish, grown to 70 - 80 % confluence and then lysed. An equal amount of cell lysate (500 µg) was incubated with the membrane arrays overnight at 4°C. Phosphorylated receptor tyrosine kinases were detected by incubating the membranes with a mixture of pan anti-phospho-tyrosine antibodies conjugated with horseradish peroxidase, which were then detected with

chemiluminescent detection reagents. The expression of the specific phosphorylated protein was determined following quantification of scanned images by ImageJ.

2.22. In vivo work

The Imperial College Animal Welfare and Ethical Review Body (AWERB) and the Home Office London approved animal experiments under the project license number 70/7997 and personal license number I8DDEFD4D. Nine animals per group are required to detect a 20% or greater difference in tumour burden between wild-type OPCML, OPCML mutants and control groups with 90% at a significance level (alpha) of 0.05% (two tailed). For most of our experiments however, we are seeking to detect differences larger than 20% and therefore typically use no more than five animals per group.

All experiments were carried out in the appropriate designated facilities under animal welfare guidelines to minimise suffering, distress and pain.

2.23. Chick Embryo Chorioallantoic membrane (CAM) assay

Fertilized chicken eggs (Henry Stewart, UK) were cleaned with a tissue and incubated at 37.5^{o}C with 60 % relative humidity (kept constant throughout the experiment). The first day of incubation was considered as day 1 or an Embryonic day (ED) 1. On ED4, in aseptic conditions, a small hole was pierced through the pointed pole of the shell using a 19 G needle, and 2-3 ml of albumin were removed and discarded, while the hole was covered with transparent film dressing (Premier healthcare excellence, UK). A semipermeable transparent sterile film was then placed on the eggshell, and another hole was pierced on the side of eggshell near the pointed

pole of the eggshell using a 19 G needle, while sharp angled scissors were used to cut a 1-2 cm-wide window through the eggshell to expose the CAM. The window was covered with sterile transparent film. On ED9, the membranes were ready for grafting. The graft was prepared by suspending SKOV cells in Matrigel (BD Biosciences, USA) at a final concentration of 1 x 10^6 / 50 µL. These cells had been previously transduced with GFP and either pLenti-OPCML mutants, pLenti-OPCML wild-type, or pLenti-Empty vector. A large blood vessel was then bruised using a 150 mm glass sterile rod, 25 µl of the prepared graft, containing 0.5x10^6 cells in Matrigel, were then initially inoculated onto this area and after a short while other 25 µl of the prepared graft was added to the same area. After inoculation, the window was closed with transparent sterile film and incubated in the incubator at 37.5ºC, 60 % relative humidity. Tumour growth and viability of the embryos were monitored daily. At ED15, photos were taken to measure tumour fluorescence and size using the stereomicroscope SteREO Discovery.V8 (Zeiss, Germany) with the Zen 2 Capture software (Zeiss, Germany). Then eggs were terminated by refrigeration for >4 hours and death was confirmed by decapitation. Tumours were excised, washed with PBS and placed in 4% PFA in PBS for 24 hours and embedded in paraffin.

2.24. *In vivo* mouse model

Five mice in each arm were used (six eight-week old athymic nude female mice) (Charles River Laboratories, UK) and they were inoculated intraperitoneally with 200 µL of PBS containing 5x10^6 SKOV-3 cells transduced with either pLenti-OPCML mutants, pLenti-OPCML WT or pLenti-Empty vector virus. The mice were controlled and

monitored carefully for signs of distress, pain and suffering, weight loss and behavioural changes. Joel Abrahams injected the mice intraperitoneally, while Dr. Chiara Recchi monitored, culled and dissected the mice.

2.25. Immunohistochemistry

Tumours grown in eggs or mice were fixed, embedded in paraffin and sections of 5 µm thickness were cut using a Leica RM 2135 Microtome (Leica, Germany) with a MX35 microtome blade (Thermo scientific, USA). Paraffin-embedded sections were then dewaxed and rehydrated in sequential steps in xylene and ethanol solutions (100-30 %) and lastly with water before proceeding with immunodetection. Antigen retrieval was done for 40 minutes at 80°C in 10 mM citrate buffer, pH 6. Samples were blocked with blocking solution (3% normal goat serum (Sigma Aldrich, USA), 0.5 % Triton in 1X TBS) for 1 hour at room temperature. Primary antibodies were diluted in diluting solution (1X TBS, 0.1% Triton, 3% normal goat serum) and incubated at 4°C overnight. Secondary antibodies were diluted in diluting solution and incubated for 2 hours at 37°C. Then, samples were washed and mounted with DAPI, covered with a coverslip that was fixed with nail polish. Sections were observed under an inverted Leica SP5 confocal microscope (Leica, Germany), and results were analysed using ImageJ.

2.26. Data analysis

Data were analysed using GraphPad Prism software (USA) unless stated otherwise. Images were compiled in Image J. Results are presented as mean +/-SEM unless otherwise indicated. Statistical analysis was performed with two-tailed student's T-test, one-way ANOVA, and two way ANOVA analysis using Prism 7 with Bonferroni correction as appropriate. A p-value <0.05 was considered significant.

3. CHAPTER 3

Mapping *OPCML* mutations on the crystal structure

Introduction

Somatic mutations occur during replication as a result of DNA duplication errors or through exposure to mutagens. In general, somatic mutations can be divided into two classes: driver mutations and passenger mutations (Greenman et al., 2007).

The majority of somatic mutations are passenger mutations, which are biologically neutral and do not alter growth properties. Conversely, the minority are the biologically active driver mutations that alter and affect the cancer characteristics of cells such as their proliferation, adhesion, invasion and migration. Hence, they play a role in cancer development and are considered valuable targets for drug discovery (Greenman et al., 2007; Chin & Gray, 2008; Chin et al., 2011).

Ovarian cancer is the most lethal gynaecological malignancy caused mainly by a loss of tumour suppressor gene (TSG) function (Bowtell et al., 2015). *OPCML* is a TSG that is frequently inactivated by methylation in ovarian cancer and also in many other tumour types including colorectal, gastric, nasopharyngeal, liver, oesophageal, breast, lung, prostate, cervix cancer and lymphomas (Sellar et al., 2003; Cui et al., 2008). Interestingly, here we could ascertain that, in a limited number of cancer patients, OPCML presents point somatic mutations, some of which are recurrent across different tumour types.

To fully recognise the potential role of these mutations, we were able to crystallise and solve the structure of OPCML through a collaboration with the University of Massachusetts. We have then mapped the mutations on the crystal structure.

Aim of this chapter

The aim of this chapter is to identify the OPCML mutations found in cancer patients and to map them onto the crystal structure in order to understand their role in ovarian cancer. In this way, we can broaden our knowledge of the function of OPCML so it can be used for potential target therapy.

In brief, the aims are:

1. To identify OPCML mutations using The Cancer Genome Atlas (TCGA) and the Catalogue of Somatic Mutations in Cancer (COSMIC);
2. To reveal the crystal structure of OPCML through a collaboration with J. Birtley at the University of Massachusetts Medical School.

In this chapter, the mutation frequency in different tissue types, the distribution of the mutated residues and of relatively critical sites in the protein domains and their possible functional impact will be discussed.

3.1. TCGA and COSMIC database

In this study, I initially performed a mutational analysis to predict the functional impact of OPCML mutations. To this end, 162 OPCML mutations were identified from the TCGA and COSMIC database that were distributed across all cancer types (Figure 3.1). The frequency of OPCML mutations found in colorectal cancer, skin and lung cancer over the total number of mutations identified is 20.2%, 15%, and 12.9%, respectively, which represents 50% of the total number of OPCML mutations.

We identified that OPCML and OPCML mutants in TCGA database are expressed and their expression ranges widely in several tumour types (Figure 9.2).

Generally, the frequency of these clinical mutations is uncommon, ranging from 5.5% in melanoma and 3.3% in gastric cancer to around 0.1% in cancers such as breast and brain (figure 3.1B).

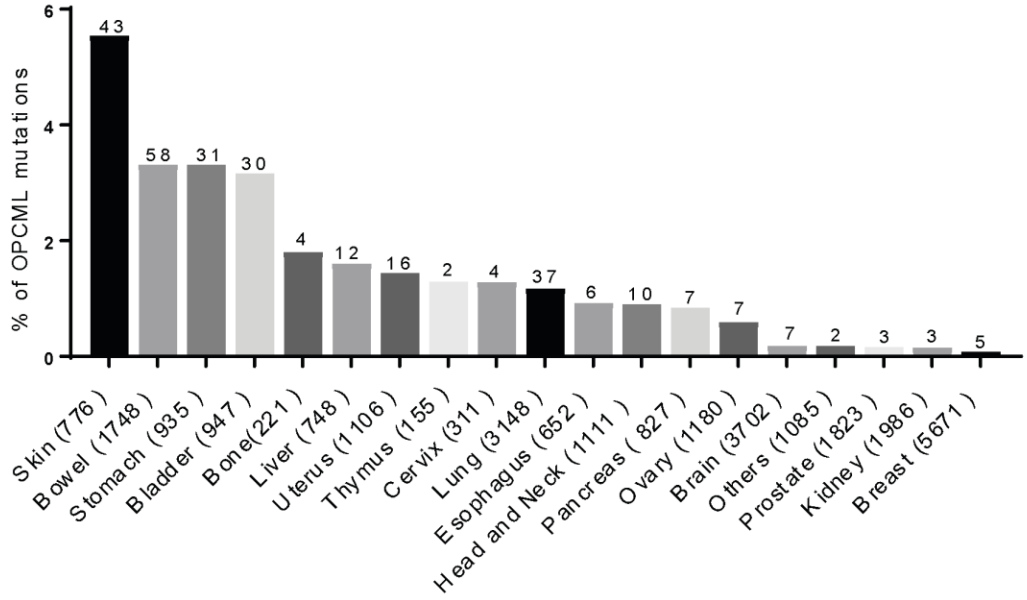
We have identified a number of potentially interesting OPCML and OPCML mutants SNP variants that need further investigation. We tried in our analysis to show the summary of OPCML SNPs identified in public GWAS database, which shows the association between OPCML and SNPs and also with some of the selected OPCML mutants. It is difficult to assume that any variant has any impact on the gene or not unless further analysis of the results is performed. Transcript variants within an intron may possibly regulate genes, which might affect alternative splicing of the mRNA, but could also be relevant as enhancers and possibly enhance the expression of many genes. To establish this it would be necessary to analyse the predicted protein binding sites and see if there is any differential binding for a specific protein (Figure 9.3).

Given the large number of mutations, in the absence of structural information on OPCML, it was difficult to predict which of these missense mutations give rise to proteins that are expressed and folded correctly and which could be destabilizing and lead to folding defects that could cause OPCML degradation. Mutant proteins able to reach the membrane could be particularly informative, especially if their phenotypic effect was a result of failure to interact correctly with an identified cognate binding partner.

A

DATA	TCGA	COSMIC
Nonsense substitution	0	8
Missense substitution	211	172
Synonymous substitution	0	68
Truncating	22	0
Frameshift insertion	0	1
Frame shift deletion	0	3
Complex mutation	0	1
Others	3	2
Total	236	258

B



C

	N-term	*D1*	*D2*	*D3*	*C-term*	*Total*
Residue numbers	1-41	42-134	135-222	223-314	315-345	345
Number of residues	41	93	88	92	31	345
% of OPCML	11.9	26.9	25.5	26.7	9.0	100
Total number of mutations	23	111	67	65	21	287
Total % of mutations	8.0	38.7	23.3	22.6	7.3	100
Actual positions mutated	11	40	24	34	9	118
% of positions mutated	9.3	33.9	20.3	28.8	7.6	100

Figure 3.1 OPCML is mutated in different tumour types according to the TCGA and COSMIC database.

A. Table summarizing the mutations found in TCGA and COSMIC. These mutations are divided into nonsense, missense, synonymous, and frameshift.
B. Bar chart showing OPCML is mutated in different tumour types. The graph shows the percentage of patients who present mutations in the OPCML gene (y-axis) classified per cancer type. The numbers in brackets on the x-axis indicate the total number of patients for each cancer type, while the number above the bars show the actual number of patients who have mutations.
C. The table indicates the actual number and the relative percentage of the residues present in OPCML, the mutations identified in the databases and the amino acids mutated in the different domains of OPCML. Table summarizing the residual number in each domain, number of residual in each domain, percentage of OPCML mutations, total number of mutations, total percentage of mutations, the actual positions mutated, and the percentage of position mutated.

3.2. OPCML crystal structure

In order to establish the role of these mutations and to understand the molecular basis for OPCML's role as a tumour suppressor, the crystal structure of OPCML was resolved in collaboration with Dr J. Birtley from the University of Massachusetts Medical School.

The soluble recombinant OPCML was crystallized, and its structure determined using a combined single-wavelength anomalous dispersion/molecular replacement approach, followed by rounds of automated and manual model building and refinement. The crystal structure of the OPCML protein was determined by X-ray diffraction at 2.65 Å. In that way, 274 of the 286 residues in the mature OPCML protein could be visualized in the crystal structure. There are six potential N-linked glycosylation sites in OPCML (asparagine at positions 44, 70, 140, 285, 293 and 306). An electron density, consistent with glycosylation, was observed at asparagine residues 70, 293 and 306 and glycans were modelled at these positions. OPCML consists of three immunoglobulin domains (D1–D3), connected by shortly extended linkers, that homodimerise via a network of D1–D1 contacts and a buried N-linked glycosylation at asparagine at position 70 (Figure 3.2). The Primary and the secondary of OPCML structure showed (Figure 3.3) with domains boundary residue in domain I (42-134), domain II (135-222), and domain III (223-314).

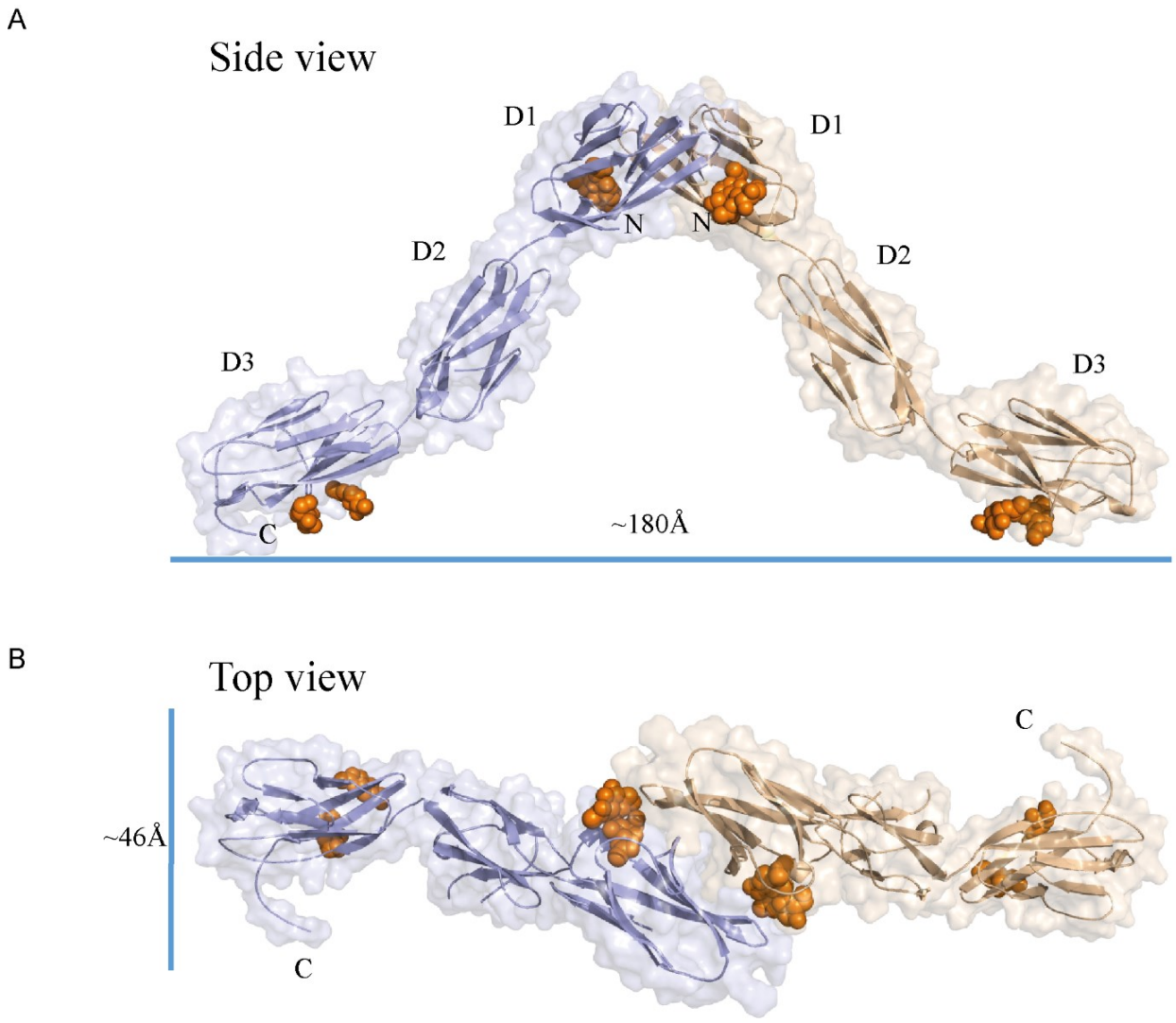


Figure 3.2 Crystal structure of the OPCML homodimer.

Ribbon representation illustrating the dimeric architecture (A, side view and B, top view) with transparent spheres. D1–D1 contacts mediate the dimerization interface. One monomer is coloured blue, and the other is wheat-coloured. N-linked glycosylations (on asparagine at positions 70, 293 and 306) are shown as orange spheres. The N- and C-termini are indicated on the structure, and the experiment was performed by Dr J. Birtely at the University of Massachusetts.

A

DOMAIN I

```
GCT ATG GAC AAC GTG ACG GTC CGG CAG GGG GAG AGC GCC ACC CTC AGG TGT ACC ATA GAT   180
 A   M   D   N   V   T   V   R   Q   G   E   S   A   T   L   R   C   T   I   D    60

GAC CGG GTA ACC CGG GTG GCC TGG CTA AAC CGC AGC ACC ATC CTC TAC GCT GGG AAT GAC   240
 D   R   V   T   R   V   A   W   L   N   R   S   T   I   L   Y   A   G   N   D    80

AAG TGG TCC ATA GAC CCT CGT GTG ATC ATC CTG GTC AAT ACA CCA ACC CAG TAC AGC ATC   300
 K   W   S   I   D   P   R   V   I   I   L   V   N   T   P   T   Q   Y   S   I   100

ATG ATC CAA AAT GTG GAT GTG TAT GAC GAA GGT CCG TAC ACC TGC TCT GTG CAG ACA GAC   360
 M   I   Q   N   V   D   V   Y   D   E   G   P   Y   T   C   S   V   Q   T   D   120

AAT CAT CCC AAA ACG TCC CGG GTT CAC CTA ATA GTG CAA GTT                           420
 N   H   P   K   T   S   R   V   H   L   I   V   Q   V                         140
```

DOMAIN II

```
                                                        CCT CCT CAG ATC ATG AAT   420
                                                          P   P   Q   I   M   N   140

ATC TCC TCA GAC ATC ACT GTG AAT GAG GGA AGC AGT GTG ACC CTG CTG TGT CTT GCT ATT   480
 I   S   S   D   I   T   V   N   E   G   S   S   V   T   L   L   C   L   A   I   160

GGC AGA CCA GAG CCA ACT GTG ACA TGG AGA CAC CTG TCA GTC AAG GAA GGC CAG GGC TTT   540
 G   R   P   E   P   T   V   T   W   R   H   L   S   V   K   E   G   Q   G   F   180

GTA AGT GAG GAT GAG TAC CTG GAG ATC TCT GAC ATC AAG CGA GAC CAG TCC GGG GAG TAC   600
 V   S   E   D   E   Y   L   E   I   S   D   I   K   R   D   Q   S   G   E   Y   200

GAA TGC AGC GCG TTG AAC GAT GTC GCT GCG CCC GAT GTG CGG AAA GTA AAA ATC ACT GTA   660
 E   C   S   A   L   N   D   V   A   A   P   D   V   R   K   V   K   I   T   V   220

AAC TAT                                                                          720
 N   Y                                                                           240
```

DOMAIN III

```
                                                        CCT CCC TAT ATC TCA AAA GCC AAG AAC ACT GGT GTT TCA GTC GGT CAG AAG GGC   720
                                                          P   P   Y   I   S   K   A   K   N   T   G   V   S   V   G   Q   K   G   240

ATC CTG AGC TGT GAA GCC TCT GCA GTC CCC ATG GCT GAA TTC CAG TGG TTC AAG GAA GAA   780
 I   L   S   C   E   A   S   A   V   P   M   A   E   F   Q   W   F   K   E   E   260

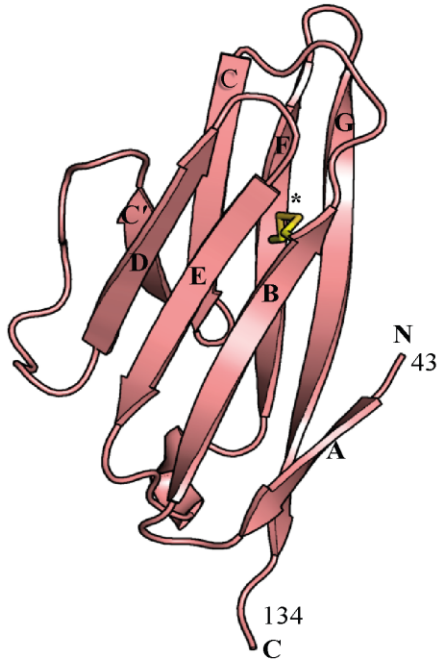
ACC AGG TTA GCC ACT GGT CTG GAT GGA ATG AGG ATT GAA AAC AAA GGC CGC ATG TCC ACT   840
 T   R   L   A   T   G   L   D   G   M   R   I   E   N   K   G   R   M   S   T   280

CTG ACT TTC TTC AAT GTT TCA GAA AAG GAT TAT GGG AAC TAT ACT TGT GTG GCC ACG AAC   900
 L   T   F   F   N   V   S   E   K   D   Y   G   N   Y   T   C   V   A   T   N   300

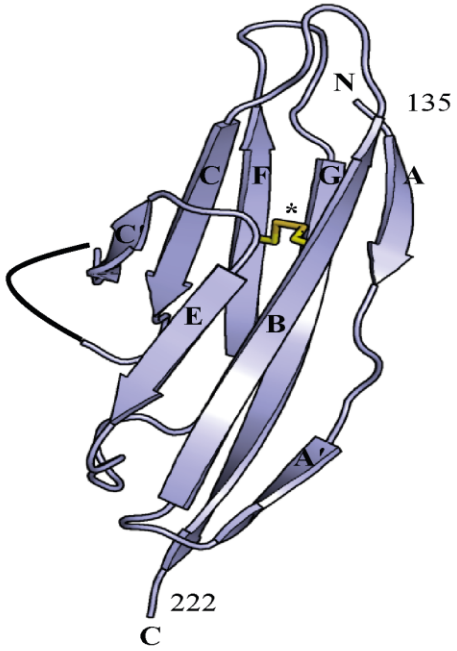
AAG CTT GGG AAC ACC AAT GCC AGC ATC ACA TTG TAT GGG CCT                           960
 K   L   G   N   T   N   A   S   I   T   L   Y   G   P                         320
```

B

DOMAIN I



DOMAIN II



DOMAIN III

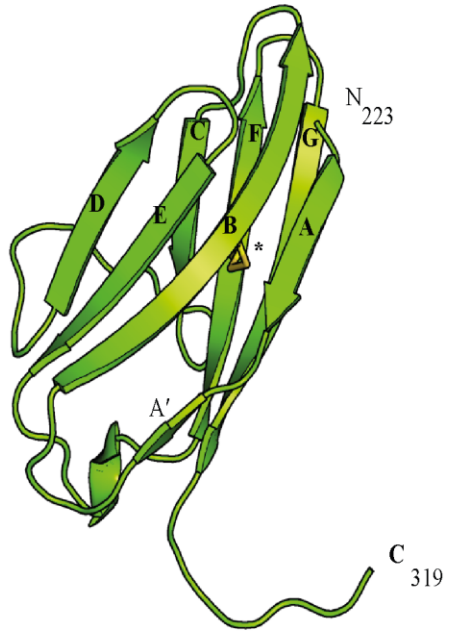


Figure 3.3 The primary and secondary structure of OPCML.

A. The figure shows the sequence of human OPCML domains (UniProt entry Q14982).

B. Ribbon diagrams of domains 1, 2 and 3 from OPCML. Domain 1, shown in salmon, belongs to the V-set subfamily of Ig domains and consists of nine β-strands. The AGFCC′ forms one sheet and BED the other. Strand A is displaced somewhat, the C-terminal end of the protein (residues 315-9, not shown) inserts between the B and G strands to make crystal contacts. Domain 2 (blue) is an I2-set Ig domain; strand D is absent. The loop between the C and C' strands (residues 175-179) is missing due to disorder and is shown as a dashed black line. Domain 3 (green) exhibits an I1-set topology (Harpaz & Chothia, 1994) with two β-sheets, ABED and A′GFC. The A–A′ segmented β-strand, crosses over between B and G respectively. Disulfide bridges connect all B and F strands and are indicated (*). The N- and C- termini are indicated and are numbered. Casanova reference inside Diedrich reference.

3.3. OPCML mutations mapped onto OPCML's crystal structure

To understand the clinical significance of the OPCML mutations found in cancer patients, these were mapped onto the crystal structure (Figure 3.4), and their possible effect on OPCML structure and function was hypothesised. Many of these mutations could potentially lead to folding defects and instability of the OPCML protein. Eleven such substitutions were found at the N-terminal secretion signal, 9 mutations at C-terminal GPI anchor site, 40 mutations in domain I, 24 mutations in domain II, and 34 mutations in domain III.

In order to assess the functional significance of these mutations, TCGA and COSMIC dataset and crystal structure were used. In order to understand the impact of these clinical mutations on the tumour suppressor properties of OPCML, we selected a panel of representative mutations, including residues at dimerization interfaces, glycosylation sites, and exposed residues localized in the aforementioned patches.

Using both the data from COSMIC and TCGA, overall mutation numbers were determined for OPCML at 118 mutations. We observed 33.9% (40/118) of missense mutations in domain I, 20.3% (24/118) in domain II, and 28.8% (34/118) in domain III.

Several of the mutations identified are expressed in several cancer type (Figure 9.2), the data from TCGA show that the OPCML expression varies depending on the tumour type.

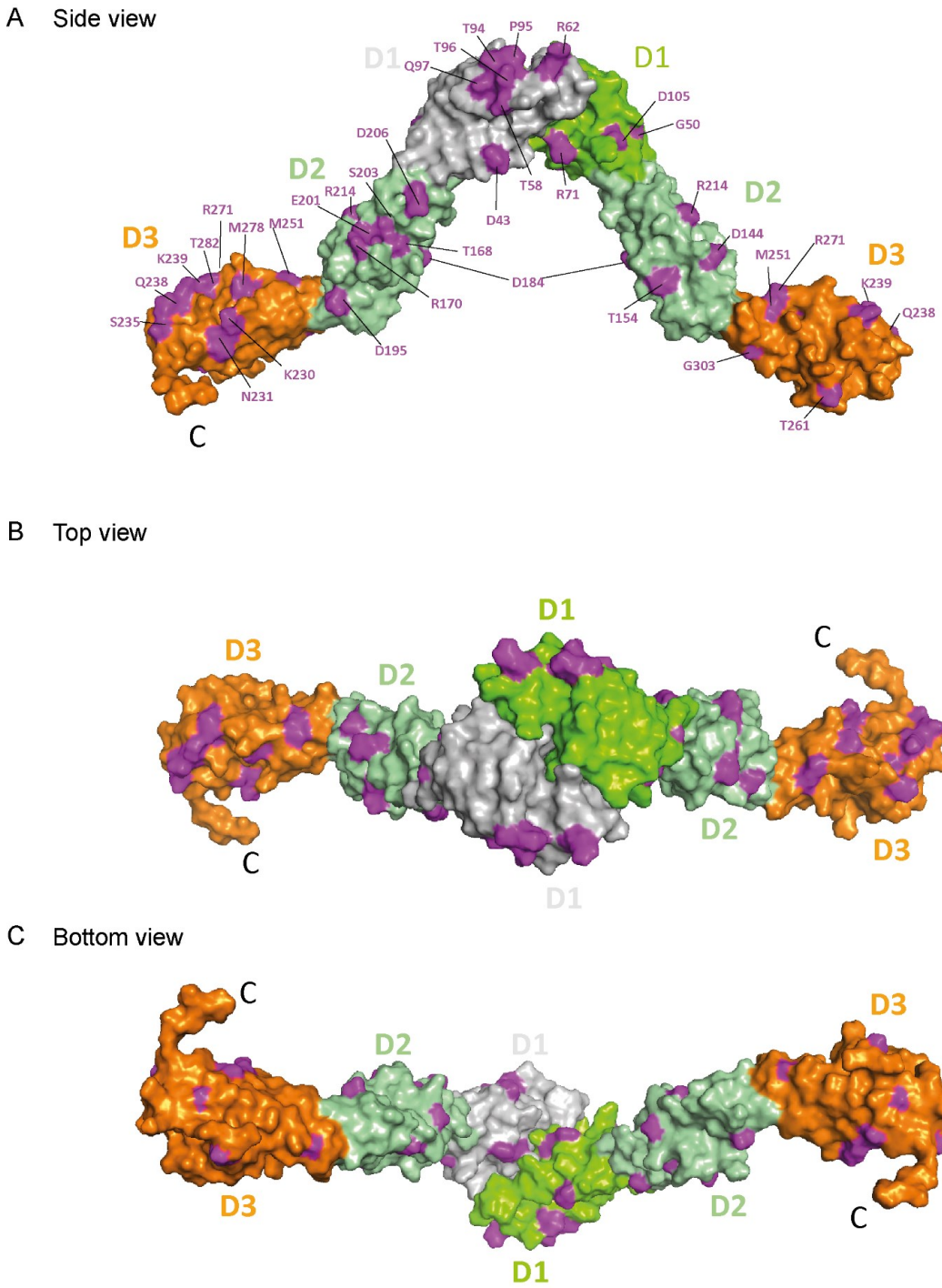


Figure 3.4 Mutational analysis of OPCML.

Three different views (A, side view; B, top view; and C, bottom view) of OPCML's crystal structure show the mutations identified through the TCGA and COSMIC dataset. The light grey, light green and orange colours represent the three domains of OPCML. The pink colour shows the sites of the mutations in the crystal structure.

3.4. Summary of the findings

Overall, 118 missense mutations were identified in OPCML using the TCGA and COSMIC dataset; the mutations in OPCML were also mapped across the identified crystal structure, and the clinical mutations were found to fall into particular classes such as a mutation in the domain I, domain II, and domain III. In conclusion, I propose a model where rare somatic missense mutations promote cancer's progression through the inactivation of this potent TSG, revealing clinically important structural features of OPCML.

4. CHAPTER 4

Role of OPCML domain I mutations

Introduction

Loss of expression of OPMCL in human tissues has been associated with tumorigenesis and cancer progression, while OPCML re-expression in cancer cells reduces proliferation, enhances intercellular attachment, and abolishes both subcutaneous and intraperitoneal tumorigenicity *in vivo* (Sellar et al.; McKie et al., 2012). However, the role of clinical OPCML mutations is still elusive and understanding how they affect OPCML function will help us to understand the mechanism of tumour suppression in terms of which part of OPCML is essential for the function of the protein.

Objective: To delineate the role of OPCML mutants in domain I in ovarian cancer development and progression.

1. Generate ovarian cancer cell lines (SKOV3, PEA1, PEO1) overexpressing OPCML mutants, OPCML wild type, and control (empty vector , CTRL).
2. Investigate the localisation of OPCML mutants compared to OPCML wild-type.
3. Analyse the effect of OPCML mutants in phenotypic assays such as cell proliferation, cell adhesion, anchorage-independent cellular growth, invasion, and migration.
4. Study the RTKs-OPCML interaction focussing mainly on the RTKs AXL and FGFR1.
5. Investigate the effects of the mutations in a target therapy context by using an AXL inhibitor as an example of targeted therapy.
6. Investigate the role of OPCML mutants in both *in vivo* and *in ovo* assays.

4.1. Identification of OPCML mutations in domain I using public data from TCGA and COSMIC and mapping into the newly discovered OPCML crystal structure.

The present study aimed to use TCGA and COSMIC datasets in conjunction with the OPCML crystal structure to identify the OPCML mutants in domain I that could be impairing OPCML function.

The analysis revealed that in a few patients (111 out of 28,132) distributed across all cancer types, OPCML presented point mutations in domain I. We identified 40 OPCML domain I mutations in these patients and we arranged them into particular classes based on mutation type and location. The mutations in OPCML domain I represent 38.7% of all the patients with a mutated OPCML, compared to domain II and III, which have 23.3% and 22.6% respectively. The amino acid length of domain I is relatively similar to domain II, and III (92, 87, and 91 amino acids respectively), which may reflect the importance of domain I mutations.

The knowledge of the OPCML structure enhances the understanding of the potential effect of a mutation associated with OPCML. Importantly, the structure presented here should allow us to predict the effect of potential OPCML mutations on its tumour suppressor function. The mutations were mapped onto the crystal structure (Figure 4.1 A). Figure 4.1 B shows all the mutations observed in domain I and their frequency.

We selected some mutations based on their frequency, occurrence in several tumours and possible impact on the functionality of the protein. We selected six mutations, namely OPCML R65L, OPCML N70H, OPCML R71C, OPCML P95R, OPCML P95L, and OPCML P95S.

The first mutation, R65L, changes the arginine residue in position 65 into leucine; it occurs exclusively in lung adenocarcinoma, but the three-dimensional molecular structure suggests that this mutant could change dimer interface interactions, which may affect the dimer stability of the protein and consequently have an effect on the folding of the mutated protein.

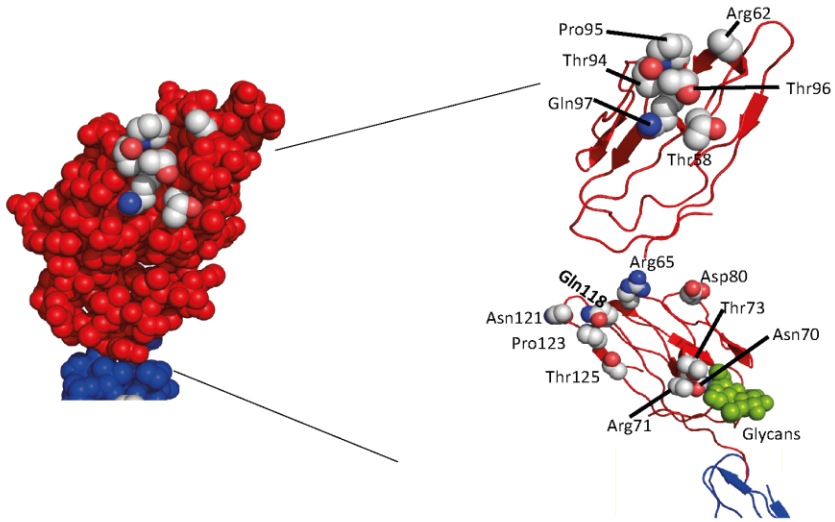
The second mutation, N70H, changes the asparagine residue in position 70 into histidine. This mutation is found in melanoma and causes a structure modification by disrupting a glycan site and possibly the dimer interface, which could be necessary for proper protein folding.

The third mutation, R71C, changes the arginine residue in position 71 into cysteine; interestingly, another mutation was identified in position 71 which changes the arginine residue into histidine. R71C, though, occurs in three different types of tumours, namely uterine, colorectal, and melanoma and we decided to focus on this mutation rather than the R71H. The three-dimensional molecular structure showed that this mutant could disrupt the dimer interface and be liable for oxidation.

The mutations in position 95, P95R, P95L and P95S, change the proline residue into arginine, leucine and serine respectively. They occur in three different types of tumours, namely ovarian, kidney, and bladder respectively. Mutations at this residue might cause the disruption of a β–turn and hinder protein folding modification related to the crystal structure. Our group previously showed that the P95R mutation, identified in primary ovarian cancer, behaved like OPCML wild-type (WT) in cell growth *in vivo* and *in vitro* but caused loss of aggregation in cells overexpressing the mutated protein (Sellar et al., 2003).

The Figure 4.1 C presents a summary of the mutations used in this study, giving their positions, the amino acid changed, the cancer type, and their possible impact on the crystal structure.

A



DOMAIN I

```
GCT ATG GAC AAC GTG ACG GTC CGG CAG GGG GAG AGC GCC ACC CTC AGG TGT ACC ATA GAT   180
 A   M   D   N   V   T   V   R   Q   G   E   S   A   T   L   R   C   T   I   D   60

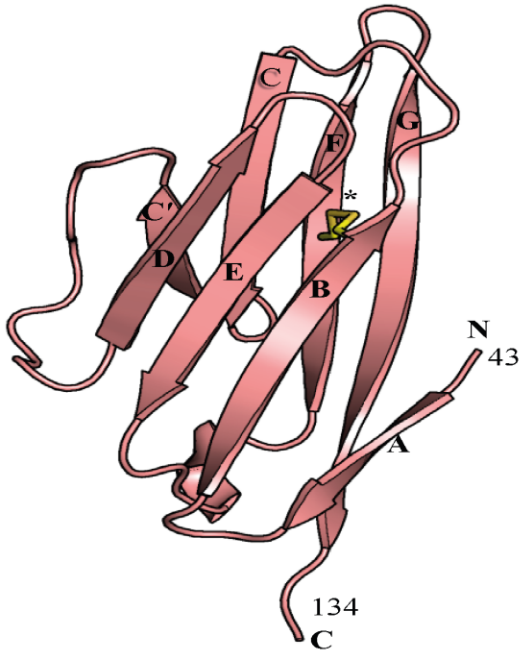
GAC CGG GTA ACC CGG GTG GCC TGG CTA AAC CGC AGC ACC ATC CTC TAC GCT GGG AAT GAC   240
 D   R   V   T   R   V   A   W   L   N   R   S   T   I   L   Y   A   G   N   D   80

AAG TGG TCC ATA GAC CCT CGT GTG ATC ATC CTG GTC AAT ACA CCA ACC CAG TAC AGC ATC   300
 K   W   S   I   D   P   R   V   I   I   L   V   N   T   P   T   Q   Y   S   I   100

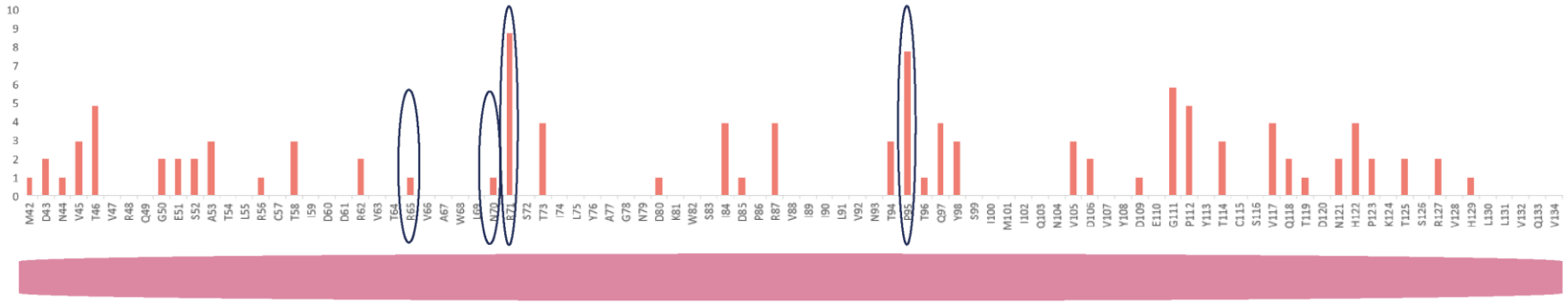
ATG ATC CAA AAT GTG GAT GTG TAT GAC GAA GGT CCG TAC ACC TGC TCT GTG CAG ACA GAC   360
 M   I   Q   N   V   D   V   Y   D   E   G   P   Y   T   C   S   V   Q   T   D   120

AAT CAT CCC AAA ACG TCC CGG GTT CAC CTA ATA GTG CAA GTT                           420
 N   H   P   K   T   S   R   V   H   L   I   V   Q   V                           140
```

DOMAIN I



B



C

Position	Cancer type	AA changed	Frequency	Modification
R65	Lung	L	1	Disrupts dimer interface
N70	Skin	H	1	Disrupts dimer interface - Glycan site
R71	Colorectal, Uterine, and Skin	C	7	Disrupts dimer interface/Exposed - liable to oxidation
	Colorectal, and Brain	H	2	Disrupts dimer interface/Exposed - liable to oxidation
P95	Ovary	R	1	Surface exposed
P95	Kidney	L	3	Surface exposed
P95	Bladder	S	4	Surface exposed

Figure 4.1 Crystal structure of OPCML with domain I mutations mapped.

A. Mutations mapped on the tertiary structure of OPCML. The right upper panel shows the sequence of human OPCML domain I with the position of the selected OPCML mutants coloured in pink. The right lower panel shows ribbon diagrams of domains I in salmon, it belongs to the V-set subfamily of Ig domains and consists of nine β-strands. Disulfide bridges connect all B and F strands and are indicated (*). The N- and C- termini are indicated and are numbered. Casanova reference inside Diedrich reference.
B. Among all mutations observed in OPCML domain I in this study, the mutations to the domain I that were chosen are encircled.
C. Summary table of the chosen domain I mutations, giving the mutation's position, cancer type, amino acid changed, and the possible modification of the crystal structure.

4.2. Creation and characterisation of ovarian cancer cell lines stably expressing OPCML mutants.

To understand the biological role of the OPCML domain I mutations and characterise these mutations in *vivo*, three ovarian cancer cell lines (SKOV3, PEA1, and PEO1) were initially selected for the creation of stable cell lines expressing OPCML wild-type, mutants, or empty vector. Our constructs were verified by sequencing before creating the viruses used to transduce the different ovarian cancer cell lines.

OPCML expression was confirmed by Western Blot analysis, where OPCML could be visualised at 55 kDa in all the transduced cell lines except in the control (CTRL) (Figure 4.2 A, left panel for cell line SKOV3; Figure 4.2 B, left panel for cell line PEA1; Figure 4.2 C, left panel for cell line PEO1).

Quantification of the Western Blot showed no statistical differences between wild-type OPCML expression and that of OPCML mutants for the three cell line SKOV3, PEA1, and PEO1 (Figure 4.2 A, right panel for cell line SKOV3; Figure 4.2 B, right panel for cell line PEA1; Figure 4.2 C, right panel for cell line PEO1).

Immunofluorescence was then employed to assess the expression and localisation of OPCML in the cells. By using an antibody against OPCML, we confirmed that the wild-type and all the mutant OPCMLs were expressed in transduced SKOV3, PEA1, and PEO1 cell lines (Figure 4.2 A, lower panel for cell line SKOV3; Figure 4.2 B, lower panel for cell line PEA1; Figure 4.2 C, lower panel for cell line PEO1).

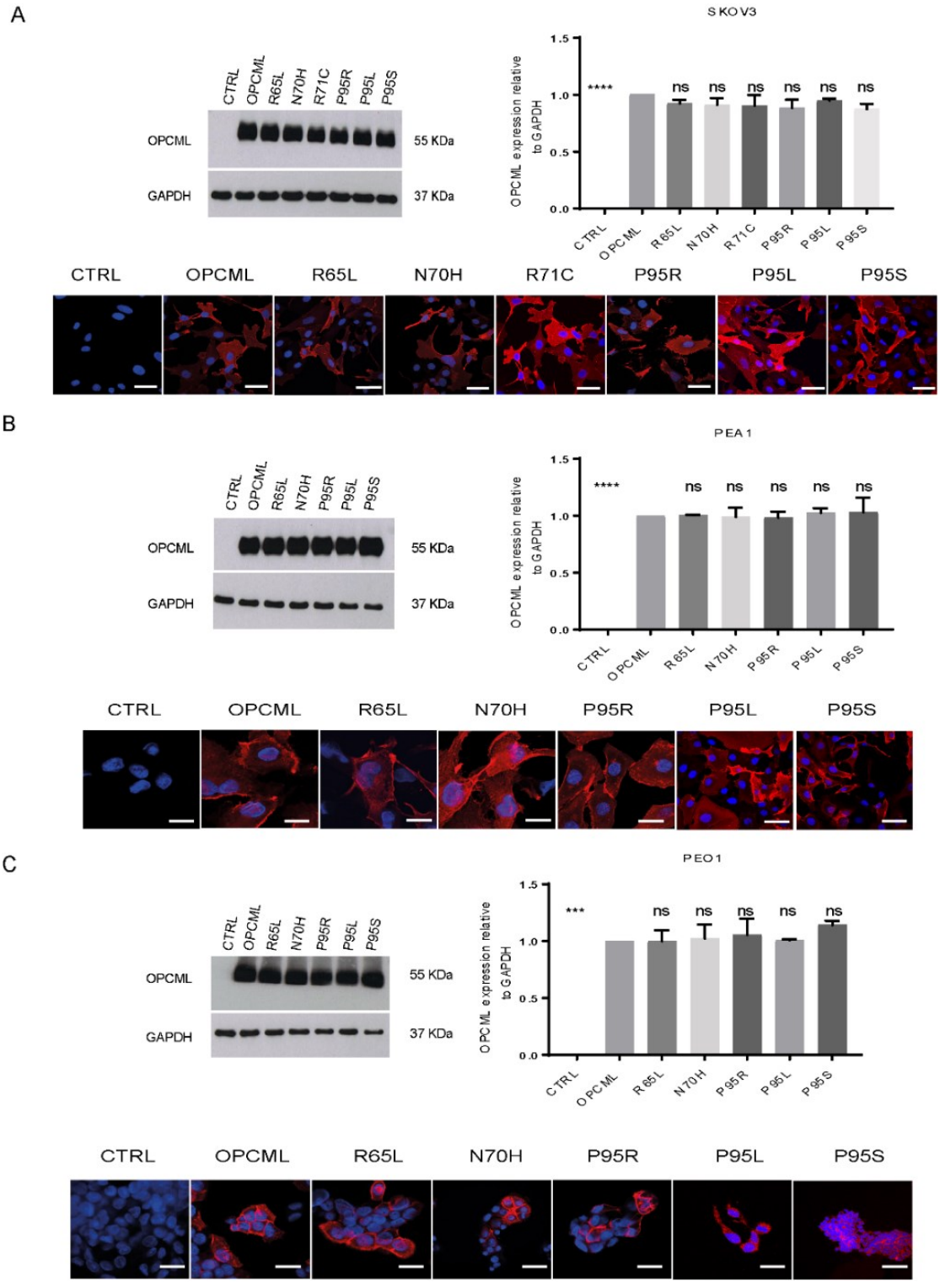

A
SKOV3
CTRL
OPCML
R65L
N70H
R71C
P95R
P95L
P95S
OPCML
GAPDH
55 KDa
37 KDa
OPCML expression relative to GAPDH
****
ns
B
PEA1
***
C
PEO1

Figure 4.2 OPCML mutants in domain I expressed in ovarian cancer cell lines.

Upper panels: Western Blot analysis showing in the left panel OPCML expression in stably transduced with wild-type OPCML or OPCML mutants compared to cell lines stably transduced with an empty vector as control (CTRL). GAPDH was used as loading control. A bar chart of the results of Western Blot analysis is shown in the right panel. The difference in expression between wild-type OPCML and OPCML mutants was statistically non-significant, but compared to the control it was very significant (n = 3; mean ± SEM; **** P < 0.00001; ns, not significant). (A) SKOV3; (B) PEA1; (C) PEO1.

Lower panels: Immunofluorescence microscopy reveals that OPCML is expressed in the cell lines (red colour); the nucleus is shown in blue. The images show OPCMLR65L, OPCMLN70H, OPCMLR71C, OPCMLP95R, OPCMLP95L and OPCMLP95S, expression compared to wild-type OPCML and control in stably transduced SKOV3 cell lines (scale bar, 20 μm). (A) SKOV3; (B) PEA1; (C) PEO1.

4.3. The localisation of OPCML mutants in domain I and OPCML wild-type in the cell membrane.

OPCML is a GPI-anchored protein, and as such, it is localised to the cell membrane (McKie et al., 2012). To confirm that the mutations do not affect the localisation of the OPCML protein, immunofluorescence was then employed to assess this.

By using an antibody against OPCML, we confirmed that the wild-type and mutants were all positioned on the cell plasma membrane and that the amino acid substitutions did not affect this position in all three the cell lines used (Figure 4.3).

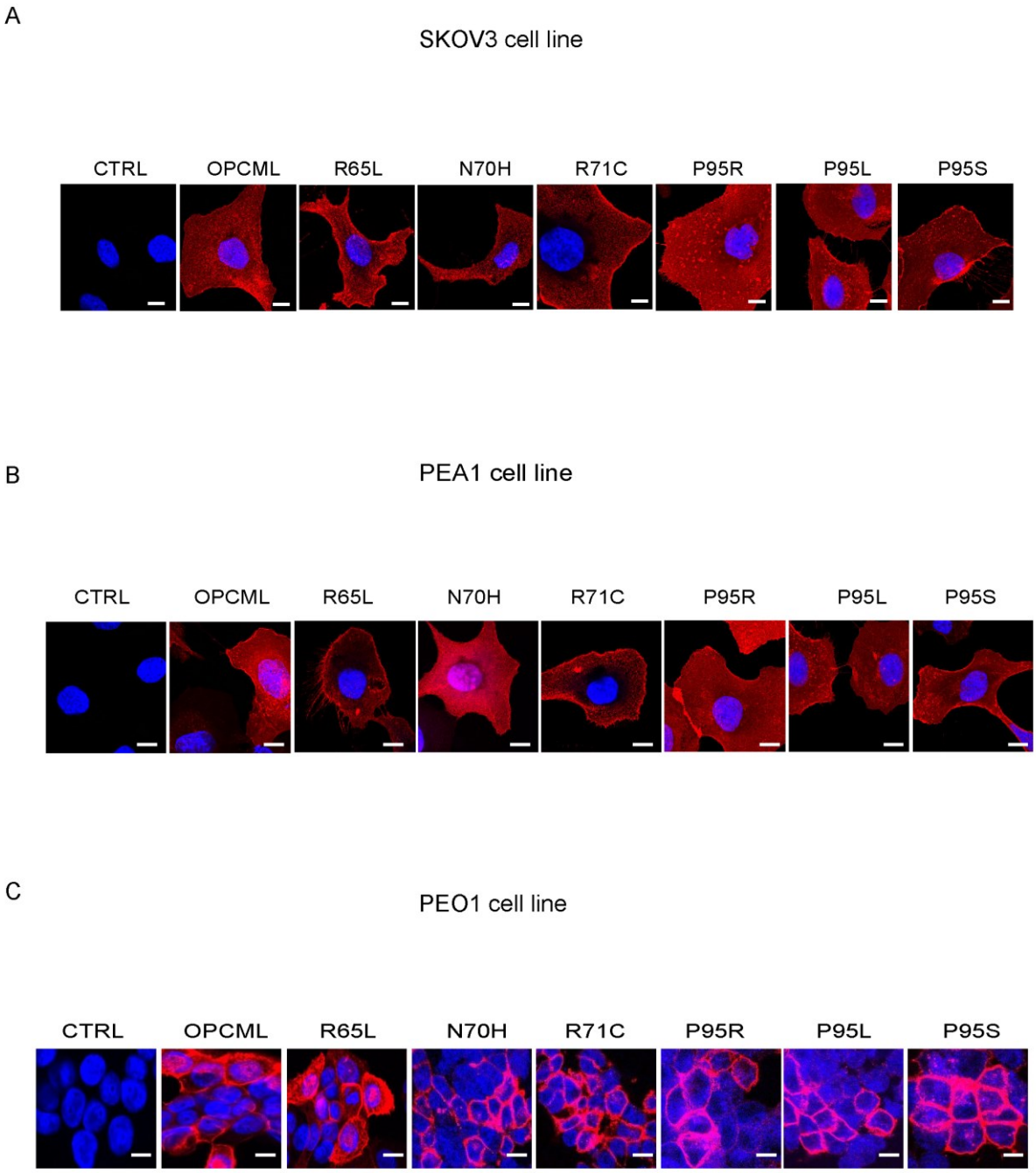


Figure 4.3 OPCML mutants localised to the cell membrane in ovarian cancer cell lines.

Immunofluorescence microscopy of the SKOV3 cell line reveals OPCML in red and the nucleus in blue. The images show that OPCMLR65L, N70H, R71C, P95R, P95L and P95S, are expressed on the cell membrane in stably transduced cell lines. Wild-type OPCML and control are shown for comparison (*n* = 3; scale bar A & B, 5 µm; scale bar C, 10 µm). (A) SKOV3; (B) PEA1; (C) PEO1.

4.4. OPCML mutants maintain the lipid raft localisation of OPCML.

Previously, we showed that OPCML is mainly localised in a portion of the membrane named lipid rafts, or detergent-resistant membranes, to understand the effect of the mutations on the localisation of OPCML in lipid rafts, we performed a cell fractionation assay.

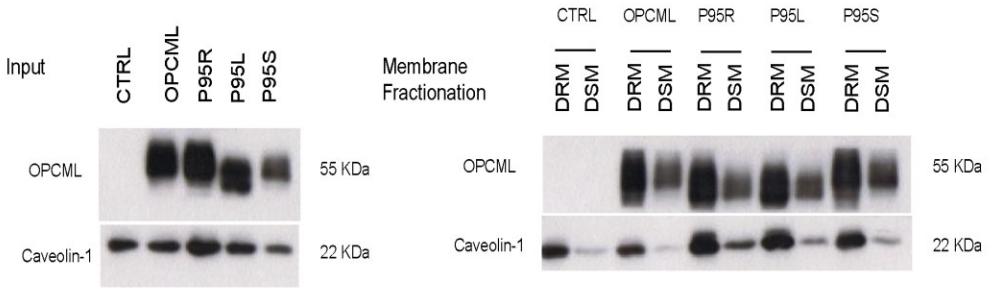
Ultracentrifugation separated detergent-soluble (DSM) and insoluble (DRM) membrane fractions following incubation with a mild non-ionic detergent like Triton X-100. Triton X-100 is considered a mild detergent due to its ability to disrupt the lipid-lipid or lipid-protein interaction rather than protein-protein interaction (Speers and Wu, 2007).

Three mutants (OPCML P95R, OPCML P95L, OPCML P95S) were selected and compared to OPCML wild-type and control.

Successful fractionation was demonstrated by the expression pattern of Caveolin-1, a marker for lipid rafts. We discovered that the OPCML mutants are localised mainly in the detergent-resistant portion of the membrane, like OPCML wild-type (Figure 4.4 A&B).

Thus, the results show that OPCML wild-type and OPCML mutants reside abundantly in the lipid raft. There, they could possibly interact with RTKs and control their function through a shift from the detergent soluble to the insoluble domain, which then would affect their downstream signalling.

A


Input
CTRL
OPCML
P95R
P95L
P95S
OPCML
55 KDa
Caveolin-1
22 KDa
Membrane Fractionation
CTRL
OPCML
P95R
P95L
P95S
DRM
DSM
OPCML
55 KDa
Caveolin-1
22 KDa

B

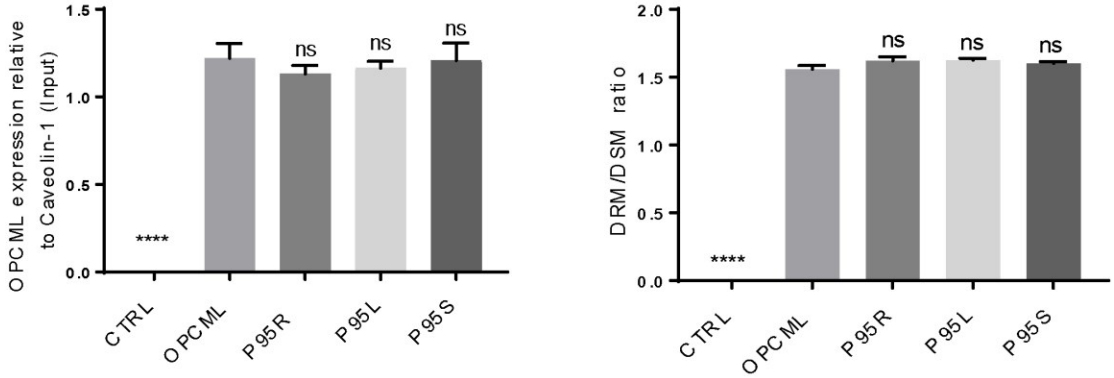

OPCML expression relative to Caveolin-1 (Input)
1.5
1.0
0.5
0.0
****
ns
ns
ns
CTRL
OPCML
P95R
P95L
P95S
DRM/DSM ratio
2.0
1.5
1.0
0.5
0.0
****
ns
ns
ns
CTRL
OPCML
P95R
P95L
P95S

Figure 4.4 OPCML wild-type and OPCML mutants reside in the lipid raft In SKOV3 ovarian cancer cell line.

A. Western Blot analysis showing in the left panel OPCML expression in SKOV3 stably transduced with wild-type OPCML or OPCML mutants compared to cell lines stably transduced with an empty vector as control (CTRL) input, and in the right panel membrane fractionation of detergent-resistant membrane (DRM, lipid raft) and detergent soluble membrane (DSM). Caveolin-1 was used as a marker for DRM.

B. A bar chart of the results of Western Blot analysis is shown in the left panel for input and right panel for membrane fractionation. The difference in the ratio between DRM and DSM between wild-type OPCML and OPCML mutants in the SKOV3 cell line was statistically non-significant. The significance of the differences was determined by one-way ANOVA analysis using Prism 7 with Bonferroni correction (n = 3; mean ± SEM;; **** P < 0.00001; ns, not significant).

4.5. The RTK AXL interacts with OPCML wild-type and OPCML mutants.

After confirming that OPCML mutants resided in the same compartment on the cell membrane and that the amino acid substitutions did not affect their localisation, we then asked whether the mutations affected OPCML interaction with RTKs in the lipid raft.

We have in fact previously described the mechanism by which OPCML negatively regulates a specific spectrum of receptor tyrosine kinases (RTK) through interactions with their extracellular domains and by altering their localisation (McKie et al., 2012). Axl has been extensively linked to metastatic features and it induces chemoresistance by activating Epithelial-Mesenchymal Transition (EMT) in a range of cancers (Asiedu et al., 2014).

In our lab, we showed that OPCML interacts with AXL in mammalian 2-hybrid and GST pull-down assay (Antony et al., manuscript in preparation). To see whether the mutations disrupt this interaction or not, I initially used a co-immunoprecipitation (co-IP) assay. The co-IP method is one of the most practical ways to determine whether two proteins associate or not in biological conditions in *vitro*.

AXL was successfully immuno-precipitated with an anti-AXL antibody, and Western Blot detected the presence of OPCML in the eluate. The co-IP showed that Axl associated with OPCML wild-type and the OPCML mutants in full medium but the relative association between the mutants look different (Figure 4.5). Although, less GAPDH expression was observed in the control input, the levels of AXL are equal and the levels of AXL in the CO-IP samples are equal.

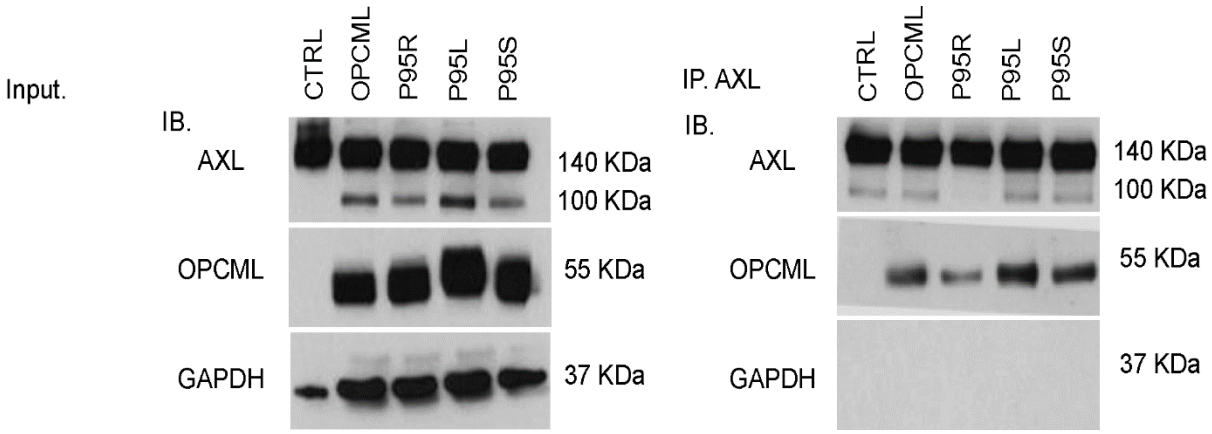


Figure 4.5 Axl interacts with OPCML wild-type and mutants.

Western Blot analysis of CO-IP experiment showing in the left panel input OPCML expression in cells stably transduced with wild-type OPCML or OPCML mutants compared to cell lines stably transduced with an empty vector as control (CTRL), and in right panel the actual immunoprecipitation (IP) showing AXL and OPCML. An anti-AXL antibody was used to immunoprecipitate OPCML; antibodies were used to immunoblot against AXL, OPCML and GAPDH (*n* = 3).

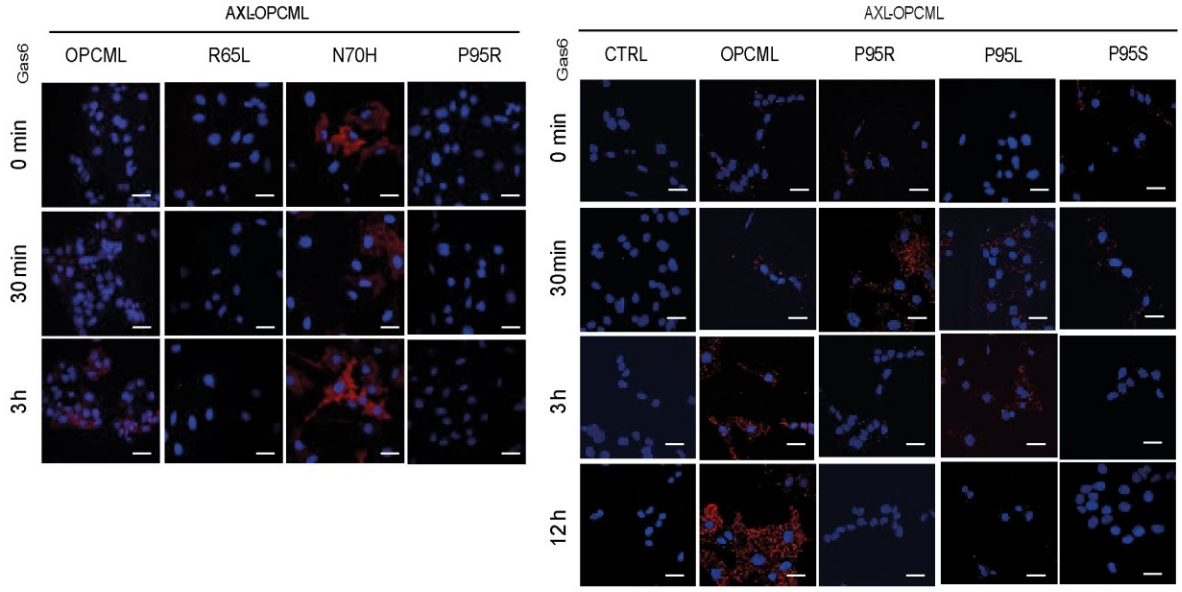
4.6. OPCML mutants disrupt the interaction with AXL upon stimulation with the AXL ligand Gas6 over time.

In our lab, we showed that OPCML inhibited Axl-mediated migration and invasion of ovarian cancer cells when stimulated with Gas6, the AXL ligand (Antony et al. manuscript in preparation).To characterise further the interaction between OPCML and AXL, we then used this ligand in an in situ proximity ligation assay (PLA, Duolink). The PLA assay can detect a protein-protein interaction in their native setting even when it is weak or transient.

We carried out this experiment in the SKOV3 cells transduced with OPCML mutants, OPCML wild-type, and control that were stimulated, after serum-starvation, with GAS6 for 0, 30 min, 3 hours or 12 hours. From this experiment we found that OPCML wild-type significantly increased the interaction with AXL upon stimulation with Gas6. The results also showed that all the investigated OPCML mutants in domain I, except for N70H, disrupted the OPCML-AXL interaction upon Gas stimulation (Figure 4.6 A). Interestingly, OPCML N70H showed a strong interaction with AXL in non-stimulated cells, and the interaction is maintained throughout all the time points.

Analysis of the results revealed a statistically significant difference between OPCML mutants in domain I and wild-type OPCML (Figure 4.6 B).

A


AXL-OPCML
Gas6
OPCML
R65L
N70H
P95R
0 min
30 min
3h
AXL-OPCML
Gas6
CTRL
OPCML
P95R
P95L
P95S
0 min
30min
3h
12h

B

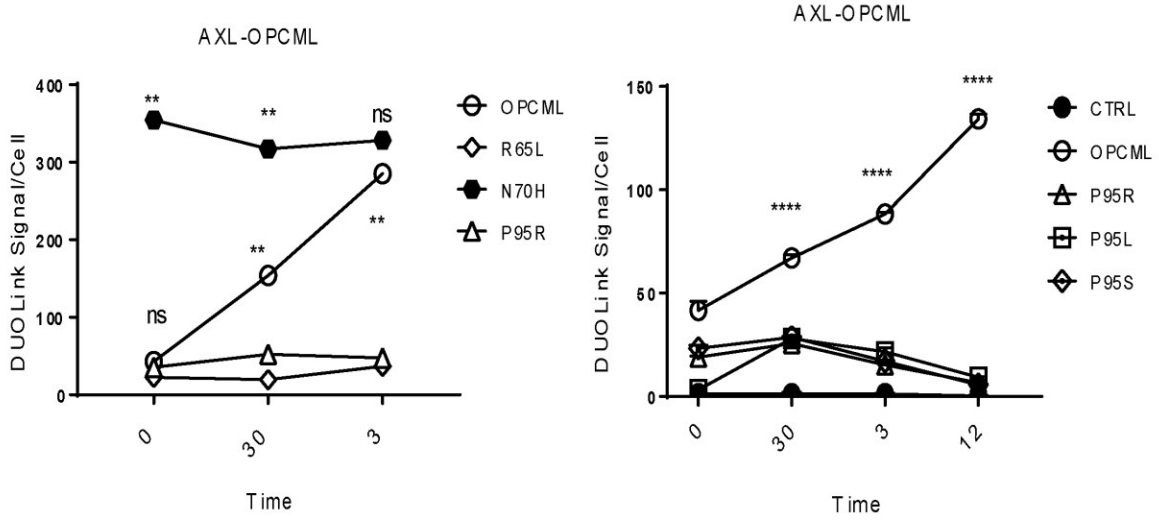

AXL-OPCML
DUOLink Signal/Cell
400
300
200
100
0
**
**
ns
ns
**
**
OPCML
R65L
N70H
P95R
0
30
3
Time
AXL-OPCML
DUOLink Signal/Cell
150
100
50
0
****
****
****
CTRL
OPCML
P95R
P95L
P95S
0
30
3
12
Time

Figure 4.6 OPCML mutants disrupt the interaction with AXL upon stimulation with the AXL ligand Gas6 over time.

A. In situ proximity ligation assay (Duolink assay) analysis reveals that OPCML interacted with AXL in the SKOV3 cell line (red dot colour represent the interaction); the nucleus is shown in blue. The images show OPCML R65L, OPCML N70H, OPCML P95R, OPCML P95L and OPCML P95S interaction with AXL compared to wild-type OPCML and control in stably transduced SKOV3 cell lines stimulated with AXL ligand rhGas6 over time (0, 30 min, 3h, 12h) (scale bar, 20 μm). (The left panel was performed by Jane Anthony).

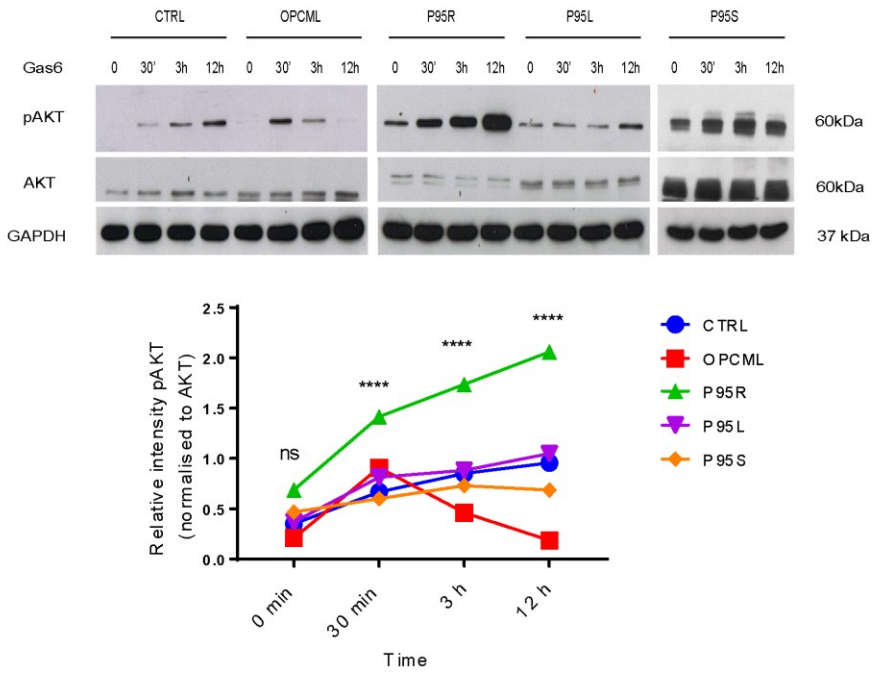
B. A line chart of the results of the Duolink assay analysis is shown in the left and right panel. The difference in interaction between wild-type OPCML and OPCML mutants with AXL in the SKOV3 cell line was statistically significant. The significance of the differences was determined by one-way ANOVA analysis using Prism 7 with Bonferroni correction (n = 3; mean ± SEM; ***p< 0.0001; **** P < 0.00001; ns, not significant).

4.7. OPCML mutants do not inhibit GAS6/AXL downstream signalling.

After showing in the Duolink and co-IP assays that there might be an interaction between OPCML and AXL, we sought to determine the functional consequences of these findings. Unpublished data from our lab showed that OPCML, by binding to AXL, causes the sequestering of the receptor into the detergent-resistant portion of the membrane, where Axl is de-phosphorylated. As a consequence, the phosphorylation of ERK upon stimulation with Gas6 is reduced. In order to understand the interaction between AXL and the OPCML mutants and their effect on the downstream signalling, we subjected the same SKOV3 ovarian cancer cell lines to stimulation with Gas6 over the time course (0, 30 min, 3 h, and 12 h). The results show that OPCML wild-type-expressing cells had a transient increase in pAKT after 30 minutes of stimulation with Gas6, followed by a decrease and complete abrogation of the signalling at 3 and 12 hours respectively. In contrast to OPCML wild-type, OPCML mutants revealed increased and sustained phosphorylation of AKT over time (Figure 4.7 A&B).

Thus, these results show that OPCML mutants are loss of function and may disrupt the interaction between OPCML and AXL in the lipid raft. As a consequence, we speculate that the free AXL in the active form in the detergent-soluble portion of the membrane can activate the downstream signalling and phosphorylation of AKT.

A


CTRL
OPCML
P95R
P95L
P95S
Gas6
0 30' 3h 12h
pAKT
AKT
GAPDH
60kDa
60kDa
37 kDa
Relative intensity pAKT (normalised to AKT)
ns
****
****
****
0 min
30 min
3 h
12 h
Time
CTRL
OPCML
P95R
P95L
P95S

B

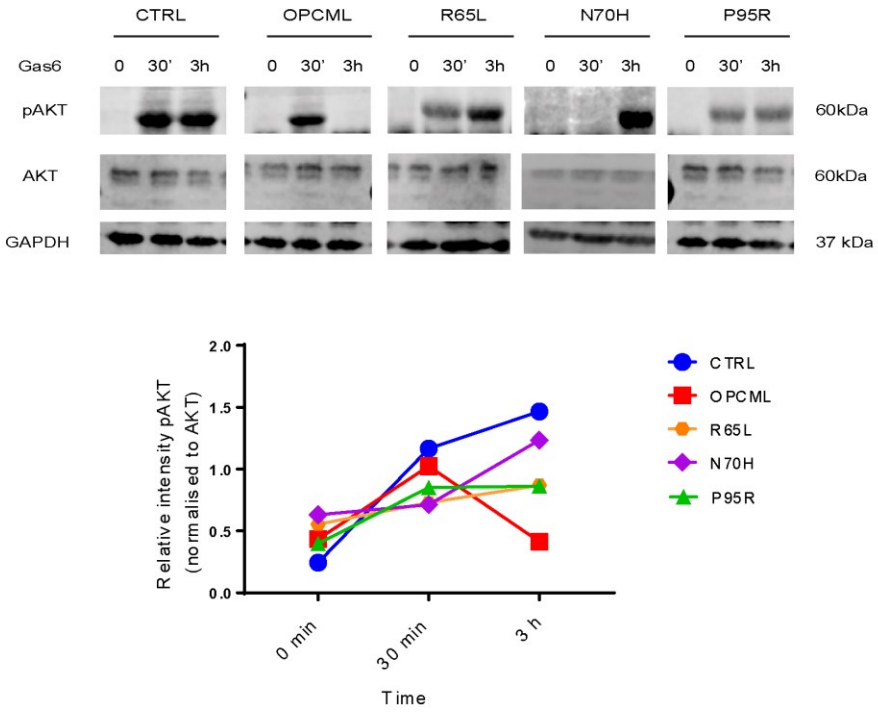

CTRL
OPCML
R65L
N70H
P95R
Gas6
0 30' 3h
pAKT
AKT
GAPDH
60kDa
60kDa
37 kDa
Relative intensity pAKT (normalised to AKT)
0 min
30 min
3 h
Time
CTRL
OPCML
R65L
N70H
P95R

Figure 4.7 OPCML mutants do not inhibit GAS6/AXL downstream signalling.

A. Western Blot analysis shows in the upper panel the phosphorylation of AKT in SKOV3 stably transduced with wild-type OPCML or OPCML mutants (OPCML P95R, OPCML P95L, and OPCML P95S) compared to cell lines stably transduced with an empty vector as control (CTRL) upon stimulation with the AXL ligand rhGAS6 (400 ng/ml) over time (0, 30 min, 3 h, 12h). GAPDH was used as loading control. A line chart of the results of Western Blot analysis is shown in the lower panel. The significance of the differences was determined by one-way ANOVA analysis using Prism 7 with Bonferroni correction .The difference in phosphorylation between wild-type OPCML and OPCML mutants in the SKOV3 cell line was statistically significant, also compared to the control it was significant (n = 3; mean ± SEM; **** $P < 0.00001$; ns, not significant).
B. Western Blot analysis shows in the upper panel the phosphorylation of AKT in SKOV3 cells stably transduced with wild-type OPCML or OPCML mutants (OPCML R65L, OPCML N70H, and OPCML P95R) compared to cell lines stably transduced with an empty vector as control (CTRL) upon stimulation with the AXL ligand rhGAS6 (400 ng/ml) over time (0, 30 min, 3 h, 12h). GAPDH was used as loading control. A line chart of the results of Western Blot analysis is shown in the lower panel, n = 1, performed by Jane Anthony.

4.8. OPCML mutants do not alter cell migration and invasion upon Gas6 stimulation compared to inhibition by wild-type OPCML.

Axl overexpression was found in several tumours and has been reported to be linked with invasiveness or metastasis in several types of tumours (Lee et al., 2014). Therefore, we then investigated the effects of the regulation, or loss of, of the downstream signalling on cell motility and invasion.

Previously, in our lab, we showed that upon stimulation with Gas6, ovarian cancer cells such as SKOV3 become more motile, while cells expressing OPCML show a strongly reduced motility. So, to identify the contribution of OPCML mutants in cell motility, we performed wound-healing assays.

To perform these experiments, we seeded the same SKOV3 ovarian cancer cell lines that were used before in commercial inserts, and the gap closure was followed live on a confocal microscope by taking images every 15 minutes over 15 hours.

The experiment was performed in the absence of serum to restrain cells proliferation and in the presence of Gas6 to constrain the effect on the GAS6/AXL pathway.

The results show that wild-type OPCML had the ability to suppress motility compared to OPCML mutants when cells were activated with the AXL ligand, GAS6 (Figure 4.9 A&B left panel). Interestingly, one of the mutants, OPCML N70H, preserved the tumour-suppressing function and reduced motility compared to the other mutants.

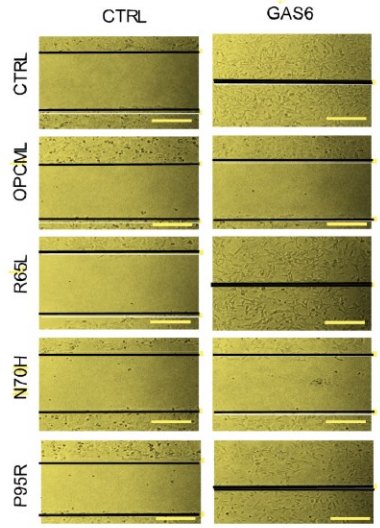
These results suggest that among the OPCML mutants in domain I, only OPCML N70H showed no statistically significant difference with wild-type OPCML (Figure 4.8 A&B right panel).

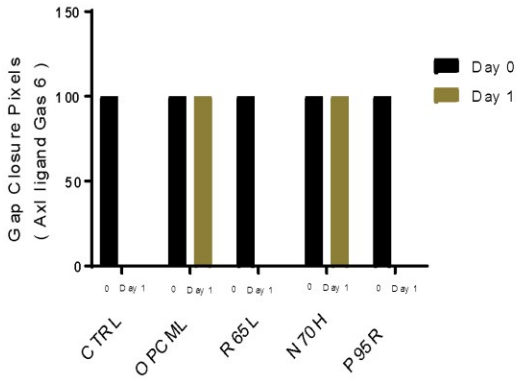
In addition, to further investigate the consequences of the mutations in domain I on cell invasion, SKOV3 cell line transduced with OPCML wild-type, OPCML mutants and control were seeded in low-adherent plate to form three-dimensional spheroids. After five days, Gas6 was added at 400 ng/ml in Matrigel matrix to stimulate the cells.

The results show that the OPCML mutants present loss of function in invasion compared to wild-type OPCML and behaved like the control cells (empty vector). As expected, wild-type OPCML suppressed the ability of the cells to invade (Figure 4.8 C).

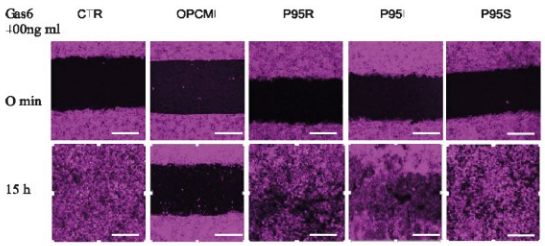
We also observed the OPCML mutants lose the inhibitory function of OPCML in invasion, and as results showed cells invading the matrix in the three-dimensional environment at the cell borders (Figure 4.8 C left panel), indicating that these cells had the characteristic of metastatic cells. In contrast, wild-type OPCML showed resistance to spheroid formation and sign of cell death around the spheroid.

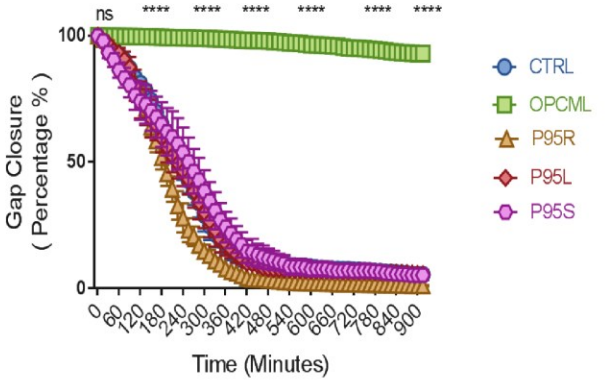
A


CTRL
GAS6
CTRL
OPCML
R65L
N70H
P95R

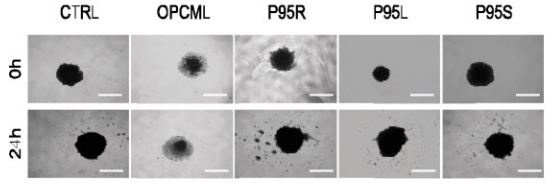

Gap Closure Pixels
(Axl ligand Gas 6)
150
100
50
0
Day 0
Day 1
CTRL
OPCML
R65L
N70H
P95R

B


Gas6
400ng ml
CTR
OPCML
P95R
P95L
P95S
0 min
15 h


ns
****
100
50
0
Gap Closure
(Percentage %)
0
60
120
180
240
300
360
420
480
540
600
660
720
780
840
900
Time (Minutes)
CTRL
OPCML
P95R
P95L
P95S

C


CTRL
OPCML
P95R
P95L
P95S
0h
24h

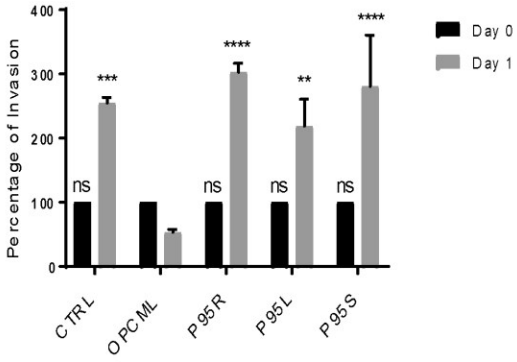

Percentage of Invasion
400
300
200
100
0
***
****
**
****
ns
Day 0
Day 1
CTRL
OPCML
P95R
P95L
P95S

Figure 4.8 OPCML mutants do not alter cell migration and invasion upon Gas6 stimulation compared to inhibition by wild-type OPCML.

A, B) Wound healing assay of the ovarian cancer SKOV3 cell line transduced with wild-type OPCML, OPCML R65L, OPCML N70H, OPCML P95R, and control (A) or wild-type OPCML, OPCML P95R, OPCML P95S, OPCML P95L, and control (B). Cells were seeded in insert in 24 well plate and three positions selected and allowed to migrate for 15 hours after stimulation with the AXL ligand rhGas6. Phase-contrast microscopy pictures were taken of the wounded area by confocal microscope and are shown on the left panels. The wound closure area was determined with ImageJ. The right panels show the results obtained. The difference in wound healing assay between wild-type OPCML and OPCML R65L, P95R, and control in the SKOV3 cell line was statistically significant, but it was non-significant compared to the OPCML N70H. Three independent experiments were performed; the obtained data are presented as a mean and standard error of the mean (SEM, error bar). The significance of the differences was determined by one-way ANOVA analysis using Prism 7 with Bonferroni correction (n = 3; **** $P <$ 0.0001; scale bar, 200 μm). Performed by Jane Anthony and Mohammad Alomary.

C) Spheroid invasion assay of the ovarian cancer SKOV3 cell line transduced with wild-type OPCML, OPCML P95R, OPCML P95L, OPCML P95S, and control. Cells were seeded in triplicate and allowed to form spheroid for 5 days, after which they were stimulated with the AXL ligand rhGas6 and allowed to invade for 24 hours. Phase-contrast microscopy pictures were taken of the wounded area with a Nikon TE2000-V Eclipse inverted microscope. The cells invading the matrix at the cell borders and the size of the spheroid area were determined with ImageJ. The right panel shows the bar chart of the results obtained. Three independent experiments were performed; the obtained data are presented as a mean and standard error of the mean (SEM, error bar). The difference in spheroid invasion assay between wild-type OPCML and control/OPCML mutants in the SKOV3 cell line was statistically significant. The significance of the differences was determined by one-way ANOVA analysis using Prism 7 with Bonferroni correction (n = 3; ** $P < 0.01$; *** $P < 0.0001$; **** $P < 0.00001$; scale bar, 50 μm).

4.9. OPCML mutants impair the sensitisation effect of OPCML to AXL inhibitor R428 by altering Caspase 3/7 activation.

Published and unpublished data obtained in our lab showed that OPCML wild-type sensitises cells to anti-EGFR/HER2 or -EGFR only therapies, such as lapatinib and erlotinib (Zanini et al., 2017), as well as to R428 (Antony et al., unpublished). To further investigate whether OPCML mutants have a role in the clinical setting, we used an AXL inhibitor, R428 (BGB324), in sensitisation studies.

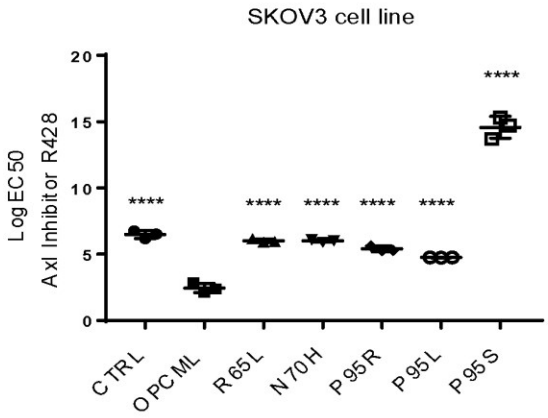
SKOV3 ovarian cancer cell lines were subjected to treatment with increasing concentrations of AXL inhibitor R428 for 48 hours before assessing the growth inhibition by cell proliferation assay. The results show that wild-type OPCML sensitised the cells to R428 by 2.7 fold compared to control cell (GI50 2.44 μM vs GI50 6.5 μM) while most of the OPCML mutants showed GI50s similar to the control (Figure 4.9 A). Interestingly, one of the mutants, OPCML P95S, showed a 2.24 fold increase above the control, and a 6 fold increase compared to wild-type OPCML (Figure 4.9 A).

We further sought to identify the events that might promote the acquired resistance to the AXL inhibitor in cells expressing OPCML. It is known that R428 markedly suppresses AXL signalling and induces apoptosis (Jian-Zhong et al., 2017). Therefore, we examined the impact of R428 on the downstream signalling pathways in our transduced cell lines. Cells were subjected treated with AXL inhibitor for 3 hours , then to stimulation with AXL ligand Gas6 for 1 hours. We found that OPCML mutants in SKOV3 cells significantly abolish the inhibitory function of OPCML on the phosphorylation level of ERK compared to the wild-type OPCML cell lines. The results showed that, like the control, OPCML mutants in domain I impair the OPCML function

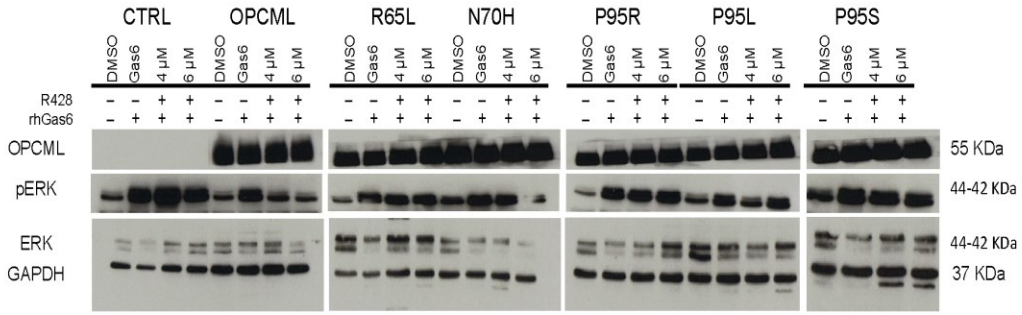
on the phosphorylation of ERK in response to treatment with AXL inhibitor (Figure 4.9 B). Analysis of the results revealed a statistically significant difference between OPCML mutants in domain I and wild-type OPCML (Figure 4.9 C).

Based on the above findings, encouraged to identify the mechanism behind this resistance, we further examined whether the OPCML mutants' effect on the sensitisation to AXL inhibition was due to evading apoptosis. The SKOV3 cell lines were then employed to assess Caspase-3/7 activity using a Caspase-Glo 3/7 assay. The results show that the Caspase 3/7 activity of the OPCML mutants was reduced by three folds compared to wild-type OPCML. This could explain why the OPCML mutants alter the OPCML inhibitory effect and sensitisation to the AXL inhibitor. In contrast, in the presence of OPCML wild-type and R428, Caspase 3/7 activity was increased compared to control (Figure 4.9 D).

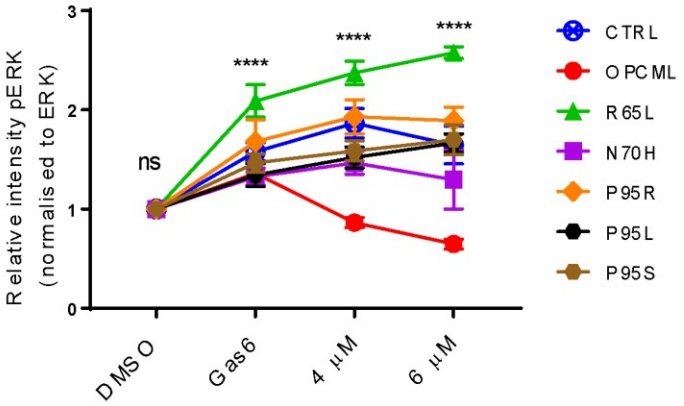
A


SKOV3 cell line
Log EC50
Axl Inhibitor R428
20
15
10
5
0
****
CTRL
OPCML
R65L
N70H
P95R
P95L
P95S

B


CTRL
OPCML
R65L
N70H
P95R
P95L
P95S
DMSO
Gas6
4 µM
6 µM
R428
rhGas6
OPCML
pERK
ERK
GAPDH
55 KDa
44-42 KDa
44-42 KDa
37 KDa

C


Relative intensity pERK
(normalised to ERK)
3
2
1
0
ns
****
****
****
DMSO
Gas6
4 µM
6 µM
CTRL
OPCML
R65L
N70H
P95R
P95L
P95S

D

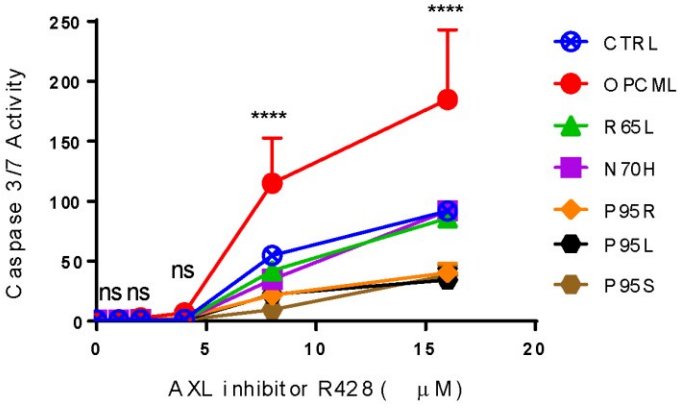

Caspase 3/7 Activity
250
200
150
100
50
0
ns ns
ns
****
****
0
5
10
15
20
AXL inhibitor R428 (µM)
CTRL
OPCML
R65L
N70H
P95R
P95L
P95S

Figure 4.9 OPCML mutants impair the sensitisation effect of OPCML to AXL inhibitor R428 by altering Caspase 3/7 activation.

A. Scatter plot of the results of determination of half maximal inhibitory concentration of AXL inhibitor R428 of the ovarian cancer SKOV3 cell line transduced with wild-type OPCML, OPCML mutants, and control grown for 48 hours in the presence of different concentrations of R428 (0, 1, 2, 4, 8, and 16 μM), determined by an MTS assay. Three independent experiments were performed; the obtained data are presented as a mean and standard error of the mean (SEM, error bar). The difference in the half maximal inhibitory concentration of R428 between wild-type OPCML and OPCML mutants in the SKOV3 cell line was statistically significant, also compared to the control it was significant. The significance of the differences was determined by one-way ANOVA analysis using Prism 7 with Bonferroni correction (n = 3; **** $P < 0.00001$).
B. Western Blot analysis shows phosphorylation and expression of ERK, and OPCML in cells stably transduced with wild-type OPCML or OPCML mutants (OPCML R65L, OPCML N70H, OPCML P95R, OPCML P95L, OPCML P95S) compared to cell lines stably transduced with an empty vector as control (CTRL) upon Cells were subjected treated with AXL inhibitor R428 (4 μM, 6 μM) for 3 hours, then to stimulation with AXL ligand rhGAS6 (400 ng/ml) for 1 hours. Dimethyl sulfoxide (DMSO) was used as control and GAPDH was used as loading control.
C. Line chart of the results of the Western Blot shown in B. The difference in the phosphorylation of ERK between wild-type OPCML and OPCML mutants in the SKOV3 cell line was statistically significant, also compared to the control it was significant. The significance of the differences was determined by one-way ANOVA analysis using Prism 7 with Bonferroni correction (n = 3; mean ± SEM; **** P < 0.00001; ns, not significant).
D. Caspase 3/7 apoptosis assays of the ovarian cancer SKOV3 cell line transduced with wild-type OPCML, OPCML mutants, and control. Cells were seeded in triplicate and treated with serial concentration (0–16 μM) of R428 for 24 hours. Caspase activity was normalised to cell density obtained by MTS for each treatment. Three independent experiments were performed; the obtained data are presented as a mean and standard error of the mean (SEM, error bar). The difference in Caspase 3/7 assay between wild-type OPCML and OPCML mutants in the SKOV3 cell line was statistically significant, also compared to the control it was significant The significance of the differences was determined by one-way ANOVA analysis using Prism 7 with Bonferroni correction (n = 3; mean ± SEM ; **** $P < 0.00001$; ns, not significant).

4.10. OPCML R65L loses the OPCML function in migration by impairing the OPCML-FGFR1 interaction and as consequence, the phosphorylation of downstream AKT.

Aberrant expression and activation of receptor tyrosine kinases (RTK) such as FGFR1 have been associated with tumour progression in a wide variety of human malignancies (Imran et al., 2012). Previously, we showed that OPCML exerts its suppressor function by interacting with RTKs such as FGFR1 and downregulates their function through attenuating their related downstream signalling.

To confirm the FGFR1-OPCML interaction and to understand the role of the OPCML mutants in the FGFR1-OPCML context we used in situ proximity ligation assay (Duolink, PLA). To perform the experiment, we used the SKOV3 cell line transduced with OPCML wild-type, OPCML R65L, OPCML N70H, OPCML P95R, and control that were stimulated with recombinant human FGF1 (rhFGF1) for 0, 30 min and 3 hours.

We found that OPCML wild-type in SKOV3 cells significantly increased the interaction with FGFR1 upon stimulation with FGF1 while the three different mutations gave three different behaviour, with R65L interfering completely, N70H not interfering at all with FGF1 stimulation and the P95R behave like wild-type OPCML interaction with FGFR1 upon stimulation with FGF1 (Figure 4.10 A).

Based on the above findings, we further examined the effects of the mutations on the downstream signalling of FGFR1. SKOV3 cell lines were then subjected to stimulation with FGFR1 ligand FGF1 over a time course of 0, 30 min, and 3 hours. The results showed that OPCML wild-type expressing cells had only a transient elevation of pAKT at 30 minutes followed by abrogation of the signalling. In contrast, OPCML

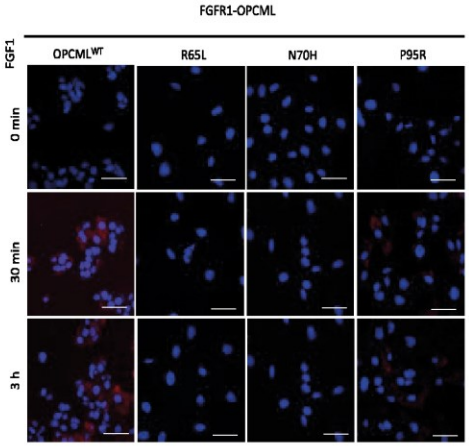
mutants showed an elevated and sustained phosphorylation of AKT like the control cells (Figure 4.10 B).

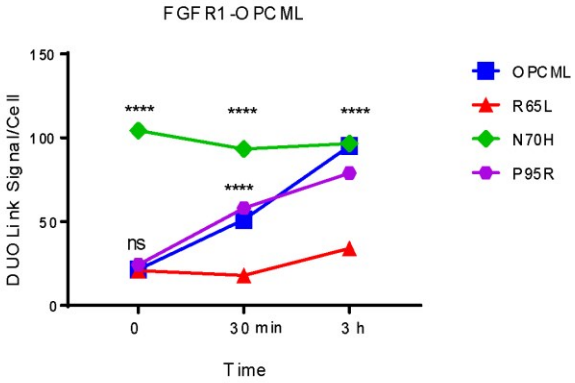
Next, we explored whether FGFR1 upregulated the migratory potential of the OPCML mutants cells by wound healing assay. The results showed that wild-type OPCML had the ability to suppress the motility compared to OPCML mutants when cells were activated with FGFR1 ligand FGF1 (Figure 4.10 C). Interestingly, two of the mutants, OPCML N70H and OPCML P95R, preserved the tumour-suppressing function and reduced motility compared to the other mutant, OPCML R65L.

Fascinatingly, OPCML N70H behaves like OPCML in conserving the properties of tumour suppressor in inhibiting the migration in the FGF1/FGFR1 context as consistent with the previous results on RTKs AXL showing that the OPCML-N70H interaction with AXL was not altered upon activation by the AXL ligand GAS6. Moreover, OPCML P95R did not respond to stimulation with rhFGF1 in the wound healing assay and behaved like OPCML, which may indicate that the stimulation with rhFGF1 is not the primary pathway for this mutation and possibly other cross-talk between RTKs could initiate the migration of the cells.

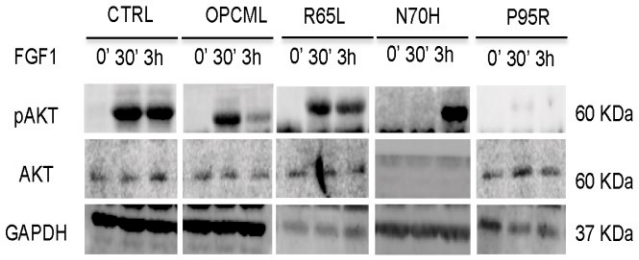
These results suggest that among the OPCML mutants in domain I, only one, OPCML R65L, displayed a loss of function for wound healing assay while the other two mutants, OPCML N70H and OPCML P95R showed no statistically significant difference with wild-type OPCML. Our results indicate that OPCML mutants in domain I behave differently to different RTKs stimuli (Figure 4.10 C right panel).

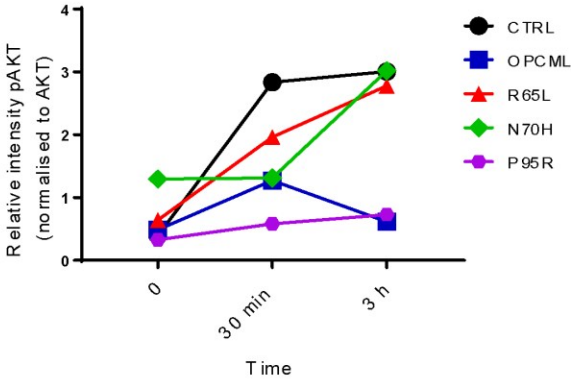
A


FGFR1-OPCML
FGF1
OPCML^WT
R65L
N70H
P95R
0 min
30 min
3 h

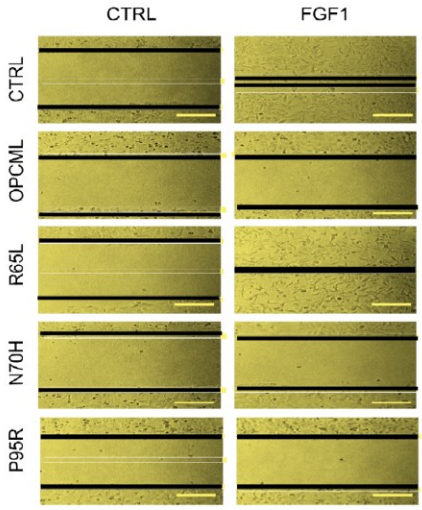

FGFR1-OPCML
DUO Link Signal/Cell
150
100
50
0
****
****
****
****
ns
0
30 min
3 h
Time
OPCML
R65L
N70H
P95R

B


CTRL
OPCML
R65L
N70H
P95R
FGF1
0' 30' 3h
0' 30' 3h
0' 30' 3h
0' 30' 3h
0' 30' 3h
pAKT
AKT
GAPDH
60 KDa
60 KDa
37 KDa


Relative intensity pAKT
(normalised to AKT)
4
3
2
1
0
0
30 min
3 h
Time
CTRL
OPCML
R65L
N70H
P95R

C


CTRL
FGF1
CTRL
OPCML
R65L
N70H
P95R

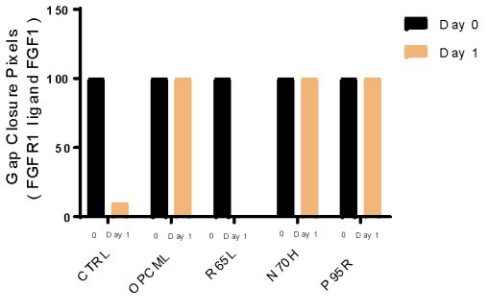

Gap Closure Pixels
(FGFR1 ligand FGF1)
150
100
50
0
Day 0
Day 1
CTRL
OPCML
R65L
N70H
P95R

Figure 4.10 OPCML R65L loses the OPCML function in migration by impairing the OPCML-FGFR1 interaction and as consequence, the phosphorylation of downstream AKT.

A. In situ proximity ligation assay (Duolink assay) analysis reveals that OPCML interacts with FGFR1 in the SKOV3 cell line (red dot colour represent the interaction); the nucleus is shown in blue. The images show OPCML R65L, OPCML N70H, and OPCML P95R interaction with FGFR1,compared to wild-type OPCML in stably transduced SKOV3 cell lines stimulated with FGFR1 ligand rhFGF1 over time (0, 30 min, 3h) (scale bar, 20 μm). In the right panel, a line chart of the results of Duolink assay analysis is shown, n=3, Performed by Jane Anthony.
B. Western Blot analysis showing in the left panel phosphorylation and expression of AKT in cells stably transduced with wild-type OPCML or OPCML mutants (OPCML R65L, OPCML N70H, and OPCML P95R) compared to cell lines stably transduced with an empty vector as control (CTRL) upon stimulated with FGFR1 ligand rhFGF1 (50ng/ml) over time (0, 30 min, 3 h). GAPDH was used as loading control. A line chart of the results of Western Blot analysis is shown in the right panel, n=1, Performed by Jane Anthony.
C. Wound healing assay of the ovarian cancer SKOV3 cell line transduced with wild-type OPCML, OPCML R65L, OPCML N70H, OPCML P95R, and control. Cells were seeded in triplicate and allowed to migrate for 15 hours after stimulation with the FGFR1 ligand rhFGF1. Phase-contrast microscopy pictures were taken of the wounded area by confocal microscope (left panel). The wound closure area was determined with ImageJ. The right panel shows a bar chart of the results obtained, n=1, Performed by Jane Anthony.

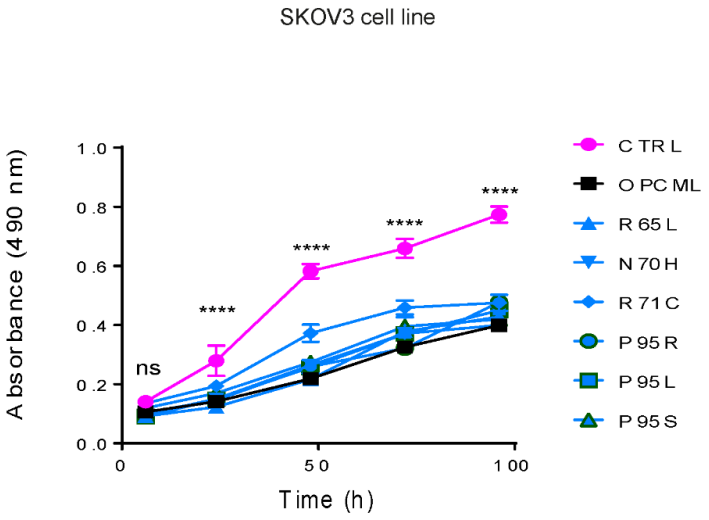
4.11. OPCML mutants in domain I behave like OPCML wild type in suppressing cell proliferation.

So far we examined the role of OPCML mutants in their interaction with RTKs. Next, we characterised their general effects on tumour growth as, in the context of ovarian cancer, we previously showed that OPCML suppresses tumour growth *in vitro* and *in vivo* (Sellar et al., 2003; McKie et al., 2012).

SKOV3 and PEA1 cell lines expressing wild-type OPCML, OPCML R65L, OPCML N70H, OPCML R71C, OPCML P95R, OPCML P95L, OPCML P95S and control were employed in proliferation assays in full cell culture medium.

We found that the wild-type and mutants all suppressed the tumour proliferation in the two different ovarian cancer cell lines (Figure 4.11; (A) SKOV3 cell line; (B) PEA1 cell line). In summary, the analysis of the results revealed a statistically significant difference between control cell line and wild-type OPCML. On the other hand, OPCML mutants show statistically insignificant proliferation compared to wild-type OPCML and statistically significant compared to control in ovarian cancer SKOV3 and PEA1 cell lines.

A



B

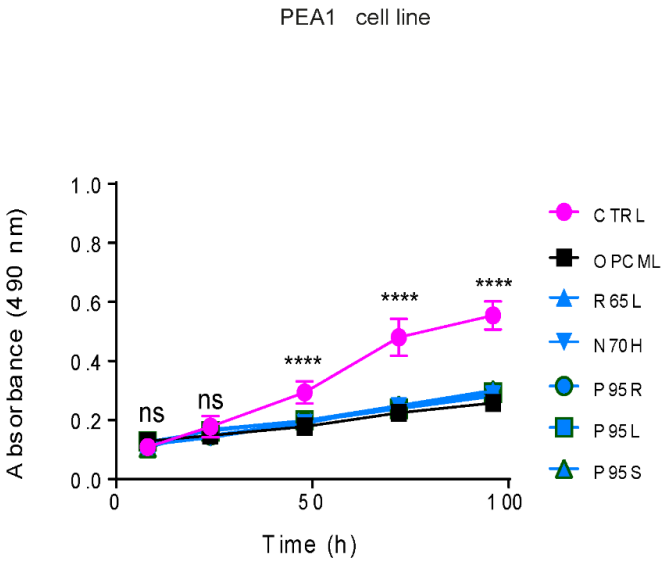


Figure 4.11 OPCML mutants in domain I behave like OPCML wild type in suppressing cell proliferation.

The proliferation of SKOV3 cell lines transduced with wild-type OPCML, OPCML R65L, OPCML N70H, OPCML R71C, OPCML P95R, OPCML P95L, OPCML P95S and control grown for 96 hours in the presence of full medium (FM) was determined by an MTS assay. The graph shows the absorbance of MTS reagent at 490 nm; the results are representative of four independent experiments. Data are presented as a mean and standard error of the mean (SEM, error bars); the significance of the differences was determined by two-way ANOVA analysis using Prism 7 with Bonferroni correction. n = 4; ns, non-significant; **** P < 0.00001. (A) SKOV3; (B) PEA1.

4.12. OPCML mutants reveal loss of function in anchorage-independent cellular growth.

To investigate further tumour-relevant phenotypes, we examined the ability of cancer cells to form colonies in anchorage-independent growth assays in soft agar.

Three ovarian cancer cell lines SKOV3, PEA1, and PEO1 transduced with OPCML wild-type, OPCML R65L, OPCML N70H, OPCML R71C and for SKOV3 only, OPCML P95R, OPCMLP95L, and OPCML P95S, and control were subjected to soft agar colony formation assay, for evaluating anchorage-independent cell growth.

Three different numbers of cells, 0.2, 0.4 and 0.8 × 10^4 cells per cell line, were seeded into 0.6% Difco Noble agar on a base of 1% Noble agar in six-well plates and cultured for four weeks (PEO1 cell line for 12 days due to massive growth of mutants and control) before the visible colonies were fixed and stained; cell colonies were determined using an inverted microscope.

The results show that OPCML mutants have the ability to survive and grow under anchorage-independent conditions; the OPCML mutants show variation in the number and size of the colonies formed. In contrast, in the presence of OPCML wild-type, colony formation was suppressed. Figure 4.12 (1) SKOV3; (2) PEA1; (3) PEO1 shows that OPCML mutants lose the colony formation inhibition contrary to wild-type OPCML (A: 2000 cells/well; B: 4000 cells/well; and C: 8000 cells/well).

These results indicate that all the OPCML mutants in domain I displayed a loss of function for anchorage-independent growth compared to OPCML wild-type, which exhibited a substantial suppression in the size and number of colonies formed.

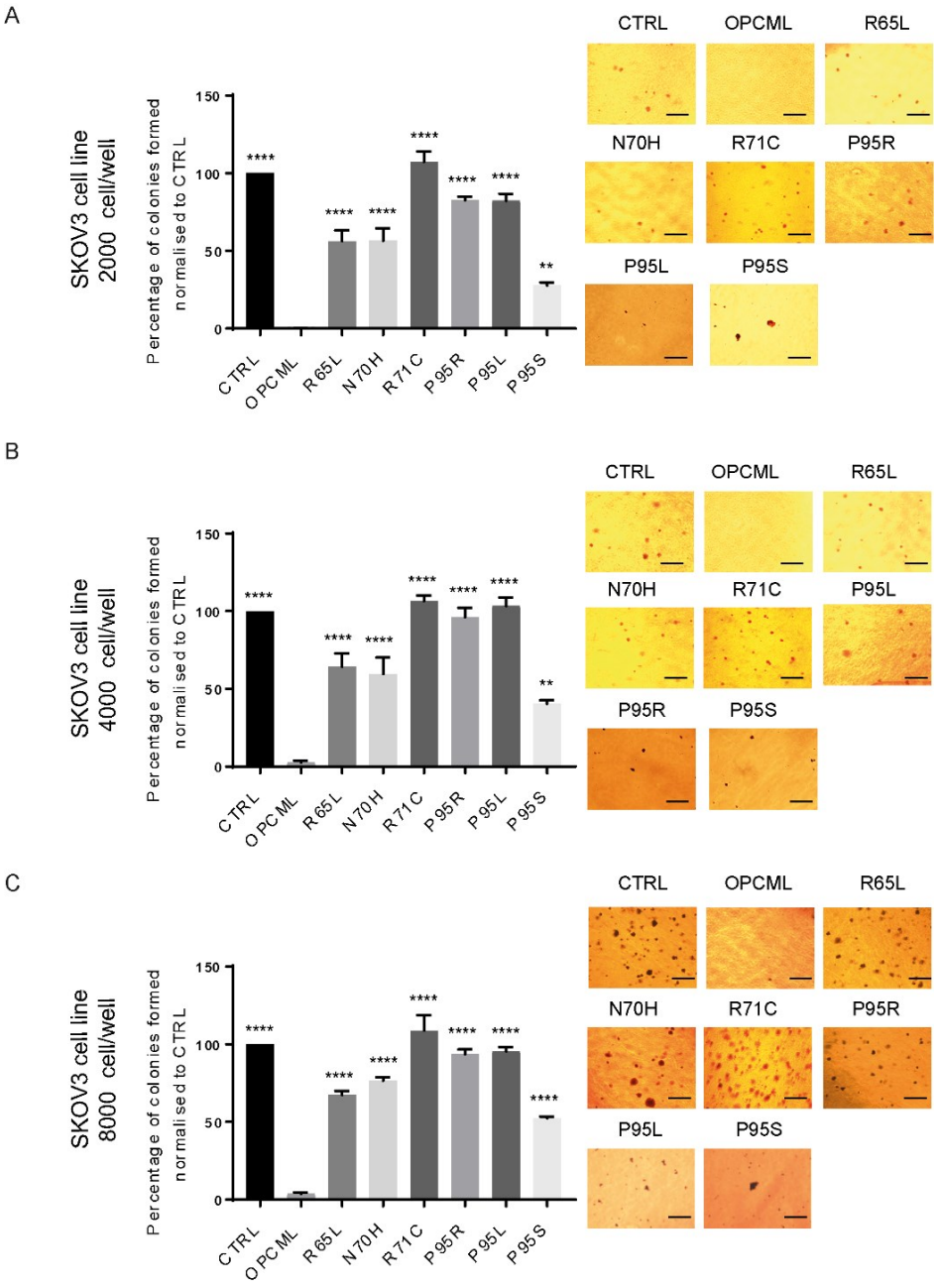

A
SKOV3 cell line
2000 cell/well
Percentage of colonies formed normalised to CTRL
150
100
50
0
****
****
****
****
****
****
**
CTRL
OPCML
R65L
N70H
R71C
P95R
P95L
P95S
CTRL
OPCML
R65L
N70H
R71C
P95R
P95L
P95S
B
SKOV3 cell line
4000 cell/well
Percentage of colonies formed normalised to CTRL
150
100
50
0
****
****
****
****
****
****
**
CTRL
OPCML
R65L
N70H
R71C
P95R
P95L
P95S
CTRL
OPCML
R65L
N70H
R71C
P95L
P95R
P95S
C
SKOV3 cell line
8000 cell/well
Percentage of colonies formed normalised to CTRL
150
100
50
0
****
****
****
****
****
****
****
CTRL
OPCML
R65L
N70H
R71C
P95R
P95L
P95S
CTRL
OPCML
R65L
N70H
R71C
P95R
P95L
P95S

Figure 4.12.1 OPCML mutants reveal loss of function in anchorage-independent cellular growth in ovarian cancer cell line SKOV3.

Soft agar colony formation assay of ovarian cancer SKOV3 cell line transduced with wild-type OPCML, OPCML R65L, OPCML N70H, OPCML R71C, OPCML P95R, OPCML P95L, OPCML P95S and control. Cells were grown on soft agar plates for four weeks before colonies were fixed and stained with 0.015% neutral red and visualised using an inverted microscope with a digital camera. Representative colour images of the colonies in soft agar acquired at 4× magnification are shown in the right panels. The average number of colonies was determined by counting them using ImageJ. The left panels show bar charts of the results obtained. Three independent experiments were performed, and the data are presented as a mean and standard error of the mean (SEM, error bar). The difference in colony formation between wild-type OPCML and OPCML mutants in the SKOV3 cell line was statistically significant, also compared to the control it was significant. The significance of the differences was determined by one-way ANOVA analysis using Prism 7 with Bonferroni correction (** $P < 0.001$; **** $P < 0.0001$; scale bar, 200 μm). (A) 0.2 x 10^4 cells/well; (B) 0.4 x 10^4 cells/well; (C) 0.8 x 10^4 cells/well.

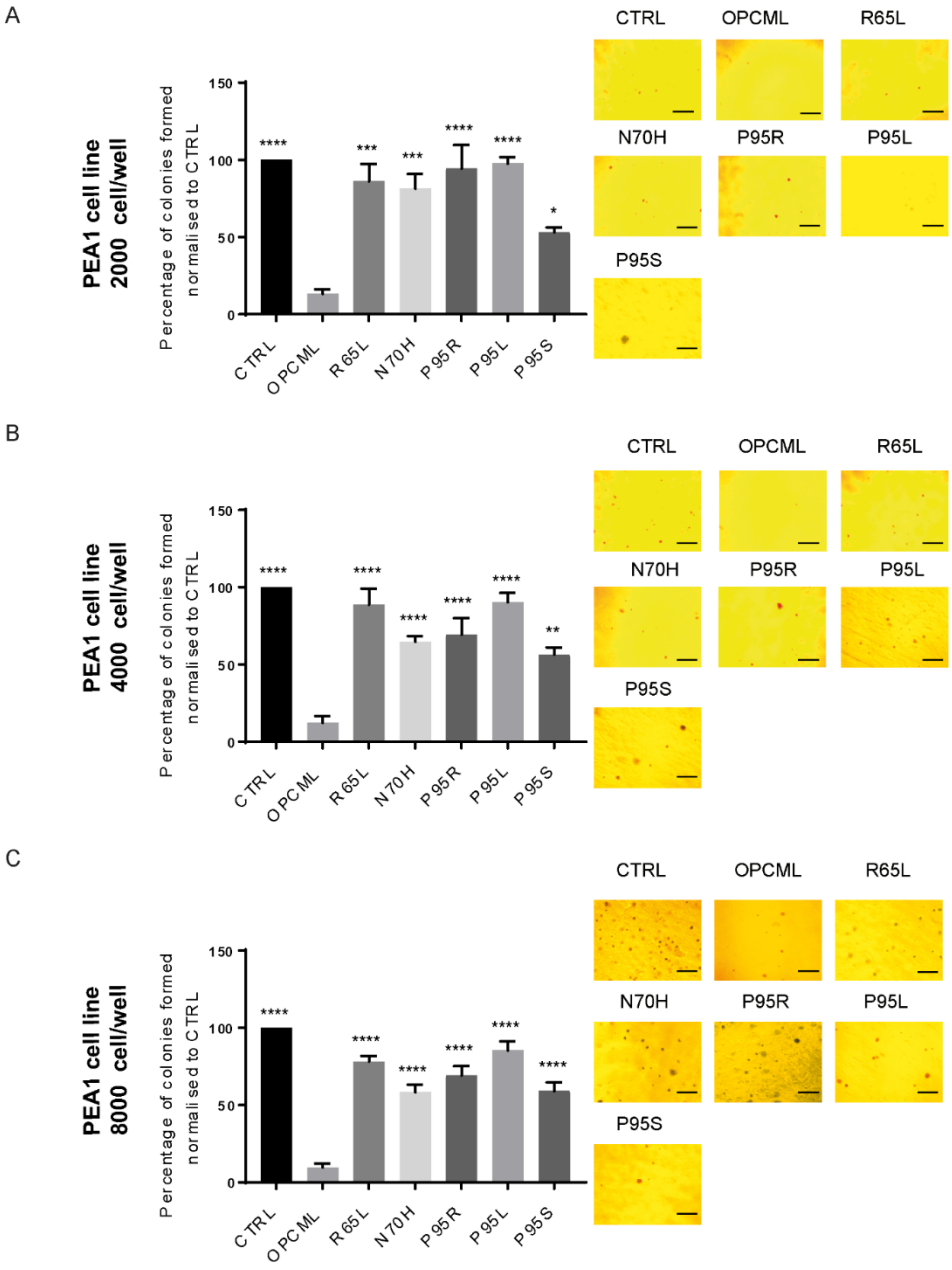

A
PEA1 cell line
2000 cell/well
Percentage of colonies formed
normalised to CTRL
150
100
50
0
****
***
***
****
****
*
CTRL
OPCML
R65L
N70H
P95R
P95L
P95S
CTRL
OPCML
R65L
N70H
P95R
P95L
P95S
B
PEA1 cell line
4000 cell/well
Percentage of colonies formed
normalised to CTRL
150
100
50
0
****
****
****
****
****
**
CTRL
OPCML
R65L
N70H
P95R
P95L
P95S
CTRL
OPCML
R65L
N70H
P95R
P95L
P95S
C
PEA1 cell line
8000 cell/well
Percentage of colonies formed
normalised to CTRL
150
100
50
0
****
****
****
****
****
****
CTRL
OPCML
R65L
N70H
P95R
P95L
P95S
CTRL
OPCML
R65L
N70H
P95R
P95L
P95S

Figure 4.12.2 OPCML mutants reveal loss of function in anchorage-independent cellular growth in ovarian cancer cell line PEA1.

Soft agar colony formation assay of ovarian cancer PEA1 cell line transduced with wild-type OPCML, OPCML R65L, OPCML N70H, OPCML P95R, OPCML P95L, OPCML P95S and control. Cells were grown on soft agar plates for four weeks before colonies were fixed and stained with 0.015% neutral red and visualised using an inverted microscope with a digital camera. Representative colour images of the colonies in soft agar acquired at 4× magnification are shown in the right panels. The average number of colonies was determined by counting them using ImageJ. The left panels show bar charts of the results obtained. Three independent experiments were performed, and the data are presented as a mean and standard error of the mean (SEM, error bar). The difference in colony formation between wild-type OPCML and OPCML mutants in the PEA1 cell line was statistically significant, also compared to the control it was significant. The significance of the differences was determined by one-way ANOVA analysis using Prism 7 with Bonferroni correction (* $P < 0.01$; *** $P < 0.001$; **** $P < 0.0001$; scale bar, 200 µm). (A) 0.2 x 10^4 cells/well; (B) 0.4 x 10^4 cells/well; (C) 0.8 x 10^4 cells/well.

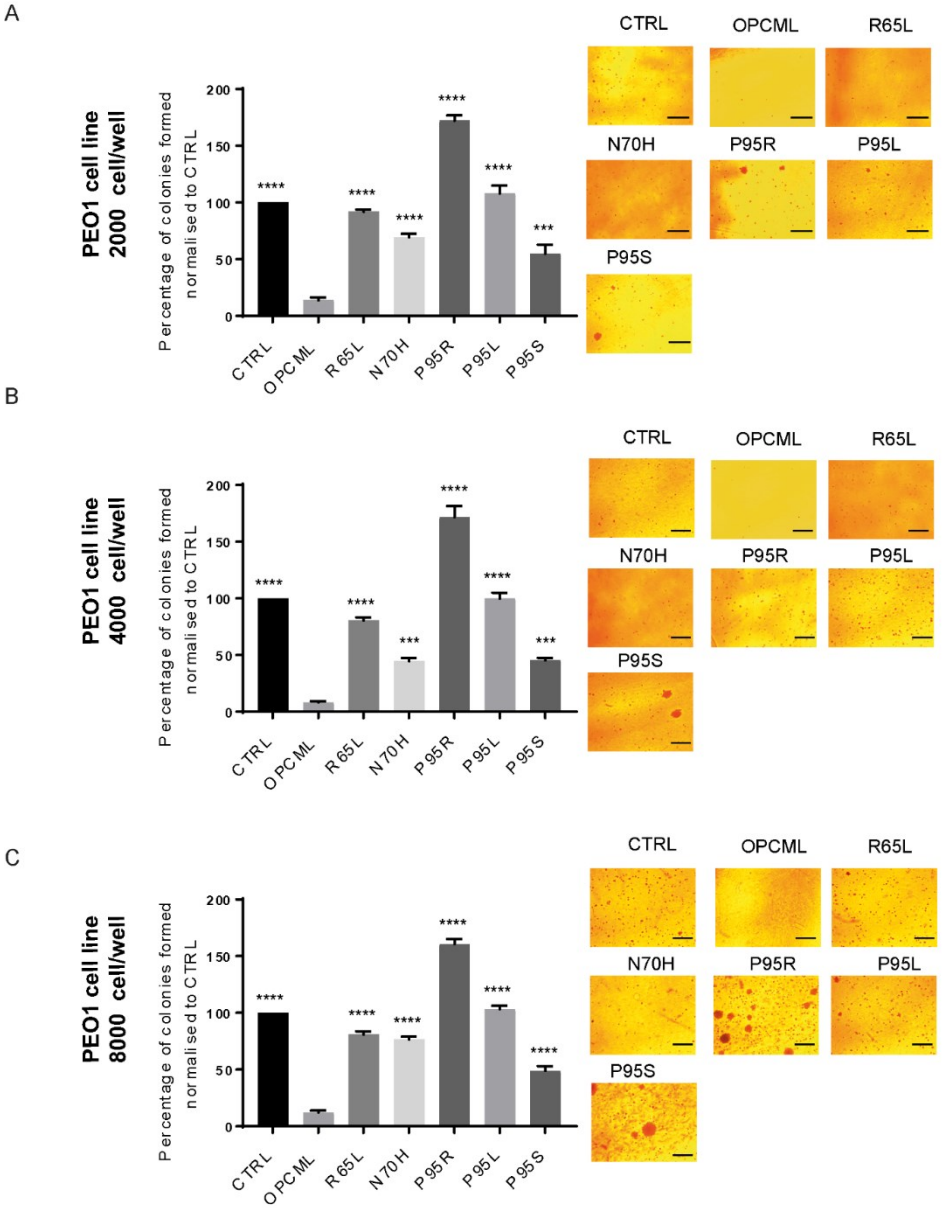

A
PEO1 cell line
2000 cell/well
Percentage of colonies formed normalised to CTRL
200
150
100
50
0
****
****
****
****
****
***
CTRL
OPCML
R65L
N70H
P95R
P95L
P95S
CTRL
OPCML
R65L
N70H
P95R
P95L
P95S
B
PEO1 cell line
4000 cell/well
Percentage of colonies formed normalised to CTRL
200
150
100
50
0
****
****
***
****
****
***
CTRL
OPCML
R65L
N70H
P95R
P95L
P95S
CTRL
OPCML
R65L
N70H
P95R
P95L
P95S
C
PEO1 cell line
8000 cell/well
Percentage of colonies formed normalised to CTRL
200
150
100
50
0
****
****
****
****
****
****
CTRL
OPCML
R65L
N70H
P95R
P95L
P95S
CTRL
OPCML
R65L
N70H
P95R
P95L
P95S

Figure 4.12.3 OPCML mutants reveal loss of function in anchorage-independent cellular growth in ovarian cancer cell line PEO1.

Soft agar colony formation assay of ovarian cancer PEO1 cell line transduced with wild-type OPCML, OPCML R65L, OPCML N70H, OPCML P95R, OPCML P95L, OPCML P95S and control. Cells were grown on soft agar plates for 12 days before colonies were fixed and stained with 0.015% neutral red and visualised using an inverted microscope with a digital camera. Representative colour images of the colonies in soft agar acquired at 4× magnification are shown in the right panels. The average number of colonies was determined by counting them using ImageJ. The left panels show bar charts of the results obtained. Three independent experiments were performed, and the data are presented as a mean and standard error of the mean (SEM, error bar). The difference in colony formation between wild-type OPCML and OPCML mutants in the PEO1 cell line was statistically significant, also compared to the control it was significant. The significance of the differences was determined by one-way ANOVA analysis using Prism 7 with Bonferroni correction (*** $P < 0.001$; **** $P < 0.0001$; scale bar, 200 μm). (A) 0.2 x 10^4 cells/well; (B) 0.4 x 10^4 cells/well; (C) 0.8 x 10^4 cells/well.

4.13. OPCML mutants show loss of suppressive function on cellular migration in ovarian cancer *in vitro*.

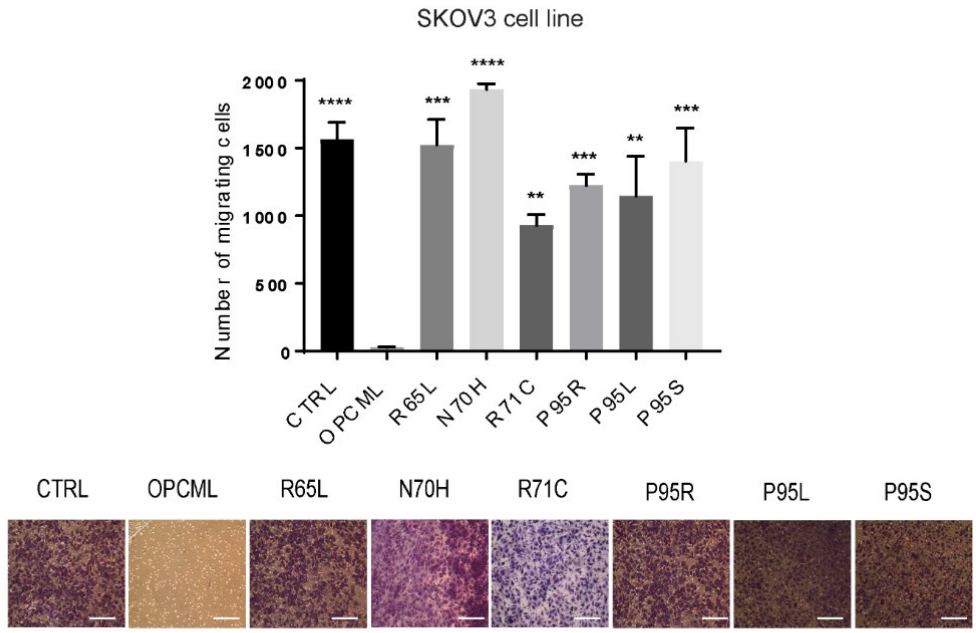
Next, to shed light on possible roles for OPCML mutants on another characteristic of cancer cells such as migration, we investigated the migration properties using Transwell Biocoat migration chamber assay in SKOV3 and PEA1 ovarian cancer cell lines.

OPCML mutants, wild-type OPCML, and the empty vector were grown in full medium and then re-suspended in serum-free media before being added to the chamber at 2.5×10^4 cells/chamber. Seeding was done in triplicate. Cells were allowed to migrate for 24 hours after which they were fixed and stained with 0.1% crystal violet in methanol solution. Complete medium with 10% serum was added to the lower chamber as a chemoattractant.

Not surprisingly, wild-type OPCML suppresses the ability of the cells to migrate. However, the results show that OPCML mutants do not suppress migration like wild-type OPCML does and behave like the control (empty vector). Figure 4.13 shows the results of the migration assay in (A) SKOV3 cell line, (B) PEA1 cell line.

Overall, OPCML mutants in domain I show loss of function and block the inhibitory effect of OPCML on migration.

A


SKOV3 cell line
Number of migrating cells
2000
1500
1000
500
0
****
***
****
**
***
**
***
CTRL
OPCML
R65L
N70H
R71C
P95R
P95L
P95S
CTRL
OPCML
R65L
N70H
R71C
P95R
P95L
P95S

B

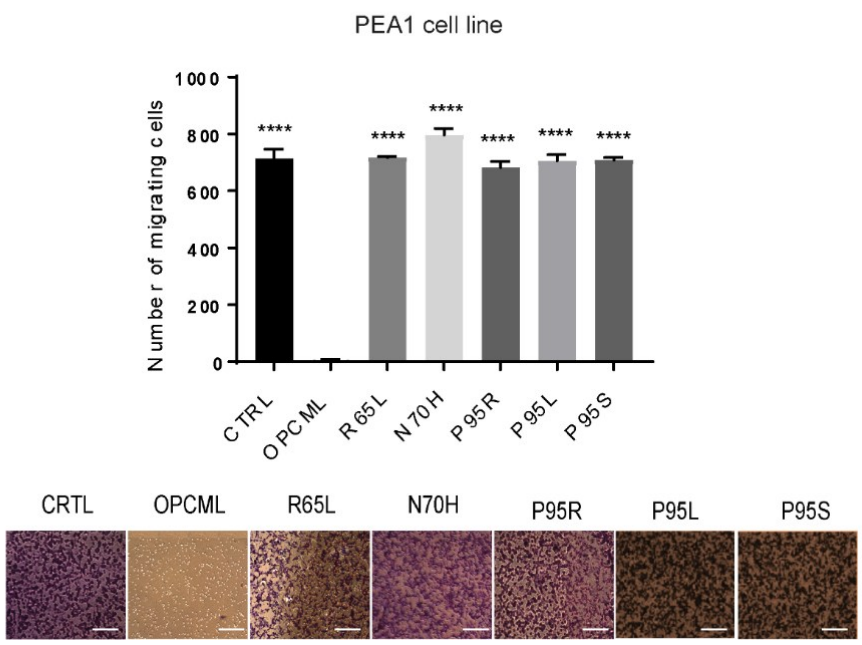

PEA1 cell line
Number of migrating cells
1000
800
600
400
200
0
****
****
****
****
****
****
CTRL
OPCML
R65L
N70H
P95R
P95L
P95S
CRTL
OPCML
R65L
N70H
P95R
P95L
P95S

Figure 4.13 OPCML mutants show loss of suppressive function on cellular migration in ovarian cancer in vitro.

Transwell migration assay of the ovarian cancer cell line transduced with wild-type OPCML, OPCML R65L, OPCML N70H, OPCML R71C, OPCML P95R, OPCML P95L, OPCML P95S and control. Chambers were seeded in triplicate with 2.5×10^4 cells/chamber. Cells were allowed to migrate for 24 hours after which they were fixed and stained with 0.1% crystal violet in methanol solution and visualised using a Nikon Eclipse TE2000-U microscope and Q-Capture Pro software. Representative colour images of the chamber containing cells acquired at 10× magnification are shown in the lower panels. At least six pictures were taken for each chamber, and the total number of cell migrated was determined by counting the cells with ImageJ. The upper panels show bar charts of the results obtained. Three independent experiments were performed; the obtained data are presented as a mean and standard error of the mean (SEM, error bar). The difference in migration between wild-type OPCML and OPCML mutants in the cell line was statistically significant, also compared to the control it was significant. The significance of the differences was determined by one-way ANOVA analysis using Prism 7 with Bonferroni correction (*n*=3; ** P=0.0012; *** P=0.006; **** P<0.0001; scale bar, 50 μm). (A) SKOV3 cell line; (B) PEA1 cell line.

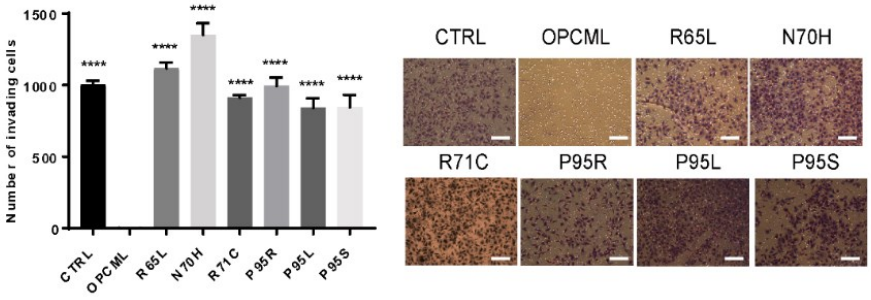
4.14. OPCML mutants block OPCML function in invasion in ovarian cancer in vitro.

Next, to investigate the potential roles of OPCML mutants on tumorigenic features such as invasion, we questioned whether OPCML mutants could affect the OPCML function and are involved in the invasion process. We investigated the invasion properties using Transwell Biocoat growth factor reduced invasion chambers with Matrigel basement membrane matrix (Corning, USA) in SKOV3, PEA1, and PEO1 ovarian cancer cell lines.

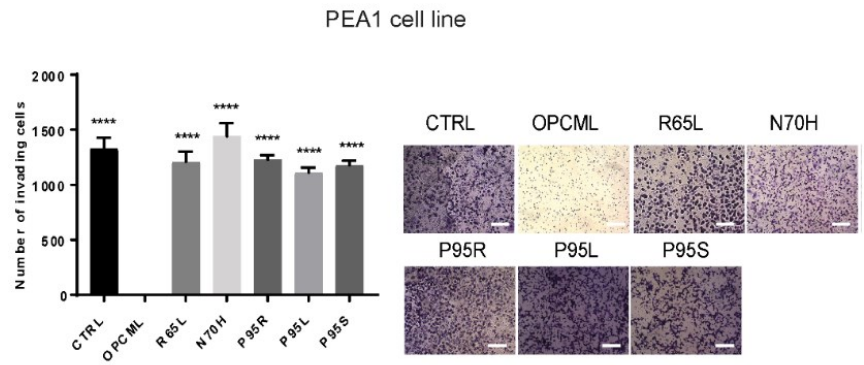
OPCML mutants, wild-type OPCML, and the empty vector were grown in full medium and then re-suspended in serum-free media before being added to the chamber coated with matrigel at 2.5×10^4 cells/chamber. Seeding was done in triplicate. Cells were allowed to invade for 24 hours after which they were fixed and stained with 0.1% crystal violet in methanol solution. Complete medium with 10% serum was added to the lower chamber as a chemoattractant.

The results showed that OPCML mutants lose the OPCML function in invasion and behaved like control (empty vector). Again, as expected, wild-type OPCML suppressed the ability of the cells to invade. Figure 4.14 shows the results of the invasion assay: (A) SKOV3 cell line, (B) PEA1, (C) PEO1 cell lines.

A


SKOV3 cell line
Number of invading cells
1500
1000
500
0
****
CTRL
OPCML
R65L
N70H
R71C
P95R
P95L
P95S

B


PEA1 cell line
Number of invading cells
2000
1500
1000
500
0
****
CTRL
OPCML
R65L
N70H
P95R
P95L
P95S

C

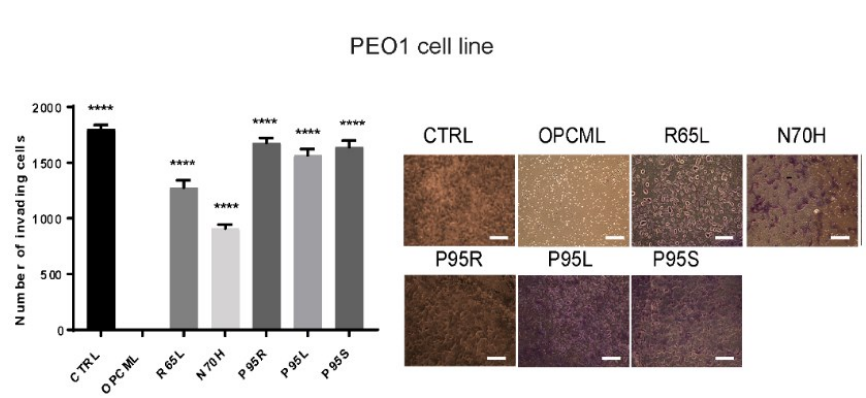

PEO1 cell line
Number of invading cells
2000
1500
1000
500
0
****
CTRL
OPCML
R65L
N70H
P95R
P95L
P95S

Figure 4.14 OPCML mutants block OPCML function in invasion in ovarian cancer in vitro.

Transwell Invasion assay of the ovarian cancer cell lines transduced with wild-type OPCML, OPCML R65L, OPCML N70H, OPCML R71C, OPCML P95R, OPCML P95L, OPCML P95S and control. Chambers were seeded in triplicate with 2.5 × 10^4 cells/chamber. Cells were allowed to invade for 24 hours after which they were fixed and stained with 0.1% crystal violet in methanol solution and visualised using a Nikon Eclipse TE2000-U microscope and Q-Capture Pro software. Representative colour images of the chamber containing cells acquired at 10× magnification are shown in the right panels. At least six pictures were taken for each chamber, and the total number of cell invade was determined by counting the cells with ImageJ. The left panels show bar charts of the results obtained. Three independent experiments were performed; the obtained data are presented as a mean and standard error of the mean (SEM, error bar). The difference in invasion between wild-type OPCML and OPCML mutants in the cell line was statistically significant, also compared to the control it was significant. The significance of the differences was determined by one-way ANOVA analysis using Prism 7 with Bonferroni correction (*n*=3; **** P<0.0001; scale bar, 50 μm). (A) SKOV3 cell line; (B) PEA1 cell line; (C) PEO1 cell line.

4.15. OPCML mutants in domain I alter OPCML -regulated adherence to extracellular matrix components.

As cell invasion and migration are considered a complex multistep cascade organised by both intracellular and extracellular signals, we asked whether OPCML mutants could also altered cell adhesion to the extracellular matrix (ECM). It is known that there is an important role of the extracellular matrix in migration, invasion, and resistance to the treatment (Liotta & Kohn, 2001).

The extracellular matrix (ECM) is composed of a complex of proteins and proteoglycans that is remodelled and contributes to cancer progression. Significant components of the ECM are collagen, laminin and proteoglycans. Cellular invasion and migration require the cell to adhere to the extracellular matrix; we assessed the effect of mutations in OPCML on cellular adhesion to extracellular matrix proteins. To evaluate whether OPCML mutants could promote adherence to extracellular matrix components, the transduced SKOV3 ovarian cancer cell lines were subjected to a cell adhesion assay.

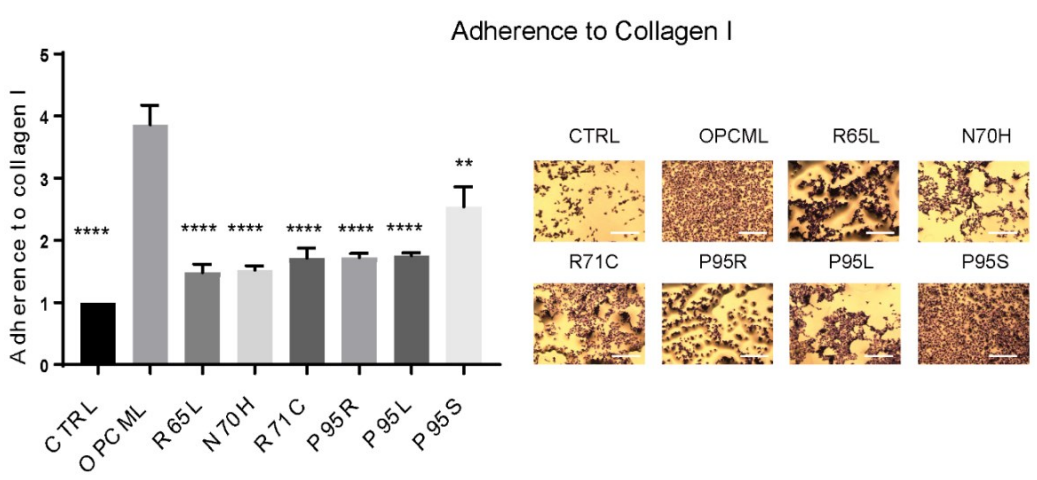
OPCML mutants, wild-type OPCML and the control (empty vector) were grown in full medium and then re-suspended in serum-free media before being added to wells that were pre-coated with different ECM proteins such as collagen I, collagen IV, laminin I, fibronectin, and fibrinogen. Cells were allowed to adhere for 90 minutes after which they were stained with 0.09% crystal violet, extracted with 10% acetic acid and subsequently measured. Bovine serum albumin (BSA) was used as negative control.

For the OPCML mutants in domain I, we found a decrease in cellular adhesion to collagen I and Collagen IV in comparison to wild-type OPCML and the levels of

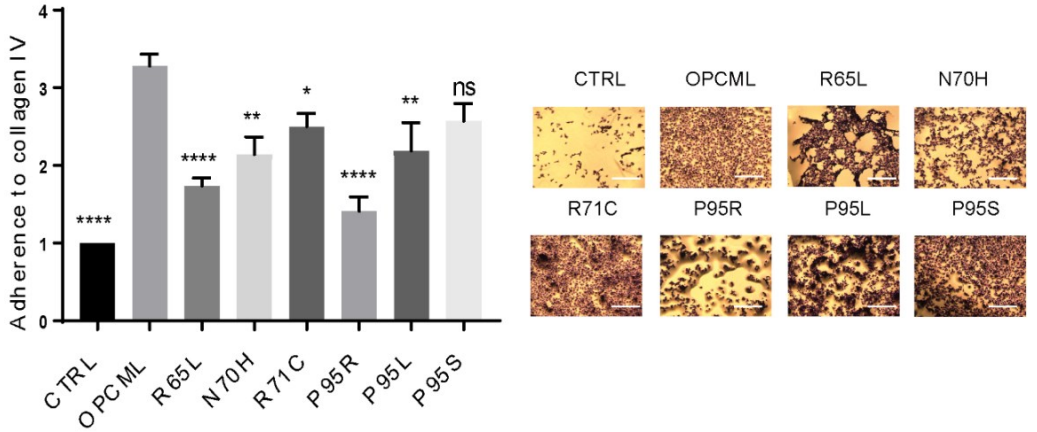
decrease were significant ($p < 0.0001$) (Figure 4.15 A and B, respectively). On the other hand, the OPCML mutants in domain I showed loss of the OPCML function on cellular adhesion to laminin I, fibronectin, and fibrinogen ($P < 0.0002$ or $P < 0.0001$) (Figures 4.15 C, D, and E). These proteins are known to play a vital role in enhancing cellular attachment to the extracellular matrix through integrin receptors, which facilitate the adhesion and migration of tumour cells and provide resistance to chemotherapeutic treatment.

Consequently, cell adhesion to the extracellular matrix suggests that OPCML mutants in domain I show loss of OPCML function and could impair the OPCML function toward the invasion, migration and resistance to chemotherapy of ovarian cancer cells *in vitro* converse to OPCML wild type.

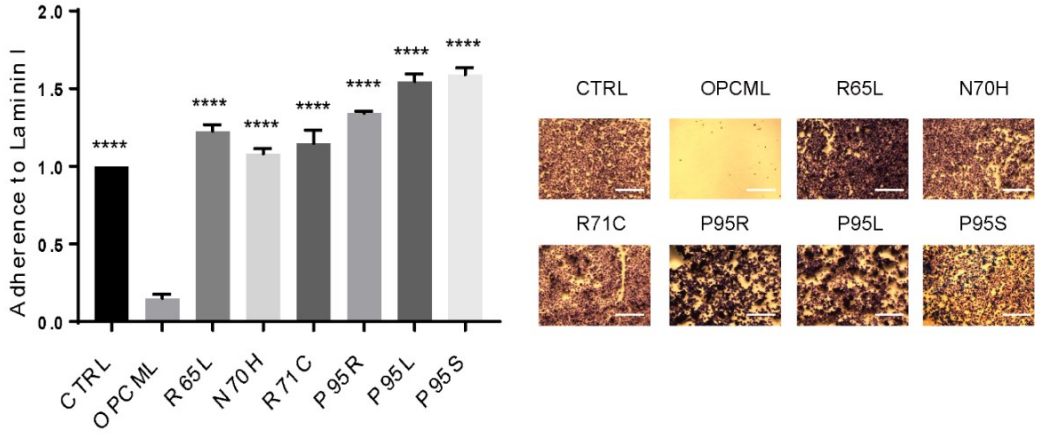
A


Adherence to Collagen I
Adherence to collagen I
CTRL
OPCML
R65L
N70H
R71C
P95R
P95L
P95S

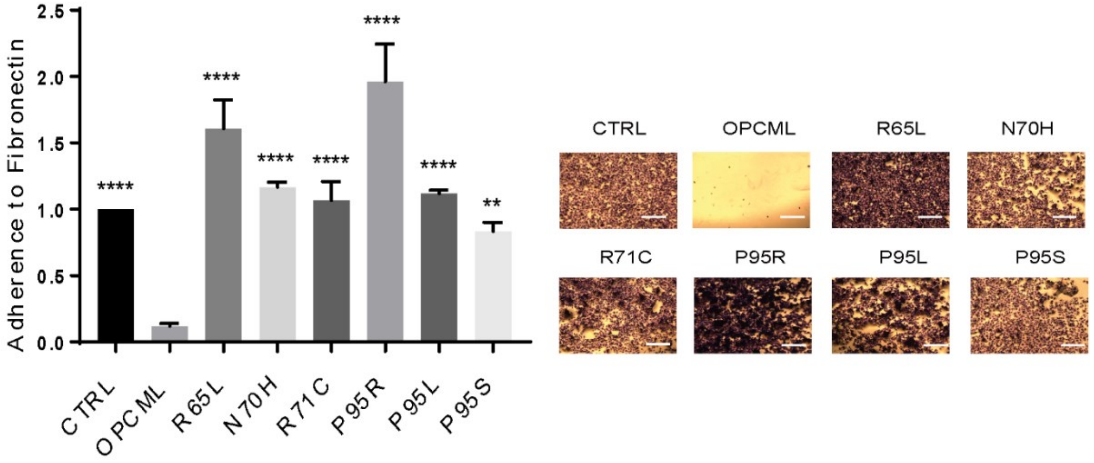
B


Adherence to Collagen IV
Adherence to collagen IV
CTRL
OPCML
R65L
N70H
R71C
P95R
P95L
P95S

C


Adherence to Laminin I
Adherence to Laminin I
CTRL
OPCML
R65L
N70H
R71C
P95R
P95L
P95S

D


Adherence to Fibronectin
Adherence to Fibronectin
2.5
2.0
1.5
1.0
0.5
0.0
****
****
****
****
****
****
**
CTRL
OPCML
R65L
N70H
R71C
P95R
P95L
P95S
CTRL
OPCML
R65L
N70H
R71C
P95R
P95L
P95S

E

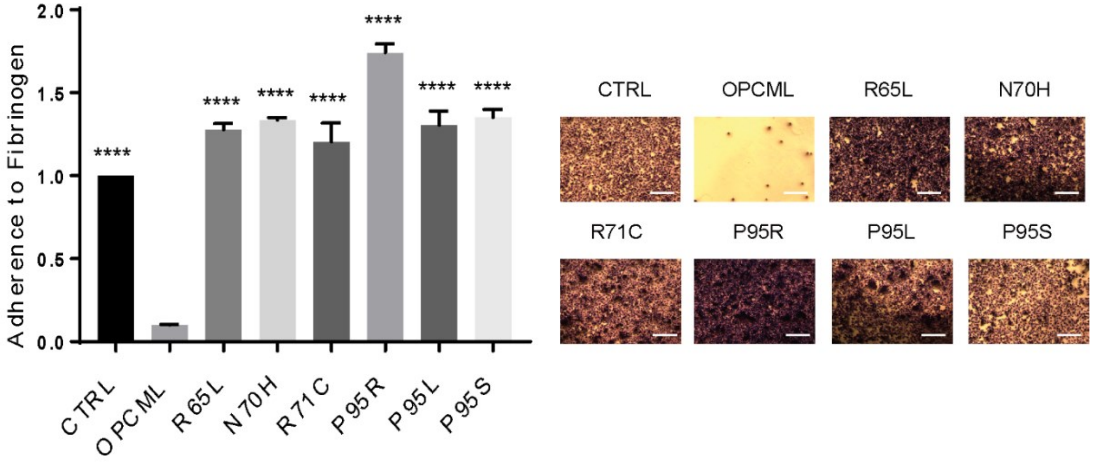

Adherence to Fibrinogen
Adherence to Fibrinogen
2.0
1.5
1.0
0.5
0.0
****
****
****
****
****
****
****
CTRL
OPCML
R65L
N70H
R71C
P95R
P95L
P95S
CTRL
OPCML
R65L
N70H
R71C
P95R
P95L
P95S

Figure 4.15 OPCML mutants in domain I alter OPCML-regulated adherence to extracellular matrix components.

The cell adhesion assay of ovarian cancer SKOV3 cells transduced with wild-type OPCML, OPCML R65L, OPCML N70H, OPCML R71C, OPCML P95R, OPCMLP95L, and OPCML P95S, and control. 1.5 X10^5 cells/ well were seeded in CytoSelect 48-well plates. Cells were allowed to adhere for 90 minutes after which they were stained with 0.09% crystal violet, extracted with 10% acetic acid and then measured at 560 nm in a computer-interfaced 96-well tunable microtiter plate reader. Bovine serum albumin (BSA) was used as negative control. The images were taken with a Nikon Eclipse TE2000-U microscope and Q-Capture Pro software, and representative colour images of the well-containing cells acquired at 10× magnification are shown the right panels. The left panels show bar charts of the results obtained colourimetrically. Three independent experiments were performed; the data are presented as a mean and standard error of the mean (SEM, error bar). The significance of the differences was determined by one-way ANOVA analysis using Prism 7 with Bonferroni correction (* $P < 0.0355$; ** $P < 0.0019$; **** $P < 0.0001$; ns= non-significant; scale bar, 50 μm). Plates were pre-coated with (A) collagen I, (B) collagen IV, (C) laminin I, (D) fibronectin, and (E) fibrinogen.

4.16. OPCML mutants impair the inhibitory interaction of OPCML with many RTKs.

Next, after identifying the OPCML mutants in domain I that show loss of many cellular functions, we decided to investigate the interaction between RTKs and OPCML as a mechanism to explain these phenotypes. To reveal the complete picture of the activated RTKs in the presence of these mutations we employed an implemented screening tool to assess and examine the activity of 42 RTKs.

In order to perform the experiment, we used a human phospho-RTK array to compare the phosphorylation status of 42 RTKs in SKOV3 cell line transduced with OPCML wild-type, OPCML R65L, OPCML N70H, OPCML P95R, OPCML P95L, and OPCML P95S.

The results showed that while OPCML wild-type inhibited the phosphorylation of many RTKs, OPCML mutants showed loss of this regulation, as summarised in table 4.1.

To validate the results of the phospho-RTK array in individual SKOV3 cell lines, we performed standard Western Blot analysis of OPCML mutants and OPCML wild-type, focussing on EGFR, HER2, H-RYK and IGFIR.

Table 4.1 Phosphoprotein screening array results for OPCML mutants, OPCML wild-type and control in ovarian cancer.

A table of the results of the Proteome Profiler Human Phospho-RTK Array shows the most phosphorylated RTKs in ovarian cancer SKOV3 cells transduced with wild-type OPCML, OPCML R65L, OPCML N70H, OPCML P95R, OPCMLP95L, and OPCML P95S, and control. (+, ++, +++) represent the level of phosphorylation of OPCML mutants and control compared to wild-type OPCML; (-) represent the level of phosphorylation not detected or very low.

RTK	CTRL	OPCML	R65L	N70H	P95R	P95L	P95S
EGFR	+++	+++	+++	+++	+++	+++	+++
HER2	+++	_	+++	+++	+++	+++	+++
HER3	+++	+++	+++	+++	+++	+++	+++
HER4	+++	_	+++	+++	+++	+++	+++
H-RYK	+++	_	+++	+++	+++	+++	+++
IGFIR	+++	_	+++	+++	+++	+++	+++
PDGFR (PDGFRα)	+++	_	+++	+++	+++	+++	+++
PDGFR (SCFR)	+++	_	+++	+++	+++	+++	+++
EphB3	+++	_	+++	+++	+++	+++	+++
EphA2	+++	_	+++	+++	+++	+++	+++
EphA10	+++	_	+++	+++	+++	+++	+++
C-RET	+	_	+++	_	_	+++	+++
ROR-1	+	_	+++	+	+	+++	+++
ROR-2	++	_	+++	+++	+++	+++	+++

4.16.1. **OPCML mutants lose of OPCML's activity on the EGFR family downstream signalling.**

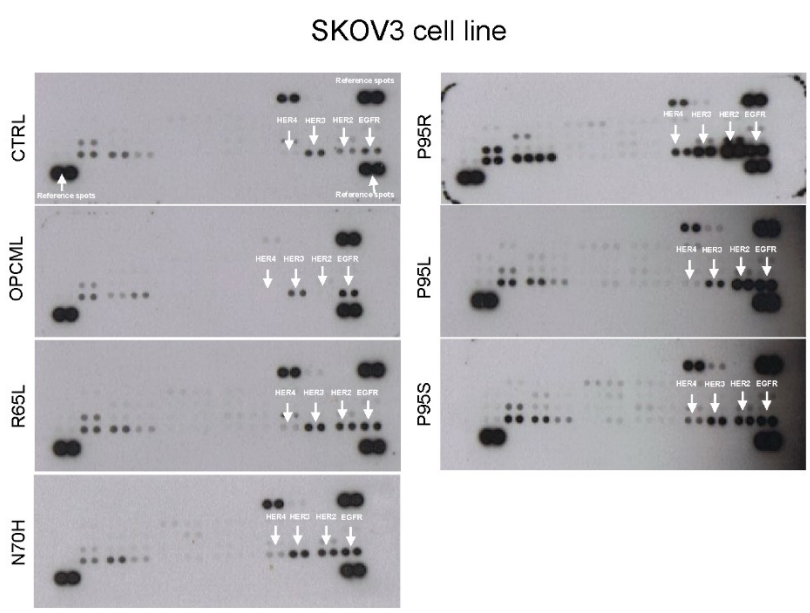
Among the 42 RTKs investigated through the proteome array, we identified the EGFR family as one of those with loss of inhibitory activity in the OPCML mutants (Figure 4.16.1 A). In particular, while OPCML wild-type suppressed the phosphorylation of HER2 and HER4, OPCML mutants showed loss of regulation for both. Strong phosphorylation of EGFR and HER3 were maintained in wild-type OPCML, OPCML mutants, and control cell lines (Figure 4.16.1 B).

Western blot analysis used to validate the protein array data confirmed these results with both the phospho- and total-HER2 levels reduced in wild-type OPCML cells compared to control and OPCML mutants. The levels of both phosphorylated and total EGFR proteins did not change in wild-type OPCML, OPCML mutants, and control confirming the results of the proteome array (Figure 4.16.1 C).

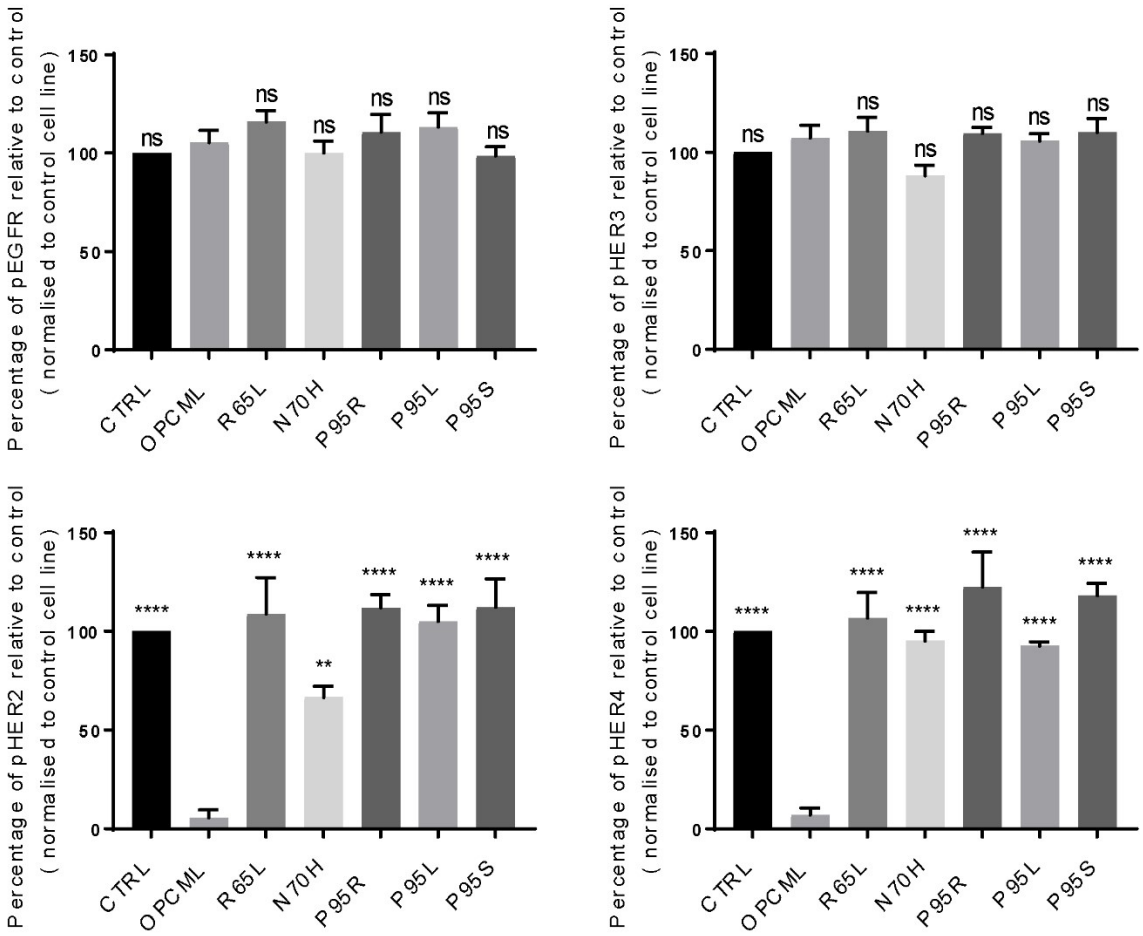
In addition to this, OPCML wild-type cells showed downregulation of the phosphorylated AKT while no difference between OPCML mutants and control was found (Figure 4.16.1 C).

Our results indicate that OPCML mutants in domain I deregulated the interaction between OPCML and RTKs compared to wild-type OPCML, which exhibits a significant suppression of HER2, HER4, and AKT.

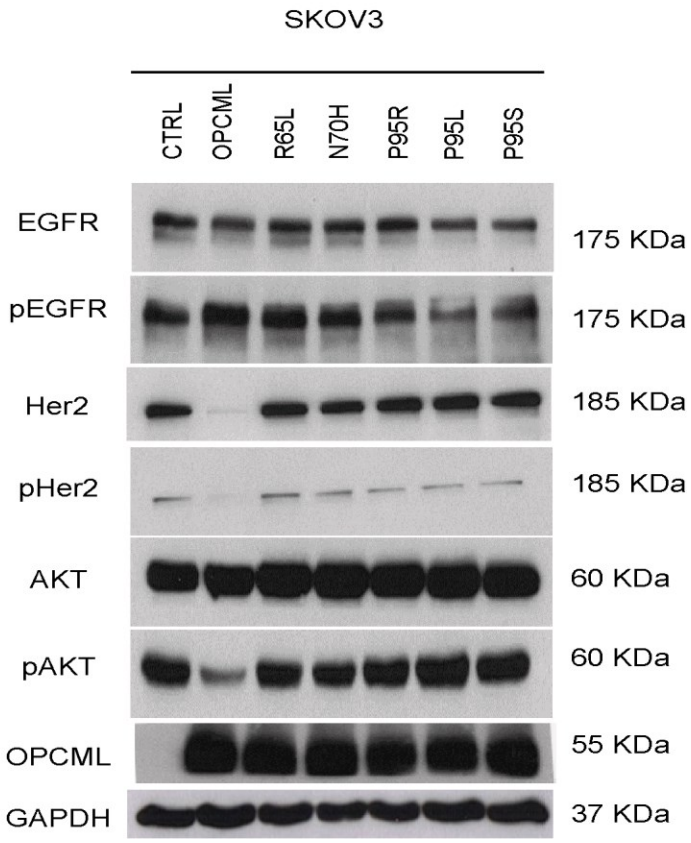
A


SKOV3 cell line
CTRL
OPCML
R65L
N70H
P95R
P95L
P95S
Reference spots
HER4 HER3 HER2 EGFR

B


Percentage of pEGFR relative to control (normalised to control cell line)
Percentage of pHER3 relative to control (normalised to control cell line)
Percentage of pHER2 relative to control (normalised to control cell line)
Percentage of pHER4 relative to control (normalised to control cell line)
150
100
50
0
ns
**
****
CTRL
OPCML
R65L
N70H
P95R
P95L
P95S

C


SKOV3
CTRL
OPCML
R65L
N70H
P95R
P95L
P95S
EGFR
175 KDa
pEGFR
175 KDa
Her2
185 KDa
pHer2
185 KDa
AKT
60 KDa
pAKT
60 KDa
OPCML
55 KDa
GAPDH
37 KDa

D

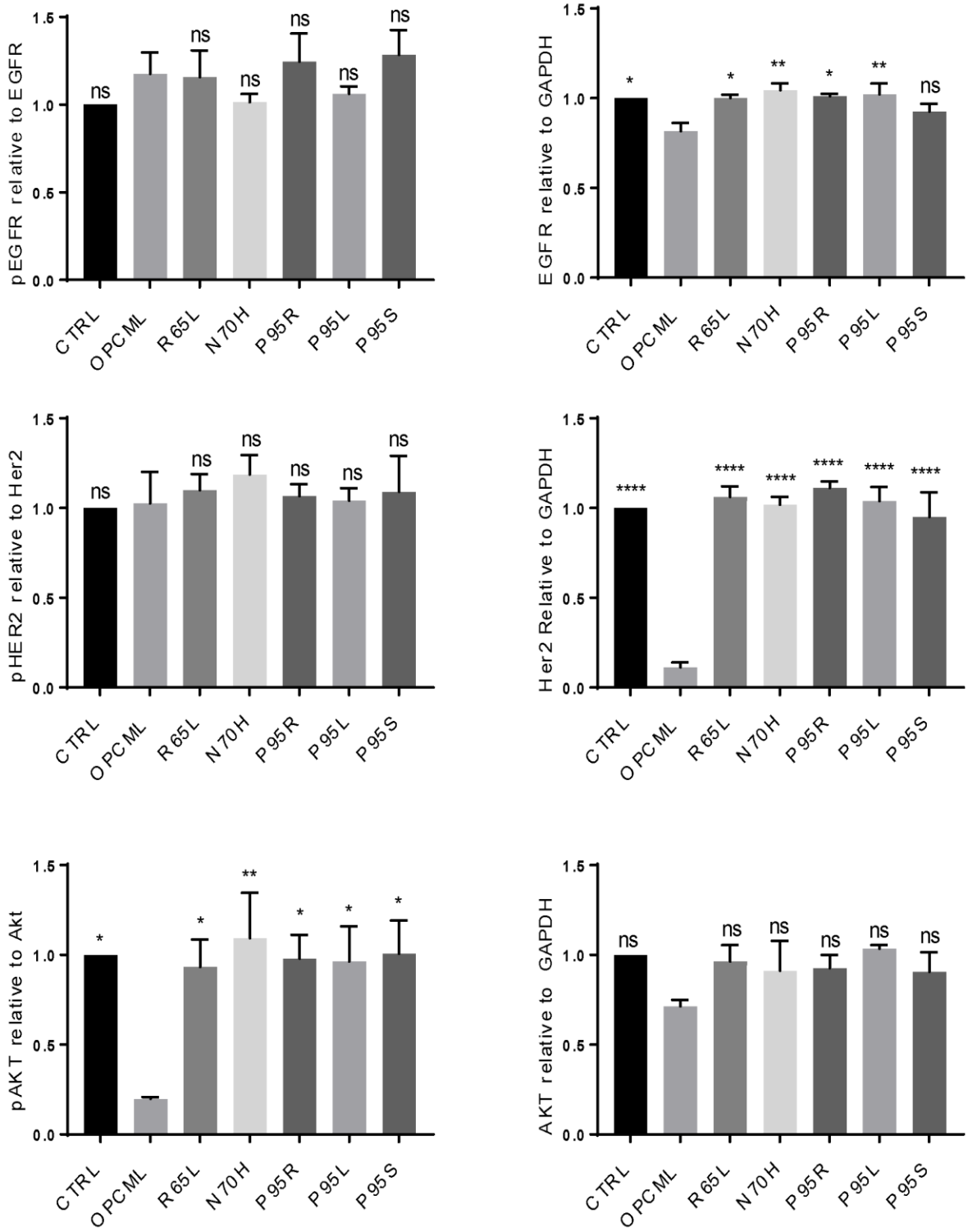

pEGFR relative to EGFR
EGFR relative to GAPDH
pHER2 relative to Her2
Her2 Relative to GAPDH
pAKT relative to Akt
AKT relative to GAPDH
CTRL
OPCML
R65L
N70H
P95R
P95L
P95S
ns
*
**
****
1.5
1.0
0.5
0.0

Figure 4.16.1 OPCML mutants lose OPCML's activity on the EGFR family downstream signalling.

A. The Human Phospho-RTK arrays of ovarian cancer SKOV3 transduced with wild-type OPCML, OPCML R65L, OPCML N70H, OPCML R71C, OPCML P95R, OPCMLP95L, and OPCML P95S, and control. 500 µg of the protein lysate were added to the membrane, incubated overnight, washed and further incubated with pan anti-phospho-tyrosine antibody conjugated to horseradish peroxidase, after which the arrays were washed and visualised using Chemiluminescence ECL. Three independent experiments were performed.

B. A bar chart of the results of the Human Phospho-RTK arrays analysis. The difference in phosphorylation of HER2, and HER4 between wild-type OPCML and OPCML mutants in the SKOV3 cell line was statistically significant, also comparing to the control was significant. The difference in phosphorylation of EGFR, and HER3 between wild-type OPCML and OPCML mutants in the SKOV3 cell line was statistically non-significant, also comparing to the control was non-significant.The significance of the differences was determined by one-way ANOVA analysis using Prism 7 with Bonferroni correction (*n* = 3; mean ± SEM; ** P = 0.0029; **** P < 0.00001; ns, not significant).

C. Western Blot analysis showing phosphorylation and the total expression of EGFR, HER2, AKT, OPCML in cells stably transduced with wild-type OPCML or OPCML mutants (OPCML R65L, OPCML N70H, OPCML P95R, OPCML P95L, OPCML P95S) compared to cell lines stably transduced with an empty vector as control (CTRL). GAPDH was used as loading control.

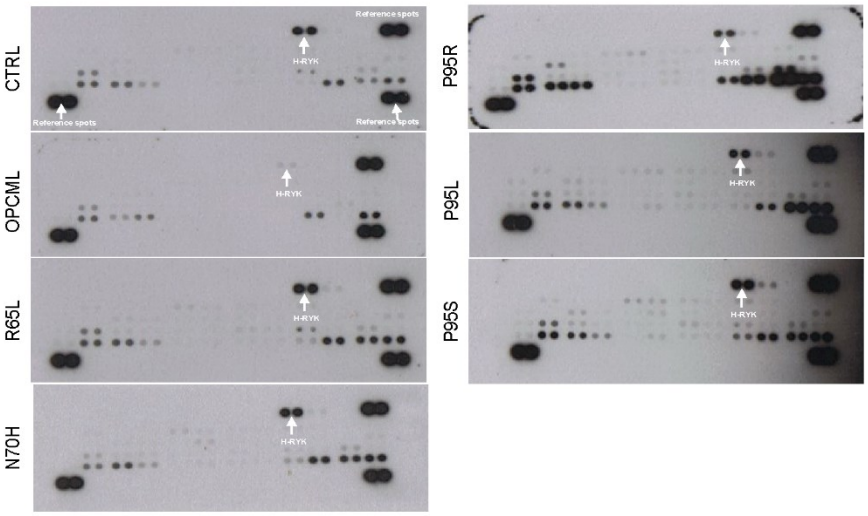
D. A bar chart of the results of Western Blot analysis is shown. The difference in phosphorylation of HER2 and AKT between wild-type OPCML and OPCML mutants in the SKOV3 cell line was statistically significant, also compared to the control it was significant. The difference in phosphorylation of EGFR between wild-type OPCML and OPCML mutants in the SKOV3 cell line was statistically non-significant, also compared to the control it was non-significant. The significance of the differences was determined by one-way ANOVA analysis using Prism 7 with Bonferroni correction (n = 3; mean ± SEM; * P = 0.0130; ** P = 0.0038; **** P<0.0001; ns, not significant).

4.16.2. **OPCML mutants block the inhibitory function on H-RYK downstream signalling.**

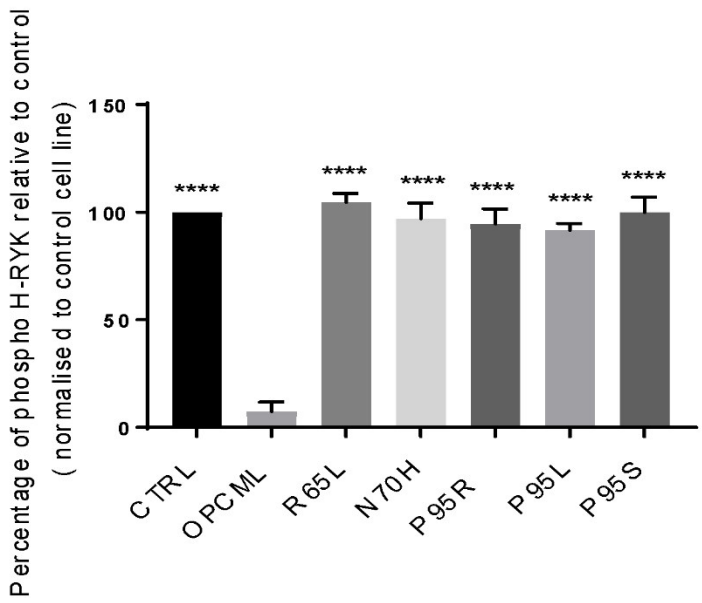
Next, we looked at H-RYK, one of the RTKs with increased phosphorylation in the OPCML mutants and control compared to OPCML wild-type (Figure 4.16.2 A). Analysis of the results revealed a statistically significant difference in the suppression of the phosphorylation of H-RYK in wild-type OPCML compared to OPCML mutants and control (Figure 4.16.2 B).

To validate these results, since there is no specific anti p-RYK antibody available against H-RYK, we validated our findings indirectly by using co-immunoprecipitation. H-RYK was then immunoprecipitated with an anti-H-RYK antibody, and we used Western Blot analysis to detect the presence of OPCML and pan phospho-tyrosines in the eluate. The co-IP showed that H-RYK associated with OPCML wild-type and the OPCML mutants. Despite the fact that wild-type OPCML cells showed a downregulated total level of H-RYK, OPCML was co-immunoprecipitated with the receptor. Furthermore, the H-RYK IP in the OPCML wild-type-expressing cells had considerable less phospho-H-RYK. In order to elucidate other possible RTK partners that could interact with H-RYK and OPCML through direct interaction or as part of a complex, we looked at EGFR, HER2 and EphA2, which have been suggested to interact with OPCML. While it was not possible to reach a conclusion for EGFR and HER2, we found that EphA2 was strongly present in the eluate with H-RYK and OPCML (Figure 4.16.2 C).

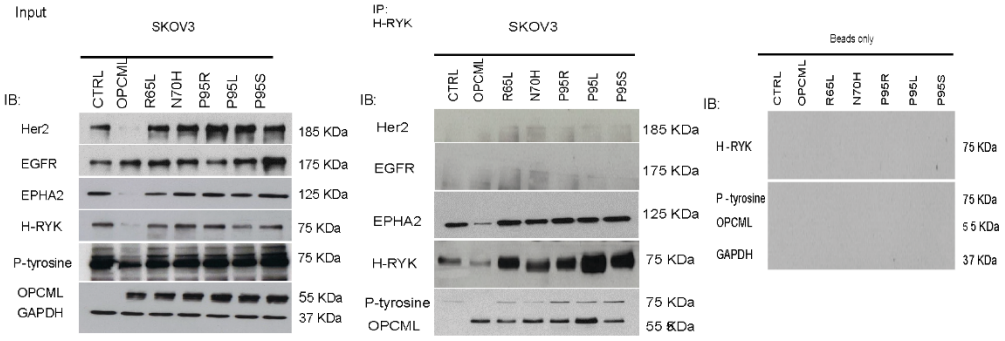
A


CTRL
OPCML
R65L
N70H
P95R
P95L
P95S
H-RYK
Reference spots

B


Percentage of phospho H-RYK relative to control
(normalised to control cell line)
150
100
50
0
****
CTRL
OPCML
R65L
N70H
P95R
P95L
P95S

C


Input
SKOV3
CTRL
OPCML
R65L
N70H
P95R
P95L
P95S
IB:
Her2
EGFR
EPHA2
H-RYK
P-tyrosine
OPCML
GAPDH
185 KDa
175 KDa
125 KDa
75 KDa
75 KDa
55 KDa
37 KDa
IP:
H-RYK
SKOV3
Beads only
55 KDa

D

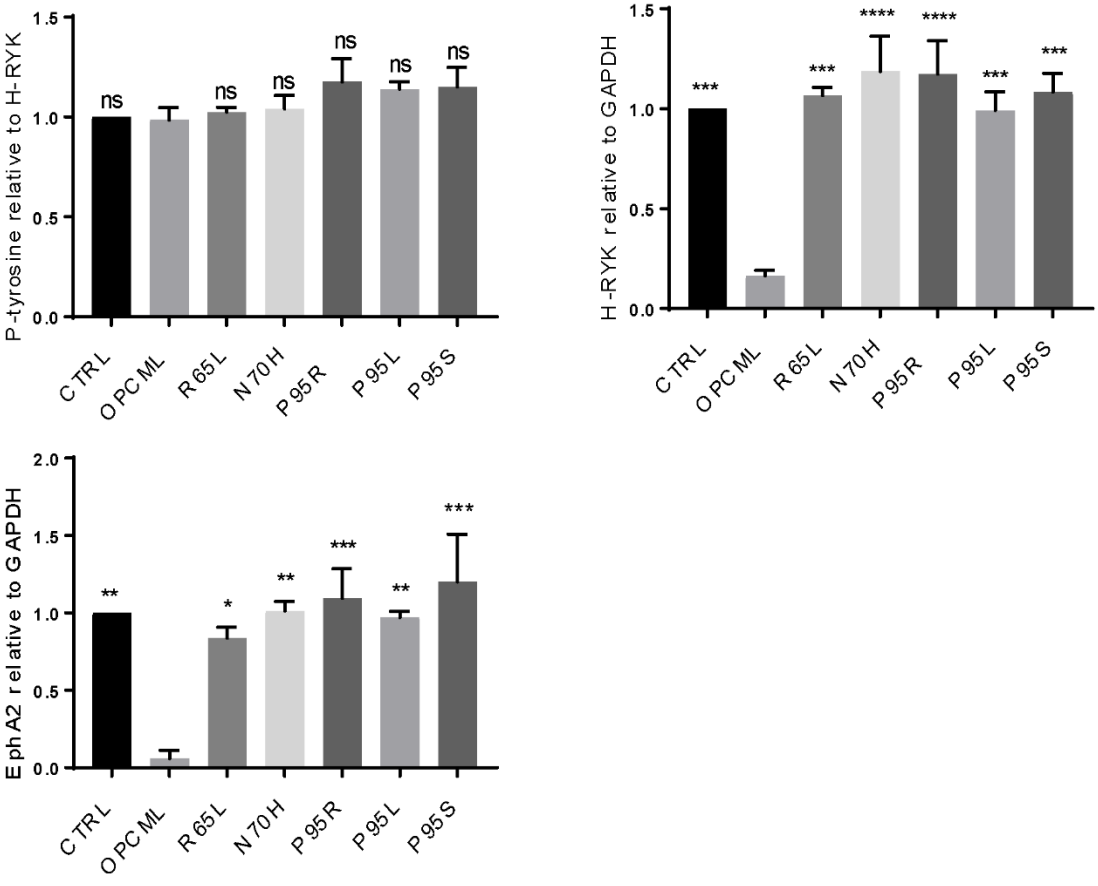

P-tyrosine relative to H-RYK
H-RYK relative to GAPDH
EphA2 relative to GAPDH
ns
*
**
***
****
CTRL
OPCML
R65L
N70H
P95R
P95L
P95S

Figure 4.16.2 OPCML mutants block the inhibitory function on H-RYK downstream signalling.

A. The Human Phospho-RTK arrays of ovarian cancer SKOV3 transduced with wild-type OPCML, OPCML R65L, OPCML N70H, OPCML R71C, OPCML P95R, OPCML P95L, and OPCML P95S, and control. 500 µg of the protein lysate were added to the membrane, incubated overnight, washed and further incubated with pan anti-phospho-tyrosine antibody conjugated to horseradish peroxidase, after which the arrays were washed and visualised using Chemiluminescence ECL. Three independent experiments were performed.

B. A bar chart of the results of the Human Phospho-RTK arrays analysis. The difference in phosphorylation of H-RYK between wild-type OPCML and OPCML mutants in the SKOV3 cell line was statistically significant, also comparing to the control was significant.The significance of the differences was determined by one-way ANOVA analysis using Prism 7 with Bonferroni correction (*n* = 3; mean ± SEM; **** P < 0.00001).

C. Western Blot analysis of co-IP experiment showing in the left panel input expression in cells stably transduced with wild-type OPCML or OPCML mutants compared to cell lines stably transduced with an empty vector as control (CTRL). The middle panel shows the actual immunoprecipitation (IP) with an anti-H-RYK antibody. Antibodies were used to immunoblot against H-RYK, OPCML, pan-p-tyrosine, HER2, EGFR, EphA2 and GAPDH. The right panel shows beads only (*n* = 3).

D. A bar chart of the results of the input co-IP experiments. The difference in expression of H-RYK between wild-type OPCML and OPCML mutants in the SKOV3 cell line was statistically significant, also comparing to the control was significant. The difference in expression of EphA2 between wild-type OPCML and OPCML mutants in the SKOV3 cell line was statistically significant, also comparing to the control was significant. The significance of the differences was determined by one-way ANOVA analysis using Prism 7 with Bonferroni correction (*n* = 3; mean ± SEM; * P = 0.0108; ** P = 0.0021; *** P = 0.0002; **** P < 0.00001; ns, not significant).

4.16.3. **OPCML mutants impair OPCML inhibitory effect on IGFIR downstream signalling.**

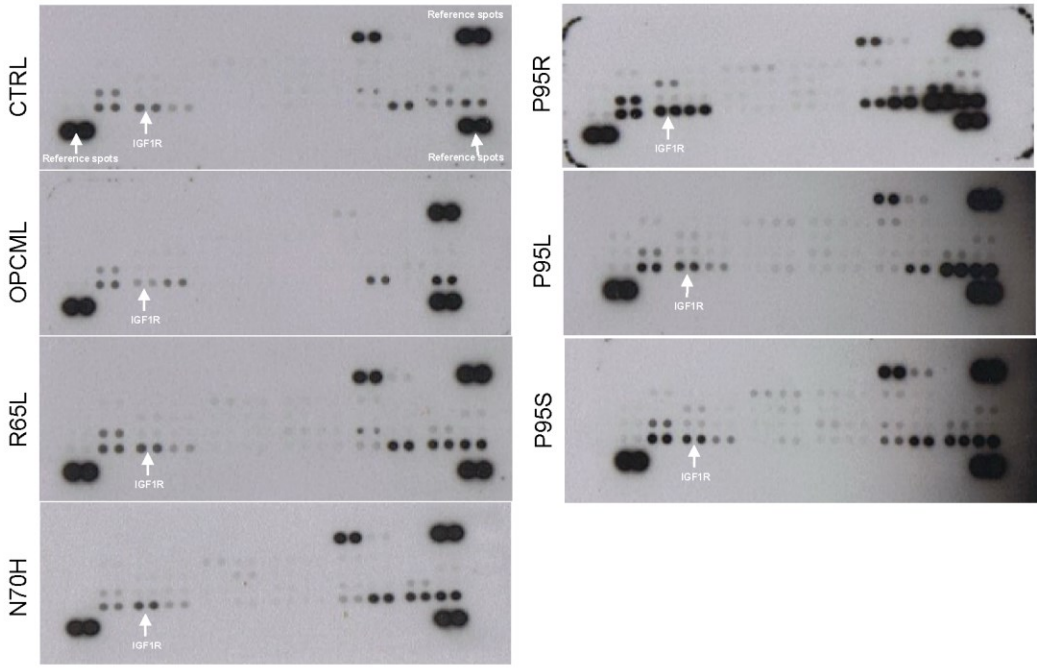
Finally, we identified the IGFIR family of RTKs as one of the families with consistently increased phosphorylation in the OPCML mutants and control compared to the OPCML wild-type (Figure 4.16.3 A). Analysis of the results showed that wild-type OPCML suppression of the phosphorylation of IGFIR is statistically significant compared to OPCML mutants and control (Figure 4.16.3 B).

To validate these results, the same SKOV3 ovarian cancer cell lines were subjected to Western Blot analysis.

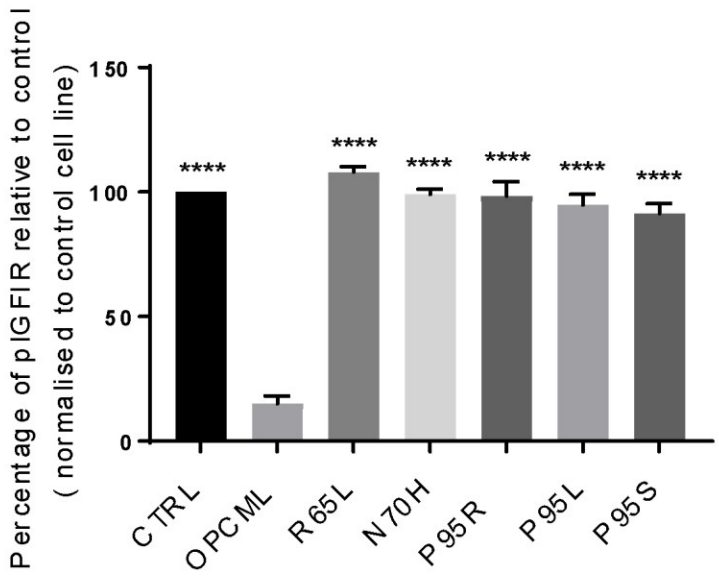
We observed that wild-type OPCML cells had suppressed phosphorylated and total IGFIR compared to OPCML mutants. Some of the OPCML mutants (the ones at position 95) showed an upregulated phosphorylation level of IGFIR compared to control cells (Figure 4.16.3 C).

Analysis of the western blot results revealed a statistical significance between OPCML mutants in domain I and wild-type OPCML in suppressing the phosphorylated and total levels of IGFIR in SKOV3 cells (Figure 4.16.3 D).

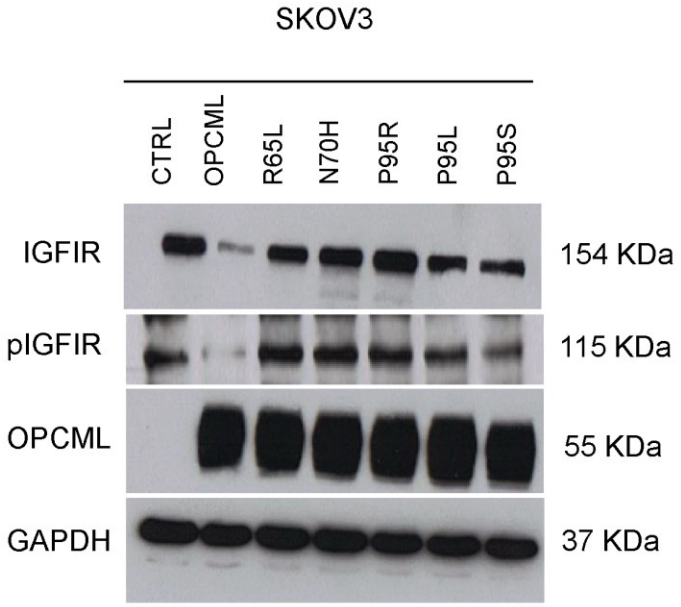
A


CTRL
OPCML
R65L
N70H
P95R
P95L
P95S
Reference spots
Reference spots
Reference spots
IGF1R

B


Percentage of pIGF1R relative to control
(normalised to control cell line)
150
100
50
0
****
CTRL
OPCML
R65L
N70H
P95R
P95L
P95S

C


SKOV3
CTRL
OPCML
R65L
N70H
P95R
P95L
P95S
IGFIR
154 KDa
pIGFIR
115 KDa
OPCML
55 KDa
GAPDH
37 KDa

D

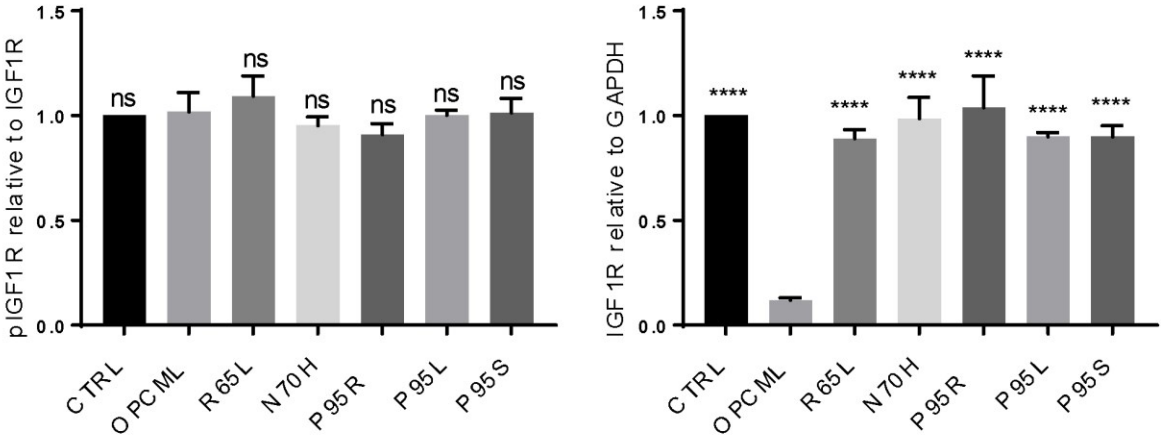

pIGF1R relative to IGF1R
1.5
1.0
0.5
0.0
ns
CTRL
OPCML
R65L
N70H
P95R
P95L
P95S
IGF1R relative to GAPDH
****

Figure 4.16.3 OPCML mutants impair OPCML inhibitory effect on IGFIR downstream signalling.

A. The Human Phospho-RTK arrays of ovarian cancer SKOV3 cells transduced with wild-type OPCML, OPCML R65L, OPCML N70H, OPCML R71C, OPCML P95R, OPCMLP95L, and OPCML P95S, and control. 500 µg of the protein lysate were added to the membrane,, incubated overnight, washed and further incubated with pan anti-phospho-tyrosine antibody conjugated to horseradish peroxidase, after which the arrays were washed and visualised using Chemiluminescence ECL. Three independent experiments were performed.
B. A bar chart of the results of the Human Phospho-RTK arrays analysis. The difference in phosphorylation of IGFIR between wild-type OPCML and OPCML mutants in the SKOV3 cell line was statistically significant, also comparing to the control was significant.The significance of the differences was determined by one-way ANOVA analysis using Prism 7 with Bonferroni correction (*n* = 3; mean ± SEM; **** P < 0.00001).
C. Western Blot analysis showing phosphorylation and the phosphorylated levels and the total expression of IGFIR, OPCML in cells stably transduced with wild-type OPCML or OPCML mutants (OPCML R65L, OPCML N70H, OPCML P95R, OPCML P95L, OPCML P95S) compared to cell lines stably transduced with an empty vector as control (CTRL). GAPDH was used as loading control.
D. A bar chart of the results of Western Blot analysis is shown. The difference in phosphorylation of IGFIR between wild-type OPCML and OPCML mutants in the SKOV3 cell line was statistically significant, also compared to the control it was significant. The significance of the differences was determined by one-way ANOVA analysis using Prism 7 with Bonferroni correction (n = 3; mean ± SEM; **** P<0.0001; ns, not significant).

4.17. OPCML mutants do not exhibit anti-tumorigenic properties *in vivo.*

After looking at the effects of the mutations *in vitro*, we went on to validate the OPCML mutants impairment of OPCML function in ovarian cancer progression *in vivo*. To this end, we generated SKOV3 xenograft mouse models with OPCML wild-type, OPCML R65L, OPCML N70H, OPCML P95R, and control expressing cells.

We used five female Athymic nude mice per cell line and injected them with 5 x 10^6 cells intraperitoneally.

Tumours grew for 8 weeks, after which time mice had to be sacrificed. As expected from cell culture experiments, the results showed that OPCML mutants significantly blocked the OPCML function on tumour growth (Figure 4.17 A) and ascites formation (Figure 4.17 B left panel) over eight weeks compared with wild-type OPCML, which impaired tumour growth and ascites formation. The only exception in the mutants was OPCML N70H, for which we saw a modest, and not statistically significant, effect on the growth and ascites formation compared to wild-type OPCML (Figure 4.17: (A) tumour images, (B) left panel for ascites and right panel for tumour weight).

Immunofluorescence was then employed to assess the expression of OPCML in paraffin-embedded sections of representative tumours. By using an antibody against OPCML, we confirmed that all the OPCML mutants were expressed (Figure 4.17 C).

We then further validated these results in another *in vivo* model, and we employed the chick embryo chorioallantoic membrane (CAM) model to assess tumour growth.

SKOV3 GFP-labelled cell line were transduced with OPCML wild-type, OPCML R65L, OPCML R214Q from OPCML domain II, OPCML M278I OPCML domain III and control.

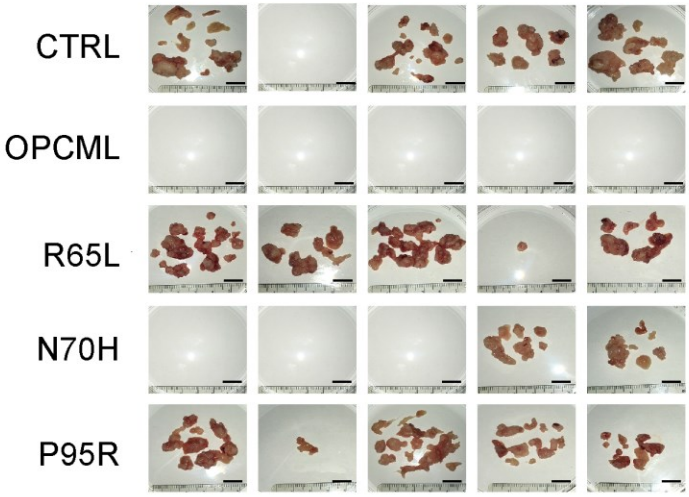
To perform this experiment, we used 1 x 10^6 cells embedded in a total volume of 50 µl of matrigel which was then grafted on embryonic day 7 (ED7) on the CAM and excised on ED15.

OPCML mutants cell lines showed significant growth in tumour size as compared with wild-type OPCML (Figure 4.17 D upper panel). Analysis of the results revealed a statistically significant difference in tumour growth between OPCML mutants and wild-type OPCML (Figure 4.21 D lower panel).

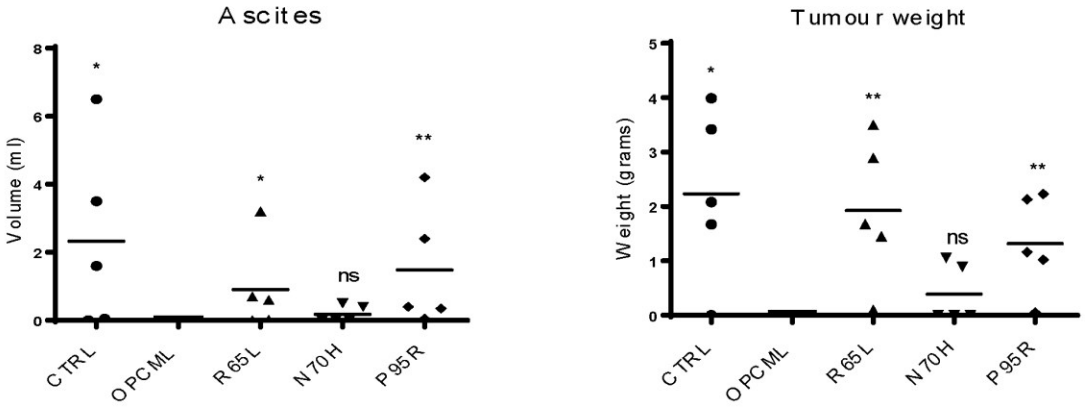
Furthermore, OPCML mutants and OPCML wild-type expression was confirmed after terminating the experiment in the excised tumours by immunofluorescence of the paraffin-embedded sections of the tumours (Figure 4.21 E).

Accordingly, the results from the mice xenograft model and the CAM model suggest that OPCML domain I mutants show loss of function in *vivo* and could block the OPCML inhibition of tumour growth in *vivo*.

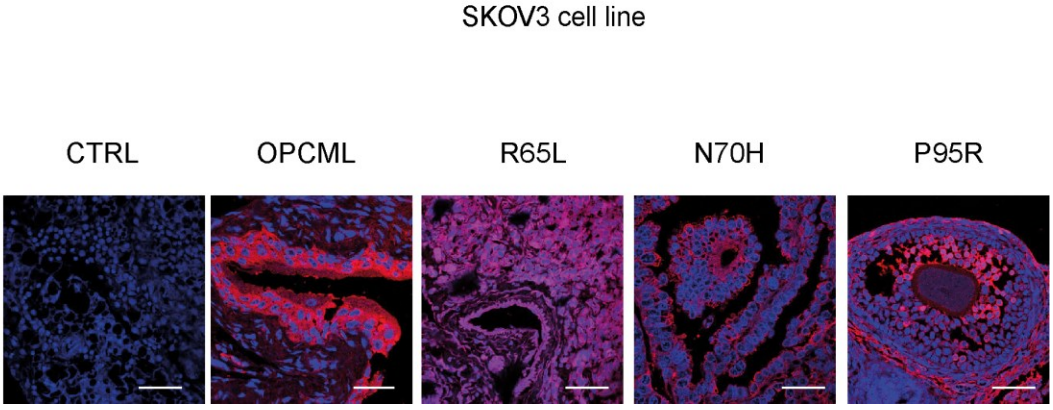
A


CTRL
OPCML
R65L
N70H
P95R

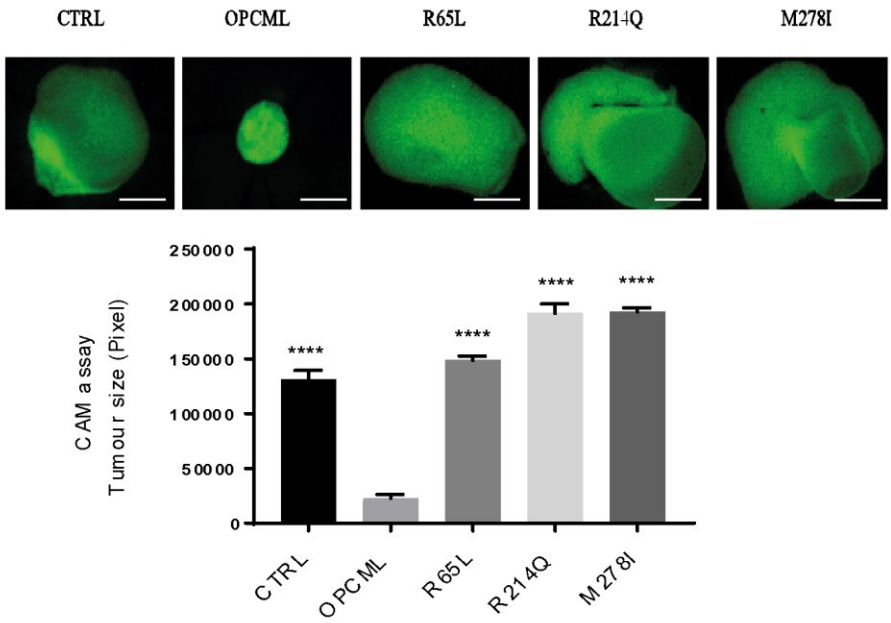
B


Ascites
Volume (ml)
0
2
4
6
8
*
*
ns
**
CTRL
OPCML
R65L
N70H
P95R
Tumour weight
Weight (grams)
0
1
2
3
4
5
*
**
ns
**
CTRL
OPCML
R65L
N70H
P95R

C


SKOV3 cell line
CTRL
OPCML
R65L
N70H
P95R

D


CTRL
OPCML
R65L
R214Q
M278I
CAM assay
Tumour size (Pixel)
250000
200000
150000
100000
50000
0
****
****
****
****
CTRL
OPCML
R65L
R214Q
M278I

E

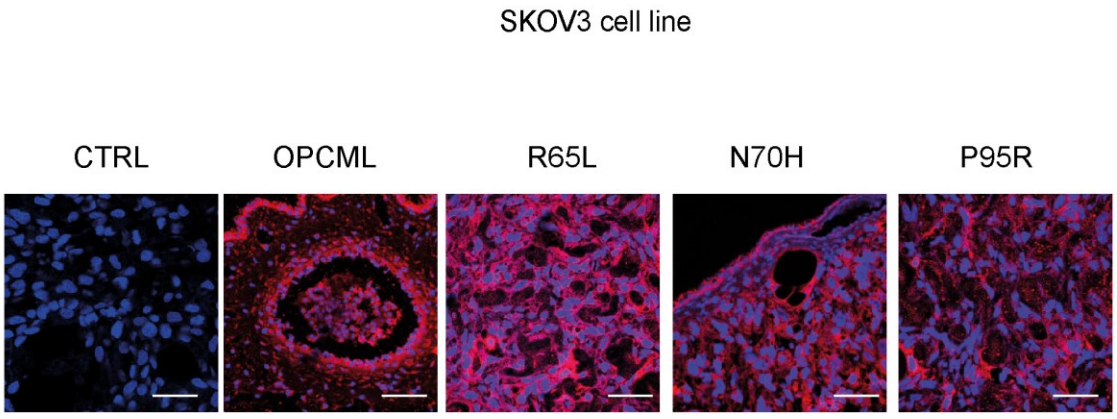

SKOV3 cell line
CTRL
OPCML
R65L
N70H
P95R

Figure 4.17 OPCML mutants do not exhibit anti-tumorigenic properties *in vivo*.

A. Xenograft mice models of ovarian cancer SKOV3 cell line transduced with wild-type OPCML, OPCML R65L, OPCML N70H, OPCML P95R, and control. Athymic mice were injected intraperitoneal with 5 $X10^6$ cells and followed for eight weeks. At the end of experiments, tumours were collected and photographed. Scale bar = 500 μm.
B. A scatter plot of the results of the mouse xenograft model analysis is shown in the left panel for ascites, and in the right panel for tumour weight. The left panel shows ascites collected at the end of the experiments. The difference in ascites volume between wild-type OPCML and OPCML mutants (OPCML R65L, OPCML P95R) and control in the SKOV3 cell line was statistically significant, but compared to the OPCML N70H it was non-significant. The right panel shows tumour weight measured at the end of the experiments. The difference in tumour weight volume between wild-type OPCML and OPCML mutants (OPCML R65L, OPCML P95R) and control in the SKOV3 cell line was statistically significant, but compared to the OPCML N70H it was non-significant. The significance of the differences was determined by one-way ANOVA analysis using Prism 7 with Bonferroni correction (*n* = 1; mean ± SEM; * P < 0.01; ** P < 0.001; ns, not significant;).
C. Immunofluorescence microscopy staining of Paraffin-embedded sections of tumours from the mouse xenograft model reveals that OPCML is expressed in the SKOV3 cell line (red colour); the nucleus is shown in blue. The images show OPCML R65L, OPCML N70H, and OPCML P95R expression compared to wild-type OPCML and control in stably transduced SKOV3 cell lines (scale bar, 20 μm).
D. Chick embryo chorioallantoic membrane (CAM) model of ovarian cancer SKOV3 GFP-labelled cell line transduced with wild-type OPCML, PCML R65L, OPCML R214Q from OPCML domain II, OPCML M278I from OPCML domain III, and control. The upper panel shows images acquired using the stereomicroscope for spatial vision SteREO Discovery.V8 (Zeiss, Germany) with Zen 2 Capture software (Zeiss, Germany).The lower panel shows a bar chart of the results of the CAM model analysis. The difference in tumour growth size between wild-type OPCML and OPCML mutants in the SKOV3 cell line was statistically significant, also comparing to the control was significant.The significance of the differences was determined by one-way ANOVA analysis using Prism 7 with Bonferroni correction (*n* = 3; mean ± SEM; **** P < 0.0001 scale bar, 50 μm).
E. Immunofluorescence microscopy staining of paraffin-embedded sections of tumours from the CAM model reveals that OPCML is expressed in the SKOV3 cell line (red colour); the nucleus is shown in blue. The images show OPCML R65L, OPCML R214Q, and OPCML M278I expression compared to wild-type OPCML and control in stably transduced SKOV3 cell lines (scale bar, 20 μm).

4.18. Summary and key findings

In this Chapter, we created three stable ovarian cancer cell lines SKOV3, PEA1, and PEO1 by transducing them with OPCML mutants in domain I, OPCML wild-type, and control, and we confirmed that OPCML mutants and wild-type OPCML were highly expressed in all of them. Furthermore, our data strongly indicated that OPCML mutants in domain I still inhibited cell proliferation but showed loss of function in colony formation, migration, invasion and resistance to target therapy. Interestingly, we showed in this study that OPCML abrogated the phosphorylation of downstream AKT and ERK signalling through interaction and downregulation of RTKs. We also showed that OPCML wild-type, but not the mutants, downregulated HER2, EPHA2, IGFIR, and H-RYK, and their downstream AKT and ERK signalling.

We have thus shown for the first time that single amino acid substitutions in OPCML are responsible for the complete loss of function of the tumour suppressor protein.

Furthermore, this evidence has been translated into *in vivo* mice xenograft models and *in ovo* experiments.

Taken together, our findings suggest that OPCML mutants expressed in ovarian cancer cell line result in loss of function that could potentially result in impairing the OPCML function in invasion, migration, tumour formation and resistance to treatment.

5. CHAPTER 5

Role of OPCML domain II mutations

Introduction

OPCML mutations in domain II represent 20.3% of all the mutations identified, compared to 33.9% for domain I and 28.8% for domain III.

In this chapter, we will investigate how mutations in the domain II affect the protein function and in order to do so we:

1. Generated an ovarian cancer cell line, SKOV3, overexpressing OPCML mutants in domain II (OPCML E201Q, OPCML S203R and OPCML R214Q), wild-type OPCML and empty vector control (CTRL).
2. Investigated the localisation of OPCML mutants compared to wild-type OPCML.
3. Analysed the effects of OPCML mutants in domain II on tumour growth, cell adhesion, anchorage-independent cellular growth, invasion, and migration.

5.1. Identification of OPCML mutations in domain II using the public datasets TCGA and COSMIC and mapping them onto the OPCML crystal structure

When we looked at the TCGA and COSMIC datasets we found that some patients (67 out of 28,132 distributed across all cancer types), presented point mutations in domain II of OPCML. These mutations were arranged into particular classes based on the type and location following mapping onto the crystal structure (Figure 5.1A).

Figure 5.1B shows all mutations observed in domain II and their frequency. We then selected some mutations based on their frequency, occurrence in several tumours and possible impact on the functionality of OPCML. Based on these criteria we finally selected three mutations, namely OPCML E201Q, OPCML S203R, and OPCML R214Q.

The first mutation, E201Q, causes a change from glutamic acid into glutamine; it occurs 9 times in three different types of tumours, namely colorectal, melanoma and lung squamous-cell carcinoma. Three-dimensional molecular modelling showed that this mutant is exposed on the protein's surface, where it may play a role in the interaction with RTKs.

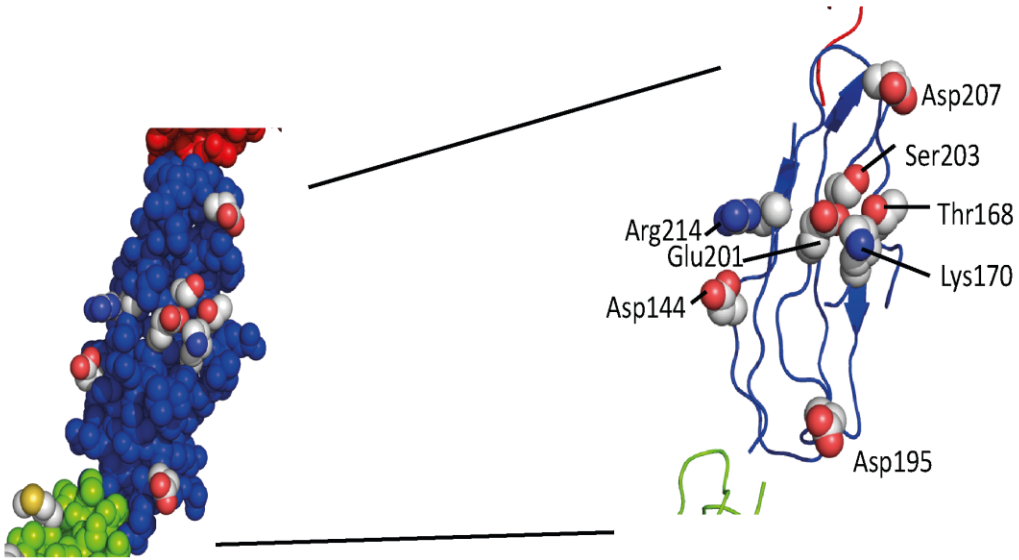
The second mutation investigated, S203R, is a serine changed into arginine. It occurs 6 times in two different types of tumours .This mutation is found in lung adenocarcinomas and head-and-neck squamous cell carcinomas. This mutant also causes a structure modification on the surface, and again could play a role in the interactions with RTKs.

The third mutation, R214Q, changes arginine to glutamine. OPCML R214Q is found 5 times in patients with bladder carcinoma and lung adenocarcinoma. Again, the

structure modification caused by this mutant is on the surface, where it may also play a role in the interaction with RTKs.

Figure 5.1C presents a summary of the mutations used in this study, giving their positions, the amino acid changes, the cancer type and their possible impact on the crystal structure.

A



DOMAIN II

```
                                                    CCT CCT CAG ATC ATG AAT   420
                                                      P   P   Q   I   M   N   140

ATC TCC TCA GAC ATC ACT GTG AAT GAG GGA AGC AGT GTG ACC CTG CTG TGT CTT GCT ATT   480
  I   S   S   D   I   T   V   N   E   G   S   S   V   T   L   L   C   L   A   I   160

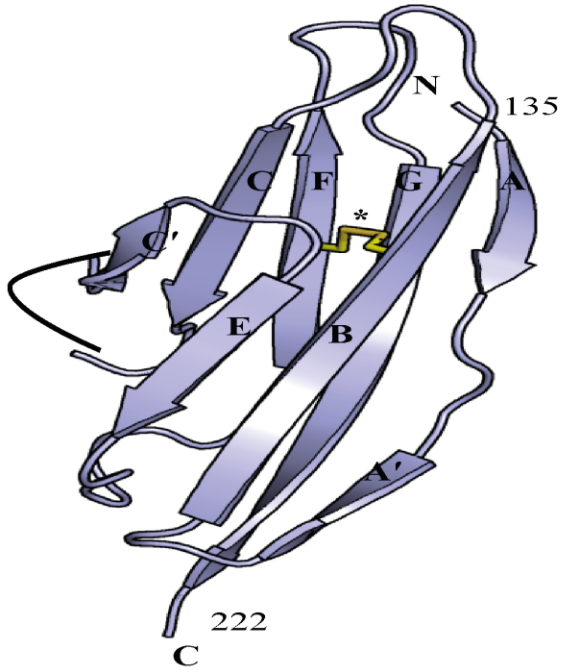
GGC AGA CCA GAG CCA ACT GTG ACA TGG AGA CAC CTG TCA GTC AAG GAA GGC CAG GGC TTT   540
  G   R   P   E   P   T   V   T   W   R   H   L   S   V   K   E   G   Q   G   F   180

GTA AGT GAG GAT GAG TAC CTG GAG ATC TCT GAC ATC AAG CGA GAC CAG TCC GGG GAG TAC   600
  V   S   E   D   E   Y   L   E   I   S   D   I   K   R   D   Q   S   G   E   Y   200

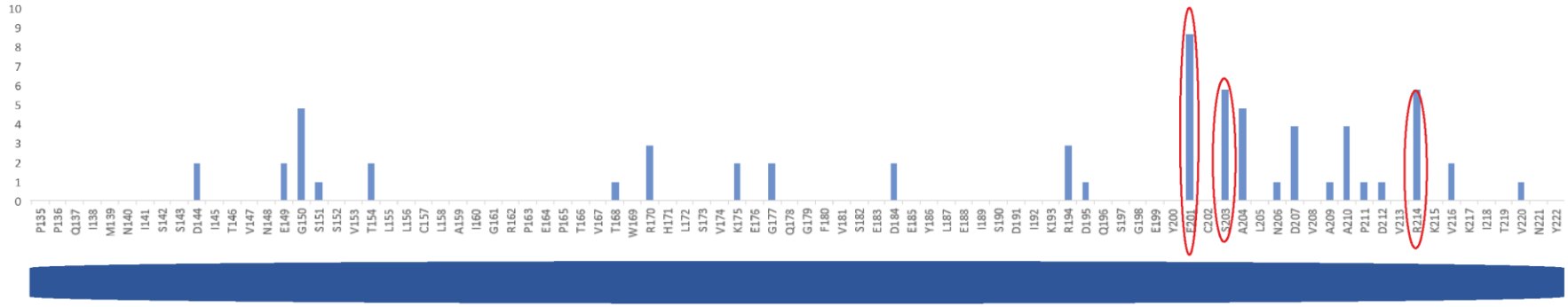
GAA TGC AGC GCG TTG AAC GAT GTC GCT GCG CCC GAT GTG CGG AAA GTA AAA ATC ACT GTA   660
  E   C   S   A   L   N   D   V   A   A   P   D   V   R   K   V   K   I   T   V   220

AAC TAT                                                                         720
  N   Y                                                                         240
```

DOMAIN II



B



C

Position	Cancer type	AA changed	Frequency	Modification
E201	Lung	Q	3	Surface exposed
	Colorectal, and Skin	K	6	Surface exposed
S203	Lung, and Head and Neck	R	6	Surface exposed
R214	Bladder	Q	3	Surface exposed
	Lung	P	2	Surface exposed
	Lung	W	1	Surface exposed

Figure 5.1 Crystal structure of OPCML with domain II mutations mapped.

A. Mutations mapped on the tertiary structure of OPCML. The right upper panel shows the sequence of human OPCML domain II with the position of the selected OPCML mutants coloured in pink. The right lower panel shows ribbon diagrams of domains II in salmon, it belongs to the V-set subfamily of Ig domains and consists of nine β-strands. Disulfide bridges connect all B and F strands and are indicated (*). The N- and C- termini are indicated and are numbered. Casanova reference inside Diedrich reference.
B. Among all mutations observed in OPCML domain II in this study, the mutations to domain II chosen are encircled.
C. Summary table of OPCML domain II mutations chosen, giving the mutation's position, cancer type, amino acid changed, and the localisation on the crystal structure.

5.2. Creation and characterisation of mutants in stable ovarian cancer cell lines

To understand the biological role of the mutations in domain II of OPCML, the SKOV3 cells were selected for the creation of stable cell lines expressing wild-type OPCML, mutants or empty vector by viral transduction.

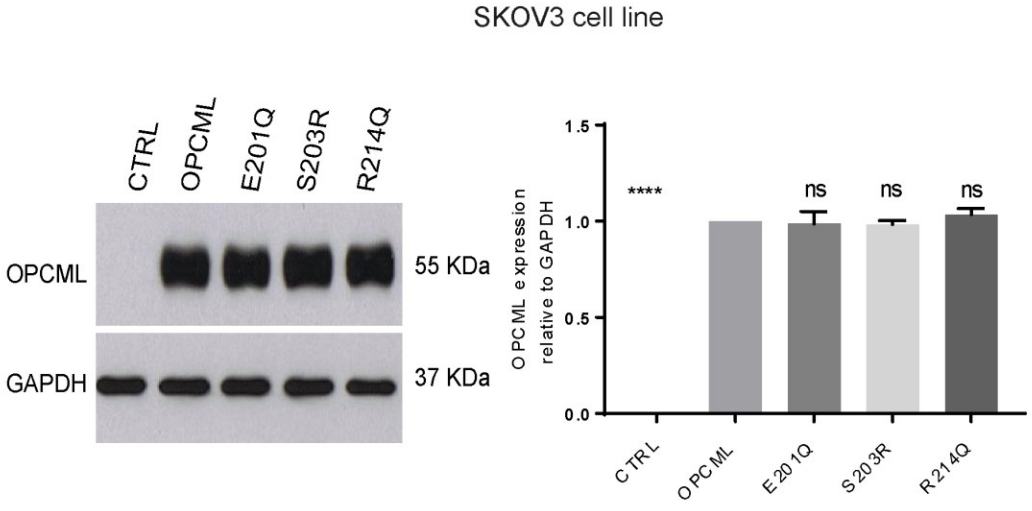
Each construct was verified by sequencing before creating the viruses used to transduce the ovarian cancer cell line.

OPCML expression was first confirmed by Western Blot analysis, where it could be visualised at 55 kDa in all the transduced cell lines except in control (CTRL) (Figure 5.2 A, left panel). Quantification of the Western Blot showed no statistical differences between wild-type OPCML expression and that of OPCML mutants (Figure 5.2 A, right panel).

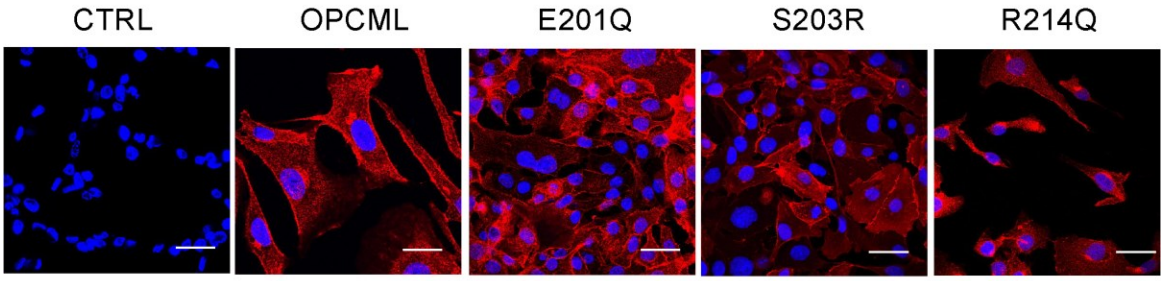
Immunofluorescence was then employed to assess the expression of OPCML. By using an antibody against OPCML, we confirmed that the wild-type and all the mutant OPCML were expressed on the membrane of transduced SKOV3 cell lines (Figure 5.2 B).

The images in Figure 5.2C show wild-type OPCML, OPCML E201Q, S203R, and R214Q localised mainly on the membrane compared to control in stably transduced SKOV3 cell lines.

A


SKOV3 cell line
CTRL
OPCML
E201Q
S203R
R214Q
OPCML
GAPDH
55 KDa
37 KDa
OPCML expression relative to GAPDH
1.5
1.0
0.5
0.0
****
ns
ns
ns
CTRL
OPCML
E201Q
S203R
R214Q

B


CTRL
OPCML
E201Q
S203R
R214Q

C

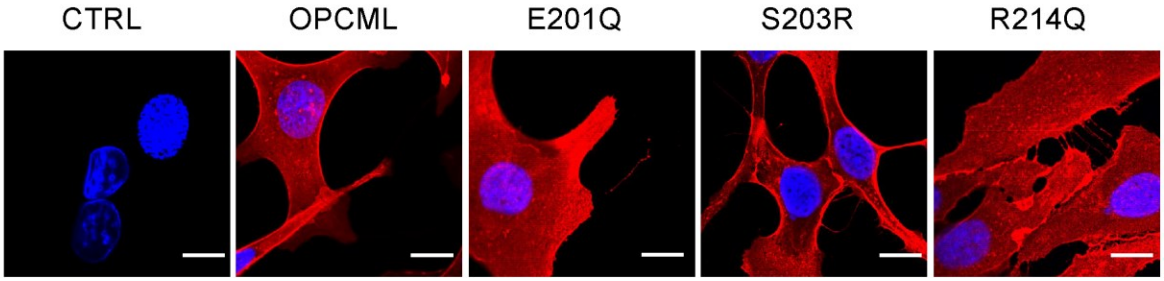

CTRL
OPCML
E201Q
S203R
R214Q

Figure 5.2 OPCML mutants in domain II behave like OPCML in expression and localisation on the cell membrane in SKOV3 cells.

A. Western Blot analysis showing in the left panel OPCML expression in SKOV3 cell lines stably transduced with wild-type OPCML or OPCML mutants compared to cells stably transduced with an empty vector as control (CTRL). GAPDH was used as loading control. A bar chart of the results of Western Blot analysis is shown in the right panel. The significance of the differences was determined by one-way ANOVA analysis using Prism 7 with Bonferroni correction .The difference in expression between wild-type OPCML and OPCML mutants was statistically non-significant, but compared to the control it was very significant (n = 3; mean ± SEM; **** P < 0.00001; ns, not significant).

B. Immunofluorescence microscopy reveals that OPCML is expressed in the SKOV3 cell line (red colour); the nucleus is shown in blue. The images show OPCML E201Q, OPCML S203R and OPCML R214Q expression compared to wild-type OPCML and control (scale bar, 20 μm).

C. Immunofluorescence microscopy of the SKOV3 cell line reveals OPCML in red and the nucleus in blue. The images show that OPCML E201Q, S203R, and R214Q, are expressed on the cell membrane in stably transduced SKOV3 cell lines. Wild-type OPCML and control are shown for comparison (n = 3; scale bar, 5 μm).

5.3. OPCML mutants in domain II block the OPCML function in ovarian cancer cell proliferation in vitro.

After confirming the correct expression and localisation of the mutated OPCML proteins, we moved on to examine the functional roles of these mutations in cell proliferation assays. Using an MTS proliferation assay in the SKOV3 cell lines in full cell culture medium, we found that the mutant-expressing cells had a significantly higher proliferation rate compared to the wild-type OPCML-expressing cells (Figure 5.3) suggesting that these mutations are loss of function.

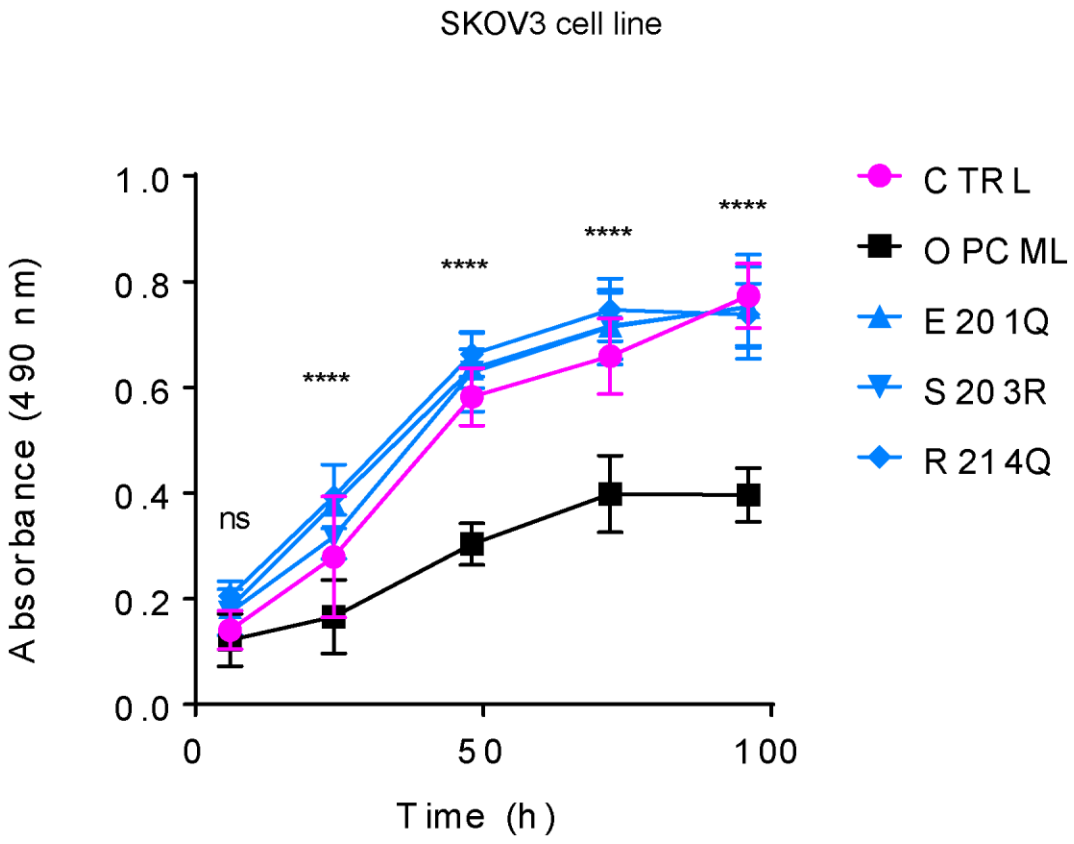


Figure 5.3 Mutants in domain II block OPCML function in proliferation ovarian cancer cells *in vitro*.

The proliferation of SKOV3 cell lines transduced with wild-type OPCML, OPCML E201Q, OPCML S203R, OPCML R214Q, and control grown for 96 hours in the presence of full medium (FM) was determined by an MTS assay. The graph shows the absorbance of MTS reagent at 490 nm; the results are representative of four independent experiments. Data are presented as a mean and standard error of the mean (SEM, error bars); the significance of the differences was determined by two-way ANOVA analysis using Prism 7 with Bonferroni correction. $n = 4$; ns, non-significant; **** $P < 0.00001$.

5.4. OPCML mutants in domain II are loss of function in anchorage-independent cellular growth assays.

Anchorage-independent growth is a hallmark characteristic of metastatic tumour cells. The same SKOV3 ovarian cancer cell lines used before were then subjected to soft agar colony formation assay, for evaluating anchorage-independent cell growth. Three different numbers of cells, 0.2, 0.4 and 0.8 × 10^4 cells per cell line were seeded into 0.6% Difco Noble agar on a base of 1% Noble agar in six-well plates and cultured for four weeks before the visible colonies were fixed and stained; cell colonies were imaged using an inverted microscope with a digital camera .

The results showed that OPCML mutants had the ability to survive and grow under anchorage-independent conditions but to different extents. Interestingly, one of the mutants, OPCML S203R, preserved partially the tumour-suppressing function and had a much-reduced number of colonies formed compared to the other mutants. As expected, in the presence of OPCML wild-type, colony formation was completely suppressed (Figure 5.4).

These results indicated that among the OPCML mutants in domain II, two of the mutants chosen, OPCML E201Q and OPCML R214Q, displayed a loss of function for anchorage-independent growth while the other mutant, OPCML S203R, showed no statistically significant difference with wild-type OPCML.

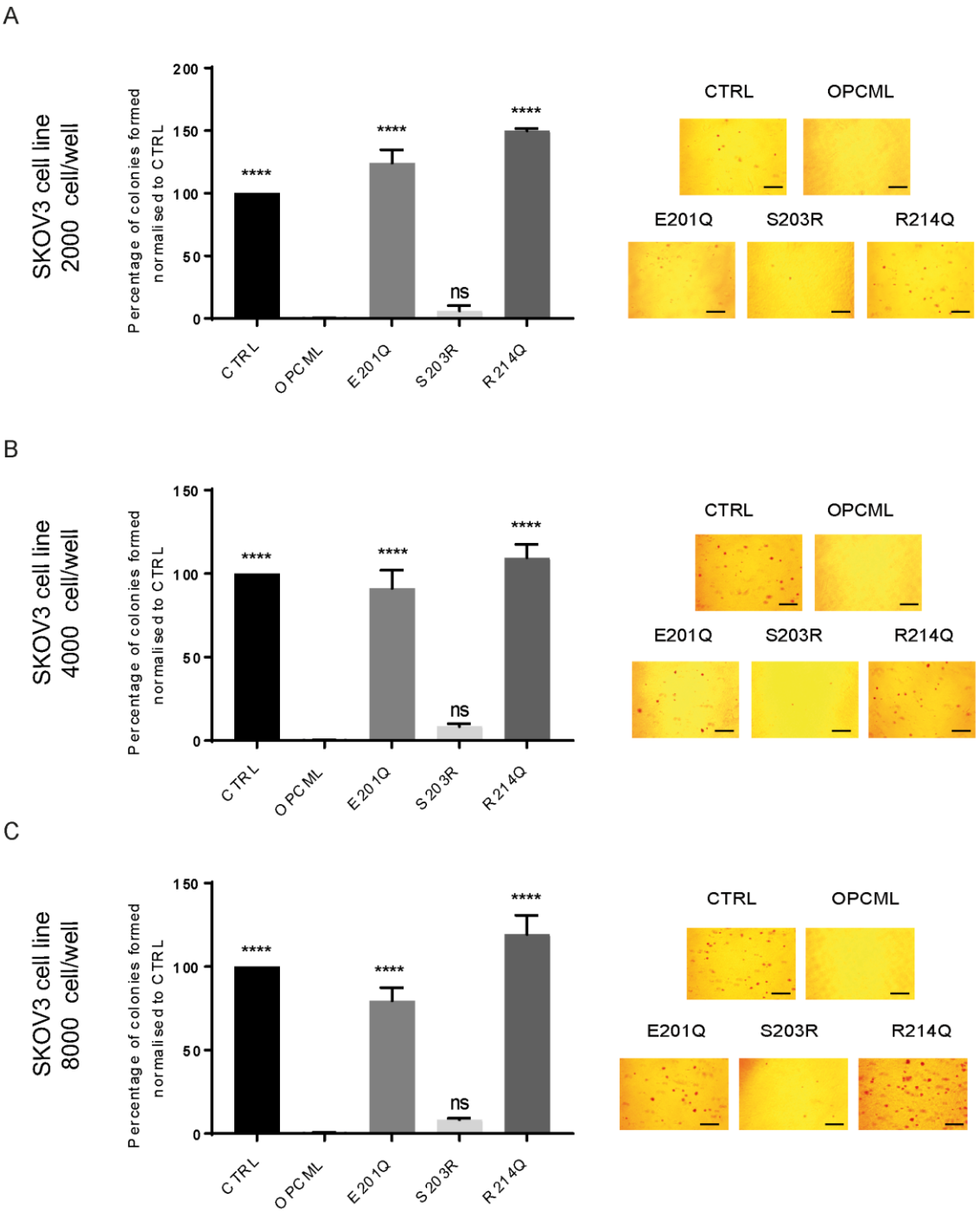

A
SKOV3 cell line
2000 cell/well
Percentage of colonies formed
normalised to CTRL
200
150
100
50
0
****
****
****
ns
CTRL
OPCML
E201Q
S203R
R214Q
CTRL
OPCML
E201Q
S203R
R214Q
B
SKOV3 cell line
4000 cell/well
Percentage of colonies formed
normalised to CTRL
150
100
50
0
****
****
****
ns
CTRL
OPCML
E201Q
S203R
R214Q
CTRL
OPCML
E201Q
S203R
R214Q
C
SKOV3 cell line
8000 cell/well
Percentage of colonies formed
normalised to CTRL
150
100
50
0
****
****
****
ns
CTRL
OPCML
E201Q
S203R
R214Q
CTRL
OPCML
E201Q
S203R
R214Q

Figure 5.4 OPCML mutants in domain II are loss of function in anchorage-independent cellular growth assays.

Soft agar colony formation assay of ovarian cancer SKOV3 cell line transduced with wild-type OPCML, OPCML E201Q, OPCML S203R, OPCML R214Q, and control. Cells were grown on soft agar plates for four weeks before colonies were fixed and stained with 0.015% neutral red and visualised using an inverted microscope and a digital camera. Representative colour images of the colonies in soft agar acquired at 4× magnification are shown in the right panels. The average number of colonies was determined by counting them using ImageJ. The left panels show bar charts of the results obtained. Three independent experiments were performed, and the data are presented as a mean and standard error of the mean (SEM, error bar). The significance of the differences was determined by one-way ANOVA analysis using Prism 7 with Bonferroni correction (ns, not significant; **** $P < 0.0001$; scale bar, 200 μm). (A) 0.2 x 10^4 cells/well; (B) 0.4 x 10^4 cells/well; (C) 0.8 x 10^4 cells/well.

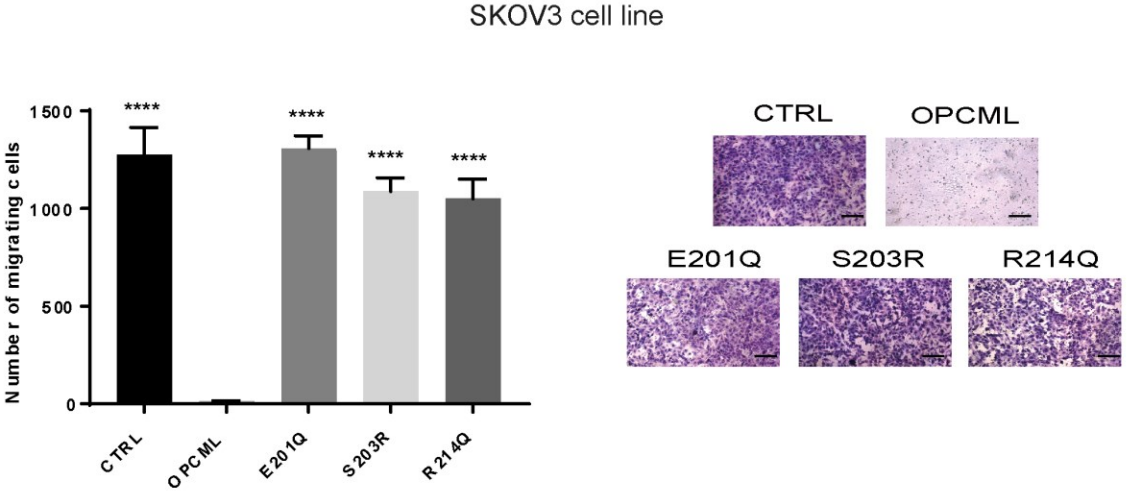
5.5. OPCML mutants block the function of OPCML in cellular migration and invasion assays

To further characterise the functional roles of these mutations we investigated the migration and invasion properties of SKOV3 cells overexpressing OPCML wild-type or mutants using the Transwell Biocoat growth factor reduced invasion chambers with Matrigel basement membrane matrix. For migration assays the same chamber but without Matrigel was used. OPCML mutants, wild-type OPCML, and the empty vector were grown in full medium and then resuspended in serum-free media before being added to the chamber in triplicate. Complete medium with 10% serum was added to the lower chamber as a chemoattractant. Cells were allowed to migrate or invade for 24 hours after which they were fixed and stained with 0.1% crystal violet in methanol solution.

The results showed that OPCML mutants had impaired the inhibitory function of OPCML in migration (Figure 5.5 A) and invasion (Figure 5.5 B) compared to wild-type OPCML and behaved like control (empty vector). Not surprisingly, wild-type OPCML suppressed the ability of the cells to migrate and invade.

Altogether, consistently with the previous results seen for the OPCML mutants in domain I, OPCML mutants in domain II showed a loss of function in migration and invasion inhibition compared to wild-type OPCML.

A


SKOV3 cell line
Number of migrating cells
1500
1000
500
0
****
****
****
****
CTRL
OPCML
E201Q
S203R
R214Q
CTRL
OPCML
E201Q
S203R
R214Q

B

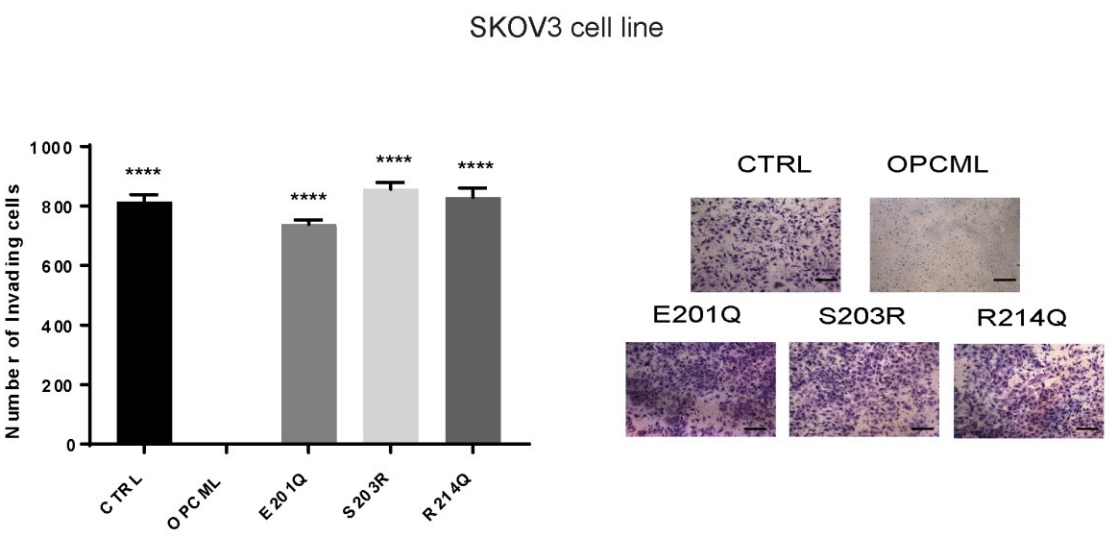

SKOV3 cell line
Number of Invading cells
1000
800
600
400
200
0
****
****
****
****
CTRL
OPCML
E201Q
S203R
R214Q
CTRL
OPCML
E201Q
S203R
R214Q

Figure 5.5 OPCML mutants block the function of OPCML in cellular migration and invasion assays.

Transwell assay of the ovarian cancer SKOV3 cell line transduced with wild-type OPCML, OPCML E201Q, OPCML S203R, OPCML R214Q, and control. Chambers were seeded in triplicate with 2.5×10^4 cells/chamber. Cells were allowed to migrate for 24 hours after which they were fixed and stained with 0.1% crystal violet in methanol solution and visualised using a Nikon Eclipse TE2000-U microscope and Q-Capture Pro software. Representative colour images of the chamber containing cells acquired at 10× magnification are shown in the right panels. At least six pictures were taken for each chamber, and the total number of cell migrated was determined by counting the cells with ImageJ. The left panels show bar charts of the results obtained. Three independent experiments were performed; the obtained data are presented as a mean and standard error of the mean (SEM, error bar). The significance of the differences was determined by one-way ANOVA analysis using Prism 7 with Bonferroni correction (**** $P < 0.0001$; scale bar, 50 μm). (A) Chambers without Matrigel coating. (B) Chambers coated with Matrigel.

5.6. OPCML mutants block the OPCML adherence to extracellular matrix components.

To evaluate whether OPCML could promote adherence to extracellular matrix components, the transduced SKOV3 ovarian cancer cell lines were subjected to a cell adhesion assay.

OPCML mutants, wild-type OPCML, and the control (empty vector) were grown in full medium and then resuspended in serum-free media before being added to wells that were pre-coated with different ECM proteins including collagen I, collagen IV, laminin I, fibronectin, and fibrinogen. Cells were allowed to adhere for 90 minutes after which they were stained with 0.09% crystal violet, extracted with 10% acetic acid and subsequently measured at 560 nm. Bovine serum albumin (BSA) was used as negative control.

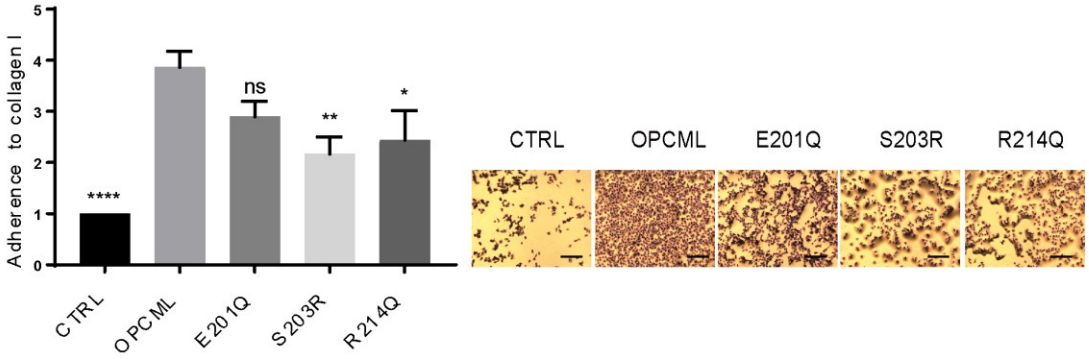
For the OPCML mutants in domain II, we found that a loss of OPCML function and a decrease in cellular adhesion to collagen I in OPCML S203R and OPCML R214Q in comparison to wild-type OPCML, but the decrease was insignificant in OPCML E201Q ($P < 0.0097$, $P < 0.0276$, and $P = 0.1544$, respectively; control, $P < 0.0001$) (Figure 5.6 A). Regarding adhesion to collagen IV, the mutations in domain II behaved like wild-type OPCML except for OPCML E201Q that showed a slight decrease compared to wild-type ($P < 0.0346$; control, $P < 0.0001$) (Figure 5.6 B). On the other hand, the OPCML mutants in domain II showed impaired OPCML function in adhesion to laminin I, fibronectin, and fibrinogen ($P < 0.0002$ or $P < 0.0001$) (Figures 5.6C, D, and E). These proteins are known to play a vital role in enhancing cellular attachment to the extracellular matrix through integrin receptors, which facilitate the adhesion and

migration of tumour cells and provide resistance to chemotherapeutic treatment (Humphries et al., 2006).

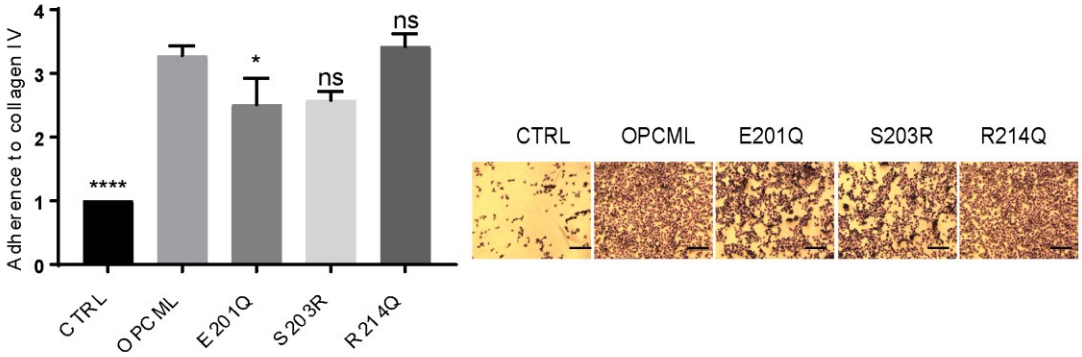
The cell adhesion to collagen I and collagen IV of the mutants in domain II was intermediate compared to the mutations in domain I, which showed a complete loss of increased adherence to collagen I and collagen IV. The inhibition of adherence to the extracellular matrix components laminin I, fibronectin and fibrinogen was completely lost in OPCML mutated in both domains I and II.

In conclusion, these results suggest that also mutations in domain II of OPCML are a partial loss of function for adhesion to collagen I and IV, and complete loss of function for adhesion to laminin I, fibronectin, fibrinogen, and invasion, and migration.

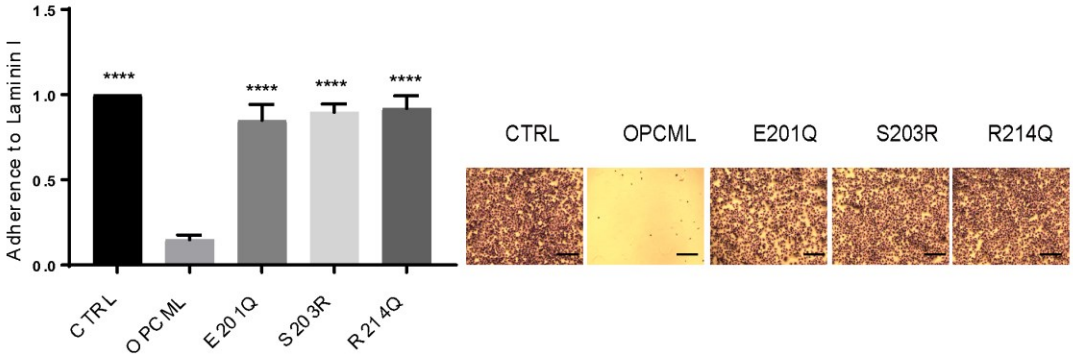
A


Adherence to collagen I
5
4
3
2
1
0
****
ns
**
*
CTRL
OPCML
E201Q
S203R
R214Q
CTRL
OPCML
E201Q
S203R
R214Q

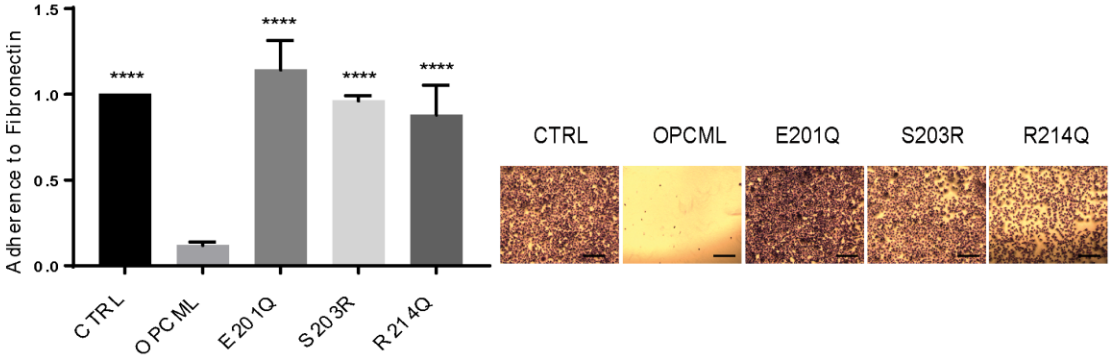
B


Adherence to collagen IV
4
3
2
1
0
****
*
ns
ns
CTRL
OPCML
E201Q
S203R
R214Q
CTRL
OPCML
E201Q
S203R
R214Q

C


Adherence to Laminin I
1.5
1.0
0.5
0.0
****
****
****
****
CTRL
OPCML
E201Q
S203R
R214Q
CTRL
OPCML
E201Q
S203R
R214Q

D


Adherence to Fibronectin
1.5
1.0
0.5
0.0
****
****
****
****
CTRL
OPCML
E201Q
S203R
R214Q
CTRL
OPCML
E201Q
S203R
R214Q

E

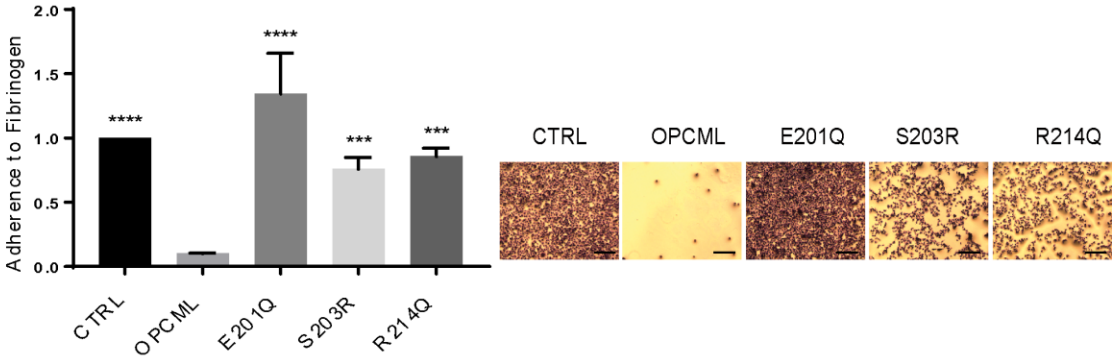

Adherence to Fibrinogen
2.0
1.5
1.0
0.5
0.0
****
****
***
***
CTRL
OPCML
E201Q
S203R
R214Q
CTRL
OPCML
E201Q
S203R
R214Q

Figure 5.6 OPCML mutants block the OPCML adherence to extracellular matrix components.

The cell adhesion assay of ovarian cancer SKOV3 transduced with wild-type OPCML, OPCML E201Q, OPCML S203R, OPCML R214Q, and control. 1.5 X10^5 cells/ well were seeded into CytoSelect 48-well plates. Cells were allowed to adhere for 90 minutes after which they were washed, stained with 0.09% crystal violet, extracted with 10% acetic acid and then measured at 560 nm in a computer-interfaced 96-well tunable microtiter plate reader. Bovine serum albumin (BSA) was used as negative control. The images were taken with a Nikon Eclipse TE2000-U microscope and Q-Capture Pro software, and representative colour images of the well-containing cells acquired at 10× magnification are shown the right panels. The left panels show bar charts of the results obtained colourimetrically. Three independent experiments were performed; the data are presented as a mean and standard error of the mean (SEM, error bar). The significance of the differences was determined by one-way ANOVA analysis using Prism 7 with Bonferroni correction (* $P < 0.0276$; ** $P < 0.0097$; *** $P < 0.001$; **** $P < 0.0001$; ns= non-significant; * scale bar, 50 μm). Plates were pre-coated with (A) Collagen I, (B) Collagen IV, (C) Laminin I, (D) Fibronectin, and (E) Fibrinogen.

5.7. Summary and key findings

To investigate the function of OPCML mutants in domain II *in vitro*, I used the SKOV3 cell line as a model to monitor the ability of OPCML mutants to affect OPCML's function as a tumour suppressor. In all the *in vitro* functional assays, these mutations were shown to diminish or completely lose OPCML function. These results support a model in which OPCML is a tumour suppressor in human cells, and loss of its function contributes to tumorigenesis. Therefore, human OPCML mutations are expected to confer tissue growth advantages modifying tumour development. Mutations could be considered another novel mechanism of OPCML inactivation in addition to the loss of heterozygosity and promoter hypermethylation, and OPCML mutants in domain II, due to their loss of function, contribute to tumour development by negatively regulating OPCML function.

6. CHAPTER 6

Role of OPCML domain III mutations

Introduction

OPCML mutants in domain III represent 28.8% of all OPCML mutations identified compared to 33.9% and 20.3% for OPCML domain I and domain II mutations, respectively.

In this chapter, we focus on the effect of these mutations on OPCML functions by:

1. Generating SKOV3 cell lines overexpressing OPCML K230R, OPCML K239N, and OPCML M278I, wild-type OPCML, and control (empty vector, CTRL).
2. Investigating the expression and localisation of the OPCML proteins.
3. Investigating the effect of OPCML mutants on tumour growth, cell adhesion, anchorage-independent cellular growth, invasion, and migration.

6.1. Identification of OPCML mutations in domain III using the public datasets TCGA and COSMIC and mapping them onto the OPCML crystal structure

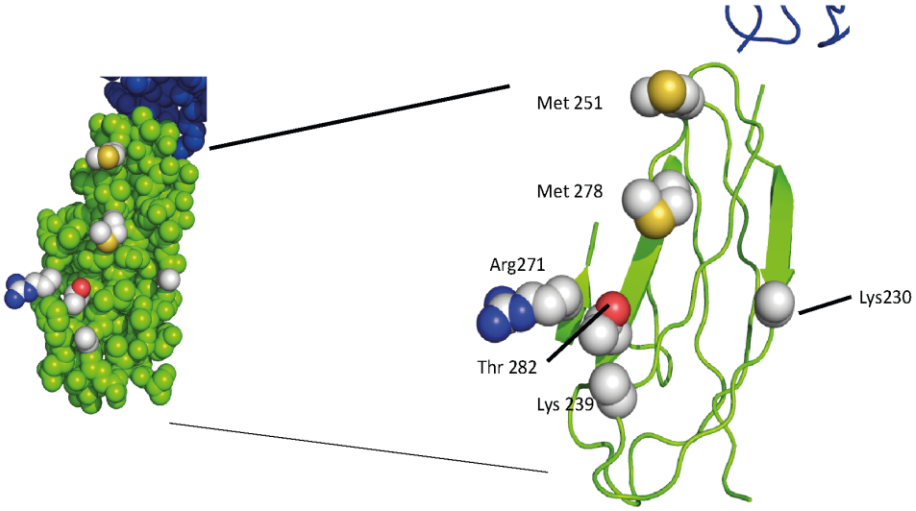
From our analysis of the TCGA and COSMIC datasets, we found that 65 out of 28,132 patients, distributed across all cancer types, presented point mutations in domain III of OPCML. The 34 different mutations identified were mapped onto the crystal structure (Figure 6.1 A), and Figure 6.1 B shows all mutations observed in domain III and their frequency. Among these 34 mutations, we selected OPCML K230R, OPCML K239N, and OPCML M278I based on their frequency, occurrence in several tumours and possible impact on the functionality of the protein.

The first mutation, K230R, changes a lysine residue in position 230 into arginine; it occurs in oesophageal tumours. Three-dimensional molecular modelling showed that this mutant is exposed on the protein's surface where it may play a role in the interaction with RTKs.

The second mutation, OPCML K239N, is a change from lysine into asparagine that occurs in melanoma. It is worth knowing that another point mutation occurs in the same location, namely K239T, where T stands for threonine. Both mutations may cause a structure modification on the surface that may play a role in the interaction with RTKs.

The third mutation is OPCML M278I, which changes a methionine to isoleucine. It occurs in ovarian cancer. Figure 6.1C presents a summary of the mutations used in this study, giving their names, positions, the amino acid changed, the cancer type and the possible impact on the crystal structure.

A



DOMAIN III

```
      CCT CCC TAT ATC TCA AAA GCC AAG AAC ACT GGT GTT TCA GTC GGT CAG AAG GGC   720
        P   P   Y   I   S   K   A   K   N   T   G   V   S   V   G   Q   K   G   240

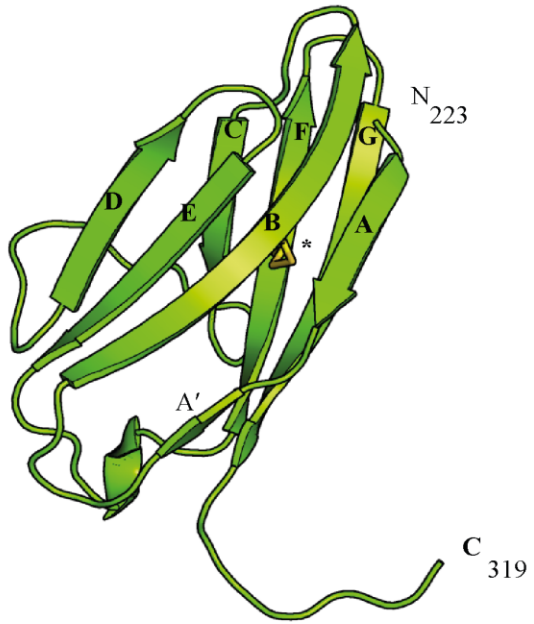
ATC CTG AGC TGT GAA GCC TCT GCA GTC CCC ATG GCT GAA TTC CAG TGG TTC AAG GAA GAA   780
  I   L   S   C   E   A   S   A   V   P   M   A   E   F   Q   W   F   K   E   E   260

ACC AGG TTA GCC ACT GGT CTG GAT GGA ATG AGG ATT GAA AAC AAA GGC CGC ATG TCC ACT   840
  T   R   L   A   T   G   L   D   G   M   R   I   E   N   K   G   R   M   S   T   280

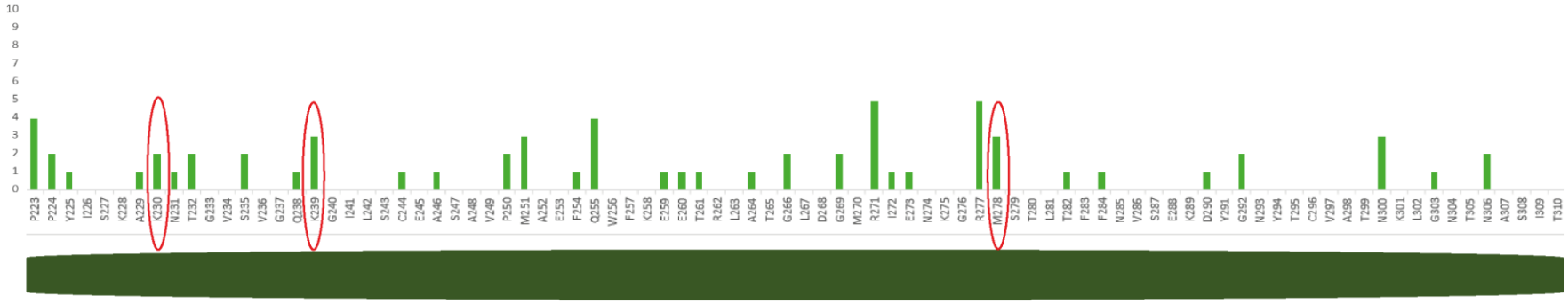
CTG ACT TTC TTC AAT GTT TCA GAA AAG GAT TAT GGG AAC TAT ACT TGT GTG GCC ACG AAC   900
  L   T   F   F   N   V   S   E   K   D   Y   G   N   Y   T   C   V   A   T   N   300

AAG CTT GGG AAC ACC AAT GCC AGC ATC ACA TTG TAT GGG CCT                          960
  K   L   G   N   T   N   A   S   I   T   L   Y   G   P                        320
```

DOMAIN III



B



C

Position	Cancer type	AA changed	Frequency	Modification
K230	Oesophagus	R	2	Surface exposed
K239	Skin	N	1	Surface exposed
	Skin	T	2	Surface exposed
M278	Ovary	I	3	Surface exposed

Figure 6.1 Crystal structure of OPCML with domain III mutations mapped.

A. Mutations mapped on the tertiary structure of OPCML. The right upper panel shows the sequence of human OPCML domain III with the position of the selected OPCML mutants coloured in pink. The right lower panel shows ribbon diagrams of domains III in salmon, it belongs to the V-set subfamily of Ig domains and consists of nine β-strands. Disulfide bridges connect all B and F strands and are indicated (*). The N- and C- termini are indicated and are numbered. Casanova reference inside Diedrich reference
B. Among all mutations observed in OPCML domain III in this study, the mutations to domain III chosen are encircled.
C. Summary table of OPCML domain III mutations chosen, giving the mutation's position, cancer type, amino acid changed, and the localisation on the crystal structur

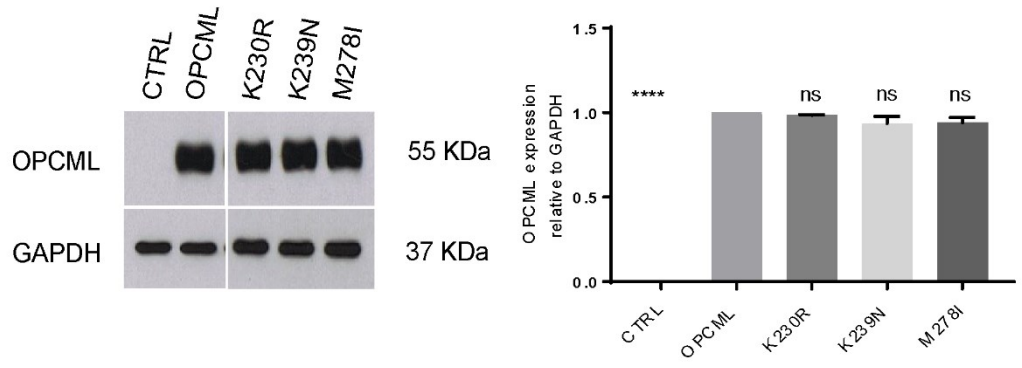
6.2. Creation and characterisation of stable ovarian cancer cell lines expressing OPCML domain III mutants.

To understand the biological role of the OPCML domain III mutations, SKOV3 ovarian cancer cell lines were created to express wild-type OPCML, mutants, or control vector. Constructs were verified by sequencing before creating the viruses used to transduce the cells.

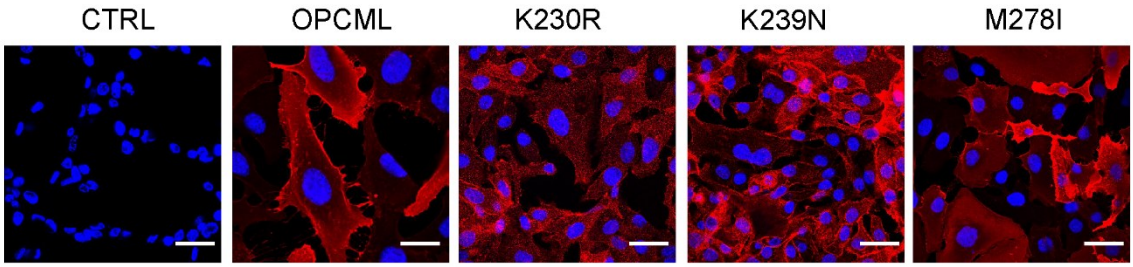
OPCML expression was confirmed by Western Blot analysis, where OPCML could be visualised at 55 kDa in all the transduced cell lines except in control (CTRL) (Figure 6.2A, left panel for cell line SKOV3). Quantification of the Western Blot showed no statistical differences between wild-type OPCML expression and that of OPCML mutants (Figure 6.2A, right panel).

Immunofluorescence was then employed to assess the expression of OPCML. By using an antibody against OPCML, we confirmed that the wild-type and mutants OPCMLs were expressed in transduced SKOV3 cell lines and that they were all mainly positioned on the cell membrane (Figure 6.2B)

A


SKOV3 cell line
CTRL
OPCML
K230R
K239N
M278I
OPCML
GAPDH
55 KDa
37 KDa
OPCML expression relative to GAPDH
1.5
1.0
0.5
0.0
****
ns
ns
ns
CTRL
OPCML
K230R
K239N
M278I

B


CTRL
OPCML
K230R
K239N
M278I

C

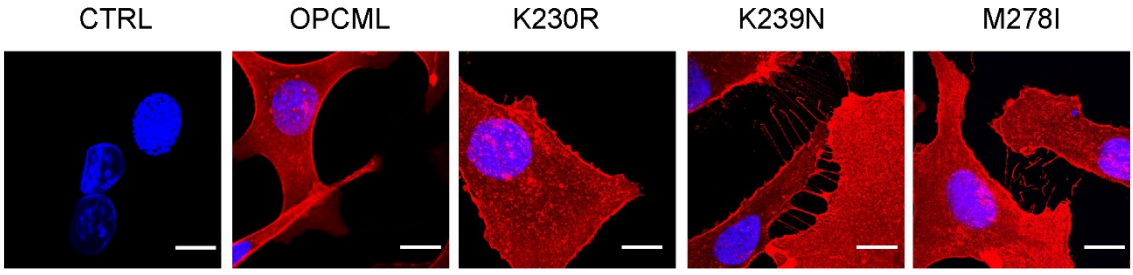

CTRL
OPCML
K230R
K239N
M278I

Figure 6.2 OPCML with mutations in domain III behaves like wild-type OPCML in expression and localisation on the cell membrane in an ovarian cancer cell line.

A. Western Blot analysis showing in the left panel of the expression OPCML in SKOV3 cells stably transduced with wild-type OPCML or OPCML mutants compared to cells stably transduced with an empty vector control (CTRL). GAPDH was used as loading control. A bar chart of the results of Western Blot analysis is shown in the right panel. The difference in expression between wild-type OPCML and OPCML mutants in the SKOV3 cell line was statistically non-significant, but compared to the control it was very significant (n = 3 mean ± SEM; **** $P < 0.00001$; ns, not significant).
B. Immunofluorescence microscopy of the SKOV3 cell line showing OPCML in red and the nucleus in blue. The images show the expression of OPCML E201Q, OPCMLS203R, OPCML R214Q, compared to wild-type OPCML and control in stably transduced cells (scale bar, 20 μm).
C. Immunofluorescence microscopy of the SKOV3 cell line. The images show OPCML K230R, OPCML K239N, and OPCML M278I expression at the cell membrane compared to wild-type OPCML and control in stably transduced SKOV3 cell lines (n = 3; scale bar, 5 μm).

6.3. OPCML mutants in domain III lose their function on proliferation in vitro in ovarian cancer cells.

To further characterise the functional significance of the OPCML mutants we assessed their role in the regulation of proliferation of tumour cells *in vitro*. To this end, we used SKOV3 cell lines transduced with wild-type OPCML, OPCML K230R, OPCML K239N, OPCML M278I, and control. Using an MTS proliferation assay in the SKOV3 cell lines in full cell culture medium we saw that, like the control, OPCML mutants in domain III had lost the OPCML function on cell growth compared to OPCML wild-type cells (Figure 6.3). Analysis of the results revealed a statistically significant difference between OPCML mutants in domain III and wild-type OPCML.

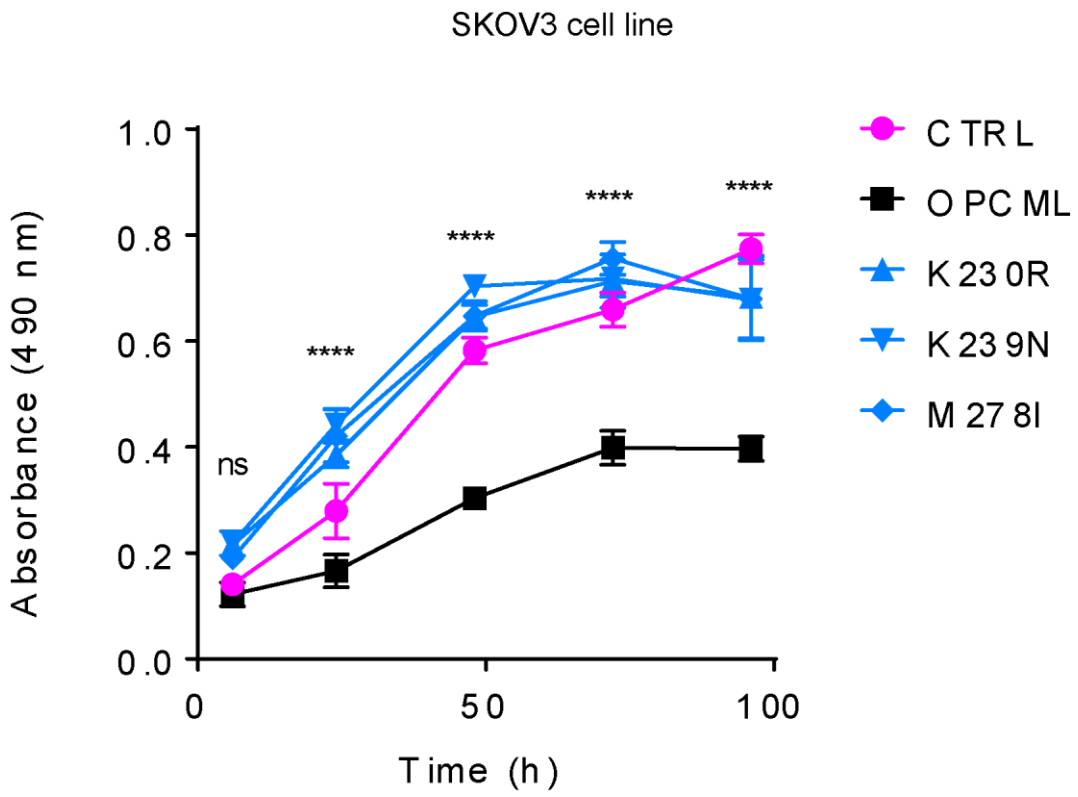


Figure 6.3 OPCML mutants in domain III lose their function on proliferation in vitro in ovarian cancer cells.

The proliferation of SKOV3 cell lines transduced with wild-type OPCML, OPCML K230R, OPCML K239N, OPCML M278I, and control grown for 96 hours in the presence of full medium was determined by an MTS assay. The graph shows the absorbance of the MTS reagent at 490 nm; the results are representative of four independent experiments. Data are presented as a mean and standard error of the mean (SEM, error bar). The significance of the differences was determined by two-way ANOVA analysis using Prism 7 with Bonferroni correction (n = 4; **** P < 0.00001; ns, non-significant).

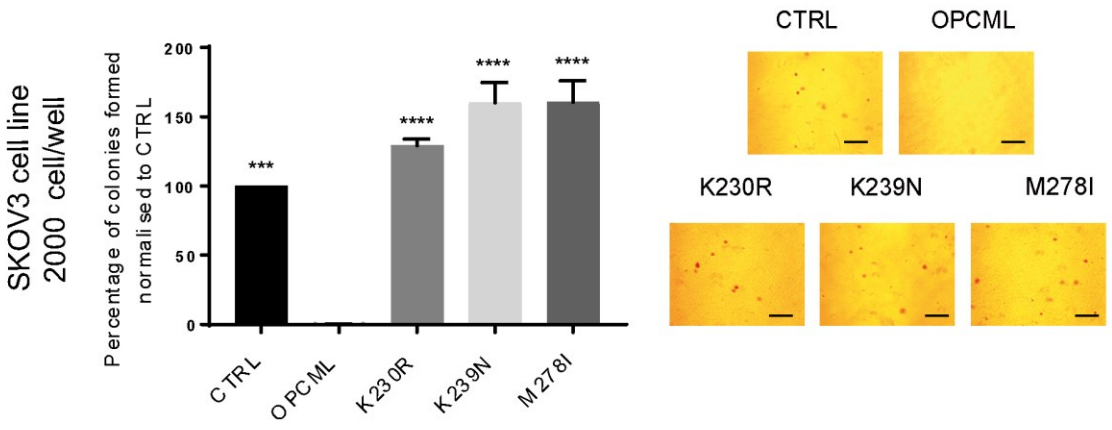
6.4. OPCML mutants in domain III reveal loss of function in the regulation of anchorage-independent cellular growth.

Anchorage-independent growth is a hallmark characteristic of metastatic tumour cells. The soft agar colony formation assay is a well-established method to evaluate anchorage-independent cell growth. To evaluate whether OPCML mutants could affect the regulation of anchorage-independent growth, SKOV3 ovarian cancer cell lines, transduced with the different OPCML domain III mutants or wild-type and control, were subjected to soft agar colony formation assay.

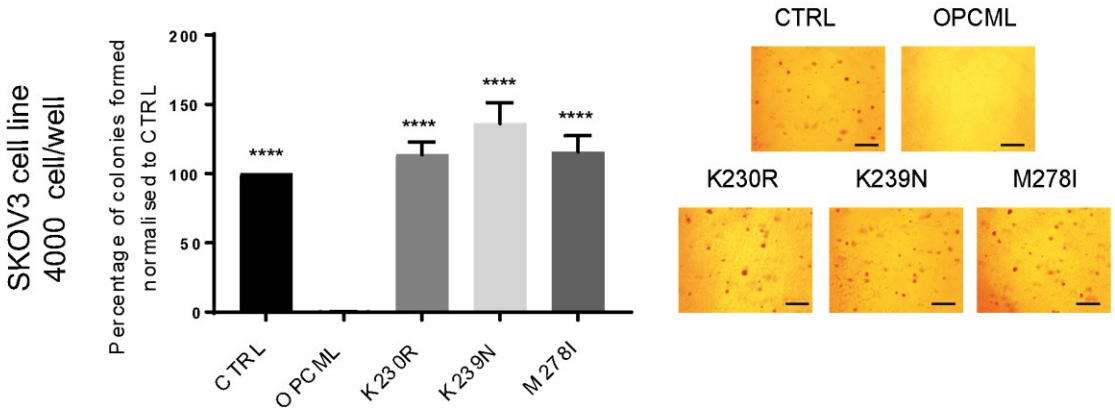
Three different numbers of cells, 0.2, 0.4 and 0.8 × 10^4 cells per cell line, were seeded into 0.6% Difco Noble agar on a base of 1% Noble agar in six-well plates and cultured for four weeks before the visible colonies were fixed and stained; cell colonies were imaged using an inverted microscope.

The results showed that OPCML mutants had the ability to survive and grow under anchorage-independent conditions; the OPCML mutants showed loss of OPCML's growth inhibition in the number and the size of the colonies formed. In contrast, the presence of OPCML wild-type resulted in suppression of colony formation (Figure 6.4).

A


SKOV3 cell line
2000 cell/well
Percentage of colonies formed normalised to CTRL
200
150
100
50
0
***
****
****
****
CTRL
OPCML
K230R
K239N
M278I
CTRL
OPCML
K230R
K239N
M278I

B


SKOV3 cell line
4000 cell/well
Percentage of colonies formed normalised to CTRL
200
150
100
50
0
****
****
****
****
CTRL
OPCML
K230R
K239N
M278I
CTRL
OPCML
K230R
K239N
M278I

C

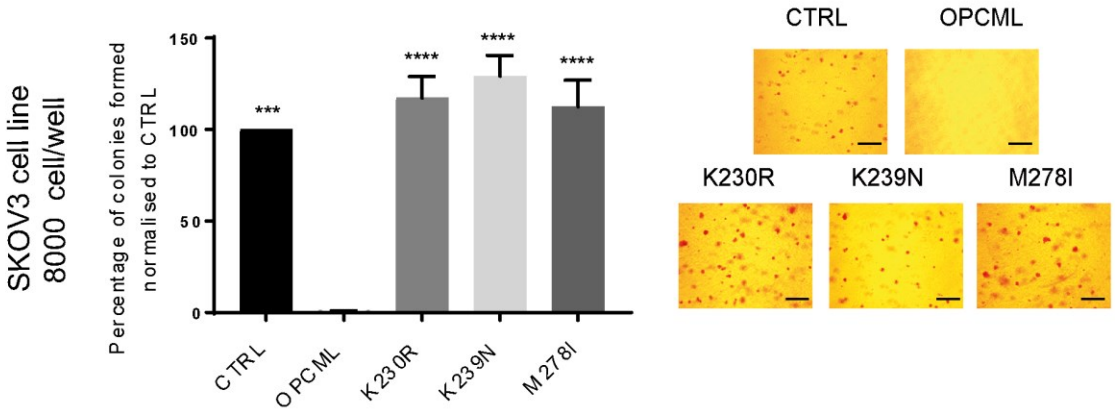

SKOV3 cell line
8000 cell/well
Percentage of colonies formed normalised to CTRL
150
100
50
0
***
****
****
****
CTRL
OPCML
K230R
K239N
M278I
CTRL
OPCML
K230R
K239N
M278I

Figure 6.4 OPCML mutants in domain III reveal a loss of function in the regulation of anchorage-independent cellular growth.

Soft agar colony formation assay of the ovarian cancer SKOV3 cell line transduced with wild-type OPCML, OPCML K230R, OPCML K239N, OPCML M278I, and control. Cells were grown on soft agar plates for four weeks before colonies were fixed and stained with 0.015% neutral red and visualised using an inverted microscope with a digital camera. Representative colour images of the colonies in soft agar acquired with ImageJ at 4× magnification are shown in the right panels. The left panels show bar charts of the results obtained. Three independent experiments were performed; the obtained data are presented as a mean and standard error of the mean (SEM, error bar). The significance of the differences was determined by one-way ANOVA analysis using Prism 7 with Bonferroni correction (*** P< 0.001; **** P< 0.0001; ns, not significant; scale bar, 200 μm). (A) 0.2 x 10^4 cells; (B) 0.4 x 10^4 cells; (C) 0.8 x 10^4 cells.

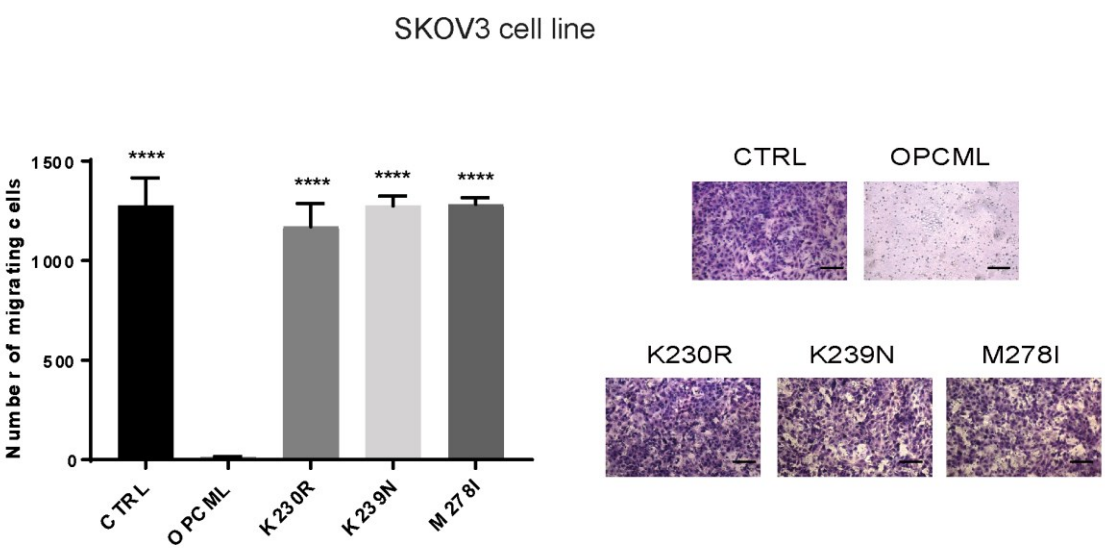
6.5. OPCML mutants abolish their function in cellular migration and invasion in ovarian cancer cells *in vitro*.

To assess the potential roles of OPCML mutants in ovarian cancer cell lines in migration and invasion, we investigated the migration and invasion properties of SKOV3 cell lines using Transwell Biocoat growth factor reduced invasion chambers with Matrigel. For migration assays, we used the same chambers but without the Matrigel. OPCML mutants, wild-type OPCML, and the empty vector were grown in full medium and then resuspended in serum-free media before being added to the chambers. Complete medium with 10% serum was added to the lower chamber as a chemoattractant. Cells were allowed to migrate or invade for 24 hours, after which they were fixed and stained with 0.1% crystal violet in methanol solution.

The results showed that OPCML mutants had increased tumour cell migration (Figure 6.5A) and invasion (Figure 6.5B), similar to control cells. Not surprisingly, wild-type OPCML suppressed the ability of the cells to migrate and invade.

Altogether, these results show that also OPCML mutants in domain III are a loss of function in the regulation of migration and invasion compared to wild-type OPCML.

A


SKOV3 cell line
Number of migrating cells
1500
1000
500
0
****
****
****
****
CTRL
OPCML
K230R
K239N
M278I
CTRL
OPCML
K230R
K239N
M278I

B

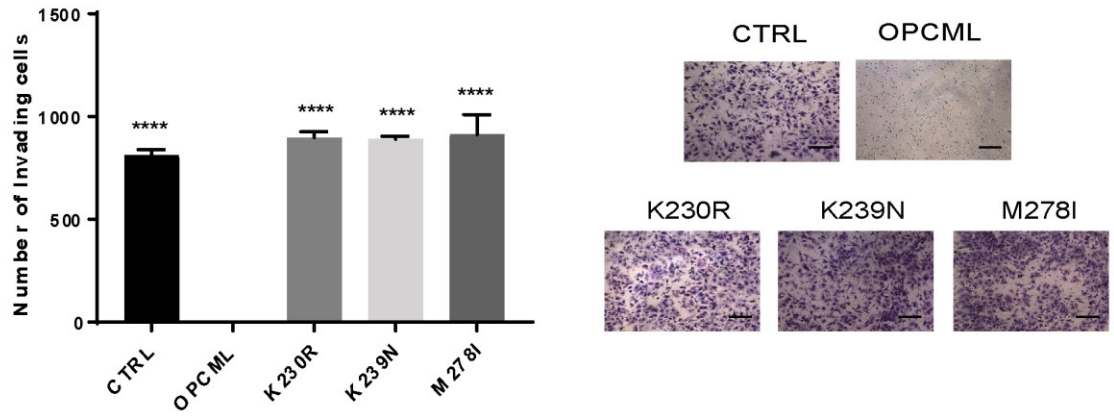

SKOV3 cell line
Number of Invading cells
1500
1000
500
0
****
****
****
****
CTRL
OPCML
K230R
K239N
M278I
CTRL
OPCML
K230R
K239N
M278I

Figure 6.5 OPCML mutants abolish their function in cellular migration and invasion in ovarian cancer cells in vitro.

A. Transwell migration assay of the ovarian cancer SKOV3 cell line transduced with wild-type OPCML, OPCML K230R, OPCML K239N, OPCML M278I, and control. Chambers without Matrigel coating were seeded in triplicate with 2.5 $\times 10^4$ cells/chamber. Cells were allowed to migrate for 24 hours after which they were fixed and stained with 0.1% crystal violet in methanol solution and visualised using a Nikon Eclipse TE2000-U microscope and Q-Capture Pro software. Representative colour images of the chambers containing cells acquired at 10× magnification are shown in the right panels. At least six pictures were taken for each chamber, and the total number of cell migrated was determined by counting the cells with ImageJ. The left panels show bar charts of the results obtained. Three independent experiments were performed; the obtained data are presented as a mean and standard error of the mean (SEM, error bar). The significance of the differences was determined by one-way ANOVA analysis using Prism 7 with Bonferroni correction (**** $P < 0.0001$; scale bar, 50 μm).

B. Transwell invasion assay of ovarian cancer transduced SKOV3 cell lines. Chambers were coated with Matrigel. Other details as in A.

6.6. OPCML mutants block its function toward adherence to extracellular matrix components.

To evaluate whether OPCML mutants could alter cell adhesion to extracellular matrix components, SKOV3 cell lines were subjected to a cell adhesion assay.

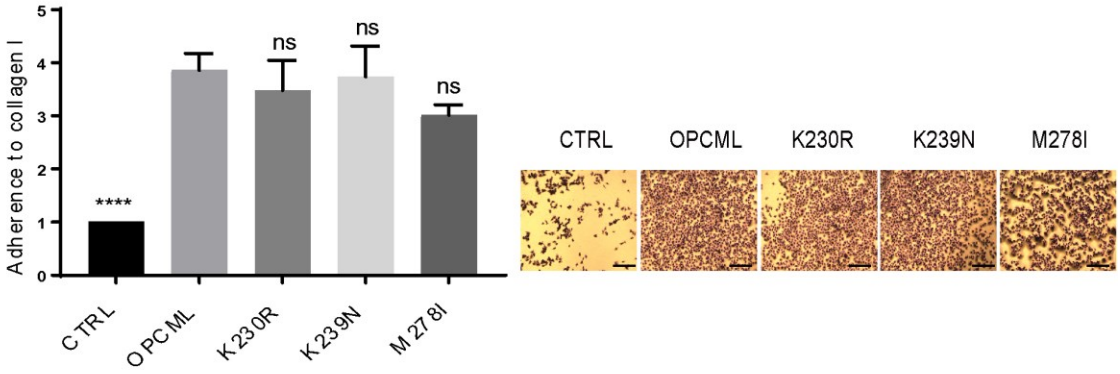
OPCML mutants, wild-type OPCML, and the control (empty vector) were grown in full medium and then resuspended in serum-free media before being added to wells that were pre-coated with different ECM proteins including collagen I, collagen IV, laminin I, fibronectin, and fibrinogen; 1.5×10^5 cells/well were seeded in triplicate. Cells were allowed to adhere for 90 minutes after which they were stained with 0.09% crystal violet, extracted with 10% acetic acid and measured at 560 nm in a computer-interfaced 96-well tunable microtiter plate reader. Bovine serum albumin (BSA) was used as negative control.

We found cellular adhesion to collagen I and collagen IV in OPCML K230R, OPCML K239N, OPCML M278I, similar to OPCML wild-type (ns > 0.9999; control $P < 0.0001$) (Figures 6.6 A, B). Remarkably, OPCML mutants in domain III showed adherence behaviour for collagen I and collagen IV that was opposite to that of OPCML mutants in domain I and domain II. OPCML mutants in domain III, however, showed loss of OPCML function in cellular adhesion to laminin I, fibronectin, and fibrinogen ($P < 0.0002$ and $P < 0.0001$) (Figures 6.6 C, D, E). SKOV3 cell lines expressing OPCML mutants in domain III, while behaving like wild-type OPCML in their adherence to collagen I and collagen IV, behaved like control cells toward laminin I, fibronectin, and fibrinogen. OPCML mutated in domain I showed a complete loss of OPCML function adherence to collagen I and collagen IV, while OPCML mutated in domain II behaved

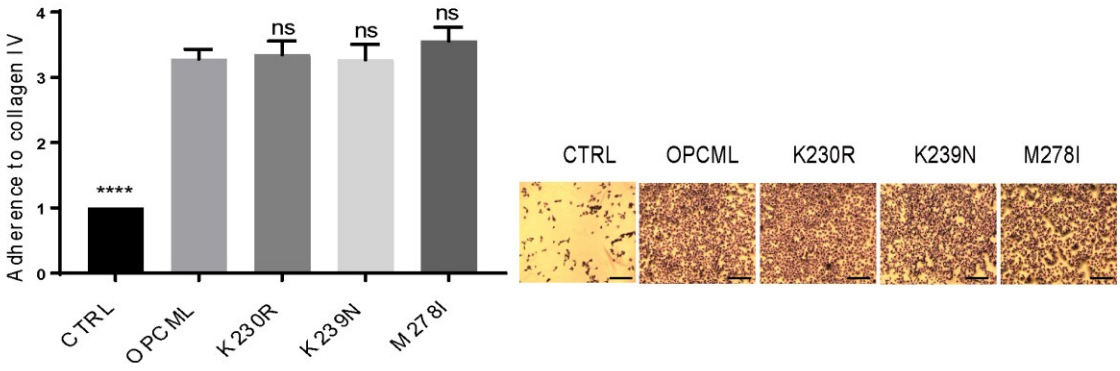
intermediately. Adherence to the extracellular matrix components laminin I, fibronectin and fibrinogen was completely lost in mutations of OPCML in all domains.

Altogether, these results for cell adhesion to the extracellular matrix suggest that the loss of OPCML function of the domain III mutants in adherence to laminin I, fibronectin, and fibrinogen could play role in the invasion and migration of ovarian cancer cells.

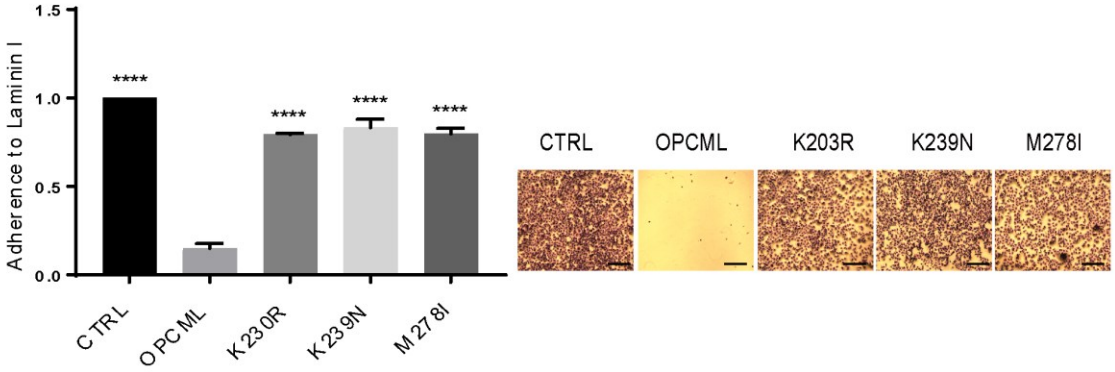
A


Adherence to collagen I
5
4
3
2
1
0
****
ns
ns
ns
CTRL
OPCML
K230R
K239N
M278I
CTRL
OPCML
K230R
K239N
M278I

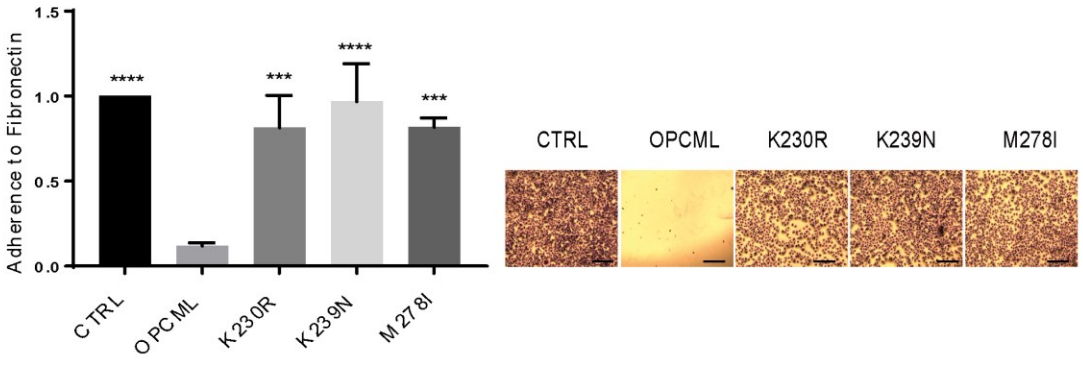
B


Adherence to collagen IV
4
3
2
1
0
****
ns
ns
ns
CTRL
OPCML
K230R
K239N
M278I
CTRL
OPCML
K230R
K239N
M278I

C


Adherence to Laminin I
1.5
1.0
0.5
0.0
****
****
****
****
CTRL
OPCML
K230R
K239N
M278I
CTRL
OPCML
K203R
K239N
M278I

D


Adherence to Fibronectin
1.5
1.0
0.5
0.0
****
***
****
***
CTRL
OPCML
K230R
K239N
M278I
CTRL
OPCML
K230R
K239N
M278I

E

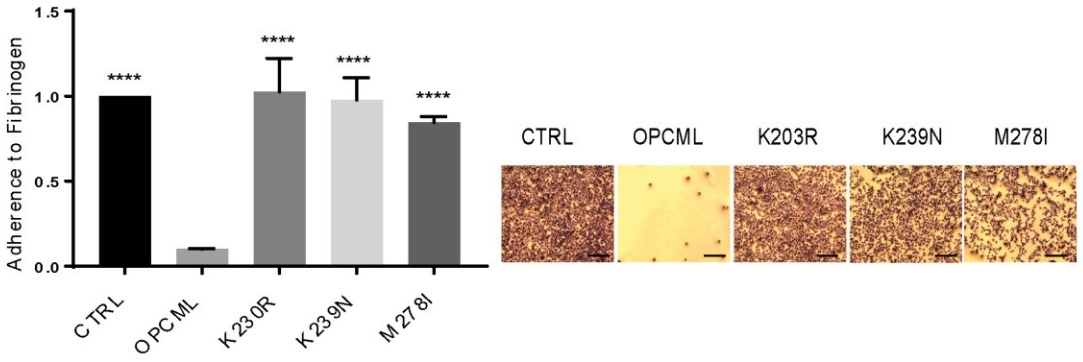

Adherence to Fibrinogen
1.5
1.0
0.5
0.0
****
****
****
****
CTRL
OPCML
K230R
K239N
M278I
CTRL
OPCML
K203R
K239N
M278I

Figure 6.6 OPCML mutants block its function toward adherence to extracellular matrix components.

Cell adhesion assay of ovarian cancer SKOV3 transduced with wild-type OPCML, OPCML K230R, OPCML K239N, OPCML M278I, and control. Cells were seeded in CytoSelect 48-well plates at 1.5×10^5 cells/well. Cells were allowed to adhere for 90 minutes after which they were stained with 0.09% crystal violet, extracted with 10% acetic acid and then measured at 560 nm in a computer-interfaced 96-well tunable microtiter plate reader. Bovine serum albumin (BSA) was used as negative control. Images were taken with a Nikon Eclipse TE2000-U microscope and Q-Capture Pro software, and representative colour images of the wells containing cells acquired at 10× magnification are shown in the right panels. The left panels show bar charts of the results obtained colourimetrically. Three independent experiments were performed, the data are presented as mean, and standard error of the mean (SEM, error bar). The significance of the differences was determined by one-way ANOVA analysis using Prism 7 with Bonferroni correction (*** $P = 0.0002$; **** $P < 0.0001$; ns, non-significant; scale bar, 50 μm). Plates were pre-coated with (A) collagen I; (B) collagen IV; (C) laminin I; (D) fibronectin; and (E) fibrinogen.

6.7. Summary and key findings

To investigate the function of OPCML mutants in domain III *in vitro*, I used the SKOV3 cell line as a model to monitor the ability of OPCML mutants to affect the function of OPCML as a tumour suppressor. OPCML mutants in domain III maintained the OPCML function in adherence to collagen I and IV, and blocked the inhibitory function of OPCML in tumour growth, anchorage-independent growth, invasion, migration, and adherence to laminin I, fibronectin, and fibrinogen. These results suggest that OPCML mutants in domain III may contribute to tumour development by negatively regulating OPCML activity due to their loss of function.

7. CHAPTER 7

General Discussion

Introduction

This thesis has discussed the gap in the current literature concerning the role of OPCML mutations in OPCML function, and the research conducted here has described the creation of OPCML mutants in ovarian cancer cell lines and has investigated the role of these mutants and their effects.

In order to explore a potential new era of ovarian cancer management, we analysed two large cohorts of patients in the TCGA and COSMIC databases to identify OPCML mutations. We found missense mutations in the OPCML gene in 287 out of 28,132 patients, distributed across all cancer types. To establish the position of these clinical mutations on the three-dimensional structure of OPCML and reveal their potential tumour suppression mechanisms, we crystalized soluble recombinant OPCML and determined its structure using a combined single-wavelength anomalous dispersion / molecular replacement approach, followed by rounds of automated and manual model building and refinement. By combining the dataset results with the correlated crystal structure, followed by a functional screening of OPCML mutations, we identified a new mechanism of OPCML inactivation through mutations that predict loss of tumour suppressor function. We then validated this function experimentally. We further showed that clinical OPCML mutations included a large number of loss of function mutations, including those that cannot prevent any more anchorage-independent tumour growth, cell adhesion to extracellular matrix, invasion, and migration in *vivo* and in *vitro*. Collectively, this work expands the current understanding of OPCML's function as a tumour suppressor and provides new opportunities to identify new methods of management for ovarian cancer and other tumours.

7.1. OPCML mutants disrupt OPCML-AXL interaction and thus abolish the inhibitory effect on the downstream signalling and on migration, invasion, and targeted therapy resistance in ovarian cancer cells.

In our study, we used functional tests such as migration and invasion assays in order to examine the effect of wild-type OPCML interaction with AXL (upon stimulation with AXL ligand Gas6) and the inhibition of the AXL/Gas6 downstream signalling, compared to OPCML mutants.

The results showed, using proximity ligation assay, that the OPCML mutants in domain I disrupt OPCML/AXL interaction, resulting in downstream signalling of AKT and, as a consequence, no inhibition of invasion and migration.

Interestingly, the strong OPCML N70H interaction with AXL was not altered either with or without stimulation with GAS6, and as a consequence, this interaction still 0blocked motility. It is possible that the N70H mutation may have an effect on the protein folding, which may affect its functional interaction with RTKs.

In previous research from this lab, we demonstrated that OPCML wild-type has a GPI- anchor associated to the cell membrane, it resides in the lipid raft compartment and accomplishes its function as a tumour suppressor through negatively regulating numerous tyrosine kinase receptors (McKie et al., 2012). More recently, in our lab (unpublished data) we demonstrated that OPCML wild-type interacts with AXL in detergent-resistant membranes, inducing its de-phosphorylation by a local phosphatase and resulting in a downregulation of downstream signalling, thus inhibiting cellular invasion and migration.

In a further investigation about the involvement of OPCML mutants in domain I in targeted therapy using AXL inhibitors in ovarian cancer, our study shows that OPCML mutants in domain I are loss of function toward target therapy sensitisation to treatment using an AXL inhibitor when compared to wild-type OPCML. This could be due cells evading apoptosis through blocking Caspase 3/7 activation by OPCML.

In the literature, AXL is known for its role in epithelial-mesenchymal transition (EMT), metastasis, cellular invasion and migration, and chemoresistance in many tumour types including ovarian cancer (Shinh, et al., 2005; Hafizi & Dahlbäck, 2006; Zhang, et al., 2008; Tai, et al., 2008; Rankin, et al., 2010; Huang et al., 2017). AXL has been found to be overexpressed and activated in many human cancers such as ovarian (Sun et al., 2004), breast (Zhang et al., 2008), and lung (Ishikawa et al., 2013). Also, AXL correlates with HER2, and motility and invasiveness in estrogen receptor-positive breast cancer (Bose et al., 2006; Berclaz et al., 2001). The ability of OPCML to negatively regulate several RTKs could have potentially important clinical implications for the management of ovarian cancer.

Taken together, we are able to report that OPCML mutations confer loss of OPCML function in invasion and migration, and targeted therapy sensitisation in the Gas6/AXL context.

7.2. OPCML mutants show different disruption of the interaction with FGFR1.

Research has shown that FGFR1 is overexpressed in ovarian cancer and plays a significant role in cellular functions such as proliferation, differentiation, apoptosis, and migration (Steele et al., 2001).

In this section, we explore the effect of OPCML mutants on the FGFR1-OPCML interaction as well as their effect on downstream signalling leading to functional consequences in ovarian cancer cells.

Our results demonstrate that some OPCML mutants disrupts the interaction between OPCML- FGFR1 while some mutations do not affect it, which then showed different responses in motility in wound healing assay.

Interestingly, the strong OPCML N70H interaction with RTK FGFR1 is not altered with or without stimulation with FGF1, and as a consequence, still shows an effect on motility. The N70H mutation may have a possible effect on OPCML protein folding, which may affect its function with its interaction with RTKs.

Also, the OPCML P95R interaction with FGFR1 is not changed and the downstream signalling phosphorylation AKT behaves as OPCML wild-type in motility function.

On the contrary, the OPCML R65L interaction with FGFR1 is disrupted compared to wild-type OPCML and showed loss of function in motility.

7.3. OPCML mutant block the inhibitory effect of OPCML on phenotypic properties of ovarian cancer.

Next, we explored the characteristics of OPCML mutants and their effects on tumour growth, invasion, migration, and the adhesion to the extracellular matrix.

We studied the effect of OPCML mutants on cell proliferation using MTS proliferation assay. Our results revealed that in ovarian cancer cells, OPCML mutants in domains II and III showed loss of function and had a significantly increased proliferation rate as compared to the wild-type OPCML cell lines. Therefore, the observed results suggest that domains II and III are necessary for the tumour growth function of wild-type OPCML. Interestingly, the OPCML mutant in domain I behaved like wild-type OPCML in two different ovarian cancer cell lines.

It is unclear how the OPCML mutants in domain I retain the OPCML function while the OPCML mutants in domains II and III lost this property. There are two possible mechanisms responsible for this difference. The first mechanism may be that the effect of the mutations in domain I on the three-dimensional structure is less significant than that of the OPCML mutations in domains II and III. This structural difference could affect RTKs' interaction with OPCML and, hence, the downstream signalling to AKT and ERK (McKie et al., 2012).

The second possible mechanism comes from previously published observation that wild-type OPCML arrests the cells in the G0/G1 phase. The checkpoint regulator p27 has been observed to be highly expressed in cell lines that expressed OPCML and pro-apoptotic caspase-3 and caspase-9; in addition, PARP levels are significantly elevated in cell lines that express OPCML (Xing et al., 2017). Furthermore, in our

previous work (McKie et al., 2012) the phosphorylation activity of AKT was downregulated in a cell line expressing OPCML as compared to the control. A recent study of gastric cancer revealed that the AKT downstream target determined that glycogen synthase kinase 3β (GSK3β) was highly expressed in gastric cancer, and its level was abrogated in the cell line expressing OPCML (Xing et al., 2017). It is worthwhile to note that GSK3β form a complex with Wnt signaling pathway components (Axin, β-catenin, APC, CK1, and DVL) (Gatcliffe et al., 2008), and in the absence of Wnt signaling, GSK3β phosphorylates the complex components, which form the complex scaffold, so the cytoplasmic increase of phosphorylated β-catenin is unable to translocate into the nucleus to activate Wnt signaling target genes.

In the presence of Wnt signalling, Wnt ligand binds to the receptor complex encircling the frizzled receptor and an LRP co-receptor. This leads to an inactivation of GSK3β that causes its separation from the Wnt complex Axin, thus preventing the phosphorylation of β-catenin, which in turn translocates into the nucleus and activates downstream target genes (Gatcliffe et al., 2008).

Moreover, we evaluated the ability of the mutants to block the inhibitory function of OPCML by examining the ability of cancer cells to form colonies in anchorage-independent growth assays in soft agar. Our study demonstrated that all the mutants in the three domains have the ability to grow and survive in anchorage-independent growth assay. Interestingly, OPCML S203R showed no statistically significant difference with wild-type OPCML. Our results indicate that OPCML mutants in domain I, domain II, and domain III have a higher likelihood of survival and growth in anchorage-

independent conditions than wild-type OPCML, which exhibits a substantial suppression in the size and number of colonies formed.

Our results are consistent with published results for OPCML in colorectal cancer which showed that SW480 and LoVo transfected with the OPCML cell line showed a significant inhibition of colony formation when compared with control-transfected cells (Li et al., 2015). Similar results have also been demonstrated in studies of gastric cancer (Xing et al., 2017).

The PI3K/AKT/ mTOR pathway perturbations have a significant role in cancer cells' ability to evade apoptosis, and there is much evidence that shows it is the most frequently altered signalling pathway in cancers, including ovarian cancer (Altomare et al., 2004; Huang et al., 2011; Cheaib et al., 2015). Our results are consistent with the hypothesis that AKT is responsible for anchorage tumour growth when comparing the loss of function of OPCML mutants in different domains with wild-type OPCML. Although OPCML S203R showed no statistically significant difference from wild-type OPCML, this result is primarily attributed to the statistical tests we used. This mutant form shows a loss of function in colony formation, and using a t-test, this result shows statistical significance ($p= 0.0010$). But if we compare it in consideration with other mutants that show massive colony formation using one way ANOVA test the results showed non-significance.

In summary, OPCML mutants show a loss of function and abolish the inhibitory effect of OPCML on the cell clonogenicity in contrast to wild-type OPCML, which suppressed tumour cell clonogenicity in ovarian cancer.

To investigate the potential roles for OPCML mutants on other tumorigenic features on migration and invasion, we then questioned whether OPCML mutants could affect OPCML function and whether they are involved in the migration and invasion process.

The results showed that OPCML mutations could significantly attenuate the OPCML function on the migration and invasion of ovarian cancer. These observations suggest that wild-type OPCML have the ability to inhibit metastasis in ovarian cancer and could be used as target therapy as multiple RTK inhibitor for ovarian metastasis tumours. Most ovarian cancer patients are diagnosed at a later stage where the cancer has progressed and become metastatic. Prevalent metastases into the abdominal cavity are the primary cause for the poor prognosis of patients with ovarian cancer (Pradeep et al., 2014).

This observation confirms previous studies conducted by Li et al. (2015) for colorectal cancer which showed that wild-type OPCML inhibits cell invasion in transwell assay, migration in wound healing and transwell assay compared to control cells.

The exact mechanism behind the migration and invasion is unknown. We speculate that during the transformation of the cells that promotes their ability to migrate, invade, survive and grow in anchorage-independent growth, the loss of OPCML function by mutation in epithelial ovarian cancers may consequently dysregulate RTKs, which lose the tight control by OPCML on their pro-oncogenic downstream signalling to ERK and AKT.

Cells require frequent adhesion and detachment to the extracellular matrix microenvironment in order to perform the invasion and migration processes, which are considered an important component of the metastatic process (Yousif, 2014). Next, as we identify the OPCML mutants that exhibit a loss of function that attenuate the OPCML function on invasion and migration, we explored whether OPCML mutants could lose or preserve the OPCML function on adhesion or possibly play a role in cell adhesion in ovarian cancer or in extracellular matrix (ECM) remodelling. Previous research has shown that there is an association between the extracellular matrix and migration, invasion, and resistance to the treatment (Liotta & Kohn, 2001).

Cellular invasion and migration require cell adhesion to the extracellular matrix; we assessed the effect of OPCML mutations occurring in several domains on cellular adhesion to extracellular matrix proteins. Our data shows that wild-type OPCML promotes cell adhesion to collagen I and collagen IV, and, conversely, it hinders adhesion to fibronectin, laminin, and fibrinogen. This is the first time that such a phenotype has been reported for OPCML.

When we investigated the adhesion properties of the mutants, we found that whilst all the domains showed loss of OPCML function in binding to fibronectin, laminin, and fibrinogen, the mutants in domain I were strongly attenuated in the OPCML function for adhesion on collagen I (and partially to collagen IV), while the mutants in domain II resulted in an intermediate phenotype, and the mutants in domain III were unaffected. Overall, OPCML mutants reveal loss of OPCML function and show that the different domains of OPCML may mediate diverse functions of this tumour suppressor.

Moreover, malignant transformation is affected by the cellular environment, which is influenced by several factors, such as surrounding stroma, growth factors, and systemic hormones, and as a result affects tumour growth, invasion, migration, and cell adhesion. Several of the extracellular matrix components related to ovarian and other tumours have been described as prognostic factors or as a biomarkers for the patient's survival. Several studies have established the importance of collagen type I in ovarian cancer adhesion, migration, and chemoresistance (Shen et al., 2012; Cho et al., 2015); fibronectin in tumour progression, promoting metastasis, angiogenesis and apoptosis evasion (Cho et al., 2015); collagen type IV and laminin I in promoting cell proliferation, cell adhesion, and migration (Cho et al., 2015; Tas et al., 2016); and fibrinogen in its role in the coagulation pathway and promoting angiogenesis, metastasis, and plasma exudates to form ascites (Wang et al., 2005, Saito et al., 2008, Von Au et al., 2013).

Also, the inhibition of phosphorylation of DDR1 and DDR2 receptor tyrosine kinase has been identified as being lost in OPCML mutants when compared to OPCML wild-type in human proteome arrays, which suggests they play a role in cell adhesion. Discoidin domain receptors (DDR) are receptor tyrosine kinases that are activated only by collagen. DDR1 and 2 expressions are associated with cellular survival, migration, and invasion in several tumours such as hepatocellular carcinoma and prostate cancer (Park et al., 2007; Shimada et al., 2008). They have also been identified in serous ovarian cancers as a prospective biomarker (Quan et al., 2011).

Cell adhesion may be important in the early steps of ovarian cancer progression and in the possible two-way communication between collagen with integrin and collagen

with DDR receptor tyrosine kinases, which promote extracellular matrix remodelling through activating matrix metalloproteinase. Thus, DDRs and integrins may play a significant role in ovarian cancer progression by being activated by collagen. This may activate matrix metalloproteinase and as a consequence initiate ECM degradation and remodelling. The difference in the collagen effect by OPCML mutants in different domains could be attributed to two reasons: the first is related to the impact of the mutant location and its effect on protein folding and function, and the second could be the effect on signaling pathways and their response to the collagen interaction with integrin and DDR receptor tyrosine kinases, as well as the possible delay in reaching maximum activation of DDRs.

Overall, OPCML mutants that show a loss of OPCML function in cell adhesion might play an essential role in ovarian cancer metastasis.

Subsequently, in order to study ovarian cancer *in vivo*, we used two in *vivo* models: Athymic nude mice and the CAM model.

The Athymic nude mice xenograft model showed that most of OPCML mutants lose the OPCML function to inhibit tumour growth and ascites formation. Our results are consistent with the previous observation that OPCML suppresses tumour growth (Sellar et al., 2003; Ntougkos et al., 2005; Reed et al., 2007; Cui et al., 2008; Fleming et al., 2009). However, although there are many advantages of using an animal to try to mimic ovarian cancer, still there are some disadvantages that may affect the reproducibility of the experiments, such as mice strain acquired mutations and the perforation of the bladder during the intraperitoneal experiment. The CAM model could be an attractive ovarian cancer model over the more commonly used xenograft mice model. We

selected three different mutants each from a different domain to confirm our results using the CAM model. As expected from cell culture experiments and the xenograft model, the results showed that OPCML mutants significantly attenuate the tumour growth inhibition. In contrast, wild-type OPCML was revealed to inhibit tumour growth strongly.

7.4. The mutants attenuate the OPCML's interaction with the spectrum of receptor tyrosine kinases.

To understand the mechanism behind the anti-tumorigenic effect of OPCML and the impact of the mutants, phospho-RTKs were detected by a commercial phospho-RTKs antibody array. OPCML mutants showed loss of inhibitory function on several RTKs, which are not activated in the wild-type OPCML expressing cell lines, such as HER2, HER4, FGFR1, IGF1R, AXL, PDGF-Rα, PDGF-Rβ, stem cell factor receptor (SCF R), ROR1, ROR2, EphA2, DDR1, DDR2, and RYK.

We selected some receptors (EGFR, HER2, EphA2, IGF1R, and H-RYK) to be validated by Western Blot. The remaining RTKs will require further investigation.

Our studies demonstrated that the mutants have lost the inhibitory effect of OPCML on the phosphorylated RTKs—EGFR, HER2, EphA2, IGF1R, and H-RYK—.

The phosphorylation of EGFR, HER2, EphA2, IGF1R, and H-RYK has already been reported in various cancers, including ovarian cancer (Ettinger, 2006; Landen et al., 2008; Bast et al., 2009; Carey et al., 2010 ;Thaker et al., 2004; Denduluri et al., 2015, and Katso et al., 2000). Previous results from McKie et al., (2012) proposed a mechanism for OPCML to downregulate the activity of receptor tyrosine kinases. The

proposal suggests that OPCML is associated with RTKs such as HER2, EphA2 and downregulates their activation, which further downregulates critical downstream signalling pathways such as AKT and ERK. These results suggest that OPCML mutants disrupt the association between OPCML and RTKs, which leads to the inactivation of OPCML.

These results suggest that using OPCML as a recombinant or mimicking the OPCML model in a drug may be a useful plan to target those RTKs with the most impact on multiple oncogenic signalling pathways. This will have the greatest translational potential for clinical ovarian cancer treatment as well as treatment for several other tumours.

The mechanism for the association of RTKs with OPCML and how these RTKs are activated in OPCML mutant cells is still elusive. One potential mechanism is that when an OPCML mutant disrupts the OPCML- association with RTKs, such as HER2, this would then heterodimerise with other RTKs partners and, thus, would lose the inhibition from OPCML on the downstream signalling, such as the AKT and ERK pathways.

Interestingly, in a cell line expressing OPCML mutants, we identified no loss of HER2 and EphA2 phosphorylation. Research has previously shown that EphA2 forms a complex with HER2 resulting in enhanced activation of Ras-MAPK and increased cell proliferation and motility in breast carcinoma cells. This indicates that EphA2 promotes breast tumour formation and metastatic progression by amplifying HER2 signalling (Zhuang et al., 2010).

There is evidence for crosstalk between Eph receptors and the Wnt signalling pathway via Ryk, a Wnt receptor containing an inactive tyrosine kinase domain. Ryk can

associate with EphB2 and EphB3, resulting in tyrosine phosphorylation (Schmitt et al., 2006). Also, we identified that EphA2 is associated with RYK using a CO-IP assay, which may help explain the role of the non-canonical Wnt signalling pathway. In the non-canonical Wnt pathway, Wnt can act through ROR (which we found to be phosphorylated in OPCML mutant cell lines through human phospho-RTK proteome arrays) and RYK tyrosine kinases, which activate Jun kinase (JNK). As a consequence, canonical signalling is inhibited (Timmermans-Sprang et al., 2015). Wnt signalling plays a significant role in the cellular processes containing differentiation, migration, invasion, adhesion, and survival (Chien et al., 2009). The dysregulation of Wnt signalling is associated with multiple cancers, including ovarian, breast, and colorectal cancer (Ying & Tao, 2009).

Moreover, our results show that OPCML mutants lose the inhibitory effect of OPCML on the activity of IGF1R. Recently, the IGF-IR has been shown to be involved in epithelial to mesenchymal transition linked to tumour metastasis and drug resistance (Wang et al., 2016). Overexpression of IGF-IR is associated with a high risk of metastasis and poor prognosis in many cancer patients (Wang et al., 2012). Also, crosstalk between IGFIR and HER2 has been involved in resistance to trastuzumab in breast cancer (Lu et al., 2001; Nahta et al., 2005).

Altogether, the results presented here demonstrate that OPCML mutations resulted in loss of the inhibitory effect on several RTKs, which contributes to ovarian progression. Wild-type OPCML negatively regulates the expression of several RTKs, including HER2, EphA2, H-RYK, and IGF-IR. OPCML mutants may also evades apoptosis and attenuate OPCML's function on tumour growth via the loss of inhibition of

downstream of PI3K/AKT and MEK/ERK signalling. Our findings suggest that OPCML as a targeted therapy would be effective and beneficial for the treatment of patients with ovarian cancer and other malignancies.

7.5. Conclusion

The investigation defined in this study was focused on the characterisation of OPCML mutations and identifying their role in ovarian cancer progression. OPCML has been found inactivated by loss of heterozygosity and hypermethylation (Sellar et al. 2003); its inactivation has been identified to increase the likelihood of tumour formation in ovarian cancer (Sellar et al. 2003).

OPCML is identified as a tumour suppressor, and the mechanisms for this suppression are thought to include a broad negative regulation of several receptor tyrosine kinases resulting in the downregulation of downstream signalling via the AKT and ERK pathways (McKie et al. 2012) and the ability to confer sensitisation to chemotherapeutic treatments (Elisa et al. 2017).

Clinical OPCML mutations were identified in several patients with ovarian cancer and other tumours, but their consequences are unknown to date. Studying the role of OPCML mutations will increase our understanding of how OPCML mutants might affect OPCML function. Several mutants were selected from different domains to identify the role of OPCML mutations in the different domains.

In Chapter 4, we clearly demonstrated that OPCML mutants in domain I show a loss of function in the phenotypic features, but preserve OPCML's tumour growth suppression when compared to mutants in domain II and domain III.

Remarkably, the interaction of OPCML mutants in domain I with AXL and FGFR1 shows some differences between the mutations that may be due to the effect of the mutations on the crystal structure and the crosstalk with other RTKs.

The *in vivo* studies we performed validated the *in vitro* studies. We showed that OPCML mutants demonstrated loss of OPCML function on tumour growth and ascites formation. Also, the CAM model showed that OPCML mutants in different domains reveal a loss of function on tumour growth.

Also, in Chapter 5, the OPCML mutants in domain II show a loss of function in proliferation, anchorage-independent, invasion, migration, and adhesion to fibronectin, laminin I, and fibrinogen.

In chapter 6, OPCML mutants in domain III revealed a loss of function in proliferation, anchorage-independent, invasion, migration, and adhesion to fibronectin, laminin I, and fibrinogen.

These findings support the consideration that OPCML mutants are an important new mechanism of OPCML inactivation.

In summary, this study provides strong evidence that mutations can inactivate OPCML's inhibitory function on proliferation, migration, invasion, tumour growth, and cell adhesion to fibronectin, fibrinogen, and laminin I of ovarian cancer cells by disrupting the negative effect of OPCML interaction with several RTKs responsible for tumorigenic properties. Furthermore, the effect of OPCML mutants caused the loss of OPCML function and loss of the downstream inhibition of the AKT and ERK signalling pathways.

7.6. Recommendation for further research

7.6.1. Further elucidate the role of OPCML in ovarian cancer metastasis.

The proteome array experiment showed that while OPCML negatively regulates the receptor tyrosine kinases, the OPCML mutants showed loss of this inhibitory function. This results urge us to further investigate the different role of each RTKs such as HER2, EphA2, IGF1R, and H-RYK in the presence or absence of OPCML. Understanding the mechanism, and the possible crosstalk, could have a great impact on our understanding of how OPCML is able to suppress growth and metastasis.

7.6.2. Explore the role of the discoidin domain receptor family in a cell line expressing OPCML in cell adhesion.

We showed in our study activated DDR1, DDR2 receptor tyrosine kinases in a cell line transduced with OPCML mutants. In contrast, wild-type OPCML showed reduced activation of DDR1 and DDR2. The DDR family is stimulated through collagen, which induces extracellular matrix remodelling. Further understanding of how OPCML mutants lose the OPCML function on adhesion to collagen will allow researchers to find ways to exploit this phenomenon for cancer treatment

7.6.3. **Role of OPCML in cartilage regeneration and osteoporosis.**

We have shown that OPCML is able to suppress the EphA2 receptor tyrosine kinase and that the inactivation of OPCML promotes the activation of the EphA2 receptor and promotes downstream signalling.

EphA2 is known for its possible role in bone remodelling through promoting osteoclastogenesis and inhibiting osteoblast differentiation (Irie et al., 2009).

Due to the OPCML role in the downregulating of EphA2, OPCML could promote osteoblast differentiation and cause reduced osteoclastogenesis.

7.6.4. **Role of OPCML dysregulation in other tumours and asthma**

One of the activated RTKs that was identified by using human proteome RTK-arrays was stem cell factor receptor c-kit.

Ovarian cancer cells transduced with OPCML mutants lose the inhibitory effect of OPCML function on stem cell factor (SCF) receptors compared to wild-type OPCML, which reduced the activation.

Signalling from the SCF receptor is critical for normal haematopoiesis, gut movement, and pigmentation. The dysregulation of SCF receptor activity has been observed in both cancer and allergies (Lennartsson & Rönnstrand, 2012).

In summary, our results demonstrate that OPCML holds tumour suppressive properties, which may be suggestive for its potential therapeutic application in treating several human diseases and malignancies characterised by unregulated SCF receptors.

Our results support the need for further investigation into the therapeutic potential of OPCML in ovarian cancer and other diseases and malignancies.

8. CHAPTER 8

REFERENCES

References

Abraham, S; Knapp, D; Cheng, L; Snyder, P; Mittal, S; Bangari, D; Kinch, M; Wu, L; Dhariwal, J; and Mohammed, S. (2006). Expression of EphA2 and Ephrin A-1 in carcinoma of the urinary bladder. *Clinical Cancer Research*, 353-60.

Adamo, A; Fiore, D; De Martino, F; Roscigno, G; Affinito, A; Donnarumma, E; Puoti, I; Vitiani, L; Pallini, R; Quintavalle, C; and Condorelli, G. (2017). RYK promotes the stemness of glioblastoma cells via the WNT/β-catenin pathway. *Oncotarget*, 13476–13487.

Adams, T., Epa, V., Garrett, T., and Ward, C. (2000). Structure and function of the type 1 insulin-like growth factor receptor. *Cellular and Molecular Life Science* , 1050-93.

Ahmed, N; Riley, C; Rice , G; and Quinn, M. (2005). Role of integrin receptors for fibronectin, collagen and laminin in the regulation. *Clinical & Experimental Metastasis*, 391–402.

Ahmed, A; Etemadmoghadam, D; Temple, J; Lynch, A; Riad, M; Sharma, S; Stewart, C; Fereday, S; Caldas, C; DeFazio, A; Bowtell, D; and Breton, J. (2010). Driver mutations in TP53 are ubiquitous in high grade serous carcinoma of the ovary. *The Journal of Pathology*, 49–56.

Altomare, DA; Wang, HQ; Skele, KL; De Rienzo, A; Godwin, AK; and Testa, JR. (2004). AKT and mTOR phosphorylation is frequently detected in ovarian cancer and can be targeted to disrupt ovarian tumor cell growth. *Oncogene*, 5853-7.

American Cancer Society, F. (2015). Global Cancer Facts & Figures 3. (3rd, Ed.) *American cancer society*. Retrieved from American cancer society.

Anatomical chart company, f. (2008). Understanding of ovarian cancer.

Angelillo-Scherrer, A; de Frutos, P; Aparicio, C; Melis, E; Savi P, P; Lupu, F; Arnout, J; Dewerchin M, M; Herbert, J; Collen, D; Dahlbäck, B; and Carmeliet, P. (2001). Deficiency or inhibition of Gas6 causes platelet dysfunction and protects mice against thrombosis. *Nature medicine*, 215-21.

Anglesio, M; Arnold, J; George, J; Tinker, A; Tothill, R; Waddell, N; Simms, L; Locandro, B; Fereday, S; Traficante, N; Russell, P; Sharma, R; Birrer, M; AOCS Study Group, For; deFazio, A; Chenevix-Trench, G; and Bowtell, D. (2008). Mutation of ERBB2 provides a novel alternative mechanism for the ubiquitous activation of RAS-MAPK in ovarian serous low malignant potential tumors. *American Association for Cancer Research*, 1678-90. doi:10.1158/1541-7786.MCR-08-0193.

Asiedu, MK; Beauchamp-Perez, FD; Ingle, JN; Behrens, MD; Radisky, DC; and Knutson, KL. (2014). AXL induces epithelial-to-mesenchymal transition and regulates the function of breast cancer stem cells. *Oncogene*, 1316–1324.

Auersperg, N., Wong, A., Choi, K., Kang, S., and Leung, P. (2001). Ovarian surface epithelium: biology, endocrinology, and pathology. *Endocrine Reviews*, 255-88.

Badgwell, D., and Bast, R. (2007). Early detection of ovarian cancer. *Disease Markers*, 397–410.

Banet, N., and Kurman, R. (2015). Two types of ovarian cortical inclusion cysts: proposed origin and possible role in ovarian serous carcinogenesis. *International journal of gynecological pathology*, 3-8.

Barøy, T; Kresse, S; Skårn, M; Stabell, M; Castro, R; Lauvrak, S; Llombart-Bosch, A; Myklebost , O; and Meza-Zepeda, L. (2014). Reexpression of LSAMP inhibits tumor growth in a preclinical osteosarcoma model. *Molecular cancer*, 1-11. doi: 10.1186/1476-4598-13-93.

Baserga, R., Peruzzi, F., and Reiss K, K. (2003). The IGF-1 receptor in cancer biology. *International Journal of Cancer*, 873-7.

Bast, R., Hennessy, B., and Mills, G. (2009). The biology of ovarian cancer: new opportunities for translation. *Nature Reviews Cancer*, 415-428.

Behan, A., Byrne, C., Dunn, M., Cagney, G., and Cotter, D. (2009). Proteomic analysis of membrane microdomain-associated proteins in the dorsolateral prefrontal cortex in schizophrenia and bipolar disorder reveals alterations in LAMP, STXBP1 and BASP1 protein expression. *Molecular Psychiatry*, 601-13. doi: 10.1038/mp.2008.7.

Bellosta, P., Costa, M., Lin, D., and Basilico, C. (1995). The receptor tyrosine kinase ARK mediates cell aggregation by homophilic binding. *Molecular Cell Biology*, 614-25.

Benedet, J; Pecorelli, S; Ngan, H; Hacker, N; Denny, L; Jones, H; Kavanagh, J; Kitchener, H; Kohorn, E; and Thomas, G. (2000). FIGO staging classifications and clinical practice gudelines in the management of gynecologic cancers. *International Journal of Gynecology and Obstetrics, 3*, 209-262. doi:10.1016/S0020-7292(00)90001-8.

Beral, V., Gaitskell, K., Hermon, C., Moser, K., Reeves, G., and Group, C. (2015). Menopausal hormone use and ovarian cancer risk: individual participant meta-analysis of 52 epidemiological studies. *Lancet*, 1835–42. Retrieved from http://dx.doi.org/10.1016/.

Beral, V; Doll, R; Hermon, C; Peto, R; Reeves, G; Brinton, L; Green, A; Marchbanks, P; Negri, E; Ness, R; Peeters, P; Vessey, M; Calle, E; Rodriguez, C; Maso, L; Talamini, R; Cramer, D; Hankinson, S; Tworoger, S; Chetrit, A; Hirsh-Yechezkel, G; Lubin, F; Sadetzki, S; Appleby, P; Banks, E; Beral, V; Berrington de Gonzalez, A; Bull, D; Crossley, B; Goodill, A; Green, I; Green, J; Hermon, C; Key, T; Reeves, G; Collins, R; Doll, R; Peto, R; Gonzalez, C; Lee, N; Marchbanks, P; Ory, H; Peterson, H; Wingo, P; Martin, N;

Pardthaisong, T; Silpisornkosol, S; Theetranont, C; Boosiri, B; Chutivongse, S; Jimakorn, P; Virutamasen, P; Wongsrichanalai, C; Titus-Ernstoff, L; Mosgaard, B; Vessey, M; Yeates, D; Chang-Claude, J; Rossing, M; Thomas, D; Weiss, N; Franceschi, S; La Vecchia, C; Negri, E; Adami, H; Magnusson, C; Riman, T; Weiderpass, E; Wolk, A; Brinton, L; Freedman, D; Hartge, P; Lacey, J; Hoover, R; Schouten, L; van den Brandt, P; Chantarakul, N; Koetsawang, S; Rachawat, D; Graff-Iversen, S; Selmer, R; Bain, C; Green, A; Purdie, D; Siskind, V; Webb, P; McCann, S; Binns, C; Lee, A; Zhang, M; Nasca, P; Coogan, P; and Rosenberg, L. (2008). Ovarian cancer and oral contraceptives: collaborative reanalysis of data from 45 epidemiological studies including 23,257 women with ovarian cancer and 87,303 controls. *Lancet*, 303-14. doi:10.1016/S0140-6736(08)60167-1.

Berclaz, G; Altermatt, HJ; Rohrbach, V; Kieffer, I; Dreher, E; and Andres, AC. (2001). Estrogen dependent expression of the receptor tyrosine kinase axl in normal and malignant human breast. *Annals of oncology*, 819-24.

Berek, J., Chalas, E., Edelson, M., Moore, D., Burke, W., Cliby, W., and Berchuck, A. (2010). Prophylactic and risk-reducing bilateral salpingo-oophorectomy: recommendations based on risk of ovarian cancer. *Obstetrics and Gynecology*, 733-43. doi:10.1097/AOG.0b013e3181ec5fc1.

Berek, J; Bast, R. (2003). Epithelial Ovarian Cancer. In D. Kufe, R. Pollock, R. Weichselbaum, R. Bast, T. Gansler, J. Holland, and E. Frei, *Holland-Frei Cancer Medicine* (6 ed.). Retrieved from https://www.ncbi.nlm.nih.gov/books/NBK12354/

Berino, F., Verdecchia, A., Lutz, J., Lombardo, C., Micheli, A., Capocaccia, R., and the EUROCARE Working Group. (2009). Comparative cancer survival information in Europe. *European Journal of Cancer*, 901-908.

Blume-Jensen, P., and Hunter, T. (2001). Oncogenic kinase signalling. *Nature*, 355-365. doi:10.1038/35077225.

Blaustein, A; Kurman, R;. (2002). *Blaustein's pathology of the female genital tract.* New York: Springer-Verlag.

Bose, R; Molina, H; Patterson, AS; Bitok, JK; Periaswamy, B; Bader, JS; Pandey, A; and Cole, PA. (2006). Phosphoproteomic analysis of Her2/neu signaling and inhibition. *Proceedings of the National Academy of Sciences of the United States of America*, 9773-8.

Boyd, J., and Rubin, S. (1997). Hereditary Ovarian Cancer: Molecular Genetics and Clinical Implications. 196-206. doi:https://doi.org/10.1006/gyno.1996.4572.

Brümmendorf, T., Spaltmann, F., and Treubert, U. (1997). Cloning and characterization of a neural cell recognition molecule on axons of the retinotectal system and spinal cord. *The European journal of neuroscience*, 1105-1116.

Calle, E., and Kaaks, R. (2004). Overweight, obesity and cancer: epidemiological evidence and proposed mechanisms. *Nature Review Cancer*, 579-91.

Campeau, E; Ruhl, V; Rodier, F; Smith, C; Rahmberg, B; Fuss, J; Campisi, J; Yaswen, P; Cooper, P; and Kaufman, P. (2009). A versatile viral system for expression and depletion of proteins in mammalian cells. *PLoS One. 2009 Aug 6;4(8):e6529. doi: 10.1371/journal.pone.0006529.*, 1-18. doi: 10.1371/journal.pone.0006529.

Carey, L; Winer, E; Viale, G; Cameron, D; and Gianni, L. (2010). Triple-negative breast cancer: disease entity or title of convenience? *Nature reviews. Clinical oncology*, 683-92.

Carpenter, G. (2003). ErbB-4: mechanism of action and biology. *Experimental Cell Research*, 66-77. Retrieved from https://doi.org/10.1016/S0014-4827(02)00100-3.

Carvalho, R; Beutler, M; Marler, K; Knöll, B; Becker-Barroso, E; Heintzmann, R; Ng T, T; and Drescher, U. (2006). Silencing of EphA3 through a cis interaction with ephrinA5. *Nature Neuroscience*, 322-30.

Cheaib, B; Auguste, A; and Leary, A. (2015). The PI3K/Akt/mTOR pathway in ovarian cancer: therapeutic opportunities and challenges. *Chinese journal of cancer*, 4–16.

Chen, J; Lui, W; Vos, M; Clark, G; Takahashi, M; Schoumans, J; Khoo, S; Petillo, D; Lavery, T; Sugimura, J; Astuti, D; Zhang, C; Kagawa, S; Maher, E; Larsson, C; Alberts, A; Kanayama, H; and Teh, B. (2003). The t(1;3) breakpoint-spanning genes LSAMP and NORE1 are involved in clear cell renal cell carcinomas. *Cancer cell*, 405-413. doi: 10.1016/S1535-6108(03)00269-1.

Chen, S., Gil, O., Ren, Y., Zanazzi, G., Salzer, J., and Hillman, D. (2001). Neurotrimin expression during cerebellar development suggests roles in axon fasciculation and synaptogenesis. *Journal of neurocytology*, 927-37.

Chen, V; Ruiz, B; Killeen, J; Cote, T; Wu, X; and Correa, C. (2003). Pathology and Classification of Ovarian Tumors. *Cancer*, 2631-42. doi:10.1002/cncr.11345.

Cheng, N., Brantley, D., and Chen, J. (2002). The ephrins and Eph receptors in angiogenesis. *Cytokine and Growth Factor Reviews* , 75-85.

Chien, A; Conrad, W; and Moon, R. (2009). A Wnt Survival Guide: From Flies to Human Disease. *Journal of Investigative Dermatology*, 1614-1627.

Cho, A; Howell, V; and Colvin, E. (2015). The Extracellular Matrix in Epithelial Ovarian Cancer – A Piece of a Puzzle. *Frontiers in oncology*, 1-16.

Cho, T., Hasegawa, J., and Loh H, H. (1986). Purification to apparent homogeneity of a mu-type opioid receptor from rat brain. *Proceedings of the National Academy of Sciences united states of America*, 4138-42.

Chunhong, L; Liping, T; Lijuan, Z; Lili, L; Qian, X; Xinrong, L; Weiyan, P; Guosheng, R; Qian, T; and Tingxiu, X. (2015). OPCML is frequently methylated in human colorectal cancer and its restored expression reverses EMT via downregulation of smad signaling. *American Journal of Cancer Research*, 1653-1648.

Citria, A., Skaria , K., and Yarden , Y. (2003). The deaf and the dumb: the biology of ErbB-2 and ErbB-3. *Experimental Cell Research*, 54-65. Retrieved from https://doi.org/10.1016/S0014-4827(02)00101-5.

Clark, C., Liu, Y., and Cooper, H. (2014). The Yin and Yang of Wnt/Ryk axon guidance in development and regeneration. *Science China Life Science*, 366-71. doi:10.1007/s11427-014-4640-3.

Clement, P. (1987). Histology of the ovary. *The American Journal of Surggical Pathology*, 277-303.

Clemmons, D. (1998). Role of insulin-like growth factor binding proteins in controlling IGF actions. *Molecular and Cellular Endocrinology . 1998* , 19-24.

Collaborative group. (2012). Ovarian Cancer and Body Size: Individual Participant Meta-Analysis Including 25,157 Women with Ovarian Cancer from 47 Epidemiological Studies. *Plos*, 1-12. doi:10.1371/journal.pmed.1001200.

Corney, D., Flesken-Nikitin, A., Choi, J., and Nikitin, A. (2008). Role of p53 and Rb in Ovarian Cancer. *Advances in Experimental Medicine and Biology*, 99–117. doi:10.1007/978-0-387-68969-2_9.

Craven , R; Xu , L; Weiner , T; Fridell , Y; Dent , G; Srivastava , S; Varnum , B; Liu , E; and Cance , W. (1995). Receptor tyrosine kinases expressed in metastatic colon cancer. *International Journal of Cancer*, 791-7.

Cui, Y; Ying, Y; van Hasselt, A; Ng, K; Yu, J; Zhang, Q; Jin, J; Liu, D; Rhim, J; Rha, S; Loyo, M; Chan, A; Srivastava, G; Tsao, G; Sellar, G; Sung, J; Sidransky, D; and Tao, Q. (2008). OPCML is a broad tumor suppressor for multiple carcinomas and lymphomas with frequently epigenetic inactivation. *Plos one*, 1-11. Retrieved from https://doi.org/10.1371/journal.pone.0002990.

Daly, M; Pilarski, R; Berry, M; Buys, S; Farmer, M; Friedman, S; Garber, J; Kauff, N; Khan, S; Klein, C; Kohlmann, W; Kurian, A; Litton, J; Madlensky, L; Merajver, S; Offit, K; Pal, T; Reiser, G; Shannon, K; Swisher, E; Vinayak, S; Voian, N; Weitzel, J; Wick, M; Wiesner, G; Dwyer, M; and Darlow, S. (2017). NCCN Guidelines Insights: Genetic/Familial High-Risk Assessment: Breast and Ovarian, Version 2.2017. *Journal of the National Comprehensive Cancer Network*, 9-20.

Davy, A., Gale, N., Murray, E., Klinghoffer, R., Soriano, P., Feuerstein, C., and Robbins, S. (1999). Compartmentalized signaling by GPI-anchored ephrin-A5 requires the Fyn tyrosine kinase to regulate cellular adhesion. *Genes Development*, 3125-3135.

Denduluri, S; Idowu, O; and Wang, Z; Liao, Z; Yan, Z; Mohammed, M; Ye, J; Wei, Q; Wang, J; Zhao, L; Luu, H. (2015). The Role of the IGF System in Cancer Growth and Metastasis: Overview and Recent Insights. *Genes & Diseases*, 13-25.

Dennis, E; Jahanshad, N; Braskie, M; Warstadt, N; Hibar, D; Kohannim, O; Nir, T; McMahon, K; de Zubicaray, G; Montgomery, G; Martin, N; Toga, A; Wright, M; and Thompson, P. (2014). Obesity gene NEGR1 associated with white matter integrity in healthy young adults. *NeuroImage*, 548-57.

Diergaarde, B., and Kurta, M. (2014). Use of fertility drugs and risk of ovarian cancer. *Curr Opin Obstet Gynecol*, 125-129. doi::10.1097/GCO.0000000000000060.

Doufekas, K., and Olaitan, A. (2014). Clinical epidemiology of epithelial ovarian cancer in the UK. *International journal of women health*, 537-545. doi:10.2147/IJWH.S40894

Drake, R., Vogl, A., and Mitchell, A. (2015). *Gray's Anatomy for Students* (3rd ed.). Elsevier.

Duarte-Pereira, S; Paiva F, F; Costa, V; Ramalho-Carvalho, J; Savva-Bordalo, J; Rodrigues, A; Ribeiro, F; Silva, V; Oliveira, J; Henrique, R; and Jerónimo, C. (2011). Prognostic value of opioid binding protein/cell adhesion molecule-like promoter methylation in bladder carcinoma. *European Journal of cancer*, 1106-14. doi:doi: 10.1016/j.ejca.2010.12.025

Dufies, M; Jacquel, A; Belhacene, N; Robert, G; Cluzeau, T; Luciano, F; Cassuto, J; Raynaud, S; and Auberger, P. (2011). Mechanisms of AXL overexpression and function in Imatinib-resistant chronic myeloid leukemia cells. *Oncotarget*, 874-85.

Dupont, J., Pierre, A., Froment, P., and Moreau, C. (2003). The Insulin-like Growth Factor Axis in Cell Cycle Progression. *Hormone and Metabolic Research*, 740-750. doi:0.1055/s-2004-814162.

Duxbury, M., Ito, H., Zinner, M., Ashley, S., and Whang, E. (2004). EphA2: a determinant of malignant cellular behavior and a potential therapeutic target in pancreatic adenocarcinoma. *Oncogene*, 1448-56.

Edmondson, R., and Monaghan, J. (2001). The epidemiology of ovarian cancer. *International Journal of Gynecological Cancer*, 423–429. doi:10.1046/j.1525-1438.2001.01053.x.

English, D., Roque, D., and Santin, A. (2013). HER2 Expression Beyond Breast Cancer: Therapeutic Implications for Gynecologic Malignancies. *Molecular diagnosis & therapy*, 85–99.

Ettinger, D. (2006). Clinical Implications of EGFR Expression in the Development and Progression of Solid Tumors: Focus on Non-Small Cell Lung Cancer. *The Oncologist*, 358-73.

Ezzati, M; Djahanbakhch, O; Arian, S; Carr, BR;. (2014). Tubal transport of gametes and embryos: a review of physiology and pathophysiology. *Journal of assisted reproduction and genetics*, 1337-47.

Falls, D. (2003). Neuregulins: functions, forms, and signaling strategies. *Experimental Cell Research*, 14-30.

Fathalla, M. (1971). INCESSANT OVULATION—A FACTOR IN OVARIAN NEOPLASIA ? *The Lancet*(7716), 163.

Fauser, B., and Heusden, A. (1997). Manipulation of Human Ovarian Function: Physiological Concepts and Clinical Consequences. *Endocrine Reviews*, 71–106.

Ferlay, J; Soerjomataram, I; Ervik, M; Dikshit, R; Eser, S; Mathers, C; Rebelo, M; Parkin, DM; Forman, D; and Bray, F. (2013). Cancer Incidence and Mortality Worldwide: IARC CancerBase No. 11. *GLOBOCAN 2012 v1.0*. Retrieved from http://gco.iarc.fr/today/online-analysis-pie?mode=cancer&mode_population=continents&population=900&sex=0&cancer=29&type=0&statistic=0&prevalence=0&color_palette=default.

Fitzmaurice, C. (2015). Global, Regional, and National Cancer Incidence, Mortality,Years of Life Lost, Years Lived With Disability, and DisabilityAdjusted Life-years for 32 Cancer Groups, 1990 to 2015A Systematic Analysis for the Global Burden of Disease Study. *JAMA Oncology*, 524-548. doi:i:10.1001/jamaoncol.2016.5688.

Fleming, J., Beaugié, C., Haviv, I., Chenevix-Trench, G., and Tan, O. (2006). Incessant ovulation, inflammation and epithelial ovarian carcinogenesis: revisiting old hypotheses. *Molecular and Cellular Endocrinology*, 4-21.

Fradkin, L., Dura, J., and Noordermeer, J. (2010). Ryks: new partners for Wnts in the developing and regenerating nervous system. *Trends in Neuroscience*, 84-92. doi:10.1016/j.tins.2009.11.005.

Funatsu, N; Miyata, S; Kumanogoh, H; Shigeta, M; Hamada, K; Endo, Y; Sokawa, Y; and Maekawa, S. (1999). Characterization of a novel rat brain glycosylphosphatidylinositol-anchored protein (Kilon), a member of the IgLON cell adhesion molecule family. *Journal of biological chemistry*, 8224-8230.

Furlanetto, R., Harwell, S., and Baggs, R. (1993). Effects of insulin-like growth factor receptor inhibition on human melanomas in culture and in athymic mice. *Cancer Research*, 2522–2526.

Folkins , AK; Jarboe , EA; Saleemuddin , A; Lee , Y; Callahan , MJ; Drapkin , R; Garber, JE; Muto , MG; Tworoger , S; Crum , CP. (2008). A candidate precursor to pelvic serous cancer (p53 signature) and its prevalence in ovaries and fallopian tubes from women with BRCA mutations. *Gynecologic oncology*, 168-73.

Gabra, H; Watson, V; Taylor, K; Mackay, J; Leonard, R; Steel, M; Porteous, D; and Smyth, J. (1996). Definition and Refinement of a Region of Loss of Heterozygosity at 11q23.3–

q24.3 in Epithelial Ovarian Cancer Associated with Poor Prognosis. *Cancer Research*, 950-954.

Gatcliffe, T., Monk, B., Planutis, K., and Holcombe, R. (2008). Wnt signaling in ovarian tumorigenesis. *International Journal of Gynecological Cancer*, 954–962.

Gennigens, C., Menetrier-Caux, C., and Droz, J. (2006). Insulin-Like Growth Factor (IGF) family and prostate cancer. *Critical reviewa in oncology/hematology*, 124-45.

George, SH; Shaw, P. (2014). BRCA and Early Events in the Development of Serous Ovarian Cancer. *Frontiers in oncology*, 1-8.

George, S; Garcia, R; Slomovitz, B. (2016). Ovarian Cancer: The Fallopian Tube as the Site of Origin and Opportunities for Prevention. *Frontiers in oncology, 6*, 1-7. doi: 10.3389/fonc.2016.00108

Ghosh, A., Secreto, C., Boysen, J., Sassoon, T., Shanafelt, T., Mukhopadhyay, D., and Kay, N. (2011). The novel receptor tyrosine kinase Axl is constitutively active in B-cell chronic lymphocytic leukemia and acts as a docking site of nonreceptor kinases: implications for therapy. *Blood*, 1928-37. doi:10.1182/blood-2010-09-305649.

Gil, O; Zhang, L; Chen, S; Ren, Y; Pimenta, A; Zanazzi, G; Hillman, D; Levitt, P; and Salzer, J. (2002). Complementary expression and heterophilic interactions between IgLON family members neurotrimin and LAMP. *Journal of neurobiology*, 190-204.

Gilks, C., Irving, J., Köbel, M., Lee, C., Singh, N., Wilkinson, N., and McCluggage, W. (2015). Incidental nonuterine high-grade serous carcinomas arise in the fallopian tube in most cases: further evidence for the tubal origin of high-grade serous carcinomas. *The American journal of surgical pathology*, 357-64.

Glickman, L., Domanski, L., Maguire, T., Dubielzig, R., and Churg, A. (1983). Mesothelioma in pet dogs associated with exposure of their owners to asbestos. *Environmental research*, 305-13.

Gobin, B; Moriceau, G; Ory, B; Charrier, C; Brion, R; Blanchard, F; Redini, F; and Heymann, D. (2014). Imatinib Mesylate Exerts Anti-Proliferative Effects on Osteosarcoma Cells and Inhibits the Tumour Growth in Immunocompetent Murine Models. *PLoS ONE*, 1-12. Retrieved from https://doi.org/10.1371/journal.pone.0090795.

Gordon, M., and Hahn, R. (2010). Collagens. *Cell Tissue Research* , 247–257.

Goff, B; Mandel, L; Drescher, C; Urban , N; Gough, S; Schurman, K; Patras, J; Mahony, B; and Andersen , R. (2007). Development of an ovarian cancer symptom index possibilities for earlier detection. *CANCER, 109*, 221-227.

Graham, D., Bowman, G., Dawson, T., Stanford, W., Earp, H., and Snodgrass, H. (1995). Cloning and developmental expression analysis of the murine c-mer tyrosine kinase. *Oncogene*, 2349-59.

Granström, C., Sundquist, J., and Hemminki, K. (2008). Population attributable fractions for ovarian cancer in Swedish women by morphological type. *British Journal of cancer*, 199-205.

Graus-Porta, D., Beerli, R., Daly, J., and Hynes, N. (1997). ErbB-2, the preferred heterodimerization partner of all ErbB receptors, is a mediator of lateral signaling. *EMBO Journal*, 1647-55.

Green, A., Purdie, D., Bain, C., Siskind, V., Russell, P., Quinn, M., and Ward, B. (1997). Tubal sterilisation, hysterectomy and decreased risk of ovarian cancer. Survey of Women's Health Study Group. *International journal of cancer*, 948-51.

Grimwood, J; Gordon, L; Olsen, A; Terry, A; Schmutz, J; Lamerdin, J; Hellsten, U; Goodstein, D; Couronne, O; Tran-Gyamfi, M; Aerts, A; Altherr, M; Ashworth, L; Bajorek, E; Black, S; Branscomb, E; Caenepeel, S; Carrano, A; Caoile, C; Chan, YM; Christensen, M; Cleland, C; Copeland, A; Dalin, E; Dehal, P; Furey, T; DeJong, P; Dickson, M; Gordon, D; Eichler, E; Pennacchio, L; Richardson, P; Stubbs, L; Rokhsar, D; Myers, R; Rubin, E; and Lucas, S. (2004). The DNA sequence and biology of human chromosome 19. *Nature*, 529-35.

Grothey, A., Voigt, W., Schöber, C., Müller, T., Dempke, W., and Schmoll, H. (1999). The role of insulin-like growth factor I and its receptor in cell growth, transformation, apoptosis, and chemoresistance in solid tumors. *Journal of Cancer Research and Clinical Oncology*, 166-73.

Gui, T., and Shen, K. (2012). The epidermal growth factor receptor as a therapeutic target in epithelial ovarian cancer. *Cancer Epidemiology*, 490-6. doi: 10.1016/j.canep.2012.06.005.

Guy, P., Platko, J., Cantley, L., Cerione, R., and Carraway, K. (1994). Insect cell-expressed p180erbB3 possesses an impaired tyrosine kinase activity. *PNAS*, 8132-6.

Hachisuka, A., Nakajima, O., Yamazaki, T., and Sawada, J. (1999). Localization of opioid-binding cell adhesion molecule (OBCAM) in adult rat brain. *Brain Research*, 482-6.

Hafizi, S., and Dahlbäck, B. (2006). Signalling and functional diversity within the Axl subfamily of receptor tyrosine kinases. *Cytokine & Growth Factor Reviews*, 295-304.

Halford, M., and Stacker, S. (2001). Revelations of the RYK receptor. *Bioessays*, 34-45.

Hanahan, D., and Weinberg, R. (2000). The hallmarks of cancer. *Cell*, 57-70.

Hankinson, S; Colditz, G; Hunter, D; Willett, W; Stampfer, M; Rosner, B; Hennekens, C; and Speizer, F. (1995). A prospective study of reproductive factors and risk of epithelial ovarian cancer. *Cancer*, 284-90.

Harlow, B., Cramer, D., Bell, D., and Welch, W. (1992). Perineal exposure to talc and ovarian cancer risk. *Obstetrics and gynecology*, 19-26.

Harrison, M., Jameson, C., and Gore, M. (2008). Mucinous ovarian cancer. *International Journal of Gynecological Cancer : Official Journal of the International Gynecological Cancer Society*, 209-14. doi:10.1111/j.1525-1438.2007.01022.x.

Hashiguchi, Y., Tsuda, H., Yamamoto, K., H Inoue, T., Ishiko, O., and Ogita, S. (2001). Combined analysis of p53 and RB pathways in epithelial ovarian cancer. *Human Pathology* , 988-96.

Hashimoto, T., Maekawa, S., and Miyata, S. (2009). IgLON cell adhesion molecules regulate synaptogenesis in hippocampal neurons. *Cell Biochemistry and Function*, 496-8. doi:10.1002/cbf.1600.

Hemminki, K., Sundquist, J., and Brandt, A. (2011). Incidence and mortality in epithelial ovarian cancer by family history of any cancer. *Cancer*, 3972-80. doi: 10.1002/cncr.26016.

Himanen, J., and Nikolov, D. (2003). Eph signaling: a structural view. *Trends in Neurosciences*, 46-51.

Himanen, J; Chumley, M; Lackmann, M; Li, C; Barton, W; Jeffrey, P; Vearing, C; Geleick, D; Feldheim, D; Boyd, A; Henkemeyer, M; and Nikolov, D. (2004). Repelling class discrimination: ephrin-A5 binds to and activates EphB2 receptor signaling. *Nature Neuroscience*, 501-9.

Holbro, T., and Hynes, N. (2004). ErbB Receptors: Directing Key Signaling Networks Throughout Life. *Annual Review of Pharmacology and Toxicology*, 195-217. Retrieved from https://doi.org/10.1146/annurev.pharmtox.44.101802.121440.

Holschneider, C., and Berek, J. (2000). Ovarian cancer: epidemiology, biology, and prognostic factors. *Seminars in surgical oncology*, 3-10.

Hovens, C., Stacker, S., Andres, A., Harpur, A., Ziemiecki, A., and Wilks, A. (1992). RYK, a receptor tyrosine kinase-related molecule with unusual kinase domain motifs. *PNAS*, 11818-22.

Hubbard, S., and Till, J. (2000). Protein tyrosine kinase structure and function. *Annual Review of Biochemistry*, 373-98.

Huang, J; Zhang, L; Greshock, J; Colligon, T; Wang, Y; Ward, R; Katsaros, D; Lassus, H; Butzow, R; Godwin, AK; Testa, JR; Nathanson, KL; Gimotty, PA; Coukos, G; Weber, BL; and Degenhardt, Y. (2011). Frequent genetic abnormalities of the PI3K/AKT pathway in primary ovarian cancer predict patient outcome. *Genes, chromosomes & cancer*, 606-18.

Huang, R., Antony, J., Tan , T., and Tan, D. (2017). Targeting the AXL signaling pathway in ovarian cancer. *Molecular & Cellular Oncology, 4*(2), 1-3.

Huncharek, M., Geschwind, J., and Kupelnick, B. (2003). Perineal application of cosmetic talc and risk of invasive epithelial ovarian cancer: a meta-analysis of 11,933 subjects from sixteen observational studies. *Anticancer research*, 1955-60.

Hyde, G; Nagle, M; Tian, C; Che, X; Paciga, S; Wendland, J; Tung, J; Hinds, D; Perlis, R; and Winslow, A. (2016). Identification of 15 genetic loci associated with risk of major depression in individuals of European descent. *NATURE GENETICS*, 1031–1036.

Innos, J; Koido, K; Philips, M; and Vasar, E. (2013). Limbic system associated membrane protein as a potential target for neuropsychiatric disorders. *frontiers in pharmacology*, 1-3. doi:10.3389/fphar.2013.00032.

Innos, J; Leidmaaa, E; Philips, M; Sütt, S; Alttoa, A; Harro, J; Kõks, S; and Vasar, E. (2013). Lsamp–/– mice display lower sensitivity to amphetamine and have elevated 5-HT turnover. *Biochemical and Biophysical Research Communications*, 413–418. doi:https://doi.org/10.1016/j.bbrc.2012.11.077.

Inoue, T; Oz , H; Wiland , D; Gharib , S; Deshpande , R; Hill , R; Katz , W; and Sternberg , P. (2004). C. elegans LIN-18 is a Ryk ortholog and functions in parallel to LIN-17/Frizzled in Wnt signaling. *Cell*, 795-806.

Irie, N; Takada, Y; Watanabe, Y; Matsuzaki, Y; Naruse, C; Asano, M; Iwakura, Y; Suda, T; and Matsuo, K. (2009). Bidirectional signaling through ephrinA2-EphA2 enhances osteoclastogenesis and suppresses osteoblastogenesis. *The Journal of biological chemistry*, 14637-44.

Ishikawa , M; Sonobe , M; Nakayama , E; Kobayashi M, , M; Kikuchi , R; Kitamura , J; Imamura , N; and Date , H. (2013). Higher expression of receptor tyrosine kinase Axl, and differential expression of its ligand, Gas6, predict poor survival in lung adenocarcinoma patients. *Annals of surgical oncology*, 467-76.

Ito, T; Ito, M; Nsito, S; Oht, A; Nagayama, Y; Kanematsu, T; Yamashita, S; and Sekine, I. (2009). Expression of the Axl Receptor Tyrosine Kinase in Human Thyroid Carcinoma. *Thyroid*, 563-567.

Itoh, S; Hachisuka, A; Kawasaki, N; Hashii, N; Teshima, R; Hayakawa, T; Kawanishi, T; and Yamaguchi, T. (2008). Glycosylation Analysis of IgLON Family Proteins in Rat Brain by

Liquid Chromatography and Multiple-Stage Mass Spectrometry. *Biochemistry*, 10132–10154.

Jervis, S; Song, H; Lee, A; Dicks, E; Tyrer, J; Harrington, P; Easton, D; Jacobs, I; Pharoah, P D; and Antoniou, A. (2014). Ovarian cancerfamilial relative risks by tumour subtypes and by known ovarian cancer genetic susceptibility variants. *Journal of Medical Genetics*, 108-113.

Jelovac, D., and Armstrong, D. (2011). Recent Progress in the Diagnosis and Treatment of Ovarian Cancer. *cancer journal for clinicians*, 1-33.

Jian-Zhong, L; Zeng-Jun, W; Wei, D; Ming, Z; Wei-Zhang, X; Hong-Fei, W; Alex, A; and Jia-Geng, Z. (2017). Targeting AXL overcomes resistance to docetaxel therapy in advanced prostate cancer. *Oncotarget*, 41064–41077.

John, R., and Ross, H. (2010). The global econonmic cost of cancer. *American cancer society and the livestrong organisation*.

Jonathan, S; Berek, M; Robert, C; and Bast, JR. (2003). *Epithelial Ovarian cancer* (6 ed.). Holland-Frei Cancer Medicine.

Jordan, S; Cushing-Haugen, K; Wicklund, K; Doherty, J; and Rossing, M. (2012). Breast-feeding and risk of epithelial ovarian cancer. *Cancer causes and control*, 919-2.

Jordan, S; Whiteman, D; Purdie, D; Green, A; and Webb, P. (2006). Does smoking increase risk of ovarian cancer? A systematic review. *Gynecologic oncology*, 1122-9.

Kalachand, R., Hennessy, B., and Markman, M. (2011). Molecular Targeted Therapy in Ovarian Cancer. *Drugs*, 947–967.

Kamiguchia, H., and Lemmon, V. (2000). IgCAMs: bidirectional signals underlying neurite growth. *Current Opinion in Cell Biology*, 598-605. Retrieved from https://doi.org/10.1016/S0955-0674(00)00138-1.

Karst, A., and Drapkin, R. (2010). Ovarian Cancer Pathogenesis: A Model in Evolution. *Journal of Oncology*, 1-13.

Katso, R; Manek, S; Biddolph, S; Whittaker, R; Charnock, M; Wells, M; and Ganesan, T. (1999). Overexpression of H-Ryk in Mouse Fibroblasts Confers Transforming Ability in Vitro and in Vivo: Correlation with Up-Regulation in Epithelial Ovarian Cancer. *CANCER RESEARCH*, 2265–2270.

Katso, R; Manek, S; Ganjavi, H; Biddolph, S; Charnock, M; Wells , M; and Ganesan, T. (2000). Overexpression of H-Ryk in Epithelial Ovarian Cancer: Prognostic Significance of Receptor Expression. *Clinical Cancer Research*, 3271–3281.

Keeble, T., and Cooper, H. (2006). Ryk: A novel Wnt receptor regulating axon pathfinding. *The International Journal of Biochemistry & Cell Biology* , 2011-2017.

Kenny, HA; Chiang, CY; White, EA; Schryver, EM; Habis, M; Romero, IL; Ladanyi, A; Penicka, CV; George, J; Matlin, K; Montag, A; Wroblewski, K; Yamada, SD; Mazar, AP; Bowtell, D; and Lengyel, E. (2014). Mesothelial cells promote early ovarian cancer metastasis through fibronectin secretion. *The Journal of clinical investigation*, 4614-28.

Khandwala, H; McCutcheon, I; Flyvbjerg, A; and Friend, K. (2000). The Effects of Insulin-Like Growth Factors on Tumorigenesis and Neoplastic Growth. *Endocrine Reviews*, 215-244. Retrieved from https://doi.org/10.1210/edrv.21.3.0399.

Kim, H; Hwang, J; Lee, B; Hong, J; and Lee, S. (2014). Newly Identified Cancer-Associated Role of Human Neuronal Growth Regulator 1 (NEGR1). *Journal of cancer*, 598-608. doi:doi: 10.7150/jca.8052.

Kinch, M., Moore, M., and Harpole, D. (2003). Predictive value of the EphA2 receptor tyrosine kinase in lung cancer recurrence and survival. *Clinical Cancer Research*, 613-8.

Knudtson, J., and Mclaughlin, J. (2013). *Female Reproductive Endocrinology.* MSD.

Koido, K; Janno, S; Traks, T; Parksepp, M; Ljubaje, U; Veiksaar, P; Must, A; Shlik, J; Vasar, V; and Vasar, E. (2014). Associations between polymorphisms of LSAMP gene and schizophrenia. *Psychiatry research*, 797-8. doi:doi: 10.1016/j.psychres.

Konstantinova, I; Nikolova, G; Ohara-Imaizumi, M; Meda, P; Kucera, T; Zarbalis, K; Wurst, W; Nagamatsu, S; and Lammert, E. (2007). EphA-Ephrin-A-mediated beta cell communication regulates insulin secretion from pancreatic islets. *Cell*, 359-70.

Kresse, S; Ohnstad, H; Paulsen, E; Bjerkehagen, B; Szuhai, K; Serra, M; Schaefer, K; Myklebost, O; and Meza-Zepeda, L. (2009). LSAMP, a novel candidate tumor suppressor gene in human osteosarcomas, identified by array comparative genomic hybridization. *GENES, CHROMOSOMES & CANCER*, 679–693.

Kulkarni, R., and Kahn, C. (2007). Ephs and ephrins keep pancreatic Beta cells connected. *Cell*, 241-3.

Kulkarni, R., and McGarry, J. (1989). Follicular stimulation and ovarian cancer. *BMJ*, 740.

Kurman, R. (2013). Origin and molecular pathogenesis of ovarian high-grade serous carcinoma. *Annals of Oncology*, 16-21. doi:doi:10.1093/annonc/mdt463.

Kurman, R., and Shih, L.-M. (2011). The Origin and Pathogenesis of Epithelial Ovarian Cancer-a Proposed Unifying Theory. *American journal of surical pathology*, 433-443. doi:10.1097/PAS.0b013e3181cf3d79.

Landen, C., Birrer, M., and Sood, A. (2008). Early events in the pathogenesis of epithelial ovarian cancer. *Journal of clinical oncology*, 995-1005.

Lauby-Secretan, B., Scocciant, C., Loomis, D., Grosse, Y., Bianchini, F., and Straif, K. (2016). *Body Fatness and Cancer — Viewpoint of the IARC Working Group.*

Lauchlan, S. (1972). The secondary Mullerian system. *Obstetrical and Gynecological Survey*, 133-146.

Lauchlan, S. (1994). The secondary müllerian system revisited. *International Journal of Gynecological Pathology*, 73-9.

Lee, Y; Miron, A; Drapkin, R; Nucci, MR; Medeiros, F; Saleemuddin, A; Garber, J; Birch, C; Birch, C; Mou, H; Gordon, RW; Cramer, DW; McKeon, FD; and Crum, CP. (2007). A candidate precursor to serous carcinoma that originates in the distal fallopian tube. *The Journal of pathology*, 26-35.

Lemmon, M., and Schlessinger, J. (2010). Cell Signaling by Receptor Tyrosine Kinases. *Cell*, 1117-1134. Retrieved from https://doi.org/10.1016/j.cell.2010.06.011.

Lennartsson, J., and Rönnstrand, L. (2012). Stem cell factor receptor/c-Kit: from basic science to clinical implications. *Physiological reviews*, 1619-49.

Leonhardt, K., Einenkel, J., Sohr, S., Engeland, K., and Horn, L. (2011). p53 signature and serous tubal in-situ carcinoma in cases of primary tubal and peritoneal carcinomas and serous borderline tumors of the ovary. *International journal of gynecological pathology*, 417-24.

Levanon, K; Ng, V; Piao, HY; Zhang, Y; Chang, MC; Roh, MH; Kindelberger, DW; Hirsch, MS; Crum, CP; Marto, JA; and Drapkin, R. (2010). Primary ex vivo cultures of human fallopian tube epithelium as a model for serous ovarian carcinogenesis. *Oncogene*, 1103-13.

Levitt, P. (1984). A monoclonal antibody to limbic system neurons. *SCIENCE*, 299-301.

Leypoldt, F., Armangue, T., and Dalmau, J. (2015). Autoimmune encephalopathies. *Annals of New York Accademy of Science*, 94-114. doi:10.1111/nyas.12553.

Lheureux , S; Shaw , PA; Karakasis, K; Oza , AM. (2015). Cancer precursor lesions in the BRCA population at the time of prophylactic salpingo-oophorectomy: Accuracy of assessment and potential surrogate marker for prevention. *Gynecologic oncology*, 235-7.

Li, J; Abushahin, N; Pang, S; Xiang, L; Chambers, S; Fadare, O; Kong, B; and Zheng, W. (2011). Tubal origin of 'ovarian' low-grade serous carcinoma. *Modern Patholology . 2011 Nov;24(11):1488-99. doi: 10.1038/modpathol.2011.106.*, 1488-99. doi:10.1038/modpathol.2011.106.

Li, C; Tang, L; Zhao, L; Li, L; Xiao, Q; Luo, X; Peng, W; Ren, G; Tao, Q; and Xiang, T. (2015). OPCML is frequently methylated in human colorectal cancer and its restored expression reverses EMT via downregulation of smad signaling. *American Journal of Cancer Research*, 1635-1648.

Linger, R., Keating, A., Earp, H., and Graham, D. (2008). TAM receptor tyrosine kinases: biologic functions, signaling, and potential therapeutic targeting in human cancer. *Advances in Cancer Reseasch*, 35-83. doi:10.1016/S0065-230X(08)00002-X.

Liotta, L; and Kohn, E. (2001). The microenvironment of the tumour–host interface. *Nature*, 375-379. doi:10.1038/35077241.

Lodge, A., Howard, M., McNamee, C., and Moss, D. (2000). Co-localisation, heterophilic interactions and regulated expression of IgLON family proteins in the chick nervous system. *Molecular Brain Research*, 84-94.

Low, E., Waller, J., Menon, U., Jones, A., Reid, F., and Simon, A. (2013). Ovarian cancer symptom awareness and anticipated time to help-seeking for symptoms among UK women. *Journal of Family Planning and Reproductive Health Care*, 163-171.

Lu, Y., Zi, X., Zhao, Y., Mascarenhas, D., and Pollak, M. (2001). Insulin-like growth factor-I receptor signaling and resistance to trastuzumab (Herceptin). *Journal of the National Cancer Institute*, 1852-7.

Luan, N.-N., Wun, Q.-J., Gong, T.-T., Vogtmann, E., Wang, Y.-L., and Lin, B. (2013). Breastfeeding and ovarian cancer risk: a meta-analysis of epidemiologic studies. *American Journal of clinical nutrition*, 1020–1031. doi:10.3945/ajcn.113.062794.

Lukanova, A., and Kaaks, R. (2005). Endogenous Hormones and Ovarian Cancer: Epidemiology and Current Hypotheses. *Cancer Epidemiology, Biomarkers & Prevention*, 98-107.

Luo, H., Yu, G., Tremblay, J., and Wu, J. (2004). Ephb6-null mutation results in compromised t cell function. *The Journal of clinical investigation* , 1762-1773.

Lyons, R., Saridogan, E., & Djahanbakhch, O. (2006). The reproductive significance of human Fallopian tube cilia. *Human reproduction update*, 363-72.

Ma, X., and Yu, H. (2006). Global Burden of Cancer. *YALE JOURNAL OF BIOLOGY AND MEDICINE*, 9.

Macheda, M; Sun, W; Kugathasan, K; Hogan, B; Bower, N; Halford, M; Zhang, Y; Jacques, B; Lieschke, G; Dabdoub, A; and Stacker, S. (2012). The Wnt receptor Ryk plays a role in

mammalian planar cell polarity signaling. *Journal of Biological Chemistry*, 29312-23. doi:10.1074/jbc.M112.362681.

Maddams, J., Utley, M., and Moller, H. (2012). Projections of cancer prevalence in the United Kingdom, 2010–2040. *British Journal of Cancer* , 1195-1202.

Mann, F., Zhukareva, V., Pimenta, A., Levitt, P., and Bolz, J. (1998). Membrane-associated molecules guide limbic and nonlimbic thalamocortical projections. *Journal of neuroscience*, 9409-19.

Marg, A; Sirim, P; Spaltmann, F; Plagge, A; Kauselmann, G; Buck, F; Rathjen, F; and Brümmendorf, T. (1999). Neurotractin, a novel neurite outgrowth-promoting Ig-like protein that interacts with CEPU-1 and LAMP. *The Journal of cell biology*, 865-876.

Marquez, RT; Baggerly, KA; Patterson, AP; Liu, J; Broaddus, R; Frumovitz, M; Atkinson, EN; Smith DI, DI; Hartmann, L; Fishman, D; Berchuck, A; Whitaker, R; Gershenson, DM; Mills, GB; Bast, RC; and Lu, KH. (2005). Patterns of gene expression in different histotypes of epithelial ovarian cancer correlate with those in normal fallopian tube, endometrium, and colon. *Clinical cancer research*, 6116-26.

Mauro, L., Salerno, M., Morelli, C., Boterberg, T., Bracke, M., and Surmacz, E. (2003). Role of the IGF-I receptor in the regulation of cell–cell adhesion: Implications in cancer development and progression. *Journal of cellular physiology*, 108-16.

McCluggage, W. (2008). My approach to and thoughts on the typing of ovarian carcinomas. *Journal of clinical pathology*, 152–163. doi:10.1136/jcp.2007.049478

McKie, A; Vaughan, S; Zanini, E; Okon, I; Louis, L; de Sousa, C; Greene, M; Wang, Q; Agarwal, R; Shaposhnikov, D; Wong, J; Gungor, H; Janczar, S; ElBahrawy, M; Lam, E; Chayen, N; and Gabra, H. (2012). The OPCML tumor suppressor functions as a cell

surface repressor-adaptor, negatively regulating receptor tyrosine kinases in epithelial ovarian cancer. *Cancer discovery*, 156-71. doi:10.1158/2159-8290.

McLemore, M., Miaskowski, C., Aouizerat, B., Chen, L.-m., and Dodd, M. (2010). Epidemiologic and Genetic Factors Associated with Ovarian Cancer. *Cancer nurs*, 281-290. doi:10.1097/NCC.0b013e31819d30d6.

McNamee, C., Reed, J., Howard, M., Lodge, A., and Moss, D. (2002). Promotion of neuronal cell adhesion by members of the IgLON family occurs in the absence of either support or modification of neurite outgrowth. *Journal of neurochemistry*, 941–948.

Medeiros, F; Muto, M; Lee, Y; Elvin, J; Callahan, M; Feltmate, C; Garber, J; Cramer, D; and Crum, C. (2006). The Tubal Fimbria Is a Preferred Site for Early Adenocarcinoma in Women With Familial Ovarian Cancer Syndrome. *The American Journal of Surgical Pathology*, 230-236.

Mehra, K., Mehrad, M., Ning, G., Drapkin, R., McKeon, F., Xian, W., and Crum, C. (2011). STICS, SCOUTs and p53 signatures; a new language for pelvic serous carcinogenesis. *Frontiers in bioscience* , 625-34.

Melén, E., Himes, B., Brehm, J., Boutaoui, N., Klanderm, B., Sylvia, J., and Lasky-Su, J. (2010). Analyses of shared genetic factors between asthma and obesity in children. *Journal of Allergy Clinical Immunology*, 631-7. doi:10.1016/j.jaci.2010.06.030.

Meric, F., Lee, W., Sahin, A., Zhang, H., Kung, H., and Hung, M. (2002). Expression profile of tyrosine kinases in breast cancer. *Clinical cancer research*, 631-7.

Mishra, S., and Joshi, P. (2007). Lipid raft heterogeneity: an enigma. *Journal of neurochemistry*, 135–142. doi:10.1111/j.1471-4159.2007.04720.x.

Miyata, S., Funatsu, N., Matsunaga, W., Kiyohara, T., Sokawa, Y., and Maekawa, S. (2000). Expression of the IgLON cell adhesion molecules kilon and OBCAM in hypothalamic magnocellular neurons. *The Journal of comparative neurology*, 74–85. doi:10.1002/1096-9861(20000814)424:1<74::AID-CNE6>3.0.CO;2-5.

Miyata, S., Matsumoto, N., Taguchi, K., Akagi, A., Iino, T., Funatsu, N., and Maekawa, S. (2003). Biochemical and ultrastructural analyses of IgLON cell adhesion molecules, Kilon and OBCAM in the rat brain. *Neuroscience*, 645-658. Retrieved from https://doi.org/10.1016/S0306-4522(02)00873-4.

Miyazaki, T., Kato, H., Fukuchi, M., Nakajima, M., and Kuwano, H. (2003). EphA2 overexpression correlates with poor prognosis in esophageal squamous cell carcinoma. *International Journal of Cancer*, 657-63.

Moasser, M. (2007). The oncogene HER2; Its signaling and transforming functions and its role in human cancer pathogenesis. *Oncogene*, 6469–6487.

Modugno, F., Ness, R., and Cottreau, C. (2002). Cigarette smoking and the risk of mucinous and nonmucinous epithelial ovarian cancer. *Epidemiology*, 467-71.

Morrison, J., Blanco, L., Vang, R., and Ronnett, B. (2015). Incidental serous tubal intraepithelial carcinoma and early invasive serous carcinoma in the nonprophylactic setting: analysis of a case series. *The American journal of surgical pathology*, 442-53.

Mullany, L., and Richards, J. (2012). Minireview: Animal Models and Mechanisms of Ovarian Cancer Development. *Endocrinology*, 1585-1592. doi:https://doi.org/10.1210/en.2011-2121.

Nagy, J., Meyers, M., Masse, E., Herzberg, K., and Dvorak, H. (1995). Pathogenesis of ascites tumor growth: fibrinogen influx and fibrin accumulation in tissues lining the peritoneal cavity. *Cancer Research*, 369-75.

Nahta, R., Yuan, L., Zhang, B., Kobayashi, R., and Esteva, F. (2005). Insulin-like growth factor-I receptor/human epidermal growth factor receptor 2 heterodimerization contributes to trastuzumab resistance of breast cancer cells. *Cancer research*, 11118-28.

Narod, S. (2016). Can advanced-stage ovarian cancer be cured? *NATURE REVIEWS CLINICAL ONCOLOGY*, 255–261. doi:10.1038/nrclinonc.2015.224.

Neubauer, A; Fiebeler, A; Graham, D; O'Bryan, J; Schmidt, C; Barckow, P; Serke, S; Siegert, W; Snodgrass, H; and Huhn, D. (1994). Expression of axl, a transforming receptor tyrosine kinase, in normal and malignant hematopoiesis. *Blood*, 1931-41.

Normanno, N., Bianco, C., De Luca, A., Maiello, M., and Salomon, D. (2003). Target-based agents against ErbB receptors and their ligands: a novel approach to cancer treatment. *Endocrine- Related Cancer*, 1-21.

Ntougkos, E., Rush, R., Scott, D., Frankenberg, T., Gabra, H., Smyth, J., and Sellar, G. (2005). The IgLON Family in Epithelial Ovarian Cancer: Expression Profiles and Clinicopathologic Correlates. *Human Cancer Biology*, 5764-5768. doi:10.1158/1078-0432.CCR-04-2388.

Obata, K., Morland, S., Watson, R., Hitchcock, A., Chenevix-Trench, G., Thomas, E., and Campbell, I. (1998). Frequent PTEN/MMAC mutations in endometrioid but not serous or mucinous epithelial ovarian tumors. *Cancer Research*, 2095-7.

Office for National Statistics. (2011). Cancer survival rates, Cancer survival in England, patients diagnosed 2005-2009 and followed up to 2010.

Olsen, C., Green, A., Whiteman, D., Sadeghi, S., Kolahdooz, F., and Webb, P. (2007). Obesity and the risk of epithelial ovarian cancer: a systematic review and meta-analysis. *European journal of cancer*, 690-709.

Onken, J; Torka , R; Korsing , S; Radke , J; Kremente, I; Nieminen , M; Bai , X; Ullrich , A; Heppner , F; and Vajkoczy , P. (2016). Inhibiting receptor tyrosine kinase AXL with small molecule inhibitor BMS-777607 reduces glioblastoma growth, migration, and invasion in vitro and in vivo. *Oncotarget*, 9876-89. doi:10.18632/oncotarget.7130.

Palmer, A; Zimmer, M; Erdmann, K; Eulenburg, V; Porthin, A; Heumann, R; Deutsch, U; and Klein, R. (2002). EphrinB phosphorylation and reverse signaling: regulation by Src kinases and PTP-BL phosphatase. *Molecular cell*, 725-37.

Pan, Y., Wang, K., and Aragam, N. (2011). NTM and NR3C2 polymorphisms influencing intelligence: family-based association studies. *Progress in Neuropsychopharmacology Biological Psychiatry*, 154-60. doi:10.1016/j.pnpbp.2010.10.016.

Pankov, R., and Yamada, K. (2002). Fibronectin at a glance. *Journal of Cell Science* , 3861-3863.

Park, H., Kim, K., Lee, H., Choi, H., Kim, D., Kim, B., and Moon, W. (2007). Overexpression of discoidin domain receptor 1 increases the migration and invasion of hepatocellular carcinoma cells in association with matrix metalloproteinase. *Oncology reports*, 1435-41.

Pasquale, E. (2005). Eph receptor signalling casts a wide net on cell behaviour. *Nature Reviews Molecular Cell Biology*, 462-75.

Paul, S; Merberg, D; Finnerty, H; Morris, G; Morris, J; Jones, S; Kriz R, R; Turner, K; and Wood, C. (1992). Molecular cloning of the cDNA encoding a receptor tyrosine kinase-related molecule with a catalytic region homologous to c-met. *International Journal of Cell Cloning*, 309-14.

Perets, R; Wyant, GA; Muto, KW; Bijron, JG; Poole, BB; Chin, KT; Chen, JY; Ohman, AW; Stepule, CD; Kwak, S; Karst, AM; Hirsch, MS; Setlur, SR; Crum, CP; Dinulescu, DM; and Drapkin, R. (2013). Transformation of the fallopian tube secretory epithelium leads to high-grade serous ovarian cancer in Brca;Tp53;Pten models. *Cancer cell*, 751-65.

Petrovicsa, G; Li , H; Stümpel, T; Tan, S; Young, D; Li, Q; Ying, K; Klocke, B; Ravindranath, L; Kohaar, I; Chen, Y; Ribli, D; Grote, K; Zou, H; Cheng, J; Dalgard, C; Zhang, S; Csabai, I; Kagan, J; Takeda, D; Loda, M; Srivastava, S; Scherf, M; Seifert, M; Gaiser, T; McLeod, D; Szallasi, Z; Ebner, R; Werner, T; Sesterhenn, I; Freedman, M; Dobi, A; and Srivastava, S. (2015). A novel genomic alteration of LSAMP associates with aggressive prostate cancer in African American men. *EBioMedicine*, 1957-1964.

Philips, M; Lilleväli, K; Heinla, I; Luuk, H; Hundahl, C; Kongi, K; Vanaveski, T; Tekko, T; Innos, J; and Vasar, E. (2015). Lsamp is implicated in the regulation of emotional and social behavior by use of alternative promoters in the brain. *Brain structure and function*, 1381-93. doi:10.1007/s00429-014-0732-x.

Piek , JM; Van Diest , PJ; Zweemer , RP; Jansen , JW; Poort-Keesom , RJ; Menko , FH; Gille , JJ; Jongsma , AP; Pals , G; Kenemans , P; Verheijen , RH. (2001). Dysplastic changes in prophylactically removed Fallopian tubes of women predisposed to developing ovarian cancer. *The Journal of pathology*, 451-6.

Piek , JM; Dorsman , JC; Zweemer , RP; Verheijen, RH; Van Diest , PJ; Colgan , TJ. (2003). Women harboring BRCA1/2 germline mutations are at risk for breast and female adnexal carcinoma. *International journal of gynecological pathology*, 315-6.

Piek, J; Kenemans, P; and Verheijen, R. (2004). Intraperitoneal serous adenocarcinoma: A critical appraisal of three hypotheses on its cause. *American Journal of Obstetrics and Gynecology*, 718-732.

Pike, M., Pearce, C., Peters, R., Wan, P., Cozen, W., and Woo, A. (2004). Hormonal factors and the risk of invasive ovarian cancer: a population-based case-control study. *Fertility and Sterility*, 186-195. Retrieved from https://doi.org/10.1016/j.fertnstert.2004.03.013.

Pollak, M; Perdue, J; Margolese, R; Baer, K; and Richard, M. (1987). Presence of somatomedin receptors on primary human breast and colon carcinomas. *Cancer letter*, 223–230.

Poveda, A., Ibáñez, M., and Rebato, E. (2014). Common variants in BDNF, FAIM2, FTO, MC4R, NEGR1, and SH2B1 show association with obesity-related variables in Spanish Roma population. *American Journal of human biology*, 660-9. doi:doi: 10.1002/ajhb.22576.

Pradeep, S; Kim, S; Wu, S; Nishimura, M; Chaluvally-Raghavan, P; Miyake, T; Pecot, C; Kim, S; Choi, H; Bischoff, F; Mayer, J; Huang, L; Nick, A; Hall, C; Rodriguez-Aguayo, C; Zand, B; Dalton, H; Arumugam, T; Jeong, L; Han, H; Cho, M; Rupaimoole, R; Mangala, L; Sehgal, V; Oh, S; Liu, J; Lee, J; Coleman, R; Ram, P; Lopez-Berestein, G; Fidler, I; and Sood, A. (2014). Hematogenous metastasis of ovarian cancer: Rethinking mode of spread. *Cancer Cell*, 77-91.

Prat, J. (2015). FIGO's staging classification for cancer of the ovary, fallopian tube, and peritoneum: abridged republication. *Journal of Gynecologic Oncology*, 87-89. Retrieved from https://doi.org/10.3802/jgo.2015.26.2.87.

Prat, J., and FIGO Committee on Gynecologic Oncology, F. (2014). Staging classification for cancer of the ovary, fallopian tube, and peritoneum. *International Journal of Gynecology and Obstetrics*, 1-5.

Quan, J., Yahata, T., Adachi, S., Yoshihara, K., and Tanaka, K. (2011). Identification of Receptor Tyrosine Kinase, Discoidin Domain Receptor 1 (DDR1), as a Potential Biomarker for Serous Ovarian Cancer. *International journal of molecular sciences*, 971-982.

Quong, R., Bickford, S., Ing, Y., Terman, B., Herlyn, M., and Lassam, N. (1994). Protein kinases in normal and transformed melanocytes. *Melanoma Res*, 313-9.

Raja, F., Chopra, N., & Ledermann, J. (2012). Optimal first-line treatment in ovarian cancer. *Annals of Oncology*, x118–x127. Retrieved from https://doi.org/10.1093/annonc/mds315.

Ramírez-González, J; Vaamonde-Lemos, R ; Cunha-Filho, J ; Varghese, A; and Swanson, R. (2016). *Overview of the Female Reproductive System.* Springer Science+Business Media New Yor. doi:10.1007/978-1-4939-3402-7_2.

Rankin, E; Fuh, K; Taylor, T; Krieg, A; Musser, M; Yuan, J; Wei, K; Kuo, C; Longacre, T; and Giaccia, A. (2010). AXL is an essential factor and therapeutic target for metastatic ovarian cancer. *Cancer Research*, 7570-9. doi:10.1158/0008-5472.

Rea, K; Pinciroli, P; Sensi, M; Alciato, F; Bisaro, B; Lozneanu, L; Raspagliesi, F; Centritto, F; Cabodi, S; Defilippi, P; Avanzi, G; Canevari, S; and Tomassetti, A. (2015). Novel Axl-driven signaling pathway and molecular signature characterize high-grade ovarian cancer patients with poor clinical outcome. *Oncotarget*, 30859-75.

Reed, J., McNamee, C., Rackstraw, S., Jenkins, J., and Moss, D. (2004). Diglons are heterodimeric proteins composed of IgLON subunits, and Diglon-CO inhibits neurite

outgrowth from cerebellar granule cells. *Journal of Cell Science*, 3961-3973. doi:doi: 10.1242/jcs.01261.

Reed, J; Dunn, J; Du Plessis, D; Shaw, E; Reeves, P; Gee, A; Warnke, P; Sellar, G; Moss, D; and Walker, C. (2007). Expression of cellular adhesion molecule 'OPCML' is down-regulated in gliomas and other brain tumours. *Neuropathology and applied neurobiology*, 77-85.

Rehn, M., Pihlajaniemi, T., Hofmann, K., and Bucher, P. (1998). The frizzled motif: in how many different protein families does it occur? *Trends in biochemical Science*, 415-417.

Renehan, A., Zwahlen, M., and Egger, M. (2015). Adiposity and cancer risk: new mechanistic insights from epidemiology. *Nature Review Cancer*, 484-98.

Rice, M., Murphy, M., and Tworoger, S. (2012). Tubal ligation, hysterectomy and ovarian cancer: A meta-analysis. *Journal of ovarian research*, 1-16.

Richards, J., and Pangas, S. (2010). The ovary: basic biology and clinical implications. *Journal of Clinical Investigation*, 963-972.

Risch, H. (1998). Hormonal etiology of epithelial ovarian cancer, with a hypothesis concerning the role of androgens and progesterone. *Journal of the National Cancer Institute*, 1774-86.

Robinson, D., Wu, Y., and Lin, S. (2000). The protein tyrosine kinase family of the human genome. *Oncogene*, 5548-57.

Roh, M., Kindelberger, D., and Crum, C. (2009). Serous tubal intraepithelial carcinoma and the dominant ovarian mass: clues to serous tumor origin? *The American journal of surgical pathology*, 376-83.

Romero, I., and Bast, R. (2012). Minireview: human ovarian cancer: biology, current management, and paths to personalizing therapy. *Endocrinology*, 2011-2123. doi:10.1210/en.2011-2123.

Rosen, D; Yang, G; Liu, G; Mercado-Uribe, I; Chang, B; Xiao, X; Zheng, J; Xue, F; and Liu, J. (2009). Ovarian cancer: pathology, biology, and disease models. *Frontiers in bioscience*, 2089–2102.

Rostgaard, K., Wohlfahrt, J., Andersen, P., Hjalgrim, H., Frisch, M., Westergaard, T., and Melbye, M. (2003). Does Pregnancy Induce the Shedding of Premalignant Ovarian Cells? *Epidemiology*, 168-173.

Roskoski, R. (2014). The ErbB/HER family of protein-tyrosine kinases and cancer. *Pharmacological Research*, 34-74.

Rotsch, M., Maasberg, M., Erbil, C., Jacques, G., Worsh, U., and Havemann, K. (1992). Characterization of insulin-like growth factor-I receptors and growth effects in human lung cancer cell lines. *Journal of Cancer Research and Clinical Oncolology* , 502-508.

Sabater, L; Gaig, C; Gelpi, E; Bataller, L; Lewerenz, J; Torres-Vega, E; Contreras, A; Giometto, B; Compta, Y; Embid, C; Vilaseca, I; Iranzo, A; Santamaría, J; Dalmau, J; and Graus, F. (2014). A novel non-rapid-eye movement and rapid-eye-movement parasomnia with sleep breathing disorder associated with antibodies to IgLON5: a case series, characterisation of the antigen, and post-mortem study. *The lancet neurology, Volume 13*(6), 575–586. Retrieved from http://dx.doi.org/10.1016/S1474-4422(14)70051-1.

Sainaghi, P., Castello, L., Bergamasco, L., Galletti, M., Bellosta, P., and Avanzi, G. (2005). Gas6 induces proliferation in prostate carcinoma cell lines expressing the Axl receptor. *Journal of Cellular Physiology*, 36-44.

Saito, N., Nishimura, H., and Kameoka, S. (2008). Clinical significance of fibronectin expression in colorectal cancer. *MOLECULAR MEDICINE REPORTS*, 77-81.

Samani, A., Yakar, S., LeRoith, D., and Brodt, P. (2007). The Role of the IGF System in Cancer Growth and Metastasis: Overview and Recent Insights. *Endocrine Reviews*, 20-47. Retrieved from https://doi.org/10.1210/er.2006-0001.

SAMCI oncology treatment: http://france-oncology.com/en/ovarian-cancer/.

Sansal, I., and Sellers, W. (2004). The Biology and Clinical Relevance of the PTEN Tumor Suppressor Pathway. *Journal of clinical oncology BIOLOGY OF NEOPLASIA*. doi:10.1200/JCO.2004.02.141.

Schlessinger, J. (2000). Cell signaling by receptor tyrosine kinases. *Cell*, 211-25.

Schmitt, A; Shi, J; Wolf, A; Lu, C; King, L; and Zou, Y. (2006). Wnt–Ryk signalling mediates medial–lateral retinotectal topographic mapping. *Nature*, 31–37.

Schofield, PR; McFarland, KC; Hayflick, JS; Wilcox, JN; Cho, TM; Roy, S; Lee, NM; Loh, HH; and Seeburg, PH. (1989). Molecular characterization of a new immunoglobulin superfamily protein with potential roles in opioid binding and cell contact. *The EMBO Journal*, 489-495.

Seidman, J., Yemelyanova, A., Cosin, J., Smith, A., and Kurman, R. (2012). Survival rates for international federation of gynecology and obstetrics stage III ovarian carcinoma by cell type: a study of 262 unselected patients with uniform pathologic review. *International Journal of Gynecological Cancer*, 367-7. doi:10.1097/IGC.0b013e31823c6f80.

Sellar, GC; Watt, KP; Rabiasz, GJ; Stronach, E; Li, L; Miller, E; Massie, C; Miller, J; Contreras-Moreira, B; Scott, D; Brown, I; Williams, A; Bates, P; Smyth, J; and Gabra, H. (2003).

OPCML at 11q25 is epigenetically inactivated and has tumor-suppressor function in epithelial ovarian cancer. *Nature genetic*, 337-343.

Sharma, K; Schmitt, S; Bergne, C; Tyanova, S; Kannaiyan, N; Manrique-Hoyos, N; Kongi, K; Cantuti, L; Hanisch, U; Philips, M; Rossner, M; Mann, M; and Simons, M. (2015). Cell type– and brain region–resolved mouse brain proteome. *NATURE NEUROSCIENCE*, 1819–1831. doi:10.1038/nn.4160.

Shen, Y., Shen, R., Ge, L., Zhu, Q., and Li, F. (2012). Fibrillar type I collagen matrices enhance metastasis/invasion of ovarian epithelial cancer via β1 integrin and PTEN signals. *International journal of gynecological cancer*, 1316-24.

Shih, I., and Kurman, R. (2004). Ovarian Tumorigenesis: A Proposed Model Based on Morphological and Molecular Genetic Analysis. *The American Journal of Pathology*, 1511-1518.

Shimada, K; Nakamura, M; Ishida, E; Higuchi, T; amamoto, H; Tsujikawa, K; and Konishi, N. (2008). Prostate cancer antigen-1 contributes to cell survival and invasion though discoidin receptor 1 in human prostate cancer. *Cancer Science*, 39-45.

Shinh, Y; Lai, C; Kao, Y; Shiah, S; Chu, Y; Lee, H; and Wu, C. (2005). Expression of Axl in Lung Adenocarcinoma and Correlation with Tumor Progression. *Neoplasia*, 1058 – 1064.

Silverberg, S. (2000). Histopathologic grading of ovarian carcinoma: a review and proposal. *International Journal of GynecologicalPathology*, 7-15.

Simons, K., and Toomre, D. (2000). Lipid rafts and signal transduction. *Nature Reviews Molecular Cell Biology* , 31-39 . doi:doi:10.1038/35036052.

Singer, G., Oldt, R., Cohen, Y., Wang, B., Sidransky, D., Kurman, R., and Shih, I. (2003). Mutations in BRAF and KRAS characterize the development of low-grade ovarian serous carcinoma. *Journal of the National Cancer Institute*, 484-6.

Singh, N., Gilks, C., Wilkinson, N., and McCluggage, W. (2015). Assessment of a new system for primary site assignment in high-grade serous carcinoma of the fallopian tube, ovary, and peritoneum. *Histopathology*, 331-7.

Slamon, D; Godolphin , W; Jones , L; Holt, J; Wong , S; Keith , D; Levin , W; Stuart , S; Udove J, J; and Ullrich , A. (1989). Studies of the HER-2/neu proto-oncogene in human breast and ovarian cancer. *Science*, 707-712.

Smittenaar, C., Petersen, K., Stewart, K., and Moitt, N. (2016). Cancer incidence and mortality projections in the UK until 2035. *British Journal of Cancer*, 1147-1155.

Soslow, R. (2008). Histologic Subtypes of Ovarian Carcinoma: An Overview. *International Journal of Gynecological Pathology*, 161-174.

Soussi, T., Ishioka, C., Claustres, M., and Béroud, C. (2006). Locus-specific mutation databases: pitfalls and good practice based on the p53 experience. *Nature Reviews Cancer*, 83-90. doi:10.1038/nrc1783.

Sriraksa, R; Zeller, C; El-Bahrawy, M; Dai, W; Daduang, J; Jearanaikoon, P; Chau-in, S; Brown, R; and Limpaiboon, T. (2011). CpG-island methylation study of liver fluke-related cholangiocarcinoma. *British Journal of cancer*, 1313–1318.

Stacker, S., Hovens, C., Vitali, A., Pritchard, M., Baker, E., Sutherland, G., and Wilks, A. (1993). Molecular cloning and chromosomal localisation of the human homologue of a receptor related to tyrosine kinases (RYK). *Oncogene*, 1347-56.

Steele, I., Edmondson, R., Bulmer, J., Bolger, B., Leung, H., and Davies, B. (2001). Induction of FGF receptor 2-IIIb expression and response to its ligands in epithelial ovarian cancer. *Oncogene*, 5878-87.

Stenhoff, J., Dahlbäck, B., and Hafizi, S. (2004). Vitamin K-dependent Gas6 activates ERK kinase and stimulates growth of cardiac fibroblasts. *Biochemical and biophysical communication*, 871-8.

Stern, D. (2000). Tyrosine kinase signalling in breast cancer: ErbB family receptor tyrosine kinases. *Breast Cancer Research* , 176-183.

Stratton, J; Gayther, S; Russell, P; Dearden, J; Gore, M; Blake, P; Easton, D; and Ponder, B. (1997). Contribution of BRCA1 mutations to ovarian cancer. *New England Journal of medicine*, 1125-30.

Struyk, A., Canoll, P., Wolfgang, M., Rosen, C., D'Eustachio, P., and Salzer, J. (1995). Cloning of neurotrimin defines a new subfamily of differentially expressed neural cell adhesion molecules. *Journal of neuroscience*, 2141–56.

Sun, W., Fujimoto, J., and Tamaya, T. (2004). Coexpression of Gas6/Axl in human ovarian cancers. *Oncology*, 450-7.

Tai, K., Shieh, Y., Lee, C., Shiah, S., and Wu, C. (2008). Axl promotes cell invasion by inducing MMP-9 activity through activation of NF-κB and Brg-1. *Oncogene*, 4044–4055.

Tas, F., Bilgin, E., Karabulut, S., and Duranyildiz, D. (2016). Clinical significance of serum laminin and type-IV collagen levels in cutaneous melanoma patients. *MOLECULAR AND CLINICAL ONCOLOGY*, 195-200.

Tavassoli, F., and Devilee, P. (2003). *World Health Organization Classification of Tumour Pathology and Genetics of Tumours of the Breast and Female Genital Organs.* International Agency for Research on Cancer (IARC).(2017, 08 23).

Thaker, P; Deavers, M; Celestino, J; Thornton, A; Fletcher, M; Landen, C; Kinch, M; Kiener, P; and Sood, A. (2004). EphA2 expression is associated with aggressive features in ovarian carcinoma. *Clinical Cancer Research*, 5145-50.

Thermo Fisher Scientific, F. (2017, 09 03). Retrieved from https://www.thermofisher.com/us/en/home/life-science/cloning/cloning-learning-center/invitrogen-school-of-molecular-biology/molecular-cloning/cloning/common-applications-strategies.html.

Timmermans-Sprang, E., Gracanin, A., and Mol, J. (2015). High basal Wnt signaling is further induced by PI3K/mTor inhibition but sensitive to cSRC inhibition in mammary carcinoma cell lines with HER2/3 overexpression. *BMC cancer*, 1-12.

Tone, A; Salvador, S; Finlayson, S; Tinker, A; Kwon, J; Lee, C; Cohen, T; Ehlen, T; Lee, M; Carey, M; Heywood, M; Pike, J; Hoskins, P; Stuart, G; Swenerton, K; Huntsman, D; Gilks, C; Miller, D; and McAlpine, J. (2012). The role of the fallopian tube in ovarian cancer. *Clinical Advances in Hematology and Oncology*, 296-306.

Tsou , A; Wu , K; Tsen, T; Chi , C; Chiu , J; Lui , W; Hu , C; Chang , C; Chou , C; and Tsai , S. (1998). Parallel hybridization analysis of multiple protein kinase genes: identification of gene expression patterns characteristic of human hepatocellular carcinoma. *Genomics*, 331-40.

Tsou, J; Galler, J; Siegmund, K; Laird, P; Turla, S; Cozen, W; Hagen, J; Koss, M; and Laird-Offrin, I. (2007). Identification of a panel of sensitive and specific DNA methylation

markers for lung adenocarcinoma. *molecular cancer*, 1-13. Retrieved from https://doi.org/10.1186/1476-4598-6-70.

Tzonou, A., Polychronopoulou, A., Hsieh, C., Rebelakos, A., Karakatsani, A., and Trichopoulos, D. (1993). Hair dyes, analgesics, tranquilizers and perineal talc application as risk factors for ovarian cancer. *International journal of cancer*, 408-10.

UK Cancer Research, F. (2017). *UK Cancer Research*. Retrieved August 2017, from http://www.cancerresearchuk.org/health-professional/cancer-statistics/statistics-by-cancer-type/ovarian-cancer/incidence#heading-One.

Ullrich, a., and Schlessinger, J. (1990). Signal transduction by receptors with tyrosine kinase activity. *Cell*, 203-212.

Valiathan, R., Marco, M., Leitinger, B., Kleer, C., and Fridman, R. (2012). Discoidin domain receptor tyrosine kinases: new players in cancer progression. *Cancer metastasis reviews*, 295-321.

Vang, R., Shih, I., and Kurman, R. (2009). Ovarian low-grade and high-grade serous carcinoma: pathogenesis, clinicopathologic and molecular biologic features, and diagnostic problems. *Advances in Anatomic Pathology*, 267-82. doi:10.1097/PAP.0b013e3181b4fffa.

Varma , R., and Mayor , S. (1998). GPI-anchored proteins are organized in submicron domains at the cell surface. *Nature*, 798-801.

Varnum, B; Young, C; Elliott, G; Garcia, A; Bartley, T; Fridell, Y; Hunt, R; Trail, G; Clogston, C; Toso, R; Yanagihara, D; Bennett, L; Sylber, M; Merewether, L; Tseng, A; Escobar, E; Yamane, H; and Liu, E. (1995). Axl receptor tyrosine kinase stimulated by the vitamin K-dependent protein encoded by growth-arrest-specific gene 6. *Nature*, 623-6.

Von Au, A; Vasel, M; Kraft, S; Sens, C; Hackl, N; Marx, A; Stroebel, P; Hennenlotter, J; Todenhöfer, T; Stenzl, A; Schot, S; Sinn, H; Wetterwald, A; Bermejo, J; Cecchini, M; and Nakchbandi, I. (2013). Circulating Fibronectin Controls Tumor Growth. *Neoplasia*, 925-938.

Vrachnis, N., Sifakis, S., Samoli, E., Kappou, D., Pavlakis, K., Iliodromiti, Z., and Botsis, D. (2012). Three-dimensional ultrasound and three-dimensional power Doppler improve the preoperative evaluation of complex benign ovarian lesions. *Clinical and Experimental Obstetrics and Gynecology*, 474-8.

Wagner, C., Sleggs, C., and Marchand, P. (1960). Diffuse Pleural Mesothelioma and Asbestos Exposure in the North Western Cape Province. *British journal of industrial medicine*, 260–271.

Walker-Daniels, J; Coffman, K; Azimi, M; Rhim, J; Bostwick, D; Snyder, P; Kerns, B; Waters, D; and Kinch, M. (1999). Overexpression of the EphA2 tyrosine kinase in prostate cancer. *The Prostate*, 275-80.

Wang, L., Zhu, J., Song, M., Chen, G., and Chen, J. (2006). Comparison of gene expression profiles between primary tumor and metastatic lesions in gastric cancer patients using laser microdissection and cDNA microarray. *World Journal of Gastroenterology*, 6949–6954. doi:10.3748/wjg.v12.i43.6949.

Wang, X; Katso, R; Butler, R; Hanby, A; Poulsom, R; Jones, T; Sheer, D; and Ganesan, T. (1996). H-RYK, an unusual receptor kinase: isolation and analysis of expression in ovarian cancer. *Molecular Medicine*, 189-203.

Wang , J., and Hielscher, A. (2017). Fibronectin: How Its Aberrant Expression in Tumors May Improve Therapeutic Targeting. *Journal of Cancer*, 674-682.

Wang, R; Li, H; Guo, X; Wang, Z; Liang, S; and Dang, C. (2016). IGF-I Induces Epithelial-to-Mesenchymal Transition via the IGF-IR-Src-MicroRNA-30a-E-Cadherin Pathway in Nasopharyngeal Carcinoma Cells. *Oncology research*, 225-31.

Wang, X; Wang, E; Kavanagh, J; and Freedman, R. (2005). Ovarian cancer, the coagulation pathway, and inflammation. *Journal of translational medicine*, 1-20.

Wang, YH; Han, XD; Qiu, Y; Xiong, J; Yu, Y; Wang, B; Zhu, ZZ; Qian, BP; Chen, YX; Wang, SF; Shi, HF; and Sun, X. (2012). Increased expression of insulin-like growth factor-1 receptor is correlated with tumor metastasis and prognosis in patients with osteosarcoma. *Journal of surgical oncology*, 235-43.

Webb, P., and Jordan, S. (2017). Epidemiology of epithelial ovarian cancer. *Best Practice & Research Clinical Obstetrics and Gynaecology*, 3-14. doi:https://doi.org/10.1016/j.bpobgyn.2016.08.006.

Weiner, H., Rothman, M., Miller, D., and Ziff, E. (1996). Pediatric brain tumors express multiple receptor tyrosine kinases including novel cell adhesion kinases. *Pediatric Neurosurgery*, 64-71.

Wenham, R., Lancaster, J., and Berchuck, A. (2002). Molecular aspects of ovarian cancer. *Best Practice & Research Clinical Obstetrics & Gynaecology*, 483-497. Retrieved from https://doi.org/10.1053/beog.2002.0298.

Whiteman, D; Webb, P; Green, A; Neale, R; Fritschi, L; Bain, C; Parkin, D; Wilson, L; Olsen, C; Nagle, C; Pandeya, N; Jordan, S; Antonsson, A; Kendall, B; Hughes, M; Ibiebele, T ; Miura, K ; Peters, S ; and Carey, R. (2015). Cancers in Australia in 2010 attributable to modiviable factors: summary and conclusions modiviable factors: summary and conclusions. *Australian and New Zealand Journal of Public Health, 15*.

Whittemore, A., Harris, R., and Itnyre, J. (1992). Characteristics relating to ovarian cancer risk: collaborative analysis of 12 US case-control studies. IV. The pathogenesis of epithelial ovarian cancer. Collaborative Ovarian Cancer Group. *American journal of epidemiology*, 1212-20.

WHO. (2014). non-communicable disease. Retrieved fromhttp://www.who.int/nmh/countries/gbr_en.pdf.

WHO, F. (2014). *GLOBAL STATUS REPORT on noncommunicable diseases 2014 "Attaining the nine global noncommunicable diseases targets; a shared responsibility"*. Switzerland: World Health Organisation. Retrieved from http://apps.who.int/iris/bitstream/10665/148114/1/9789241564854_eng.pdf?ua=1.

Wilken, J; Badri, T; Jaso Cross, S; Raji, R; Santin, A; Schwartz, P; Branscum, A; Baron, A; Sakhitab, A; and Maihle, N. (2012). EGFR/HER-targeted therapeutics in ovarian cancer. *FUTURE MEDICINAL CHEMISTRY*, 447–469. doi:10.4155/fmc.12.11.

Wise, S., and Weiss, A. (2009). Tropoelastin. *The international journal of biochemistry & cell biology*, 494-7.

Wu, C; Li, A; Chi, C; Lai, C; Huang, C; Lo, S; Lui, W; and Lin, W. (2002). Clinical significance of AXL kinase family in gastric cancer. *Anticancer Research*, 1071-8.

Wu, J., and Yu, E. (2014). Insulin-like growth factor receptor-1 (IGF-IR) as a target for prostate cancer therapy. *Cancer Metastasis Review*, 607-617.

Wykosky, J., Gibo, D., Stanton, C., and Debinski, W. (2005). EphA2 as a novel molecular marker and target in glioblastoma multiforme. *Molecular Cancer Research*, 541-51.

Xing, X; Cai, W; Ma, S; Wang, Y; Shi, H; Jiao, J; Yang, Y; Liu, L; Zhang, X; and Chen, M. (2017). Down-regulated expression of OPCML predicts an unfavorable prognosis and promotes disease progression in human gastric cancer. *BMC Cancer2017*, 17:268.

Yamaguchi, Y., and Pasquale, E. (2004). Eph receptors in the adult brain. *Current Opinion in Neurobiology*, 288-296.

Yamamoto, Y; Ning, G; Howitt, BE; Mehra, K; Wu, L; Wang, X; Hong, Y; Kern, F; Wei, TS; Zhang, T; Nagarajan, N; Basuli, D; Torti, S; Brewer, M; Choolani, M; McKeon, F; Crum, CP; and Xian, W. (2016). In vitro and in vivo correlates of physiological and neoplastic human Fallopian tube stem cells. *The Journal of pathology*, 519-530.

Yan, M., Schwaederle, M., Arguello, D., Millis, S., Gatalica, Z., and Kurzrock, R. (2015). HER2 expression status in diverse cancers: review of results from 37,992 patients. *Cancer metastasis reviews*, 157–164.

Yang, W., Godwin, A., and Xu, X. (2004). Tumor necrosis factor-alpha-induced matrix proteolytic enzyme production and basement membrane remodeling by human ovarian surface epithelial cells: molecular basis linking ovulation and cancer risk. *Cancer Research*, 1534-40.

Yap, T., Carden, C., and Kaye, S. (2009). Beyond chemotherapy: targeted therapies in ovarian cancer. *Nature Reviews Cancer*, 167-81. doi:10.1038/nrc2583.

Yarden, Y. (2001). The EGFR family and its ligands in human cancer: signalling mechanisms and therapeutic opportunities. *European Journal of Cancer*, 3-8.

Yarden, Y., and Pines, G. (2012). The ERBB network: at last, cancer therapy meets systems biology. *Nature Reviews Cancer*, 553-563. doi:10.1038/nrc3309

Yee, D., Morales, F., Hamilton, T., and Von Hoff, D. (1991). Expression of insulin-like growth factor I, its binding proteins, and its receptor in ovarian cancer. *Cancer Research*, 5107-12.

Ying, Y., and Tao, Q. (2009). Epigenetic disruption of the WNT/beta-catenin signaling pathway in human cancers. *Epigenetics*, 307-312.

Yousif, N. (2014). Fibronectin promotes migration and invasion of ovarian cancer cells. *Cell Biology International*, 85–91.

Yu, B., Qian, T., Wang, Y., Zho, S., Ding, G., Ding, F., and Gu, X. (2012). miR-182 inhibits Schwann cell proliferation and migration by targeting FGF9 and NTM, respectively at an early stage following sciatic nerve injury. *Nucleic Acids Research*, 10356–10365.

Yuan, W; Chen, Z; Wu, S; Ge, J; Chang, S; Wang, X; Chen, J; and Chen, Z. (2009). Expression of EphA2 and E-cadherin in gastric cancer: correlated with tumor progression and lymphogenous metastasis. *Pathology Oncology Research*, 473-8.

Zanini, E; Louay , L; Antony, J; Karali, E; Okon, I; McKie, A; Vaughan, S; El-Bahrawy, M; Stebbing, J; Recchi, C; and Gabra, H. (2017). The tumor suppressor protein OPCML potentiates anti-EGFR and anti-HER2 targeted therapy in HER2-positive ovarian and breast cancer. *Molecular Cancer Therapeutics*, 1-22. doi:Molecular Cancer Therapeutics.

Zelinski, D., Zantek, N., Stewart, J., Irizarry, A., and Kinch, M. (2001). EphA2 overexpression causes tumorigenesis of mammary epithelial cells. *Cancer Research*, 2301-6.

Zhang, Y; Knyazev, P; Cheburki, Y; Sharma, K; Knyazev, Y; Őrfi, L; Szabadkai, I; Daub, H; Kéri, G; and Ullrich, A. (2008). AXL Is a Potential Target for Therapeutic Intervention in Breast Cancer Progression. *American Association for Cancer research*, 1905-1915.

Zhao, C; Irie, N; Takada, Y; Shimoda, K; Miyamoto, T; Nishiwaki, T; Suda, T; and Matsuo, K. (2006). Bidirectional ephrinB2-EphB4 signaling controls bone homeostasis. *Cell Metabolism*, 111-21.

Zhou, B., Sun, Q., Cong, R., Gu, H., Tang, N., Yang, L., and Wang, B. (2008). Hormone replacement therapy and ovarian cancer risk: a meta-analysis. *Gynecologic oncology*, 641-51. doi:10.1016/j.ygyno.2007.12.003.

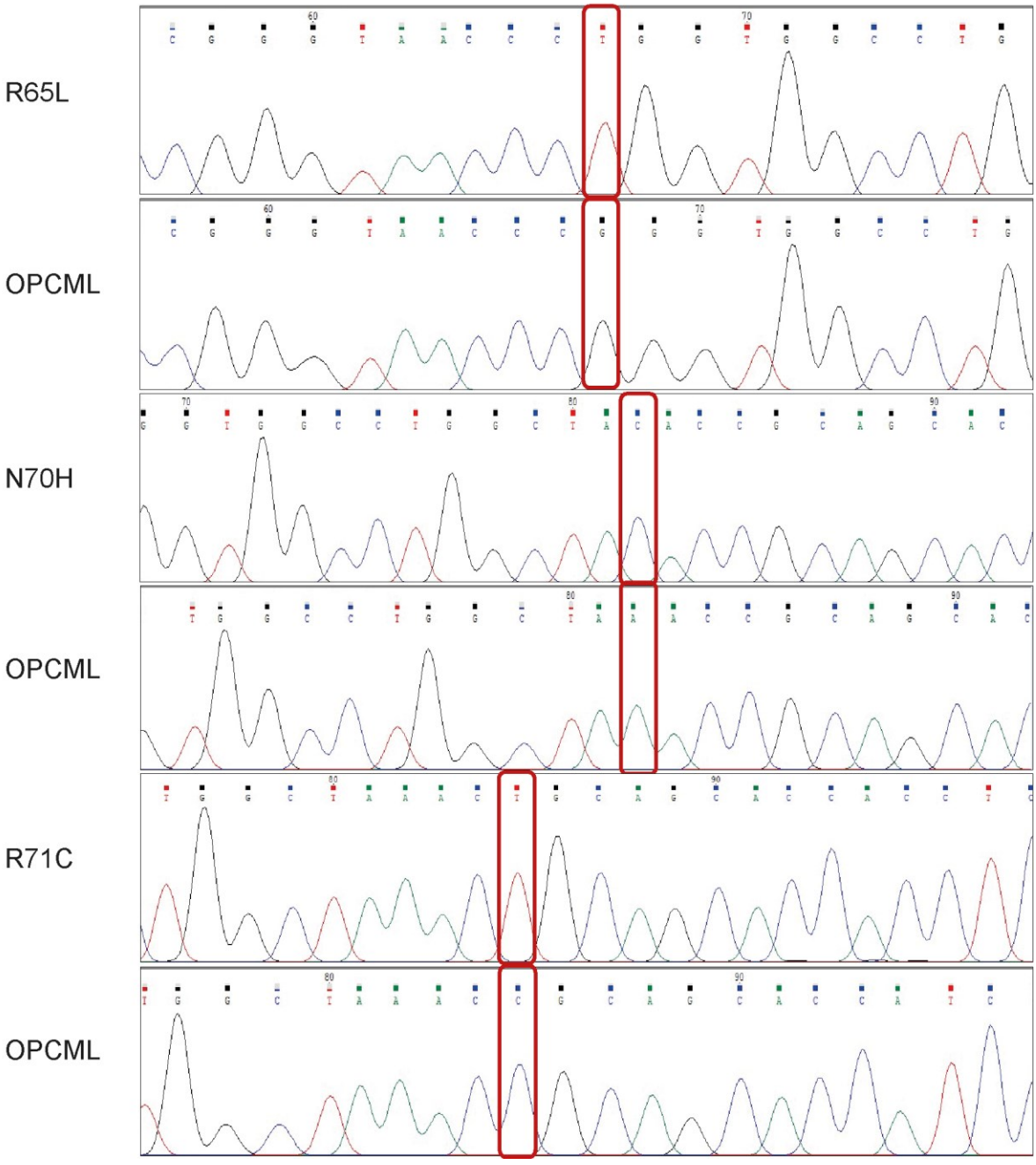
Zhuang, G; Brantley-Sieders, D; Vaught, D; Yu, J; Xie, L; Wells, S; Jackson, D; Muroaka-Cook, R; Arteaga, C; and Chen, J. (2010). Elevation of receptor tyrosine kinase EphA2 mediates resistance to trastuzumab therapy. *Cancer research*, 1-16.

Zhukareva, V., Chernevskaya, N., Pimenta, A., Nowycky, M., and Levitt, P. (1997). Limbic System-Associated Membrane Protein (LAMP) Induces Neurite Outgrowth and Intracellular Ca21 Increase in Primary Fetal Neurons. *Molecular and Cellular Neuroscience*, 43–55.

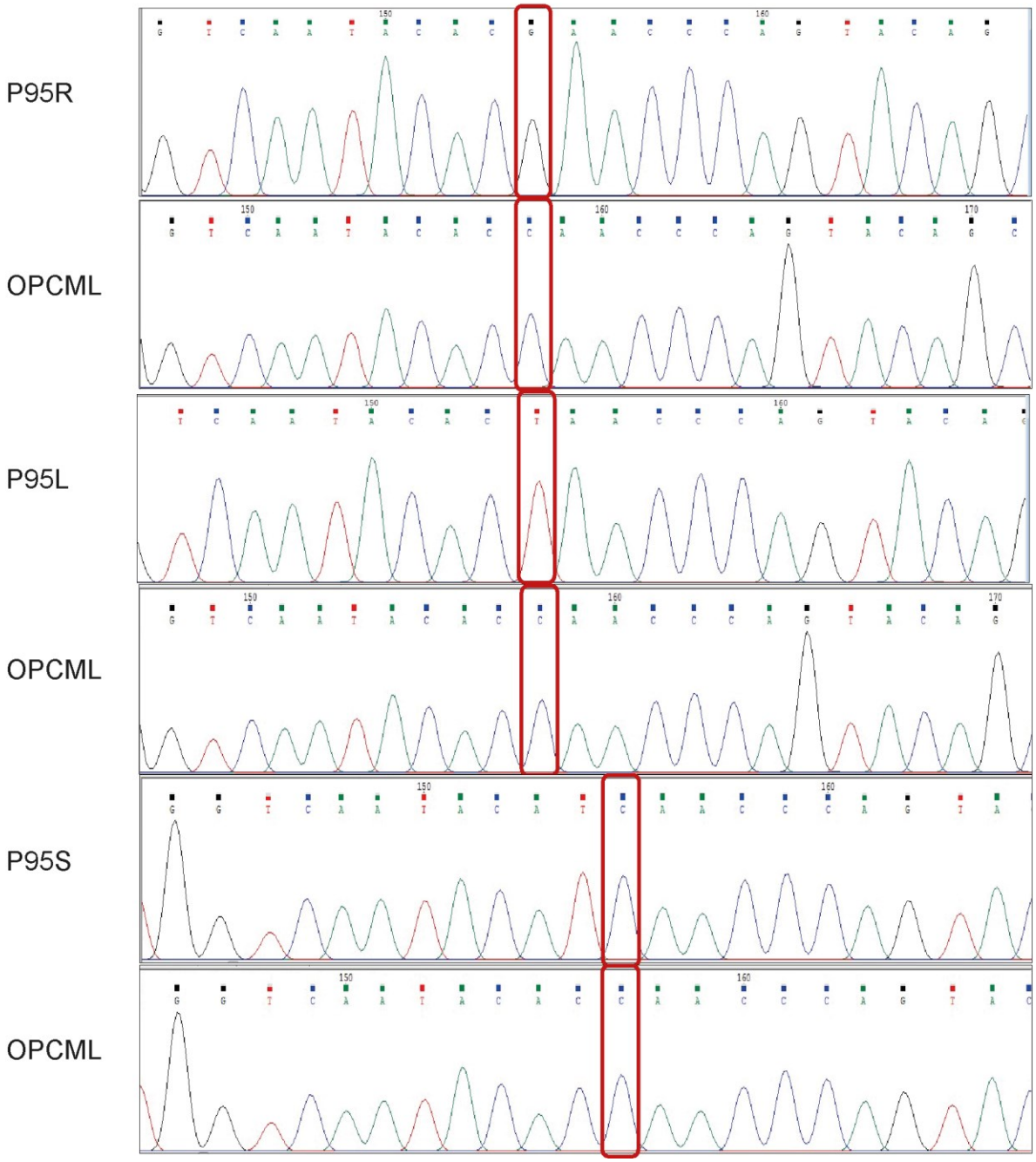
9. CHAPTER 9

Supplementary Data

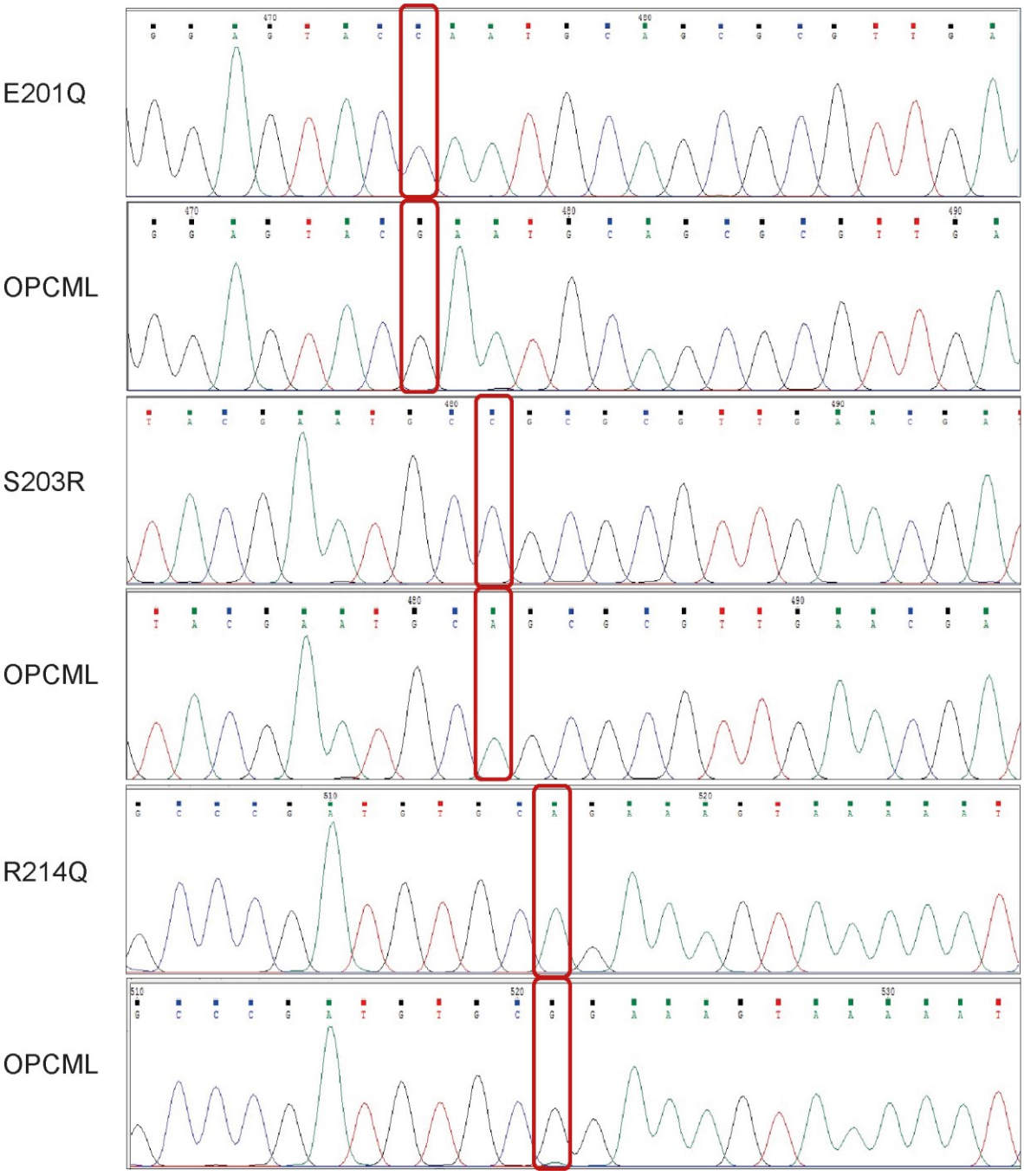
A



B



C



D

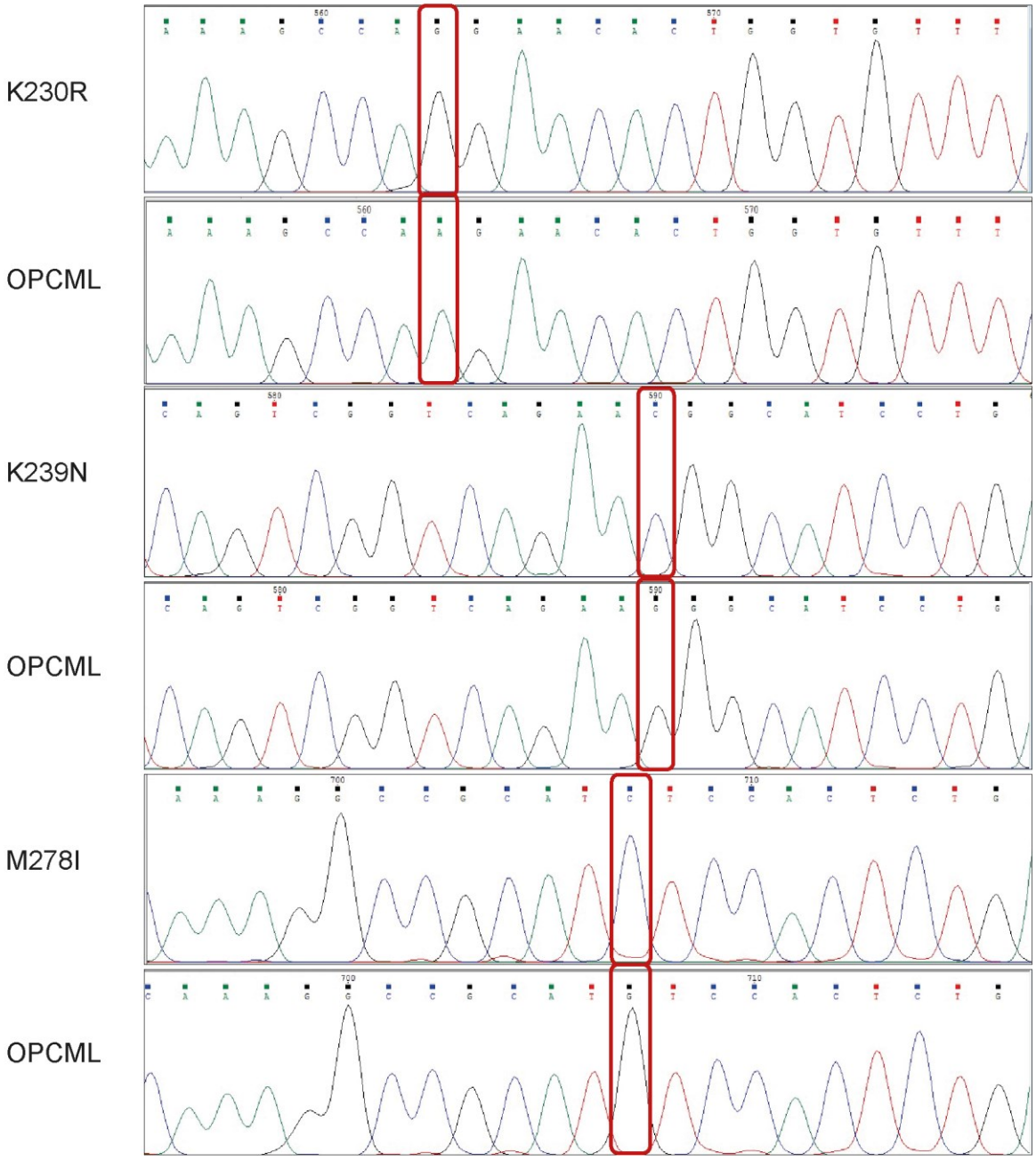


Figure 9.1Sequencing traces of the OPCML mutants and OPCML Wild-type plasmids.

The sequence traces of OPCML wild-type and OPCML mutants.

A. Wild-type OPCML compared to the selected mutants R65L, N70H, and R71C in Domain I.
B. Wild-type OPCML compared to the selected mutants P95R, P95L, and P95S in Domain I.
C. Wild-type OPCML compared to the selected mutants E201Q, S203R, and R214Q in Domain II
D. Wild-type OPCML compared to the selected mutants K230R, K239N, and M278I in Domain III.

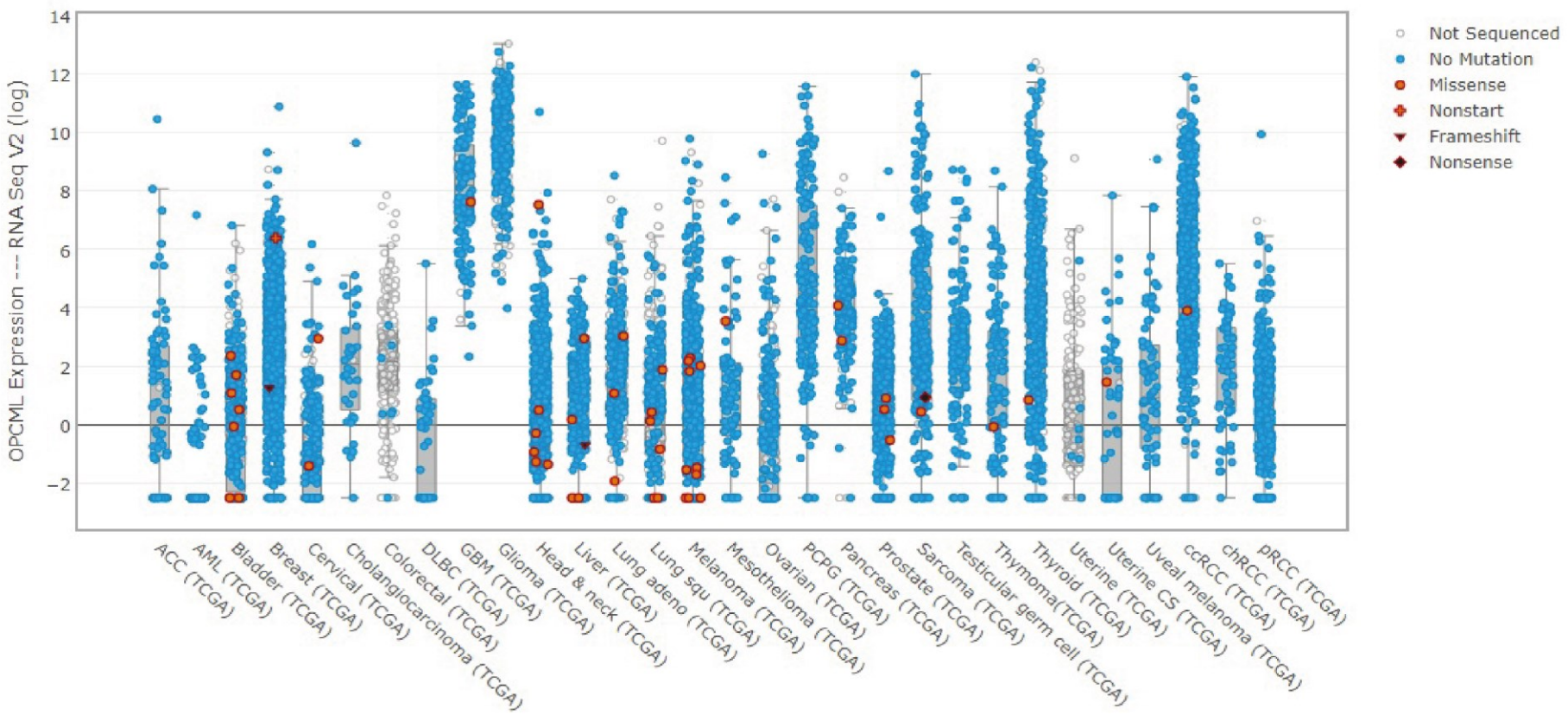


Figure 9.2 RNA-seq data from TCGA showing OPCML Wild-type and mutants mRNA expression in different cancers.

The data showed that the level of OPCML mRNA expression varied widely in different tumour types, the data are adapted from TCG

Table 9.3 Summary of the number of OPCML SNPs from genome-wide association studies.

The table shows the OPCML, SNPs ID, disease, number of SNPs, strongest SNPs- risk allele, risk allele frequency, p-value and contexts

Number	REPORTED GENE(S)	SNPS	DISEASE/TRAIT	Number of SNPs	STRONGEST SNP-RISK ALLELE	RISK ALLELE FREQUENCY	P-VALUE	PVALUE_MLOG	CONTEXT
1	OPCML	rs1940013	Heart rate variability traits (SDNN)	3	rs149496015-C	NR	6.00E-06	5.22184875	intron_variant
2	OPCML	rs9787796	Alcohol dependence	4	rs1793257-A	0.152	2.00E-06	5.698970004	intron_variant
3	OPCML	rs80068859	Gastric cancer	4	rs4578395-C	0.0309	9.00E-06	5.045757491	intron_variant
4	OPCML	rs1567127	Sleep-related phenotypes	5	rs1940013-?	0.2	1.00E-06	6	downstream_gene_variant
5	OPCML	rs1793257	Waist-hip ratio	6	rs10894604-T	0.037	7.00E-06	5.15490196	non_coding_transcript_exon_variant
6	OPCML	rs7117082	Middle childhood and early adolescence aggressive behavior	7	rs9787796-T	0.21	8.00E-09	8.096910013	intron_variant
7	OPCML	rs7104871	Coffee consumption (cups per day)	9	rs4245116-T	NR	7.00E-08	7.15490196	intron_variant
8	OPCML	rs4578395	Smooth-surface caries	11	rs2078454-A	0.092	2.00E-06	5.698970004	intron_variant
9	OPCML	rs149496015	Docetaxel-induced peripheral neuropathy in metastatic castrate-resistant prostate cancer	12	rs1027796-?	0.98	8.00E-07	6.096910013	intron_variant
10	OPCML	rs2078454	Menopause (age at onset)	13	rs4397868-?	0.2094	6.00E-06	5.22184875	intergenic_variant
11	OPCML	rs79916885	Facial morphology (factor 19)	32	rs11601484-T	NR	9.00E-06	5.045757491	intron_variant
12	OPCML	rs4397868	Blood pressure (smoking interaction)	37	rs7104871-?	NR	3.00E-07	6.522878745	intron_variant
13	OPCML	rs11601484	Rubella	38	rs79916885-?	0.1522	4.00E-06	5.397940009	intron_variant
14	OPCML	rs10894604	Visceral adipose tissue/subcutaneous adipose tissue ratio	42	rs1567127-G	0.83	4.00E-07	6.397940009	intron_variant
15	OPCML	rs1027796	Chronic obstructive pulmonary disease-related biomarkers	34	rs4468361-T	NR	4.00E-06	5.397940009	intron_variant
16	OPCML	rs4245116	Venous thromboembolism adjusted for sickle cell variant rs77121243-T	86	rs80068859-G	NR	2.00E-06	5.698970004	intron_variant
17	OPCML	rs2917569	Amyotrophic lateral sclerosis (sporadic)	175	rs7117082-?	NR	4.00E-07	6.397940009	intron_variant
18	OPCML, NTM	rs4468361	Schizophrenia	620	rs2917569-T	0.32	8.00E-06	5.096910013	intron_variant